

WestminsterResearch

<http://www.westminster.ac.uk/westminsterresearch>

Strategies for Improving the Bacterial Biodegradation of PET

Ahmaditabatabaei, Seyedehazita

This is a PhD thesis awarded by the University of Westminster.

© Miss Seyedehazita Ahmaditabatabaei, 2023.

<https://doi.org/10.34737/w74wy>

The WestminsterResearch online digital archive at the University of Westminster aims to make the research output of the University available to a wider audience. Copyright and Moral Rights remain with the authors and/or copyright owners.

Strategies for Improving the Bacterial Biodegradation of PET

Seyedehazita Ahmaditabatabaei

Supervisor: Professor Tajalli Keshavarz

A thesis submitted in the partial fulfilment of the requirements of the University of
Westminster for the degree of Doctor of Philosophy

September 2023

Abstract

Plastic waste and its persistent presence in the environment pose significant global challenges. Among various types of plastics, synthetic ones like polyethylene terephthalate (PET) are mostly used for packaging and has comprised a major part of plastic waste. PET is particularly resistant to degradation, mainly due to its high content of aromatic terephthalate units. While biodegradation is an environmentally friendly method for tackling this waste, it is proven to be somewhat inefficient. One contributing factor is that the temperature required for bacterial growth is significantly lower than the glass transition temperature of PET.

To circumvent this limitation, various complementary techniques have been proposed in this project to enhance biodegradation of PET using *Ideonella sakaiensis* (*I. sakaiensis*) and *Pseudomonas mendocina* (*P. mendocina*). These methods encompass physical approaches (e.g., UV radiation), chemical treatments (e.g., alkaline treatment), biochemical strategies (utilizing surfactants like cationic surfactant dodecyl trimethylammonium bromide (DTAB) and non-ionic surfactant Dodecyl polyethylene oxide-23 ether (Brij-35)), as well as enzymatic treatment using *Fusarium culmorum* supernatant (FSC) which contains cutinase. Furthermore, the impact of the quorum sensing molecule (QSM) (specifically, 3-oxo-C₁₂-HSL) on PET degradation was investigated in the context of DTAB-treated, FSC-treated, and DTAB-FSC-treated PET up to eight weeks in the presence of the mentioned bacteria with particular emphasis on *I. sakaiensis* for its better performance compared to *P. mendocina* under the chosen process conditions.

A range of analytical techniques, including Fourier Transform Infra-Red spectroscopy (FTIR), biofilm assays, high-pressure liquid chromatography (HPLC), high-resolution microscopy, and scanning electron microscopy (SEM), were employed to evaluate the outcomes of these treatments on PET and its biodegradation potential.

Notably, FSC treatment, in conjunction with the presence of the *I. sakaiensis* bacterial culture supplemented with QSM in Yeast Extract-Sodium Carbonate and Vitamins (YSV) medium, exhibited significant promise for enhancing PET degradation within one week.

FTIR spectroscopic analyses were employed to probe structural alterations within the PET polymer. The FTIR findings demonstrated the substantial progress achieved, unveiling an impressive ~89.0% transmittance rate post FSC treatment of PET followed by one week of incubation using the *I. sakaiensis* culture supplemented by QSM. This enhanced transmittance reflects notable modification in PET molecular bonds, signifying successful polymer breakdown.

Furthermore, assessments of microstructural transformations were carried out through high-resolution microscopy and Scanning Electron Microscopy (SEM). These observations concurred with the FTIR results, visually attesting to the efficacy of FSC treatment in the *I. sakaiensis* culture supplemented by QSM. The surfaces of FSC-treated PET exhibited notable roughness compared to untreated PET, coupled with an increased surface porosity. These structural modifications validate the findings derived from FTIR spectroscopy, fortifying the substantial strides made in PET biodegradation.

ABSTRACT	I
LIST OF FIGURES	VI
LIST OF TABLES	X
ACKNOWLEDGEMENT.....	XI
LIST OF ABBREVIATIONS	XIII
CHAPTER 1. INTRODUCTION	1
1. INTRODUCTION	2
1.1. Plastics structure and degradation.....	3
1.1.1. Plastic disposal.....	7
1.1.1.1. Landfill	7
1.1.1.2. Incineration	7
1.1.1.3. Recycling	8
1.1.2. Degradation of plastics	9
1.1.2.1. Mechanical degradation.....	9
1.1.2.2. Chemical degradation	9
1.1.2.3. Biological degradation	10
1.2. Polyethylene terephthalate.....	13
1.3. <i>Ideonella sakaiensis</i> (<i>I. sakaiensis</i>).....	16
1.3.1. Classification.....	16
1.3.2. Morphology and Physiology	16
1.4. <i>Pseudomonas mendocina</i> (<i>P. mendocina</i>)	17
1.4.1. Classification.....	17
1.4.2. Morphology	17
1.5. <i>Fusarium</i> species	17
1.5.1. Morphology	17
1.6. Doubling time calculations	18
1.7. Pre-treatment approaches for PET degradation	19
1.7.1. Sodium hydroxide (NaOH) pre-treatment.....	19
1.7.2. UV light pre-treatment	19
1.7.3. Surfactant.....	20
1.7.3.1. Surfactant types.....	20
1.7.3.1.1. Non-ionic surfactants.....	21
1.7.3.1.2. Anionic surfactants.....	22
1.7.3.1.3. Cationic surfactants	22
1.7.3.1.4. Amphoteric surfactants.....	23
1.8. Enzymatic degradation of PET	23
1.8.1. Limitations Hindering Enzymatic PET Biodegradation.....	29
1.8.2. Strategies to Enhance Enzyme-Based PET Biodegradation.....	30
1.8.2.1. Thermostable Enzymes	30
1.8.2.2. Use of Surfactants and Additives	30
1.9. Biofilm formation	32
1.10. Fourier Transform Infrared (FTIR) spectroscopy	35
1.11. High-performance liquid chromatography (HPLC).....	37
1.11.1. Normal-phase chromatography	37
1.11.2. Reversed-phase chromatography	38
1.11.3. Mobile phase elution mode	38
1.12. Quorum sensing	39
1.12.1. QSM types	41
1.12.2. Application and potential of QSM	42
1.12.3. N-(3-oxododecanoyl) L-Homoserine lactone (3-oxo-C ₁₂ -HSL)	43
1.13. Aim and objectives	45
CHAPTER 2. MATERIALS AND METHODS.....	46
2. MATERIALS AND METHODS.....	47
2.1. Materials	47
2.1.1. Microorganisms	47
2.1.1.1. Bacteria	47

2.1.1.2. Fungi	47
2.1.2. Media	47
2.1.3. Surfactants	49
2.1.4. Quorum sensing molecule.....	49
2.1.5. Plastic.....	49
2.1.6. Equipment.....	49
2.1.6.1. FTIR.....	49
2.1.6.2. Microplate reader	50
2.1.6.3. High-Performance Liquid Chromatography (HPLC).....	50
2.1.6.4. High Resolution Microscopy.....	50
2.1.6.5. Scanning electron microscopy (SEM).....	50
2.1.6.6. Other equipment.....	50
2.2. Methods	51
2.2.1. Media preparation	51
2.2.1.1. Hipolypeptone broth.....	51
2.2.1.2. Hipolypeptone agar	51
2.2.1.3. Nutrient broth.....	52
2.2.1.4. Nutrient agar	52
2.2.1.5. Stock solutions for M9 minimal medium preparation	52
2.2.1.5.1. M9 minimal salt (10 X)	52
2.2.1.5.2. Glucose (20% w/v).....	53
2.2.1.5.3. MgSO ₄ (1 M).....	53
2.2.1.5.4. CaCl ₂ (1 M).....	53
2.2.1.5.5. Biotin.....	53
2.2.1.5.6. Thiamine-HCl.....	53
2.2.1.5.7. trace elements solution (100 X).....	54
2.2.1.5.8. M9 minimal media	54
2.2.1.6. YSV medium.....	55
2.2.1.6.1. Vitamins for YSV.....	55
2.2.1.6.2. Trace element for YSV.....	55
2.2.1.7. Potato dextrose broth.....	56
2.2.1.8. Potato dextrose agar	56
2.2.2. Reagents preparation.....	56
2.2.2.1. Phosphate buffer saline	56
2.2.2.2. Phosphate Buffer (20 mM, pH 2.5).....	56
2.2.3. Preparing the pre-treatment solutions.....	57
2.2.3.1. NaOH solution	57
2.2.3.2. Dodecyltrimethylammonium bromide (DTAB)	57
2.2.3.3. Dodecyl polyethylene oxide ether (Brij-35).....	57
2.2.4. preparation of QSM	57
2.2.4.1. N-(3-oxododecanoyl) L-Homoserine lactone (3-oxo-C ₁₂ -HSL).....	57
2.2.5. Inocula preparation	58
2.2.5.1. Long-term storage of bacterial strains	58
2.2.5.2. Preparation of working culture.....	58
2.2.5.2.1. Inoculation for growth curve experiment	58
2.2.5.2.2. Inoculation for biofilm formation	59
2.2.5.2.3. Inoculation of <i>I. sakaiensis</i> for larger scale experiments including DTAB, FSC and QSM.....	60
2.2.5.2.4. Preparation of fungi species	60
2.2.6. PET preparation	60
2.2.7. Pre-treatments of PET pieces	61
2.2.7.1. Alkaline treatment.....	61
2.2.7.2. UV treatment.....	61
2.2.7.3. Surfactant treatment	61
2.2.7.4. FSC treatment.....	61
2.2.7.5. FSC-DTAB treatment	61
2.2.8. 3-oxo-C ₁₂ -HSL concentrations preparation.....	62
2.2.8.1. 3-oxo-C ₁₂ -HSL concentrations biofilm formation.....	62
2.2.8.2. DTAB large scale in 3-oxo-C ₁₂ -HSL supplemented culture	63
2.2.8.3. FSC larger scale in 3-oxo-C ₁₂ -HSL supplemented culture.....	64
2.2.9. Biofilm formation	65
2.2.9.1. Biofilm Assay.....	65
2.2.9.1.1. Staining biofilm.....	65
2.2.9.1.2. Quantifying the biofilm	66

2.2.10. FTIR.....	66
2.2.11. HPLC.....	66
2.2.11.1. TPA standard sample preparation.....	66
2.2.11.2. The sample preparation.....	66
CHAPTER 3. RESULTS.....	67
3. OVERVIEW.....	68
CHAPTER 3.1. EFFECT OF PET PRE-TREATMENT ON PET BIODEGRADATION.....	71
3.1. Overview.....	72
3.1.1. Growth profile.....	73
3.1.1.1. <i>I. sakaiensis</i> growth profile.....	73
3.1.1.2. <i>P. mendocina</i> growth profile.....	75
3.1.2. Pre-treated PET FTIR profile in the presence of <i>I. sakaiensis</i>	77
3.1.2.1. PET FTIR profile of samples in different media.....	78
3.1.2.1.1. PET pre-treatment profile in HPP medium.....	78
3.1.2.1.2. PET pre-treatment profile in YSV medium.....	79
3.1.2.1.3. PET pre-treatment profile in M9 minimal medium.....	79
3.1.2.2. PET FTIR profile of samples based on pre-treatment.....	80
3.1.2.2.1. NaOH-treatment.....	80
3.1.2.2.2. DTAB treatment.....	81
3.1.2.2.3. Brij-35 treatment.....	82
3.1.2.2.4. UV treatment.....	82
3.1.2.3. Comprehensive tables of data.....	83
3.1.3. Pre-treated PET biofilm profile in the presence of <i>I. sakaiensis</i>	87
3.1.4. Pre-treated PET FTIR profile in the presence of <i>P. mendocina</i>	89
3.1.4.1. PET FTIR profile for different media.....	89
3.1.4.1.1. PET pre-treatment profile in HPP medium.....	89
3.1.4.1.2. PET pre-treatment profile in YSV medium.....	89
3.1.4.1.3. PET pre-treatment profile in M9 minimal medium.....	89
3.1.4.2. PET FTIR profile based on pre-treatment.....	90
3.1.4.2.1. NaOH treatment.....	90
3.1.4.2.2. DTAB treatment.....	90
3.1.4.2.3. Brij-35 treatment.....	91
3.1.4.2.4. UV treatment.....	92
3.1.4.3. Comprehensive table of data.....	92
3.1.5. Pre-treated PET biofilm profile in the presence of <i>P. mendocina</i>	94
CHAPTER 3.2. EFFECT OF DTAB TREATMENT (IN LARGE SCALE) ON PET BIODEGRADATION.....	95
3.2. Overview.....	96
3.2.1. Effect of DTAB treatment on PET degradation: FTIR results.....	97
3.2.2. Effect of DTAB treatment on PET degradation: biofilm results.....	98
3.2.3. Effect of DTAB treatment on PET degradation: HPLC results.....	99
CHAPTER 3.3. EFFECT OF <i>FUSARIUM CULMORUM</i> SUPERNATANT TREATMENT ON PET BIODEGRADATION.....	102
3.3. Overview.....	103
3.3.1. Effect of <i>Fusarium culmorum</i> supernatant and DTAB in 96-well plate: biofilm results.....	104
3.3.2. Effect of <i>F. culmorum</i> supernatant in 6-well plate.....	105
3.3.2.1. Effect of <i>F. culmorum</i> supernatant in 6-well plate: biofilm results.....	105
3.3.2.2. Effect of <i>F. culmorum</i> supernatant in 6-well plate: FTIR results.....	106
3.3.3. Effect of <i>F. culmorum</i> supernatant and DTAB in large scale.....	107
3.3.3.1. Effect of <i>F. culmorum</i> supernatant and DTAB in large scale: biofilm results.....	107
3.3.3.2. Effect of <i>F. culmorum</i> supernatant and DTAB in large scale: FTIR results.....	108
3.3.3.3. Effect of <i>F. culmorum</i> supernatant and DTAB in large scale: HPLC results.....	110
3.3.3.4. Effect of <i>F. culmorum</i> supernatant and DTAB in large scale: high resolution microscopy results.....	110
3.3.3.5. Effect of <i>F. culmorum</i> supernatant and DTAB in large scale: SEM results.....	114
CHAPTER 3.4. THE EFFECT OF 3-OXO-C ₁₂ -HSL ON PRE-TREATED PET BY DTAB, FSC, AND FSC-DTAB.....	116
3.4. Overview.....	117
3.4.1. Effect of different concentrations of 3-oxo-C ₁₂ -HSL on PET samples.....	118
3.4.1.1. Effect of different concentrations of 3-oxo-C ₁₂ -HSL on PET samples: biofilm results.....	118
3.4.1.2. Effect of different concentrations of 3-oxo-C ₁₂ -HSL on PET samples: FTIR results.....	119
3.4.2. Effect of 3-oxo-C ₁₂ -HSL on DTAB-treated PET samples in large scale.....	119
3.4.2.1. Effect of 3-oxo-C ₁₂ -HSL on DTAB-treated PET samples in large scale: biofilm results.....	120
3.4.2.2. Effect of 3-oxo-C ₁₂ -HSL on DTAB-treated PET samples in large scale: FTIR results.....	121
3.4.2.3. Effect of 3-oxo-C ₁₂ -HSL on DTAB-treated PET samples in large scale: HPLC results.....	122

3.4.3. Effect of 3-oxo-C ₁₂ -HSL on FSC-treated and FSC-DTAB-treated PET samples in 96-well plate	123
3.4.3.1. Effect of 3-oxo-C ₁₂ -HSL on FSC-treated and FSC-DTAB-treated PET samples in 96-well plate: biofilm results	123
3.4.4. Effect of 3-oxo-C ₁₂ -HSL on FSC-treated and FSC-DTAB-treated PET samples in large scale	124
3.4.4.1. Effect of 3-oxo-C ₁₂ -HSL on FSC-treated and FSC-DTAB-treated PET samples in large scale: biofilm results	124
3.4.4.2. Effect of 3-oxo-C ₁₂ -HSL on FSC-treated and FSC-DTAB-treated PET samples in large scale: FTIR results	125
3.4.4.3. Effect of 3-oxo-C ₁₂ -HSL on FSC-treated and FSC-DTAB-treated PET samples in large scale: HPLC results	126
3.4.4.4. Effect of 3-oxo-C ₁₂ -HSL on FSC-treated and FSC-DTAB-treated PET samples in large scale: high resolution microscopy results	127
3.4.4.5. Effect of 3-oxo-C ₁₂ -HSL on FSC-treated and FSC-DTAB-treated PET samples in large scale: SEM results	128
CHAPTER 4. DISCUSSION	129
4.1. Overview	130
4.2. Different pre-treatment effects on PET biodegradation	130
4.2.1. PET pre-treatment in the presence of <i>I. sakaiensis</i> : FTIR and biofilm	130
4.2.2. PET pre-treatment in the presence of <i>P. mendocina</i> : FTIR and biofilm	139
4.2.3. Comparison between <i>I. sakaiensis</i> and <i>P. mendocina</i>	141
4.3. DTAB-treatment at larger scale: effect on PET biodegradation	143
4.4. FSC-treatment effect on PET biodegradation	145
4.5. QSM effect on PET biodegradation	149
CHAPTER 5. CONCLUSION AND FUTURE WORK	152
5.1. Conclusion	153
5.2. Future work	154
CHAPTER 6. APPENDIX	156
REFERENCES	165

List of figures

Figure 1.1. Growth trend of single used plastics (SUPs) (Chen et al., 2021).	3
Figure 1.2. Sanitary landfilling (Aziz et al., 2013)	7
Figure 1.3. Polymer recycling process (Soong et al., 2022).	9
Figure 1.4. Schematic biodegradation process.	12
Figure 1.5. Microbial degradation of PET.	15
Figure 1.6. <i>I. sakaiensis</i> microscopy.	16
Figure 1.7. <i>Fusarium</i> species a) <i>F. asiaticum</i> , b) <i>F. culmorum</i> , c) <i>F. graminearum</i>	17
Figure 1.8. Chemical hydrolysis of PET with alkaline solution (Bhogle and Pandit, 2018).	19
Figure 1.9. Norrish I and II reactions.	20
Figure 1.10. Chemical structure of an anionic surfactant, ammonium lauryl sulfate (National Center for Biotechnology Information, 2021).	21
Figure 1.11. Surfactant categories based on their charge at the hydrophilic portion.	21
Figure 1.12. Chemical structure of Brij-35 (National Center for Biotechnology Information, 2021). ..	22
Figure 1.13. Chemical structure of DTAB (National Center for Biotechnology Information, 2021)...	23
Figure 1.14. Cutinases mediated catalytic breakdown of PET into its subunits (Ahmaditabatabaei et al., 2021).	29
Figure 1.15. Different stages of biofilm development (Goel et al., 2021).....	33
Figure 1.16. Reversible and irreversible attachment of bacterial cell on the surface of the plastic (Kalgudi, 2018). (a) and (b) show the reversible attachment and (c) shows the irreversible attachment.	34
Figure 1.17. The sample pathway through the HPLC diagram (Scherf-Clavel, 2016).	37
Figure 1.18. Reversed-phase chromatography HPLC diagram (Kobayashi et al., 2019)	38
Figure 1.19. Different mobile phase elution mode; a) isocratic b) gradient (Robards et al., 2004).	39
Figure 1.20. QS mechanism in Gram-negative bacteria (Amache, 2014)	40
Figure 1.21. QS process effect on the surface of the squid by increasing the cell concentration of <i>V. fischeri</i> (Amache, 2014)	40
Figure 1.22. Molecular structure of AHLs (Amache, 2014).....	41
Figure 1.23. Molecular structure of butyrolactone- containing compounds (Amache, 2014).	42
Figure 1.24. Molecular structure of 3-oxo-C ₁₂ -HSL.....	44
Figure 2.1. The schematic shows the pre-treatment process of PET using FSC.....	62
Figure 2.2. The schematic diagram illustrates the experimental setup used to investigate the biodegradation of PET in the presence of QSM and DTAB.	63
Figure 2.3. The schematic diagram illustrates the experimental setup used to investigate the biodegradation of FSC and FSC-DTAB treated PET in QSM supplemented culture.....	64
Figure 2.4. Biofilm formation on non-treated and treated PET pieces experiment set-up (created with BioRender.com).....	65
Figure 3.1. Diagram highlighting the experiments and the pathway pursued to attain the optimal approach for the biodegradation of PET film.	70
Figure 3.2. The figure shows the results of three independent shaken flask cultures (100 ml culture in 500 ml shaken flask) in HPP medium over 36 hrs of incubation at 30 °C, 180 rpm.	73
Figure 3.3. The figure shows the results of three independent shaken flask cultures (100 ml culture in 500 ml flask) in YSV medium over 8 hrs of incubation at 30 °C, 180 rpm.	75
Figure 3.4. FTIR transmittance percentages of carbonyl group after pre-treatment of PET samples and inoculation in HPP in the presence of <i>I. sakaiensis</i> culture over three weeks incubation at 30 °C.	78
Figure 3.5. FTIR transmittance percentages of carbonyl group after pre-treatment of PET samples and inoculation in YSV in the presence of <i>I. sakaiensis</i> culture over three weeks incubation at 30 °C.	79
Figure 3.6. FTIR transmittance percentages of carbonyl group after pre-treatment of PET samples and inoculation in M9-minimal in the presence of <i>I. sakaiensis</i> culture over three weeks incubation at 30 °C.	80
Figure 3.7. FTIR transmittance percentages of carbonyl functional group after NaOH treatment of PET samples and inoculation by HPP, YSV and M9 minimal medium in the presence of <i>I. sakaiensis</i> culture over three weeks incubation at 30 °C.	81

Figure 3.8. FTIR transmittance percentages of carbonyl group after DTAB treatment of PET samples and inoculation by HPP, YSV and M9 minimal medium and <i>I. sakaiensis</i> culture after three weeks incubation at 30 °C.	81
Figure 3.9. FTIR transmittance percentages of carbonyl group after Brij-35 treatment of PET samples and inoculation by HPP, YSV and M9 minimal medium and <i>I. sakaiensis</i> culture over three weeks incubation at 30 °C.	82
Figure 3.10. FTIR transmittance percentages of each functional group after Brij-35- treatment of PET samples and inoculation by HPP and YSV and <i>I. sakaiensis</i> culture after three weeks incubation at 30 °C.	83
Figure 3.11. The biofilm formation on non-treated and treated (NaOH, DTAB, Brij-35 and UV) PET samples were inoculated in HPP, YSV and M9 minimal medium with <i>I. sakaiensis</i> , and were incubated at 30 °C for one week. (n=8, P < 0.0001 (****)).	87
Figure 3.12. The biofilm formation on non-treated and treated (NaOH, DTAB, Brij-35 and UV) PET samples were inoculated in HPP, YSV and M9 minimal medium with <i>I. sakaiensis</i> , and were incubated at 30 °C for two week. (n=8, P < 0.0001 (****)).	88
Figure 3.13. The biofilm formation on non-treated and treated (NaOH, DTAB, Brij-35 and UV) PET samples were inoculated in HPP, YSV and M9 minimal medium with <i>I. sakaiensis</i> , and were incubated at 30 °C for three weeks. (n=8, P < 0.0001 (****)).	88
Figure 3.14. FTIR transmittance percentages of carbonyl group after pre-treatment of PET samples and inoculation in HPP, YSV and M9-minimal in the present of <i>P. mendocina</i> culture after one week incubation at 30 °C.	89
Figure 3.15. FTIR transmittance percentages of carbonyl group after NaOH-treatment of PET samples and inoculation in HPP, YSV and M9-minimal in the presence of <i>P. mendocina</i> culture after one week incubation at 30 °C. (n=3, P < 0.001 (***)).	90
Figure 3.16. FTIR transmittance percentages of carbonyl group after DTAB-treatment of PET samples and inoculation in HPP, YSV and M9-minimal in the presence of <i>P. mendocina</i> culture after one week incubation at 30 °C. (n=3, P < 0.0001 (****)).	91
Figure 3.17. FTIR transmittance percentages of carbonyl group after Brij-35-treatment of PET samples and inoculation in HPP, YSV and M9-minimal in the presence of <i>P. mendocina</i> culture after one week incubation at 30 °C. (n=3, P < 0.01 (**)).	91
Figure 3.18. FTIR transmittance percentages of carbonyl group after UV-treatment of PET samples and inoculation in HPP, YSV and M9-minimal in the presence of <i>P. mendocina</i> culture after one week incubation at 30 °C. (n=3, P < 0.01 (**), P < 0.0001 (****)).	92
Figure 3.19. The biofilm formation on non-treated and treated (NaOH, DTAB, Brij-35 and UV) PET samples were inoculated in HPP, YSV and M9 minimal medium with <i>P. mendocina</i> , and were incubated at 30 °C for one week.	94
Figure 3.20. The carbonyl percentage of non-treated and DTAB-treated PET samples inoculated in YSV medium in the presence of <i>P. mendocina</i> , or <i>I. sakaiensis</i> . Cultures were incubated at 30 °C for one week.	97
Figure 3.21. The biofilm formation on non-treated and DTAB-treated PET samples. Cultures were inoculated in YSV medium in the presence of <i>P. mendocina</i> , and <i>I. sakaiensis</i> , and were incubated at 30 °C for one week.	98
Figure 3.22. TPA calibration curve. The area related to different TPA concentrations containing 1.2, 2.5, 5, 8, 10, 12, 15, 20 µg/ml were collected by HPLC.	99
Figure 3.23. Chromatograms of YSV medium.	99
Figure 3.24. Chromatograms of non-treated and DTAB-treated PET samples after incubation in the presence of <i>I. sakaiensis</i> over eight weeks.	100
Figure 3.25. Chromatograms of non-treated and DTAB-treated PET samples after incubation in the presence of <i>P. mendocina</i> over eight weeks.	100
Figure 3.26. The TPA concentration (µg/ml) of non-treated and DTAB-treated PET samples were inoculated in YSV medium in the presence <i>I. sakaiensis</i> was incubated at 30 °C over eight weeks.	101
Figure 3.27. Biofilm formation on different treated PET (non, FSC, FSC-DTAB) in the presence of <i>I. sakaiensis</i> in 96-well plate after 24 hrs at 30 °C.	105
Figure 3.28. Biofilm formation of non-treated and FSC-treated PET in 6-well plate in the presence of <i>I. sakaiensis</i> over three weeks at 30 °C.	106
Figure 3.29. FTIR of non-treated and FSC-treated PET in YSV medium in the presence of <i>I. sakaiensis</i> over three weeks in 6-well plate.	107

Figure 3.30. Biofilm formation of different treatments of PET (non, FSC and FSC-DTAB) in 500 ml shaken flask in the presence of <i>I. sakaiensis</i> over eight weeks.....	108
Figure 3.31. FTIR on different treatments of PET (non, FSC, FSC-DTAB) in 500 ml shaken flask in the presence of <i>I. sakaiensis</i> over eight weeks.....	109
Figure 3.32. Using high resolution microscopy to visual presentation of the non-treated, FSC-treated and FSC-DTAB-treated PET after one and eight weeks of incubation in the presence of <i>I. sakaiensis</i> at 30 °C (magnification ×20).	112
Figure 3.33. Using high resolution microscopy to visual presentation of the non-treated, FSC-treated and FSC-DTAB-treated PET after one and eight weeks of incubation in the presence of <i>I. sakaiensis</i> at 30 °C (magnification ×100).....	113
Figure 3.34. SEM presentation of the non-treated, FSC-treated and FSC-DTAB-treated PET samples after one and eight weeks of incubation in the presence of <i>I. sakaiensis</i> at 30 °C.....	115
Figure 3.35. <i>I. sakaiensis</i> biofilm formation in YSV medium in the presence of different concentrations (0.5, 1, 5, 10, 15 and 20 µg/ml) of QSM (3-oxo-C ₁₂ -HSL) was investigated.	118
Figure 3.36. Carbonyl group transmittance percentage in the presence of different concentrations (0.5, 1, 5, 10, 15 and 20 µg/ml) of QSM (3-oxo-C ₁₂ -HSL) was investigated.	119
Figure 3.37. Biofilm formation on non-treated and DTAB-treated PET in 500 ml shaken flask in the presence of <i>I. sakaiensis</i> and QSM over eight weeks.	121
Figure 3.38. FTIR on non-treated and DTAB-treated PET in 500 ml shaken flask in the presence of <i>I. sakaiensis</i> and QSM over eight weeks.	122
Figure 3.39. Biofilm formation on non-treated, FSC-treated and FSC-DTAB-treated PET in 96-well plate in the presence of <i>I. sakaiensis</i> and QSM after 24 hrs.	123
Figure 3.40. Biofilm formation on non-treated, FSC-treated and FSC-DTAB-treated PET in 500 ml shaken flask in the presence of <i>I. sakaiensis</i> and QSM after over eight weeks.	125
Figure 3.41. FTIR on non-treated and DTAB-treated PET in 500 ml shaken flask in the presence of <i>I. sakaiensis</i> and QSM over eight weeks.	126
Figure 3.42. High resolution microscopy on FSC-treated and FSC-DTAB-treated PET in the presence of <i>I. sakaiensis</i> and QSM over eight weeks (magnification ×20).	127
Figure 3.43. SEM on FSC-treated and FSC-DTAB-treated PET in the presence of <i>I. sakaiensis</i> and QSM over eight weeks. Red arrow shows the pores.....	128
Figure 4.1. Presence of functional groups in molecular structure of PET (Roberts et al., 2020).....	132
Figure 4.2. The PET sample after hydrolysis reaction breaks down to Bis (2-hydroxyethyl) terephthalate (BHET), Mono (2-hydroxyethyl) terephthalate MHET, Terephthalic acid (TPA) and ethylene glycol (EG). The figure shows the presence of hydroxyl groups in cited molecules (Roberts et al., 2020).....	133
Figure 4.3. Transmittance percentages of carbonyl group related to DTAB and Brij-35 pre-treated PET pieces in YSV and M9 minimal medium over three weeks of incubation with <i>I. sakaiensis</i> at 30 °C.	137
Figure 4.4. Transmittance percentages of carbonyl group related to DTAB and Brij-35 pre-treated PET pieces in YSV and M9 minimal medium after one week of incubation with <i>P. mendocina</i> at 30 °C.	140
Figure 4.5. Comparing the carbonyl functional groups related to DTAB and Brij-35- treated PET pieces in the presence of <i>I. sakaiensis</i> and <i>P. mendocina</i> in defined media (YSV and M9) after one week.	141
Figure 4.6. Comparing the biofilm formation related to DTAB and Brij-35- treated PET pieces in the presence of <i>I. sakaiensis</i> and <i>P. mendocina</i> in defined media (YSV and M9) after one week..	142
Figure 6.1. FTIR of PET samples (non-treated and treated) using HPP and <i>I. sakaiensis</i> culture after one week incubation at 30 °C	156
Figure 6.2. FTIR on PET samples (non-treated and treated) using HPP and <i>I. sakaiensis</i> culture after two week incubation at 30 °C.	156
Figure 6.3. FTIR on PET samples (non-treated and treated) using HPP and <i>I. sakaiensis</i> culture after three weeks incubation at 30 °C.....	157
Figure 6.4. FTIR on PET samples (non-treated and treated) using YSV and <i>I. sakaiensis</i> culture after one week of incubation at 30 °C.	157
Figure 6.5. FTIR on PET samples (non-treated and treated) using YSV and <i>I. sakaiensis</i> culture after two week of incubation at 30 °C.	158
Figure 6.6. FTIR on PET samples (non-treated and treated) using YSV and <i>I. sakaiensis</i> culture after three weeks of incubation at 30 °C.	158

Figure 6.7. FTIR on PET samples (non-treated and treated) using M9 minimal and <i>I. sakaiensis</i> culture after one week of incubation at 30 °C.....	159
Figure 6.8. FTIR on PET samples (non-treated and treated) using M9 minimal and <i>I. sakaiensis</i> culture after two week of incubation at 30 °C.....	159
Figure 6.9. FTIR on PET samples (non-treated and treated) using M9 minimal and <i>I. sakaiensis</i> culture after three weeks of incubation at 30 °C.....	160
Figure 6.10. FTIR on PET samples (non-treated and treated) using HPP and <i>P. mendocina</i> culture after one week of incubation at 30 °C.....	160
Figure 6.11. FTIR on PET samples (non-treated and treated) using YSV and <i>P.mendocina</i> culture after one week of incubation at 30 °C.....	161
Figure 6.12. FTIR on PET samples (non-treated and treated) using M9 minimal and <i>P.mendocina</i> culture after one week of incubation at 30 °C.....	161
Figure 6.13. FTIR on non-treated and DTAB-treated PET samples using YSV medium in the presence of <i>I. sakaiensis</i> and <i>P.mendocina</i> culture after one week of incubation at 30 °C (large-scale).	162
Figure 6.14. HPLC chromatogram of TPA standard samples with concentrations ranging 1.2, 2.5, 5, 8, 10, 12, 15, 20 µg/ml.....	162
Figure 6.15. HPLC chromatograms of water.....	163
Figure 6.16. FTIR on FSC-treated PET in the presence of <i>I. sakaiensis</i> in 6-well plate after one week.	163
Figure 6.17. FTIR on FSC-treated PET with QSM in the presence of <i>I. sakaiensis</i> in large scale after one week.....	163
Figure 6.18. FTIR on different treatments of PET (non, non with QSM, FSC, FSC with QSM FSC-DTAB and FSC-DTAB with QSM) in the presence of <i>I. sakaiensis</i> in large scale after eight weeks.	164
Figure 6.19. HPLC chromatogram on non-treated, FSC-treated and FSC-DTAB-treated PET in the presence of <i>I. sakaiensis</i> in large scale after one week. Non-treated, FSC-treated and FSC-DTAB-treated.	164
Figure 6.20. HPLC chromatogram on non-treated, non-treated with QSM, FSC-treated, FSC-treated with QSM, FSC-DTAB-treated and FSC-DTAB-treated PET in the presence of <i>I. sakaiensis</i> in large scale after one week. Non-treated, non-treated with QSM, FSC-treated, FSC-treated with QSM, FSC-DTAB-treated and FSC-DTAB-treated.	164

List of Tables

Table 1.1. Some general properties and applications of common plastics (Mariotti et al., 2019)	5
Table 1.2. Some features of PET, HDPE, LDPE, PS, PHAs and PLAs	6
Table 1.3. Different functional group and the related wavenumber	36
Table 2.1. List of media and their applications.....	47
Table 2.2. Comprehensive inventory of chemicals employed as media constituents or reagents.....	48
Table 2.3. Surfactants suppliers and product numbers	49
Table 2.4. QSM supplier and product number.....	49
Table 2.5. PET supplier and product number	49
Table 2.7. HPP broth ingredients in 1-litre distilled water	51
Table 2.8. HPP agar ingredients in 1-litre distilled water.....	51
Table 2.9. Nutrient Broth ingredients in 1-litre distilled water.....	52
Table 2.10. Nutrient agar ingredients in 1-litre distilled water.....	52
Table 2.11. M9 minimal salt (10 X) ingredients in 1-liter distilled water	52
Table 2.12. Glucose (20%) ingredients in 100 ml distilled water.....	53
Table 2.13. Magnesium sulfate (1 M) ingredients in 100 ml distilled water	53
Table 2.14. Calcium chloride (1 M) ingredients in 100 ml distilled water	53
Table 2.15. Biotin ingredients in 100 ml distilled water.....	53
Table 2.16. Thiamine-HCl ingredients in 100 ml distilled water	53
Table 2.17. Trace element solution (100X) ingredients in 1-liter distilled water	54
Table 2.18. M9 minimal medium ingredients in 1-liter distilled water	54
Table 2.19. YSV ingredients in 100 ml distilled water.....	55
Table 2.20. YSV vitamins ingredients in 100 ml distilled water	55
Table 2.21. Trace element solution ingredients in 100 ml distilled water	55
Table 2.22. Potato dextrose broth ingredients in 1-litre distilled water	56
Table 2.23. Potato dextrose agar ingredients in 1-litre distilled water.....	56
Table 2.24. PBS ingredients in 1-litre distilled water.....	56
Table 2.25. 20 mM Phosphate Buffer ingredients in 1-litre distilled water.....	56
Table 2.26. NaOH (10 %) solution ingredients in 100 ml distilled water	57
Table 2.27. DTAB solution ingredients in 100 ml distilled water	57
Table 2.28. Brij-35 solution ingredients in 100 ml distilled water	57
Table 2.29. 3-oxo-C ₁₂ -HSL stock solution in 10 ml DMSO	57
Table 3.1. Transmittance percentages of non-treated and treated (NaOH, DTAB, Brij-35 and UV) PET samples after one week inoculation in HPP, YSV and M9 minimal medium and <i>I. sakaiensis</i> culture at 30 °C.	84
Table 3.2. Transmittance percentages of non-treated and treated (NaOH, DTAB, Brij-35 and UV) PET samples after two week inoculation in HPP, YSV and M9 minimal medium and <i>I. sakaiensis</i> culture at 30 °C.	85
Table 3.3. Transmittance percentages of non-treated and treated (NaOH, DTAB, Brij-35 and UV) PET samples after three weeks inoculation in HPP, YSV and M9 minimal medium and <i>I. sakaiensis</i> culture at 30 °C.	86
Table 3.4. Transmittance percentages of non-treated and treated (NaOH, DTAB, Brij-35 and UV) PET samples after one week inoculation in HPP, YSV and M9 minimal medium and <i>P. mendocina</i> culture at 30 °C.	93
Table 4.1. Functional groups of PET and the related wavenumber	133

Acknowledgement

Firstly, I would like to express my sincere gratitude to my Director of Studies, Prof. Tajalli Keshavarz for his valuable guidance, unwavering support, and insightful feedback throughout the journey of completing this doctoral thesis. His profound insights into research and life have opened a new perspective for me, and it was an honour to be part of his team. I am also wanting to thank you Dr. Godfrey, my second supervisor, for his valuable feedback and encouragement.

I am also grateful for technical team, especially Thakor Tandel and Vanita Amin for their kind support.

I am also deeply thankful to the members of our research laboratory. Their discussions, and collaborative spirit have created an enriching environment for learning and exploration.

I am extremely grateful to my close friends, Dr. Zeynab Moinipoor, Dr. Ghazal Hatamifard and Dr. Samane Faramehr for their all advice, support and camaraderie through my most challenging journey.

My heartfelt thanks go to my family for their unconditional love and endless encouragement. Their belief in my abilities has been a driving force behind every milestone achieved during my PhD.

Declaration

I, Seyedehazita Ahmaditabatabaei, declare that the work presented in this thesis is my own and was carried out in accordance with the guidelines and regulations of the University of Westminster. I confirm where information has been obtained from other sources, it is indicated in this thesis.

Seyedehazita Ahmaditabatabaei September 2023

List of Abbreviations

• AHLs	Acyl homoserine lactones
• ANOVA	Analysis of variance
• Asp	Aspartate
• ATR	Attenuated total reflectance
• BHET	Bis (2-hydroxyethyl) terephthalate
• BPA	Bisphenol A
• °C	Degree Celsius
• Δ	Delta
• DNA	Deoxyribonucleic acid
• DMSO	Dimethyl sulfoxide
• Brij-35	Dodecylpolyethylene oxide-23 ether
• DTAB	Dodecyl trimethylammonium Bromide
• t_d	Doubling time
• <i>E. Coli</i>	<i>Escherichia coli</i>
• EG	Ethylene glycol
• EPS	Extracellular polymeric substances
• FTIR	Fourier transform infrared spectroscopy
• <i>F. asiaticum</i>	<i>Fusarium asiaticum</i>
• <i>F. culmorum</i>	<i>Fusarium culmorum</i>
• FSC	<i>Fusarium culmorum</i> supernatant containing cutinase
• <i>F. graminearum</i>	<i>Fusarium graminearum</i>
• <i>F. oxysporum</i>	<i>Fusarium oxysporum</i>
• <i>F. solani</i>	<i>Fusarium solani</i>
• G	Generation time
• r	Growth rate
• HDPE	High-Density Polyethylene
• HPLC	High-performance liquid chromatography
• HPP	Hipolypeptone
• His	Histidine
• hrs	Hours
• <i>H. insolens</i>	<i>Humicola insolens</i>
• HFB	Hydrophobins
• <i>I. sakaiensis</i>	<i>Ideonella sakaiensis</i> 201-F6
• IR	Infrared
• LDPE	Low-Density Polyethylene
• μ_{max}	Maximum specific growth rate
• μ	Micro
• μm	Micrometre
• MHET	Monohydroxyethyl terephthalate
• MHETase	Monohydroxyethyl terephthalate hydrolase
• mAU	Milli absorbance unit
• ml	Millilitre

• mM	Mili Molar
• min	Minute
• nm	Nanometre
• $N_{(0)}$	Number of cells at time 0
• $N_{(t)}$	Number of cells at time t
• n	Number of generations
• NA	Nutrient agar
• NB	Nutrient broth
• OD	Optical density
• PBS	Phosphate buffer saline
• PAHs	Polyaromatic hydrocarbons
• PBS	Polybutylene succinate
• PC	Polycarbonate
• PCBs	Polychlorinated biphenyls
• PE	Polyethylene
• PET	Polyethylene Terephthalate
• PETase	Polyethylene Terephthalate hydrolase
• PHEs	Polyethylene Terephthalate hydrolytic enzymes
• PHAs	Polyhydroxyalkanoates
• PLA	Polylactic acid
• PP	Polypropylene
• PS	Polystyrene
• PVAc	Polyvinyl acetate
• PVA	Polyvinyl alcohol
• PVC	Polyvinyl chloride
• pNPB	P-nitrophenyl butyrate
• pNPP	P-nitrophenyl palmitate
• PDA	Potato dextrose agar
• PDB	Potato dextrose broth
• <i>P. mendocina</i>	<i>Pseudomonas mendocina</i>
• QS	Quorum sensing
• QSM	Quorum sensing molecules
• K	Rate constant
• Rpm	Revolutions per minute
• RNA	Ribonucleic acid
• SEM	Scanning electron microscopy
• Ser	Serine
• SUPs	Single-use plastics
• SPI	Society of the Plastic Industry
• SDS	Sodium dodecyl sulfate or sodium lauryl sulfate
• NaOH	Sodium hydroxide
• TDOC	Sodium taurodeoxycholate
• TPA	Terephthalic acid
• t	Time
• Tg	Transition temperature

- TCA cycle
 - Surfactants
 - UV
 - *V. fischeri*
 - YSV
- Tricarboxylic acid cycle
Surface active agents
Ultraviolet
Vibrio fischeri
Yeast extract sodium carbonate and vitamins

Chapter 1. Introduction

1. Introduction

Today, plastic pollution of land and oceans is one of the main concerns of scientists and the public. The majority of plastics are mineral-based and non-biodegradable. Besides, plastics are mostly single use, and they are disposed after a short time of usage. Examples of single-use plastics (SUPs) are plastic bottles, plastic bags, and plastic packaging. Between 1950 and 2018, production of these plastics increased from 2 million tonnes to 360 million metric tonnes worldwide (PlasticsEurope, 2019). The growth trend of SUPs is shown in figure 1.1. Since, the end of 1900s the popularity of plastic has come to scrutiny due to the concerns about the plastics waste that are being accumulated in the landfills, and in the oceans through the spread of smaller pieces of plastic (Geyer et al., 2017).

These small pieces of plastics, called micro plastics (< 5mm), are the prominent threat for the ocean and the soil. Around 8 million tons plastics end up in the oceans every year. This plastic waste enters the life cycle of sea animals and eventually humans. Besides, micro plastics leaked to the soil enter the food cycle of animals and finally humans. So, plastic waste is considered as one of the main global pollution problems (Thevenon et al., 2014; Boucher and Friot, 2017).

Consumer products such as packaging bags, bottles, foil and films are mainly made from PET, High-Density Polyethylene (HDPE), and to some extent Low-Density Polyethylene (LDPE). Among these plastic types, degradation of PET is the focus of this project due to the excessive use of single use plastics including beverages bottles, medicine jars, rope and clothing. Moreover, the highest percentage (47 %) of plastics wastes is from packaging (Soong et al., 2022).

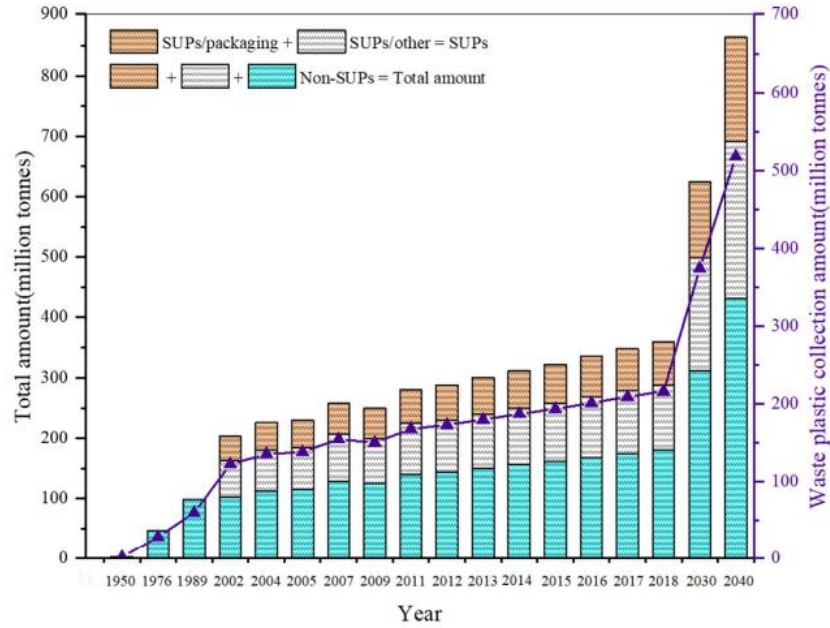


Figure 1.1. Growth trend of single used plastics (SUPs) (Chen et al., 2021).

SUPs/packaging
 SUPs/other,
 Non-SUPs.

Several routes are practised for the treatment of plastics: Disposal (landfill, open-air), incineration, recycling and biodegradation. Biodegradation of plastics is the most environmentally friendly method to degrade the plastics by using both enzymes and microbes. Ideal Plastics, for both consumers and environment, should provide durability during and degradability after their life span. A very small proportion of mainly non-mineral based plastics (approximately 1-5 %) such as polyhydroxyalkanoates (PHAs) and polylactic acid (PLA) are biodegradable. These plastics can be degraded by some microorganism and their enzymes. There are several reports on efficient biodegradation of recalcitrant plastics such as PET, polyethylene (PE), and Polystyrene (PS) (Shah and Hasan, 2008; Mohanan et al., 2020; Zhang et al., 2022). A recent study reports degradation of PET by the Gram-negative bacterium, *Ideonella sakaiensis* 201-F6 (*I. sakaiensis*) (Yoshida et al., 2016; Yoshida et al., 2021). However, this process is time-consuming with low efficiency, and at present, inefficient.

1.1. Plastics structure and degradation

Plastics are made from raw organic or inorganic materials such as carbon-silicon, hydrogen, nitrogen, oxygen and chlorine. There are mainly seven varieties of non-degradable plastics: PET, HDPE, LDPE, Polypropylene (PP), PS, Polyvinyl chloride

(PVC), and other plastics such as nylons and polycarbonate (Shimao, 2001; Shah and Hasan, 2008). These plastics also known as single used plastics.

Plastics can be divided into two groups of biological and synthetics. Biological plastics are produced from microorganisms. For example, PHAs and PLA are biological plastics. Synthetic plastics such as PET, PVC, PS, PE, polyvinyl alcohol (PVA) and polybutylene succinate (PBS) are produced from minerals such as crude oil (Scott and Wiles, 2001; Shah and Hasan, 2008; Hassan et al., 2022).

Plastics are categorized under different classification. Table 1.1 illustrates the classification offered by The Society of the Plastic Industry (SPI) in 1988. According to this classification, one code is allocated to every seven main types of plastics. Plastics with code 2, 4 and 5 are less harmful than the others (Mariotti et al., 2019).

The first code is related to PET. This type of plastic has high heat and solvent resistance. It is hard and tough. PET is harmful as it leaks antimony trioxide and phthalates, which both are serious dangers to health (Hurd, 2014). Second code is allocated to HDPE. This group is much safer, and it does not release chemicals into the packaged foods. It is used mostly for the milk bottles, shampoo containers and bleach ware. Third code is related to PVC. This group is used in pipes and tiles. This type is very harmful as it can release toxic chemicals such as phthalates, mercury, and dioxins, and cannot be used as a food container (Cao et al., 2016; Hassan et al., 2022). Fourth code is LDPE. This type is durable and flexible. LDPE can be used for cling film, sandwich bags and grocery bags as it is known as the healthy plastic. However, it can release estrogenic chemicals specifically under sunlight. Fifth code is allocated to PP which is strong and has a high melting point. It can be used for lunch boxes and yogurt pots. It can release plastic additives such as Bisphenol A (BPA) and phthalates which are toxic to environment and general population (Eyerer, 2010). Sixth code is related to PS. Egg cartons, food containers and medicine bottles are some examples of this type of plastic. It can release styrene which affects the immune system, liver and lungs. The seventh category is related to other plastics such as polycarbonate (PC) which are used for baby bottles. It can leach bisphenol A (BPA) which affects neurological and cardiovascular health (Proshad et al., 2018).

This classification with some other general properties and applications of plastics are shown in table 1.1. Also, table 1.2 shows the molecular structure and molecular weight of some plastics.

Table 1.1. Some general properties and applications of common plastics (Mariotti et al., 2019)








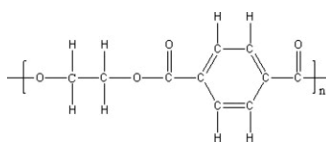
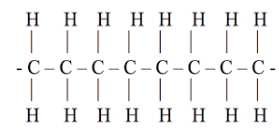
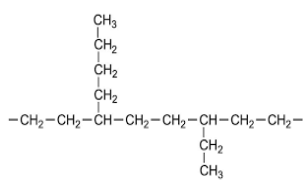
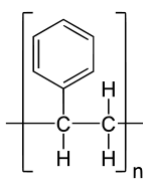
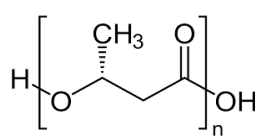
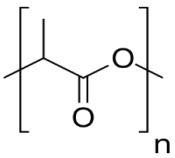
<i>Symbol</i>	<i>Type of Plastics</i>	<i>Main Use</i>
	Polyethylene Terephthalate (PET)	PET is used for containers for foods and liquid, soft drink bottles, fibers for clothing.
	High Density Polyethylene (HDPE)	HDPE is used for bottles, piping for water and sewer, milk jugs, detergent bottles, nursery pots, oil containers, snowboards, boats and chairs
	Polyvinyl Chloride (PVC)	PVC (or vinyl) is common for products such as plumbing products, medical tubing, pressure pipes, electrical cable insulation, outdoor furniture, liquid detergent containers, etc.
	Low Density Polyethylene	This polyethylene is ductile and, thus, used for shopping bags, food containers, films or bags and stretch wrap
	Polypropylene (PP)	PP is a thermoplastic polymer and one of the worldwide most common used plastic. It is used for laboratory equipment, automotive parts, medical devices, etc.
	Polystyrene (PS)	PS is commonly used for yoghurt pots, foodservice containers, CD cases, envelope windows, video cassettes, appliance housings as televisions.
	Other types of plastics	Various usages.

Table 1.2. Some features of PET, HDPE, LDPE, PS, PHAs and PLAs

Name of Polymer	Molecular weight per repetitive unit (g/mol)	Solubility	Molecular formula	Structure
PET	192	Insoluble	$C_{10}H_8O_4$	
HDPE	28	Insoluble	C_2H_4	
LDPE	28	Insoluble	C_2H_4	
PS	104	Insoluble	$(C_8H_8)_n$	
PHAs	71	Low permeation of water	$C_3H_3O_2$	
PLAs	16	Insoluble	$(C_3H_4O_2)_n$	

1.1.1. Plastic disposal

In 2015, 79% of plastics was discarded, 12% incinerated, and 9% recycled worldwide. Each of these methods has serious drawbacks (Geyer et al., 2017).

1.1.1.1. Landfill

The landfill is the most common and oldest method used for disposal of the waste materials where the waste accumulates. In the landfilling process, the degradation occurs mainly by microorganisms. This process is very slow. For some materials such as plastics that have the high durability the biodegradation time is very long, approximately 10-100 years. The landfill process starts in open dumps (Peirce et al., 1997).

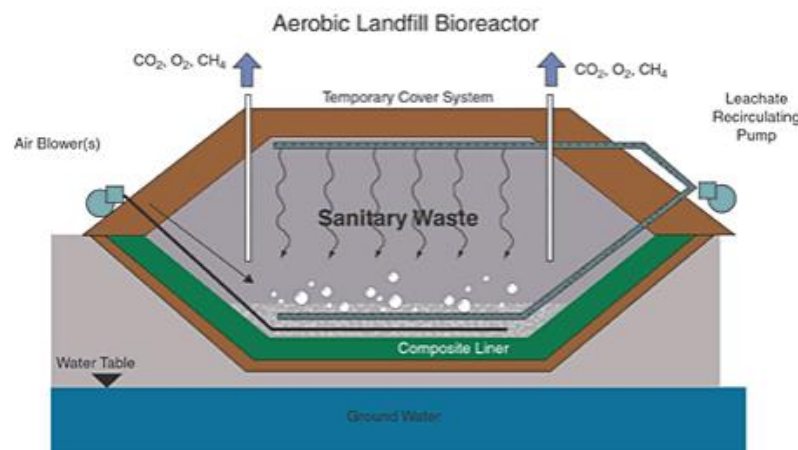


Figure 1.2. Sanitary landfilling (Aziz et al., 2013)

In this process, the waste just accumulates on the landfill site. However, another method called sanitary landfill is used to dispose off the waste materials more efficiently (Fig 1.2). This engineered operation improves disposal standards too. In this method the waste materials are collected in excavated earth lined with plastic (PVC) and covered with the soil. This method has some drawbacks such as emission of toxic leachate. Also, the risk of consumption of plastics by wild animals increases. In addition, the leachate can affect the fertility of soil. Furthermore, due to the lack of bioavailability, degradation of the plastics chemical structure is a serious drawback (Peirce et al., 1997; Pereira et al., 2017).

1.1.1.2. Incineration

Another waste treatment process is incineration. In this method, very high temperature (850 °C) is used to burn waste materials ending in ash, flue gases and heat. This process

is divided into five steps. At first, the waste is stored. Then, it is burnt in the furnace at a high temperature. During this step, hot gases and ash residues are produced. The next step involves gas temperature reduction. Then the pollutants such as methane and carbon dioxide are removed from the cooled gas and the residues are disposed of. Finally, clean gas disperses (National Research Council, 2000). However, the problem with this method is that the combustion of the waste materials is energy-consuming. Besides, incineration of plastics releases toxic compounds such as dioxins, furans, mercury and polychlorinated biphenyls into the air, affecting air quality, resulting in respiratory diseases and potentially cancer. Also, the leftover of this process, the ash, contains hazardous material such as Polyaromatic hydrocarbons (PAHs), Polychlorinated biphenyls (PCBs), toxic carbon and benzene (Mihucz et al., 2016).

1.1.1.3. Recycling

Recycling is one of the most prominent methods to tackle plastic waste. Recycling is the process during which the material at the end of its life cycle is processed back to the consumption phase (Fig 1.3). Plastics have lower percentage of recycling among the other waste materials such as papers, glasses and steel. This lower percentage is due to the differences in the characteristics of plastics, and the additives in their structure (Webb et al., 2013; Worrell and Reuter, 2014).

Most plastics are recycled mechanically. However, some plastics such as thermosets (e.g. silicone and epoxy) cannot be recycled in this way as they make some cross links in their structure once heated and retain their strength. So, other methods such as chemical recycling (such as depolymerisation) are needed. Chemical recycling has been used for most plastics including PET (Aguado and Serrano, 1999; Aziz., 2021). Mechanical recycling is divided into four steps. Firstly, the collected materials are sorting out based on plastic types. Secondly, the sorted materials are shredded. Then, they are washed and dried. Finally, they are melted and reprocessed to be used again as products (Shen et al., 2010). In chemical recycling, the polymers are broken down to their monomers by using depolymerisation techniques. The mechanical recycling is much more cost-effective than chemical recycling. The advantage of chemical recycling compared with the mechanical one is that the quality of virgin polymer can be maintained. The chemical technologies that are used at commercial scale are glycolysis, methanolysis and alkaline hydrolysis. However, these methods are very costly and cannot be used to recycle the plastics at the end of their life cycle. While the recycling of the plastics is a plausible route, only 9% of 5800 m tonnes of primary

plastics, accumulated since 1950, have been recycled. As different plastics have different molecular structure, there is no single recycling procedure. However, in general, depolymerization occurs during the chemical route (Shen et al., 2011; Moges et al., 2022).

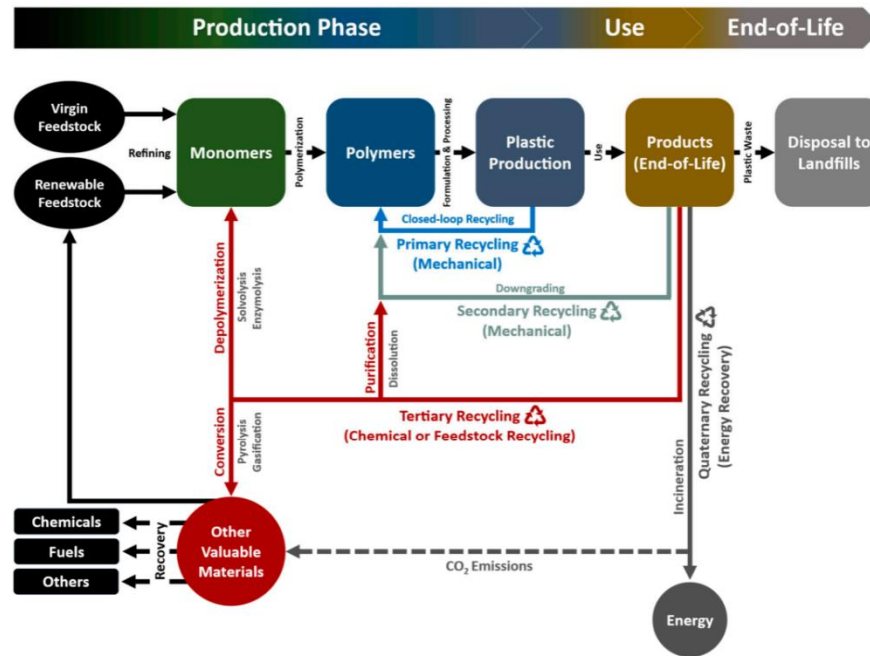


Figure 1.3. Polymer recycling process (Soong et al., 2022).

1.1.2. Degradation of plastics

Another approach to deal with plastic waste is degradation of the plastics. Treatment of plastics to degrade them can be categorized into three main groups including mechanical, chemical and biological treatment.

1.1.2.1. Mechanical degradation

Different modes of mechanical treatment are grinding to reduce the size of particles, ultraviolet (UV) treatment and photo-oxidative degradation. The mechanical treatment methods have the drawback that they cannot completely degrade the plastics waste (Grassie and Scott, 1985; Gilan et al., 2004).

1.1.2.2. Chemical degradation

Chemical treatment is the usage of chemical interactions to break down the polymer molecules to their monomers. The main problem is the disposal of the chemicals that are used for the degradation (Lin and Yang, 2009; Al-Salem et al., 2009).

1.1.2.3. Biological degradation

The biodegradable plastics have the sensitivity to the microbial attack. Microbial degradation of plastics by bacteria, fungi and algae has been reported (Gu et al., 2000). For example, *I. sakaiensis* and *Pestalotiopsis microspora* are used for degradation of PET. *Rhodococcus*, *Enterococcus faecalis*, *Pseudomonas putida* and *Salmonella* are used for PS degradation. *Bacillus sp.*, *Gracilibacillus sp.*, *Pseudomonas stutzeri* and *Aspergillus oryzae* (*A. oryzae*) can degrade PHAs (Ghosh et al., 2013; Meereboer et al., 2020).

These microorganisms attack the polymers and break them down to their oligomers and monomers. Biodegradation is verified by loss of polymer weight, carbon dioxide production and change in tensile strength, dimension, chemical and physical properties and molecular weight distribution of the polymer. Biodegradation process can be affected by methods that the polymer was synthesised, presence of the additives in the polymers' structure, effects of substituents, effects of stress and environmental conditions. Also, chemical bonding, polymer composition, molecular weight, hydrophobic character and size of the polymer molecules can affect the process (Dussud and Ghiglione, 2014).

Currently, abiotic non-biological hydrolysis is the most prevalent and important initial reaction that leads to degradation, followed by the enzymatic or microbial degradation. Biodegradation process can be divided into four steps including biodeterioration, depolymerisation, assimilation and mineralisation. Biodeterioration of plastics is the process in which microorganisms, and abiotic factors' activities such as mechanical, light, thermal and chemical degradation lead to tiny plastic fractions. Depolymerisation or bio-fragmentation is the next stage. In this step, microorganisms secrete the catalytic agents (enzymes and free radicals) that break down the material to the monomers. Depolymerisation can happen through the action of physical forces such as heating/cooling, freezing/thawing, wetting/drying, or biological forces such as the growth of microbes or by microbial enzymes. Assimilation is the process that the transported molecules of plastic integrate into the microbial metabolism to produce energy. Mineralisation is the last stage during which the plastic monomers are converted to the minerals such as nitrogen, methane, carbon dioxide and water (Fig 1.4) (Singh and Sharma, 2008; Dussud and Ghiglione, 2014; Pathak and Navneet, 2017; Gong; 2018).

Polymer degradation occurs through four different mechanisms: solubilisation, ionisation, hydrolysis and enzyme catalysed degradation.

The percentage of solubility of polymers depends on their hydrophilicity. Hydration is caused by disruption in secondary and tertiary structures of polymers. These structures bind with van der Waals forces and hydrogen bonds. During the hydration process polymers become water soluble and they lose their strength. Plastics are hydrophobic and for degrading them bio-surfactants are used to enhance the solubility of their surface (Ishigaki et al., 1999).

Another mechanism is ionisation. Some polymers that are insoluble in water can be degraded by ionisation or protonation of pendent groups. For example, polyacids become hydrophilic at high pH (Chambliss, 1983). The next mechanism is hydrolysis. Some polymers containing pendent anhydride or ester groups are insoluble in water. They can become soluble by hydrolysing these pendent groups to form ionised acids on the polymer chain. Poly acrylic acid and poly methacrylic acid are examples of these types of polymers that become soluble by hydrolysing their ester groups. The chemical structure of polymers and their molecular weight affect the hydrolysis process (Murphy et al., 1986).

The last but not the least mechanism is enzyme catalysed degradation. Enzymes play a critical role as catalysts in many reactions such as oxidation, reduction, hydrolysis, esterification and molecular inter-conversions. Enzymes can enhance assimilation by microorganisms of hydrophobic polymers which are highly stable such as PE, PP and PS. For example, previous studies show that lipase can catalyse degradation of poly vinyl acetate (PVAc) where its ester bonds are broken (Singh and Sharma, 2008).

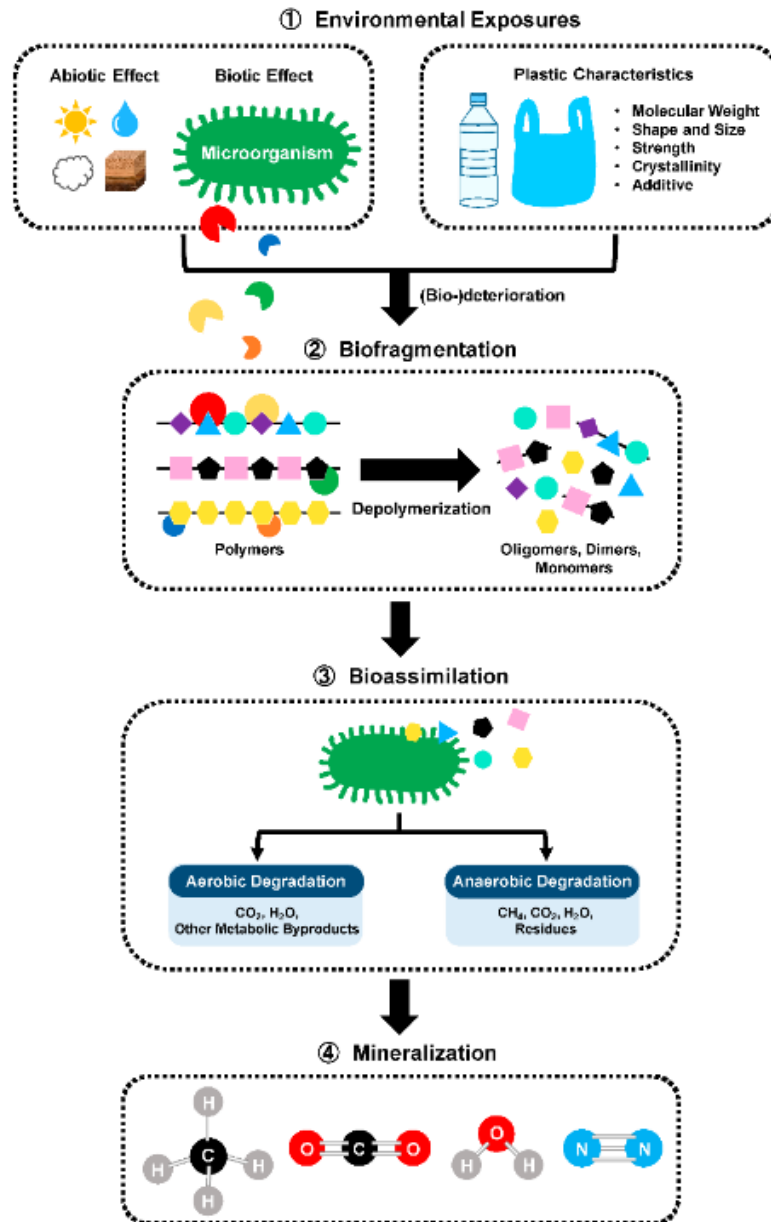


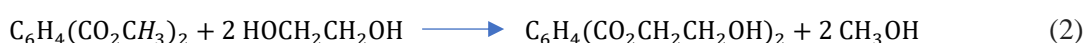
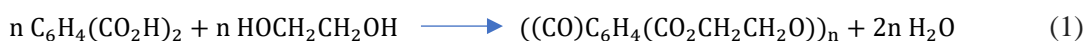
Figure 1.4. Schematic biodegradation process.
 1) environmental exposure, 2) biofragmentation, 3) bioassimilation, 4) mineralization (Soong et al., 2022).

1.2. Polyethylene terephthalate

Using PET started in the 1940s by DuPont in the manufacturing of textile fibres. PET's use as bottle, jars and beverages containers began in 1973. Since the 1980s, they have been used as disposable bottles. The waste from this polymer reached 55 million tons in 2015. PET contains 8 % of the weight and 12 % of the volume of the world solid waste. Its lightweight, low coefficient of friction, flexibility, high durability and low market price makes it a top candidate in the daily usage. As PET is transparent and shatterproof, it is used for manufacturing of polymer films. This polymer is highly used in packaging too (McIntyre, 2004; Taniguchi et al., 2019).

PET is derived from crude oil. It is the most common thermoplastic polymer in the polyester family. PET monomer repeating unit is $C_{10}H_8O_4$. This polymer is present in both amorphous and semi-crystalline structure, and it has high yield strength of around 40 MPa and tensile strength of around 170 MPa. Its intrinsic viscosity is its prominent characteristic. The longer is the polymer chain, the higher is the viscosity. Upon heating, PET's resilience decreases as the absorbed water hydrolyses it. Currently, the most common degradation of PET is by hydrolytic and thermal oxidation (Vegt and Govaert, 2005).

The monomer bis(2-hydroxyethyl) terephthalate (BHET) can be synthesised by the esterification reaction between terephthalic acid (TPA) and ethylene glycol (EG). In this reaction, the by-product is water as equation 1 shows. The esterification (condensation) process begins by interaction between alcohol and acid. The alcohol loses the H bond, and the acid loses its O-H and ester is formed. Binding of H and O-H forms water. Another route to synthesis of the ester is transesterification reaction between EG and dimethyl terephthalate (DMT) which produces methanol as their by-product (Reimschuessel, 1980).



Previously recycling was one of the common routes to modulate the waste from post-consumer PET. The recycling process has been encouraged due to resistance of PET to biodegradation. However, the amount of available PET to recycle is much higher than recycling capacity. Another type of disposal of PET is incineration which emits high amount of carbon dioxide. So, attention has focused on the biodegradation process as a green approach to the environment.

Some processes can break down PET into smaller pieces. These include drying, heating, mechanical pressure, thawing and freezing. After converting PET to smaller pieces, degradation can be facilitated by photo-degradation with UV light and thermo-oxidative process for the enzymes to adhere to the polymer. PET's ester bonds can be broken by esterase enzyme which changes the wettability and hydrophobicity of the surface of the PET (Pospisil and Nespurek, 1997).

PET, due to its hydrocarbon bonds and ester groups, has a high resistance to degradation. The hydrocarbon bonds have resistance to degradation by bacteria due to the lack of water in their structure. The high ratio of aromatic terephthalate units reduces chain mobility, which leads to a reduction in degradation. This also reduces the hydrolysis of the esters. Besides, as the crystallinity of the polymer increases, it becomes more difficult for microorganisms to attack the polymer. In addition to functional groups in the backbone of the polymer, the crystallinity, surface hydrophobicity and chain mobility affects their resistance to degradation by microorganisms (Tokiwa, 2009; Wei and Zimmermann, 2017). The pretreatment of PET can be through the use of acid, alkaline, temperature and UV to enhance the subsequent degradation process. The rate of degradation is measured by visual observation, weight loss, changes in mechanical properties, carbon dioxide evolution/oxygen consumption, scanning electron microscopy (SEM), Fourier transform infrared spectroscopy (FTIR), clear-zone formation, pigment production, enzyme assay and biofilm formation (Shah and Hassan, 2008).

PET hydrolytic enzymes (PHEs) including cutinases that can hydrolyse the cutin, the lipases and a few esterases. However, these enzymes have limited degradation effect on PET. Some examples of microorganisms that can degrade PET include filamentous fungi such as *Fusarium oxysporum* (*F. oxysporum*) and *Fusarium solani* (*F. solani*). However, they cannot degrade PET completely; they only modify its surface for better degradation (Wei and Zimmermann, 2017).

Recently, a new bacterium isolated from the soil, *I. sakaiensis* has shown promise for PET degradation. It can provide PET hydrolytic enzymes PETase and MHETase. Both enzymes act in their specific roles, with PETase being responsible for hydrolytic conversion of PET into oligomers that include MHET as their main component, and MHETase further hydrolyses MHET into PET monomers, TPA, and EG (Yoshida et al., 2016) (Fig 1.5).

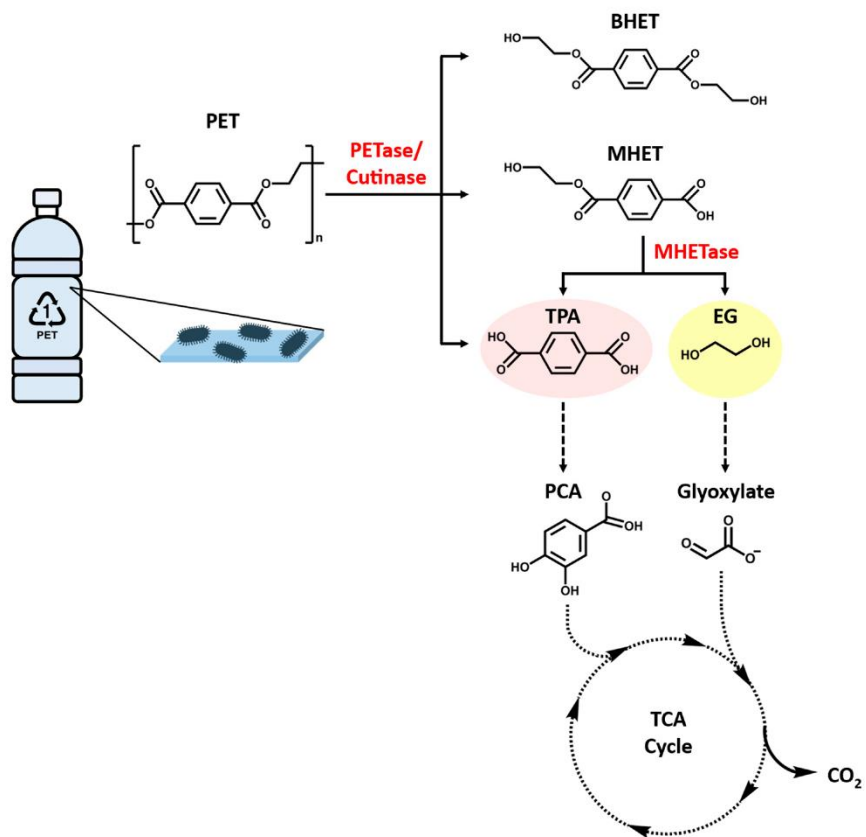


Figure 1.5. Microbial degradation of PET.

PETase and MHETase using to convert PET to its monomers including TPA and EG (Soong et al., 2022).

1.3. *Ideonella sakaiensis* (*I. sakaiensis*)

1.3.1. Classification

I. sakaiensis was isolated from soil in a microbial consortium in Japan. This bacterium comes from *Proteobacteria* phylum, *Betaproteobacteria* class, *Burkholderiales* order, *Comamonadaceae* family, *Ideonella* genus and *I. sakaiensis* species (Yoshida et al., 2016).

1.3.2. Morphology and Physiology

I. sakaiensis is a Gram-negative (Fig 1.6 (a)), aerobic, non-spore forming and rod-shaped bacterium. *I. sakaiensis* grows at 15-42 °C (optimally 30-37 °C) and the pH range 5.5- 9 (optimally 7-7.5). The cell length is 1.2- 1.5 µm and the cell width is 0.6- 0.8 µm. It is motile by monotrichous polar flagellum as can be seen by transmission electron micrograph (Fig 1.6 (b)). The incubation period for this bacterium is two days on agar. *I. sakaiensis*' colonies are circular, smooth and non-pigmented. Their colony size is 0.5-1 mm after two days of incubation at 30 °C (Yoshida et al., 2016). *I. sakaiensis* is established as a microorganism of choice for biodegradation of PET. It can use PET as the main carbon and energy source for its growth.

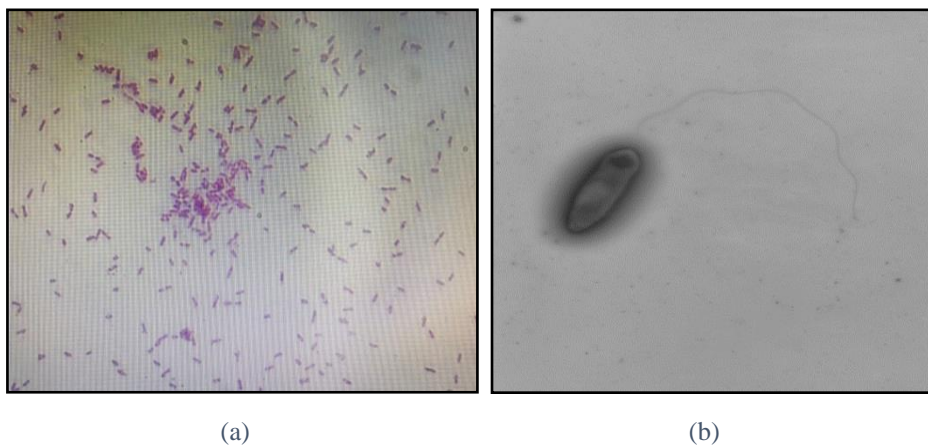


Figure 1.6. *I. sakaiensis* microscopy.

(a) *I. sakaiensis* microscopy $\times 100$ magnification, (b) Transmission electron micrograph of *I. sakaiensis* (Yoshida et al., 2016).

1.4. *Pseudomonas mendocina* (*P. mendocina*)

1.4.1. Classification

P. mendocina isolated by N. J. Palleroni in 1969. This bacterium was isolated from water and soil in the province of Mendoza, Argentina. This bacterium belongs to *Proteobacteria* phylum, *Gammaproteobacteria* class, *Pseudomonadales* order, *Pseudomonadaceae* family, *Pseudomonas* genus and *P. mendocina* species (Palleroni et al., 1970; Kao et al., 2005).

1.4.2. Morphology

P. mendocina is a G-negative, aerobic, polar monotrichous flagellated and rod-shaped bacterium. *P. mendocina* can grow in temperatures ranging from 25 °C to 42 °C (optimally 30 °C). The optimal pH for this strain is 6. The colonies of this bacterium are flat, smooth, smelly and brownish yellow in colour. The cell length is 1.4-2.8 µm and the cell width is 0.75-0.85 µm. A typical medium used for the cultivation of this strain is nutrient broth (NB) (Palleroni et al., 1970; Kao et al., 2005).

1.5. *Fusarium* species

Fusarium asiaticum (*F. asiaticum*), *Fusarium culmorum* (*F. culmorum*) and *Fusarium graminearum* (*F. graminearum*) are fungal plant pathogens (Fig 1.7, a-c). These fungi come from *Ascomycota* division, *Sordariomycetes* class, *Hypoceales* order, *Nectriaceae* family and *Fusarium* genus (Schmidt-Heydt et al., 2010; Iwahashi, 2018).

1.5.1. Morphology

F. asiaticum grows at 25-30 °C. *F. culmorum* grows at 25-33 °C (optimally 30 °C). *F. graminearum* grows at 25-35 °C (optimally 25 °C). Colonies of these fungi are coloured yellowish-brown to reddish-brown. The macroconidia are short, wide and slightly curved. The medium that is used for the cultivation of all of them is potato dextrose agar (PDA) and potato dextrose broth (PDB). The incubation period for this bacterium is 7 days on agar (Schmidt-Heydt et al., 2010; Iwahashi, 2018).

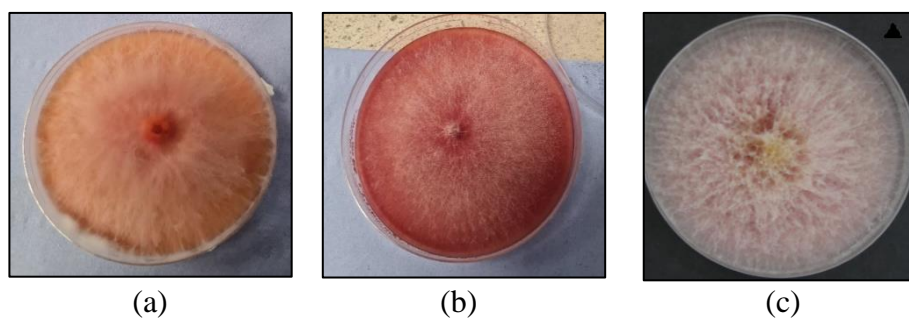


Figure 1.7. *Fusarium* species a) *F. asiaticum*, b) *F. culmorum*, c) *F. graminearum*.

1.6. Doubling time calculations

The growth process can be interpreted by using growth curve of bacteria which represents the number of cells over time. Each division cycle which during that each cell is transferred to two cells is called generation. The number of bacteria after passing some generations can be obtained through equation (3). In which $N_{(t)}$ is the number of cells at time t , $N_{(0)}$ is the number of cells at time 0 and n is the number of generations (Stanbury et al., 1995; Wang et al., 1979).

$$N_{(t)} = N_{(0)} \times 2^n \quad (3)$$

The generation time is the time takes by the cells to pass one generation cycle. Each cell division occurs in the same time interval. This time can be calculated by equation (4). In which G is the generation time, n is the number of generations and t is time (Stanbury et al., 1995; Wang et al., 1979).

$$G = \frac{t}{n} \quad (4)$$

The generation time depends on many conditions such as oxygen, light, pH, temperature and the nature of the species. For example, one of the fast-growing bacteria called *Clostridium perfringens* has the optimum generation time of 10 minutes. *Escherichia coli* (*E. Coli*) can double every 20 minutes and numbers become over 1,000,000 under 7 hrs. The *Mycobacterium tuberculosis* generation time is 12 to 16 hrs which means its growth rate is slow. Additional factors such as osmotic pressure and atmospheric pressure also can affect the generation time (Stanbury et al., 1995; Wang et al., 1979).

Other relevant terminologies are growth rate and doubling time. Growth rate refers to the growth increase by the number of cells. It can be calculated using equation (5). In which “ r ” is the growth rate, “ t ” is time, $N_{(t)}$ is the number of cells at time t and $N_{(0)}$ is the number of cells at time 0 (Stanbury et al., 1995; Wang et al., 1979).

$$r = \frac{\ln(N_{(t)}/N_{(0)})}{t} \quad (5)$$

Doubling time is the time that takes for the number of the cells to double. Equation (6) which derived by equation (5) presents the doubling time.

$$t = \frac{\ln(2)}{r} \quad (6)$$

A simplified growth curve has 4 phases that can be categorised as lag phase, log phase, stationary phase and death phase (Stanbury et al., 1995).

1.7. Pre-treatment approaches for PET degradation

Physicochemical pre-treatments play a prominent role in biodegradation of plastics such as PET. PET, due to its durability can remain in environment for a longer period of time (over 400 years) without treatment (Falkenstein et al., 2020). Pre-treatments can alter the hydrophobicity, surface morphology and crystallinity of PET by exposing the oxygen to the surface of the PET (Falkenstein et al., 2020). So, germane pre-treatment methods can play an important role in efficient biodegradation of PET. In this project, three methods (Sodium hydroxide (NaOH), surfactants (Dodecyl trimethylammonium Bromide (DTAB) and Dodecylpolyethylene oxide-23 ether (Brij-35)) and UV are investigated for pre-treatment of PET.

1.7.1. Sodium hydroxide (NaOH) pre-treatment

Chemical pre-treatments such as NaOH can be used for PET treatment. Several studies show the effect of NaOH treatment on PET. However, due to high temperature that is required during the reaction this process is costly (Rahman et al, 2009; Ügdüler et al., 2020). Also, the NaOH is a hazardous material, and it can produce toxic pollutants. During the pre-treatment process NaOH affect the ester bonds and cleave them to make the disodium terephthalate and EG (Bhogle and Pandit, 2018) (Fig 1.8).

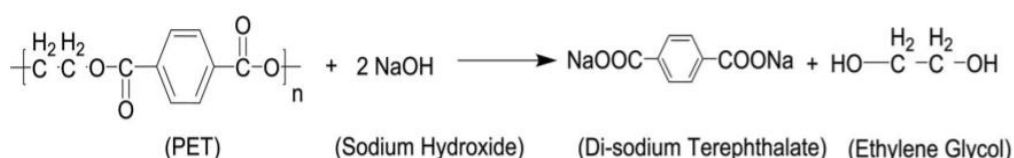


Figure 1.8. Chemical hydrolysis of PET with alkaline solution (Bhogle and Pandit, 2018).

1.7.2. UV light pre-treatment

Using the UV light (100-380 nm) can lead to photodegradation of polyolefins by generating free radicals and enhancing the microbial degradation (Fechinec et al., 2004; Ammala et al., 2011; Falkenstein et al., 2020).

Structural changes of PET have been studied by Fechine et al., 2002. The structural change on the surface of the PET causes a decrease in molecular weight and an increase in the carbonyl and O-H group. When UV radiates to the PET, chain scission occurs

through two reactions: Norrish type I and type II (Fig 1.9). In Norrish I reaction, the free radicals are generated during ester bond cleavage. In Norrish II reaction, intramolecular rearrangement occurs where a hydrogen atom is abstracted as a result of photolysis.

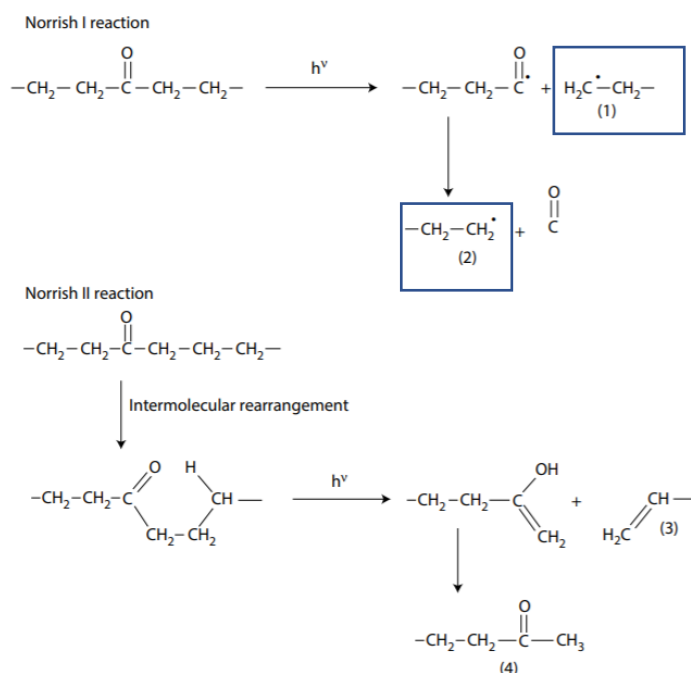


Figure 1.9. Norrish I and II reactions.

(1) and (2) free radical formation (blue boxes), (3) terminal double bond compound, (4) methyl ketone compound. (Devi et al., 2016).

1.7.3. Surfactant

1.7.3.1. Surfactant types

The word surfactant is an abbreviation for **surface active agents**. Surfactants play a prominent role in production of detergents, paints, paper products, pharmaceuticals and cosmetics. The Surfactants are the amphiphilic molecules which have both hydrophilic and hydrophobic segments in their molecular structure. This property can help in biodegradation through surface modification of plastics. The hydrophobic part of the surfactant can attach to the surface of the plastic while the hydrophilic part attaches to the water. The figure below (Fig. 1.10) shows the molecular structure of the ammonium lauryl sulfate surfactant and its hydrophilic and hydrophobic parts as an example (Dave and Joshi, 2017; Badmus et al., 2021).

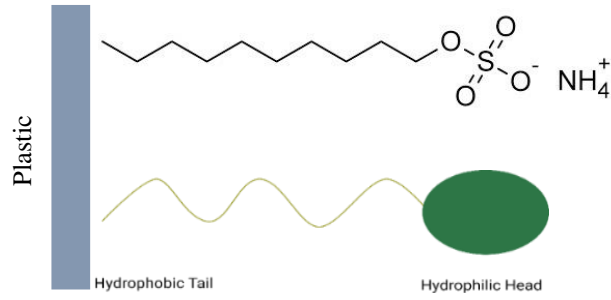


Figure 1.10. Chemical structure of an anionic surfactant, ammonium lauryl sulfate (National Center for Biotechnology Information, 2021).

Surfactants are categorized into four groups including non-ionic, anionic, cationic and amphoteric based on their charge at the hydrophilic portion of their structure (Fig 1.11).

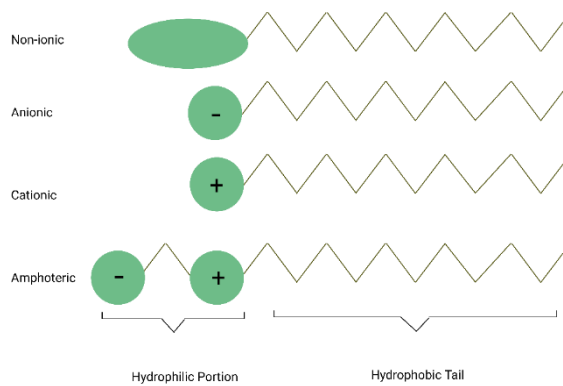


Figure 1.11. Surfactant categories based on their charge at the hydrophilic portion. (Created by Biorender.com)

1.7.3.1.1. Non-ionic surfactants

Non-ionic surfactants are neutral in terms of charge and do not have any charge at the hydrophilic end of their structure. The hydrophilic group in these surfactants can be alcohol, phenol, ether, ester or amide (Tiwari et al., 2018). Example of this type of surfactant are Dodecylpolyethylene oxide-23 ether and Triton X-100.

1.7.3.1.1.1. Dodecylpolyethylene oxide-23 ether (Brij 35)

In the current project Brij-35 was used for pre-treatment of PET. Brij-35 is the commercial name for the dodecylpolyethylene oxide-23 ether with the molecular formula of $\text{CH}_3(\text{CH}_2)_{11}(\text{OCH}_2\text{CH}_2)_{23}\text{OH}$ (Tomšič et al., 2004) (Fig 1.12).

This surfactant is categorized as a non-ionic group of surfactants based on the charge of its hydrophilic head. The number 35 in Brij-35 refers to the length of the alkyl chain

and ethylene oxide group. Polyethylene oxide end of the Brij-35 refers to the hydrophilic part of the surfactant and alkyl chain is the hydrophobic part of it. This surfactant is applicable in solubilizing the protein of the membrane and surrounding the hydrophobic part of the substrates in liquid enzyme reactions (Tomsic et al., 2004).

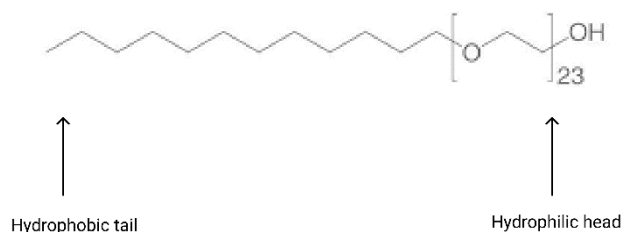


Figure 1.12. Chemical structure of Brij-35 (National Center for Biotechnology Information, 2021).

1.7.3.1.2. Anionic surfactants

Anionic surfactants become negatively charged at the end of the hydrophilic tail when they dissolve in the water. This negative charge leads the surfactant to make the micelle structure much easier. Most of the anionic surfactants contain carboxylate, sulfate and sulfonate ions in their structures. The example of the anionic surfactants are alkyl sulphates, alkyl ethoxylate sulphates and soaps. The main structure of these surfactant is C₁₂-C₁₈ aliphatic group (Tiwari et al., 2018).

1.7.3.1.3. Cationic surfactants

Cationic surfactants have the positive charge at the end of hydrophilic structure in solution. They are known as emulsifying agents, bactericides and antiseptics. These surfactants get attracted to the negatively charge sites (Tiwari et al., 2018;). Example of this type of surfactants are Dodecyl trimethylammonium Bromide and Dimethyl dioctadecylammonium Chloride.

1.7.3.1.3.1. Dodecyl trimethylammonium Bromide (DTAB)

In the current project DTAB used for pre-treatment of PET. This surfactant with the molecular formula of CH₃(CH₂)₁₁N(CH₃)₃Br is categorized as a cationic surfactant based on the charge of its hydrophilic head. Ammonium end of the chain refers to the

hydrophilic part and hydrocarbon chain is the hydrophobic part (National Centre for Biotechnology Information, 2021) (Fig 1.13).

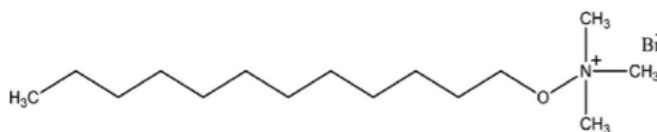


Figure 1.13. Chemical structure of DTAB (National Centre for Biotechnology Information, 2021).

1.7.3.1.4. Amphoteric surfactants

These types of surfactants have dual charge (both positive and negative) at their hydrophilic end. These opposite charges neutralise their effects and create zero charge which is referred to as zwitterionic. The charge of amphoteric surfactants depends on the pH of the solution. In an acidic solution, the charge of the surfactant becomes positive and in an alkaline solution it becomes negative. The positive charge of these surfactants is ammonium, and the negative charge could be carboxylate, sulphate or sulphonate (Tiwari et al., 2018). Example of this type of surfactants are cocoamidpropyl betaine and sodium cocoamphoacetate.

Surfactants can change the hydrophobicity of the microorganism's cell wall by adsorption to the cell wall (Kaczorek et al., 2018). The cells hydrophobicity enhances their ability to interact with hydrophobic surfaces (Obuekwe et al., 2009). The studies show the relation between the cell surface hydrophobicity (CSH) and degradation of hydrocarbons (Obuekwe et al., 2009). Plastics due to their hydrophobic surface have a higher tendency to attach to the hydrophobic molecules. However, for microbial attachment, the more hydrophilic surface desire. This modification makes the surface more hydrophilic and increase the access to the enzyme active site. Two different surfactants were used in this project: DTAB and Brij-35.

1.8. Enzymatic degradation of PET

While there are enzymes known for natural ability to breaking down PET, the rate of degradation they achieve is relatively limited. For instance, enzymes like PETase (Austin et al., 2018), cutinase (Sulaiman et al., 2012; Anbalagan et al., 2022; Din et al., 2023), and lipase (Macedo and Pio, 2005) have been employed to convert BHET into MHET through hydrolysis. *I. sakaiensis* secretes two enzymes that have similar structure to cutinases. They both have α/β hydrolase fold that can attack ester bonds.

PETase is an extracellular enzyme and MHETase is an intracellular enzyme (Yoshida et al., 2016; Falkenstein et al., 2020).

MHET can then be further enzymatically decomposed into TPA and EG using MHETase, (Koshti et al., 2018). These hydrolases have been sourced from various organisms, including bacteria like *I. sakaiensis* and *Thermobifida fusca*, as well as fungi such as *F. solani*, *Humicola insolens* (*H. insolens*), and *A. oryzae*, as reported in studies by Wang et al. in 2008, Zimmermann and Billig in 2011, Herrero Acero et al. in 2011 and Benavides Fernández et al. in 2022.

Typically, these enzymes belong to the category of serine hydrolases and are characterized by an active site featuring a catalytic triad comprising serine, histidine, and aspartate amino acids, as well as an α/β hydrolase fold, according to Wei et al. in 2016. Most of the PET hydrolases that have been functionally verified also possess a C-terminal disulfide bond, which plays a crucial role in enhancing their thermal and kinetic stability, as noted in studies by Roth et al. in 2014, Sulaiman et al. in 2012, and Then et al. in 2015.

Over the past decades some enzymes from plastic degrading microbes are reported to hydrolyse PET. These include lipases, esterases, carboxylesterases and cutinases (Longhi and Cambillau, 1999; Anbalagan et al., 2022). However, among these enzymes cutinases provide a better result for PET degradation.

PETase hydrolyses PET to MHET. The by-products of this reaction are TPA and BHET. Then, PET hydrolysates are transported through an outer membrane protein (e.g. porin) into the periplasmic space, and MHETase converts MHET to TPA and EG (Yoshida et al., 2016; Falkenstein et al., 2020; Qi et al., 2022). Then, TPA undergoes a conversion into protocatechuic acid (PCA), which can subsequently be degraded through various pathways, as documented in studies by Qi et al. in 2022. This aspect holds significance when devising bioprocesses based on PET because different pathways yield a distinct spectrum of metabolites, each with diverse applications. For instance, PCA itself has found utility in the synthesis of industrially relevant compounds like adipic acid, as indicated by Qi et al., 2022. On the other hand, EG, which can be broken down into acetate or glyoxylate (GLA), exhibits an even broader range of metabolic possibilities than TPA, as discussed in studies by Qi et al., 2022.

Notably, EG has been converted into the biodegradable bioplastic polyhydroxyalkanoate (PHA) by a specially engineered strain of *Pseudomonas putida*

KT2440. This opens up the opportunity to utilize PET monomers as a raw material for producing an environmentally friendly alternative, as demonstrated in research by Franden et al. in 2018. Also, an extracellular cutinase from *P. mendocina* can degrade the PET and produce TPA and EG.

PETase (3.1.1.101) was originally identified in the bacterium *I. sakaiensis* 201-F6 by Yoshida et al. in 2016. PETase shares a high sequence identity with cutinases, suggesting the presence of crucial structural elements responsible for substrate binding (Fecker et al., 2018; Kawai et al., 2019). Even minor distinctions between these enzymes play a pivotal role and determine their specific activities, as emphasized by Chen et al. in 2018. The high-resolution crystal structure analysis of PETase underscores its active site, which appears to be wider than that of other cutinases, potentially contributing to the enzyme's high specificity for the dense PET substrate, as discussed by Chen et al. in 2018, Knott et al. in 2020 and Kawai et al. in 2022.

PETase exhibits an elongated connecting loop due to the presence of three additional residues, namely Ser245, Asn246, and Gln247. This extension in the loop creates additional room for PET to bind, as elaborated by Taniguchi et al. in 2019 and Knott et al. in 2020.

PETase possesses two disulfide bonds, labelled as 1 and 2, according to Taniguchi et al. in 2019. In contrast, previously studied cutinases only feature disulfide bond 1, making disulfide bond 2 unique to PETase. This additional disulfide bond serves to connect the alpha and beta loops containing the catalytic triad. It also imparts greater flexibility to the active site compared to PET-active cutinases, as highlighted by Taniguchi et al. in 2019. This flexibility allows PETase to accommodate the rigidity of the PET substrate without compromising the enzyme's structural integrity. Removing disulfide bond 2 results in reduced enzymatic activity and a weakening of the catalytic triad, as observed by Fecker et al. in 2018.

In a general context, carboxylic ester hydrolases are categorized based on their activity on p-nitrophenol (p-NP) acyl esters. Lipases are specialized in acting on medium to long-chain acyl esters (>C10), cutinases target short to medium-chain acyl esters (up to C8–C10), and esterases focus on short-chain acyl esters. Although the specificity of PET hydrolytic activities does not correlate with p-NP acyl esters, these substrates prove valuable for biochemically characterizing the enzymes under investigation, as highlighted by Kawai et al. in 2022.

Esterases cleave the ester bonds (short-chain acyl ester) found in PET monomers and also facilitate the surface modification of the target PET (Liebminger et al., 2007; Carr et al., 2020). The ester linkages that connect PET monomers can be enzymatically cleaved, a process commonly facilitated by esterases found in nearly all living organisms, as indicated by Koshti et al. in 2018. In their work, Ribitsch et al. in 2011 employed *Bacillus subtilis* nitrobenzylesterase (BsEstB) to catalyse the hydrolysis of PET into TPA and MHET. Likewise, Kawai et al. in 2019 harnessed a recombinant thermostabilized polyesterase sourced from *Saccharomonospora viridis* AHK190, demonstrating its effectiveness in PET hydrolysis, with enhanced activity observed in the presence of calcium ions. Another notable contribution comes from Ribitsch et al. in 2012, who reported the use of recombinant esterase derived from *Thermobifida halotolerans* (Thh_Est) for the degradation of PET into TA and MHET.

Lipases are widely known for their catalytic hydrolysis of PET fabrics to some extent through enhancing their wettability, and the interfacial activation phenomenon characterizes them. Cutinases are lipolytic esterolytic enzymes with assertive catalytic behaviour toward PET degradation (Eberl et al., 2009; Herrero Acero et al., 2011; Carr et al., 2020; Khairul Anuar et al., 2022). Several researchers have utilized lipase enzymes for the hydrolysis of PET, and Ma et al. in 2018 reported the successful degradation of PET nanoparticles using lipase sourced from *Candida cylindracea* and *Pseudomonas sp.* Similarly, Wang et al. in 2008 utilized BHET/TPA-induced lipase from *A. oryzae* to facilitate PET hydrolysis. Furthermore, Carniel et al. in 2017 and de Castro et al. in 2017 employed a combination of lipase from *Candida antarctica* (*C. antarctica* lipase IB CALB) and HiC for efficient PET hydrolysis into TPA.

While HiC exhibited superior performance in PET hydrolysis, it had limitations in converting MHET (an intermediate product of PET hydrolysis) into TPA (Khairul Anuar et al., 2022; Shi et al., 2023). On the other hand, CALB demonstrated a greater capacity to convert MHET into TPA but was less efficient in the initial PET hydrolysis when used alone. However, when both enzymes were used together, they synergistically improved overall PET hydrolysis. Nevertheless, comprehensive investigations into the influence of enzyme dosages, temperature, and pH are still lacking in the existing research.

Cutinase (E.C. 3.1.1.74) is primarily generated by either saprophytic microorganisms, which employ cutin as a carbon source, or by phytopathogenic microorganisms to breach the cutin barrier and infiltrate host plants. It functions as a serine esterase,

featuring a catalytic triad composed of Ser–His–Asp residues, and is categorized within the α/β hydrolase superfamily. The active site of cutinase can accommodate large molecules like cutin and related synthetic compounds. Cutinase has been employed in the hydrolysis of synthetic polymers such as PET (Dimarogona et al., 2015; Magalhães et al., 2021), polycaprolactone (Adigüzel and Tunçer, 2017), polystyrene (PS) (Ho et al., 2018), polyethylene furanoate (Weinberger et al., 2017), polybutylene succinate (Hu et al., 2016), and polylactic acid (Masaki et al., 2005; Kitadokoro et al., 2019; Carr et al., 2020; Khairul Anuar et al., 2022).

This enzyme is widely distributed among fungal and bacterial species. Cutinase exhibits maximum catalytic efficiency with p-nitrophenyl butyrate and p-nitrophenyl acetate, indicating a preference for substrates with shorter carbon chains compared to others.

Due to its versatility in hydrolysing various ester bonds and catalysing esterification and transesterification reactions, cutinase holds promise for numerous industrial applications. It finds use in the production of oil, dairy products, flavour compounds, and phenolic compounds, as well as in insecticide and pesticide degradation. Additionally, cutinase has been explored for fibre modification. Its valuable properties, especially relevant for PET degradation, have attracted significant attention from researchers. Cutinases are also capable of synthesizing polyesters in non-aqueous environments through polycondensation reactions using various diacids and alcohols. For example, Hunsen et al. (2007) utilized cutinase from *H. insolens* (HiC) immobilized on Lewatit beads for polyester synthesis through condensation reactions, while Pellis et al. (2016) employed cutinase 1 from *Thermobifida cellulositica* for polycondensation to create high-molecular-weight polyesters.

Several fungal strains are significant sources of cutinases. For instance, cutinases from *A. oryzae*, *Aspergillus nidulans* (Bermúdez-García et al., 2017), *Penicillium citrinum* (Liebminger et al., 2007), *H. insolens* (Ronkvist et al., 2009), *F. solani* (Tournier et al., 2020; Alisch-Mark et al., 2006), *F. solani pisi* (Vertommen et al., 2005), and *F. oxysporum* (Dimarogona et al., 2015; Kanelli et al., 2015; Carr et al., 2020) have shown hydrolyzing activity towards low-crystallinity PET.

The PET subunits of cutinases-mediated hydrolytic breakdown e.g., BHET, MHET, TPA and EG, have been identified as the water-soluble products of PET films and fibres (Fig 1.14) (Eberl et al., 2009). In the presence of cutinase, PET hydrolysis is

catalysed by endo-type scission that cleaves internal ester bonds into end-products TA and EG (Sánchez et al., 2020; Carr et al., 2020; Khairul Anuar et al., 2022). The active catalytic site of fungal cutinase from *F. solani* includes Serin (Ser) 120, Aspartate (Asp) 175, and Histidine (His) 188. During the initial reaction, the electrons from the oxygen of Ser120 react with the carbonyl group of PET, which leads to the formation of serine-terephthalate complex and ether compound. The fungal cutinase-assisted catalytic reaction causes the breakdown of PET into BHET, MHET, and TA (Martinez et al., 1992; Anbalagan et al., 2022; Wagner-Egea et al., 2023). The oxygen of the ether moiety forms a covalent bond with the hydrogen of His188 residue of cutinase and forms EG. The oxygen from the Ser120 binds the hydrogen from the His188, and two molecules of cutinase and TA are released. The liberated cutinase molecules begin a new catalytic cycle (Martinez et al., 1992; Carr et al., 2020; Knott et al., 2020; Anbalagan et al., 2022).

The enzymatic hydrolytic reactions of PET are supposed to take place under the temperatures close to the glass transition temperature (T_g) of PET (65~80 °C). Under such reaction conditions, the polymer chains in the amorphous PET domains can gain enough mobility to access the active sites of PET hydrolases (Ronkvist et al., 2009; Wei et al., 2019). Hence, it is supposed that faster PET degradation rates could be achieved by increasing the temperatures of the enzymatic hydrolysis reaction (for heat-tolerant enzymes) up to the glass transition temperature of PET (Oda et al., 2018). Nevertheless, the high-crystallinity PET (30~40%) represents the amplest types of post-consumer plastic, and methods for lowering the crystallinity of PET to enhance the enzymatic degradation are of high interest (Ru et al., 2020).

The enzymatic degradation of PET is a heterogeneous catalytic process. However, the end products of the PET hydrolysis differ due to the reaction type, e.g., a catalytic reaction with or without additional supplementation of natural biosurfactants (i.e., hydrophobins), or synthetic surfactants (i.e., sodium lauryl sulfate), enzyme source and concentration, incubation temperature, and reaction period (Oda et al., 2018; Barth et al., 2015)

During enzymatic treatment, the surface pendant ester linkages on the PET can be easily hydrolysed to polar hydroxyl and carboxylic groups, which further decompose to carbon dioxide and water.

The studies illustrate that *F. culmorum* produce cutinase (Canavati-Alatorre et al., 2016). This production has a prominent impact on plant infection. So, these fungi will be used in this project due to their cutinase production to investigate their ability to pre-treatment of PET and enhance the degradation and biofilm formation process (Ahmaditabatabaei et al., 2021).

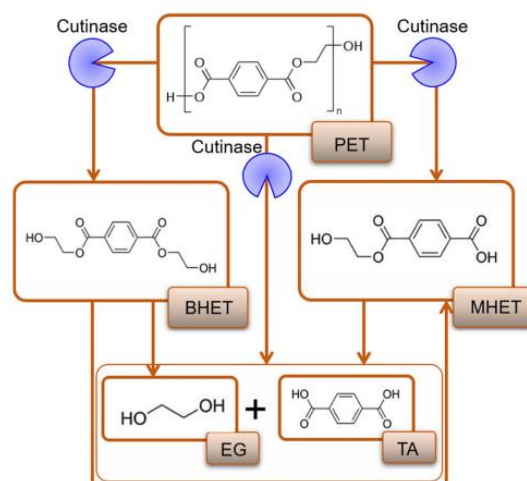


Figure 1.14. Cutinases mediated catalytic breakdown of PET into its subunits (Ahmaditabatabaei et al., 2021).

1.8.1. Limitations Hindering Enzymatic PET Biodegradation

As described above, several fungal enzyme classes, i.e., esterases, lipases, and cutinases, have been identified with significant PET biodegradation potential in various routes, including direct or indirect catalytic breakdown. This has led to the formation of PET oligomeric and monomeric units, i.e., BHET, MHET, TA, and EG (Martinez et al., 1992; Eberl et al., 2009; Sánchez et al., 2020). However, some limitations lower or hinder the efficacy of the PET biodegradation process. For instance, high-crystalline PET has low catalytic turnover due to the limited approachability of the active sites. Furthermore, the high-crystalline PET has a higher T_g that causes kinetic uncertainty (enzyme saturation and unexpected alteration in its activity and stability) and loss of enzyme activity at the temperature above PETs T_g (Shirke et al., 2018; Lu et al., 2022; Chow et al., 2023). Thus, there is a need for high-temperature-tolerant enzymes for efficient hydrolysis of high-crystalline PET. Inhibition by MHET or intermediate metabolites of the catalytic reaction process is another limitation in the enzymatic PET biodegradation (Martinez et al., 1992; Shirke et al., 2018; Maurya et al., 2020; Chow et al., 2023). Moreover, the formation of by-

products during the biodegradation or hydrolysis process increases the acidity of the reaction solution (Maurya et al., 2020), hence slowing down the reaction rate by inactivating the wild-type enzyme.

Owing to these limitations, native wild-type enzymes do not function or efficiently. Improved catalytic performance can be accomplished through adopting various strategies, such as screening for high-temperature enzymes from hyper thermophilic strains, enzyme tailoring, genetic modification of the enzyme-producing strains, and/or deploying surfactants and additives. Each of these strategies that can assist in enhancing PET biodegradation is discussed in the following section with relevant examples.

1.8.2. Strategies to Enhance Enzyme-Based PET Biodegradation

1.8.2.1. Thermostable Enzymes

Hyperthermophile microbial strains with optimal activity and stability temperatures of >80 °C are important sources of high-temperature thermostable enzymes, so-called “thermo-zymes” (enzymes resistant to irreversible inactivation at high temperatures). Thermo-zymes are considered ideal candidates for catalytic processes that need to be operated at high temperatures. Several adaptive strategies can be followed to screen or synthesize enzymes giving them functionality in a high-temperature environment.

Screening thermophiles and engineered high-temperature enzymes, several other methods, such as the exploitation of ionic liquids, or deployment of suitable modifiers such as Ca^{2+} , and various immobilization methods using robust support matrices have been adopted to increase the thermostability of PET hydrolases (Jia et al., 2013; Singh et al., 2013; Miyakawa et al., 2015). Thus, these thermophilic PET hydrolases could efficiently be used for PET biodegradation purposes. For example, the thermo-stability and catalytic activity of PET-degrading cutinase-like enzyme, Cut190, was boosted by high concentrations of Ca^{2+} , which is essential for efficient enzymatic hydrolysis of amorphous PET (Miyakawa et al., 2015). The Cut190, a member of the lipase family, encompasses an α/β hydrolase fold and a Ser-His-Asp catalytic triad, thus hydrolysing the inner block of PET (Miyakawa et al., 2015; Magalhães et al., 2021).

1.8.2.2. Use of Surfactants and Additives

The catalytic turnover of enzyme-based reactions can be facilitated/boosted by using various surfactant molecules or surface-active additives in the enzymatic hydrolysis. Surfactants stabilize the enzymes, thereby effectively prevent enzyme denaturation

during hydrolysis, which is a significant limitation of enzymatic PET biodegradation. The supplemented surfactant molecules tend to bind with the enzymes and alter the secondary and tertiary structures or flexibility of the enzyme, thereby shielding the enzyme kinetic properties (Rubingh et al., 1996). Furthermore, the integration of surfactant molecules in the reaction medium can additionally improve the dispersibility of PET particles and thus may increase the accessibility of the substrate to enzymes.

As mentioned earlier, the limited accessibility to substrate-binding active sites of the enzymes causes low activity for PET hydrolysis. This phenomenon may be ascribed to the hydrophobic force that prevents the enzyme from directly accessing the substrate (Eberl et al., 2009; Zimmermann and Billing, 2011). The accessibility of the substrate to enzymes is very important as the presence of hydrophobic forces between the PET surface and reaction substrate is one of the significant limitations of the entire PET biodegradation process (Kawai et al., 2019).

One considerable way to tackle this issue of surface hydrophobic/hydrophilic balance and substrate accessibility is the interfacial activation employing surfactant (Eberl et al., 2009). Hence, increasing the surface hydrophilization of PET near the substrate-binding region should promote cutinase-PET interactions, in the presence of surfactants, which is essential for its enzyme-assisted biodegradation. The ends of polymer chains on the PET surface are expected to protrude or form a loop (Oda et al., 2018). Surface hydrophilicity could be increased through the hydrolysis of these loops to carboxylic acid and hydroxyl residues. The overall PET degradation can be further escalated by PET surface modification that is performed by the available microbial culture or its PET hydrolytic enzymes. PET surface properties can be improved by introducing surface-active additives to the PET surface to increase its hydrophilicity. In this context, the PET biodegradation potential of fungal cutinase from *F. solani pisi* was induced by using various surfactants, including sodium dodecyl sulfate or sodium lauryl sulfate (SDS), Triton X-100, Tween 20, and sodium taurodeoxycholate (TDOC) at different concentrations in the presence of 20 mM Tris-HCl buffer of pH 8 (Chen et al., 2010). Furthermore, various substrates, i.e., p-nitrophenyl butyrate (pNPB), p-nitrophenyl palmitate (pNPP), tributyrin, and triolein were also used to initiate the reaction.

Likewise, the incorporation of additive molecules, such as hydrophobins which are cysteine-rich surface-active proteins produced by filamentous fungi, has also been

used to increase enzymatic PET hydrolysis (Espino-Rammer et al., 2013; Fukuoka et al., 2016; Joo et al., 2018). Espino-Rammer et al. 2013 tested two hydrophobins (HFBs), HFB4 and HFB7 of *Trichoderma* spp., to enhance the rate of enzymatic hydrolysis of PET. Both HFB4 and HFB7 displayed a dosage-dependent stimulation effect on PET hydrolysis by cutinase from *H. insolens*.

Moreover, the simultaneous addition of *H. insolens* cutinase and HFB4 to PET resulted in stimulation of the cutinase activity. This was observed by measuring the released soluble hydrolysis products, TA and MHET (Espino-Rammer et al., 2013).

1.9. Biofilm formation

Evolution and adaptation have conferred to bacteria the ability to survive under the extreme environments in soil, rivers and oceans. Living under extreme circumstances encourages biofilm formation by bacteria (Pop Ristova et al., 2017). The first discovery of biofilms is attributed to Antoine van Leeuwenhoek, who identified biofilm formation on his teeth in 1684. Biofilms are comprised of living bacteria and macromolecules such as polysaccharides, proteins, glycoproteins, nucleic acids, and phospholipids arranged within an intricate matrix. This matrix plays two prominent roles: production of biofilm structure and provision of channels for flow of water, nutrients and metabolic waste (Costerton, 2007; Bhagwat et al., 2021).

Biofilm development can be explained through physiology of the sessile cells and extracellular polymeric substances (EPS) in the biofilm (Branda et al., 2005; Stewart and Franklin, 2008). The EPS composition and concentration ratio vary in different biofilms and consists of a wide variety of molecules as specified above.

Stages of biofilm formation can be categorized into following steps as can be seen in figure 1.15: reversible and irreversible attachment of cells to a substratum, formation of micro-colonies, formation of macro-colonies and maturation of the biofilm by rapid production and accumulation of EPS and finally dispersal of cells from within the biofilm (Douterele et al., 2014).

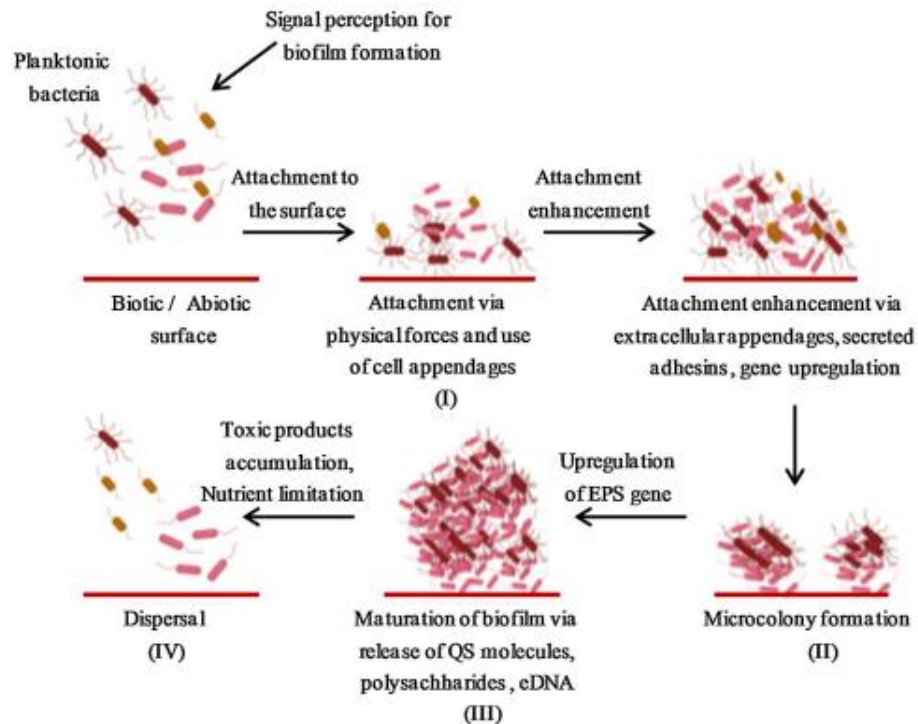


Figure 1.15. Different stages of biofilm development (Goel et al., 2021)

The attachment of bacteria to the surface of the substratum is the first step of biofilm formation. There are two stages of attachment on the surface of the substratum based on the bacterial cell's orientation (Fig 1.16). In the first stage the reversible attachment occurs. During this step bacterial cells adhere to a surface by single polar flagellum. In this stage, the bacteria overcome the repelling electrostatic forces when they come to contact with a surface. Next, irreversible microbial attachment occurs where a monolayer of cells is established and the flagellar movement on the surface stops (O'Toole and Wong., 2016). Besides, the substratum features affect the attachment. (Petrova and Sauer, 2012).

Adhesion of bacteria to the surface of plastics does not occur readily. Chemical and physical properties of plastic, hydrophilicity and hydrophobicity and physiochemical interactions can affect the adhesion. Hydrophobic bacterial cells adhere strongly to hydrophobic surfaces, and hydrophilic bacterial cells tend to adhere to hydrophilic surfaces (Ploux et al., 2010; Bhagwat et al., 2021). The structure of plastics makes their surfaces hydrophobic and this feature make them difficult to degrade. For this reason, some pretreatment is required to enhance the surface properties for better attachment of bacteria (Arkatkar et al., 2010). Pretreatment process can be divided to

three categories including mechanical (such as sand-blasting, grinding and brushing), chemical (such as chromic-sulfuric acid treatment, pickling, ozone treatment, coating with amphiphilic substances) and physio-chemical processes (such as low pressure plasma, thermal treatment, flame treatment, laser, ion etching and UV light) (Kruse et al., 1995).

After attachment bacterial cells form micro-colonies. As the thickness of biofilm reaches to 10-25 μm , the surface of substratum becomes anaerobic with a different gene expression in comparison to the cells present at the surface of the biofilm (Kalgudi, 2018). The final step in biofilm formation is the dispersal of bacterial cells. During this step the released planktonic bacterial cells attach to the new surface to make another biofilm on the new surface (Wood, 2014; Song et al., 2021; Ramakrishnan et al., 2022).

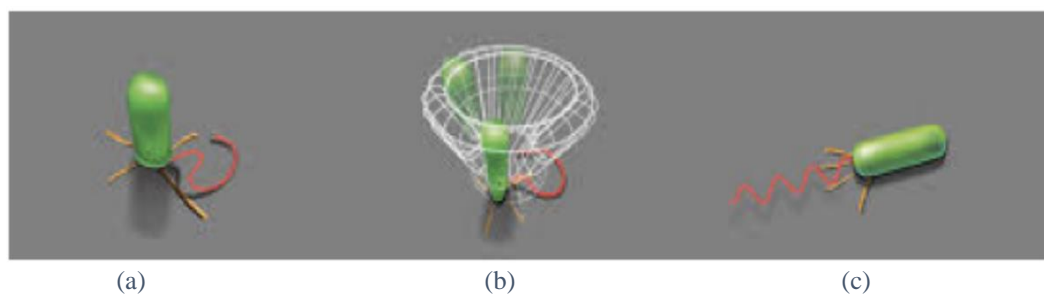


Figure 1.16. Reversible and irreversible attachment of bacterial cell on the surface of the plastic (Kalgudi, 2018). (a) and (b) show the reversible attachment and (c) shows the irreversible attachment.

Biofilm formation can play a significant role in the degradation of PET. The microbes within biofilms can produce enzymes known as PETases, which are specialized enzymes capable of breaking down PET into its constituent monomers, such as TPA and EG. These enzymes play a crucial role in the initial depolymerization of PET.

Also, Biofilms are structured communities of microorganisms that attach to surfaces and are encased in a matrix of extracellular polymeric substances (EPS). Within biofilms, various microorganisms, including bacteria and fungi, can work together synergistically to degrade complex organic materials like PET (Wood, 2014; Song et al., 2021).

Besides, Biofilms are structured communities of microorganisms that attach to surfaces and are encased in a matrix of extracellular polymeric substances (EPS).

Within biofilms, various microorganisms, including bacteria and fungi, can work together synergistically to degrade complex organic materials like PET.

1.10. Fourier Transform Infrared (FTIR) spectroscopy

FTIR, Fourier transfer infrared, is used typically as a qualitative analysis method, but it is also possible to be used as a quantitative method to quantify specific functional groups. This method is used for characterisation and identification of the organic components of the samples. FTIR can also analyse the material of the surface of the sample. FTIR analysis comes from interpreting the absorbance data. The infrared (IR) light is the main source of the energy for providing the spectrum. IR beam is one part of the electromagnetic spectrum. This beam allocates the higher wavelength (700-1050 nm) rather than visible light (400-700 nm). IR light passes through the sample. Some of the rays are transmitted and some are absorbed by the sample. The IR beam can alter the atomic vibration which provides different absorption and transmission of energy. The different behaviour of passing light through the sample provides a spectrum that act as the chemical fingerprint, and it's unique for each sample. This unique spectrum is because of the difference in chemical structures of the molecules (Rohman et al., 2020).

In FTIR there are two mirrors, interferometer and detector. The interferometer is the investigation device that uses two or more sources of lights and reaches the pattern from the interference of these lights. The obtained wave can be measured and analysed. The mentioned waves can be constructive or destructive based on their direction during the overlapping. The waves are constructive if their height increases because of the collision, and they are destructive if cancel each other intensity. The beam arrives at the beam splitter. The beam splitter breaks down the light into two parts, the reflected light, and the transmitted light. Then, the beams reach the mirrors and reflect from the mirror to the splitter and because of the interference effect they reintegrate and reaches the sample to provide the unique spectrum of the sample. To obtain the sample spectrum the background noise and environmental effects should be removed from the spectrum. The related spectrum to the noise is called interferogram (Rohman et al., 2020).

There are various types of sampling methods for FTIR analysis such as attenuated total reflectance (ATR), specular reflectance and transmission. In this project, the ATR technique was used to accomplish the required spectrum of PET. This technique was chosen due its ability to provide the spectrum from the surface of the PET. In this

technique the IR beam radiates from the IR source to the optical dense crystal and because of the difference of the refractive index between the crystal and the sample the part of the beam reflects and the part of that absorb with the sample that called evanescent wave which gives the specific spectrum related to the sample (Rohman et al., 2020).

The X-axis of FTIR spectrum shows the wavenumber (cm^{-1}), and the Y-axis shows the transmittance (%). The wavenumber range is between $4000\text{-}400\text{ cm}^{-1}$ and is called mid-IR spectral region. In this region the more the wavenumber moves toward the 400 cm^{-1} end of the spectrum, the stronger bonds peaks can be seen such as benzene structure which have strong C-C bonds. In conversion, the weaker bonds presenting towards the 4000 cm^{-1} end of the spectrum such as O-H or C-H bonds. The percentage of transmittance (Y-axis) represents the energy that requires to vibrate the specific molecules related to the specific wavenumber. The higher peak (lower percentage of transmittance) illustrates the higher energy requires for motion of molecules (Pereira et al., 2017).

The FTIR spectrum can be divided into two categories, under 1500 cm^{-1} which called fingerprint region and above that which called diagnostic region or functional group region. Signals in the spectrum can be varied in terms of the shape (broad or sharp) and intensity (weak, medium, strong). The broad signals usually have hydrogen bond in their structures such as OH- and NH-. The table 1.3 illustrates the specific wavenumber that related to each functional group (Pereira et al., 2017).

Table 1.3. Different functional group and the related wavenumber

Fingerprint and functional group region	Wavenumber (cm^{-1})
Fingerprint	400-1500
C-O	1200-1300
C-C, C-N	2100-2200
O-H (acid)	2400-3000
O-H (alcohol)	3300-3600
C=O (ester)	1740-1750
C-H	2800-3100
N-H	3400

1.11. High-performance liquid chromatography (HPLC)

High-performance liquid chromatography (HPLC) is a separation technique for identifying the targeted components in the liquid sample (Fig 1.17). HPLC system includes mobile phase, pumps, stationary phase, and detector. The mobile phase is the liquid that the target compound dissolves in it. The stationary phase is a part of the column that interacts with the target compound. Samples and mobile phase are passing through the column at different speeds, based on different characteristics of the target material such as particle size and charge of the particles. Then, the results are obtained from the detector at different times, which is called retention time. The X-axis of the HPLC spectrum shows the retention time (min), and the Y-axis shows the intensity (mAU). When there is no compound to detect by the detector the line parallel to the X-axis is shown on the plot which is called the baseline. For interpreting the result and identifying the target compound in the sample, the calibration curve is required. The known sample is prepared in different concentrations to be used to compare with the unknown sample (Khaneghah et al., 2014; Scherf-Clavel, 2016).

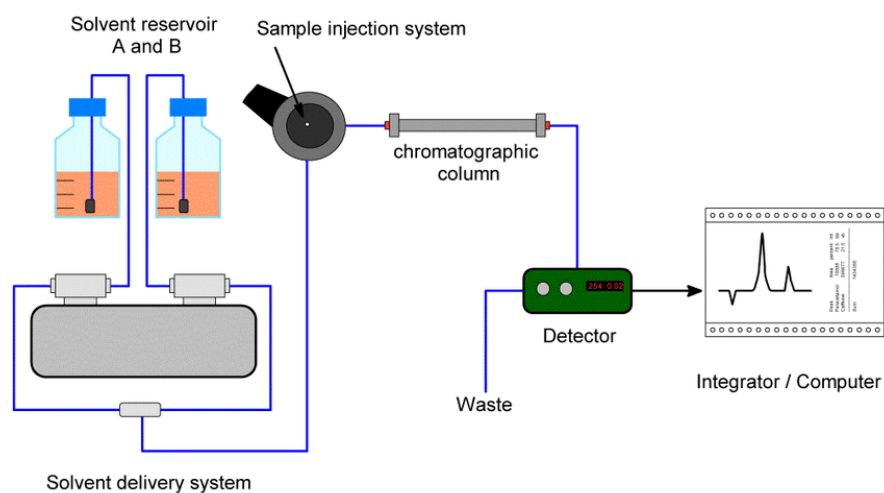


Figure 1.17. The sample pathway through the HPLC diagram (Scherf-Clavel, 2016).

There are different types of columns that can be used in HPLC including normal phase and reversed-phase, size-exclusion and ion-exchange.

1.11.1. Normal-phase chromatography

In the normal phase column, the stationary phase is polar, and the mobile phase is non-polar. It is useful for separating the non-polar solvents in the sample. In this method,

the hydrophilic solvents have a shorter retention time, and the hydrophobic material releases slower than hydrophilic molecules (Robards and Ryan, 2022).

1.11.2. Reversed-phase chromatography

In the reverse phase the column is filled with hydrophobic particles, and the mobile phase is polar such as methanol/water or acetonitrile mixture (Fig 1.18). Reversed-phase chromatography is also called hydrophobic chromatography. In this kind of stationary phase, the polar molecules have a shorter retention time. The hydrophobic molecules have a higher affinity with the stationary phase and adsorb to the column. However, the hydrophilic molecules pass through the column faster and have a shorter retention time. Elution of the hydrophobic molecules that adsorb in the column requires a higher concentration of hydrophobic or non-polar solvent in the mobile phase (Kobayashi et al., 2019).

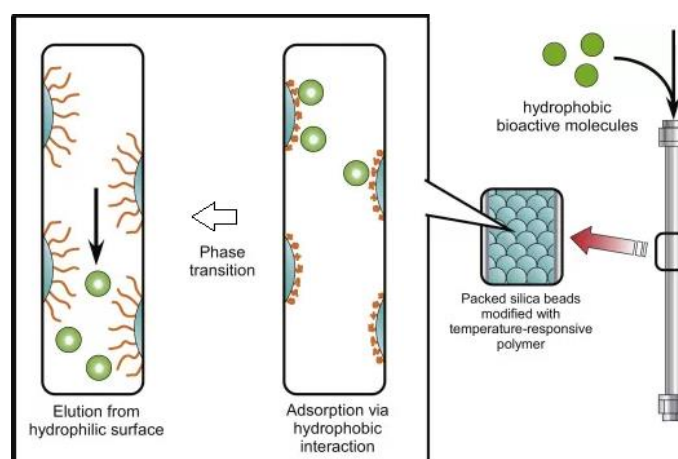


Figure 1.18. Reversed-phase chromatography HPLC diagram (Kobayashi et al., 2019)

1.11.3. Mobile phase elution mode

The mobile phase composition can be constant, isocratic elution mode, or it can be varied over time which is called gradient elution mode. For example, if there are two mobile phases in the system A and B, they can release to the system at constant percentages like 25 % of A and 75 % of B for the whole period of running the experiment. On the other hand, they can elute in the system in the form of a gradient such as increasing the A concentration from 25 % to 100 % over a period and decrease the B concentration in the system from 75 % to 0 %. The reason for using the gradient

system is that the sharper peaks can be obtained by this system. Figure 1.19 shows the isocratic and gradient diagram of one mobile phase in the system. As can be seen in the figure 1.19 the F peak which is not very intense in the isocratic mode, becomes sharper in the gradient mode (Robards et al., 2004).

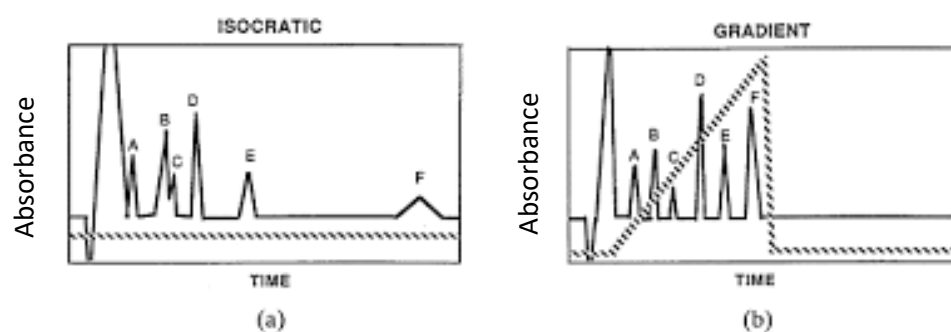


Figure 1.19. Different mobile phase elution mode; a) isocratic b) gradient (Robards et al., 2004).

1.12. Quorum sensing

Microorganisms are not considered as solitary cells without any communications. They need to communicate with their environment and each other for survival and multiplication. The cell density is one of the factors that help cells to communicate with each other and improve their adaptability to the environment (Dong et al., 2001; Hardman et al., 1998). The alteration in cells' density affects their gene expression and change the behaviour of the cells (Elasri et al., 2001; Subramoni et al., 2021).

This regulatory process which uses the cell density to affect gene express is called Quorum sensing (QS). QS depends on the production of chemical signalling molecules in the extracellular milieu. These signalling molecules contributing in communication between the cells are autoinducers and are known as quorum sensing molecules (QSM) (Fig 1.20). They can bind to some receptor molecules on the cell surface or in the cytoplasm after reaching a threshold concentration. These bindings give them the ability to function as transcriptional regulators (Miller and Bassler, 2001; Subramoni et al., 2021).

Quorum sensing was discovered in the late 1960s. This discovery began by researching on the luminous bacterium, *Vibrio fischeri* (*V. fischeri*). This bacterium lives in symbiosis with Hawaiian bobtail squid. As *V. fischeri* concentration increases on the surface of the squid's light organ, the concentration of QS molecule increases leading, through QS process, to the expression of signals that result in bioluminescence (Ruby, 1996).

As can be seen in figure 1.21, there are eight genes involved in the process of bioluminescence. At low density of *V. fischeri* cells, the concentration of QSM is lower and they can diffuse freely across the cell membrane without effecting a change in genetic response. However, by increasing the cell density, the concentration of QSM increases and goes beyond the threshold which is 1-10 $\mu\text{g/l}$ for *V. fischeri*. This concentration level is for binding the QSM to the receptors on the surface or in the cytoplasmic environment. This process leads to the emission of light (Nealson and Hastings, 1979; Amache, 2014).

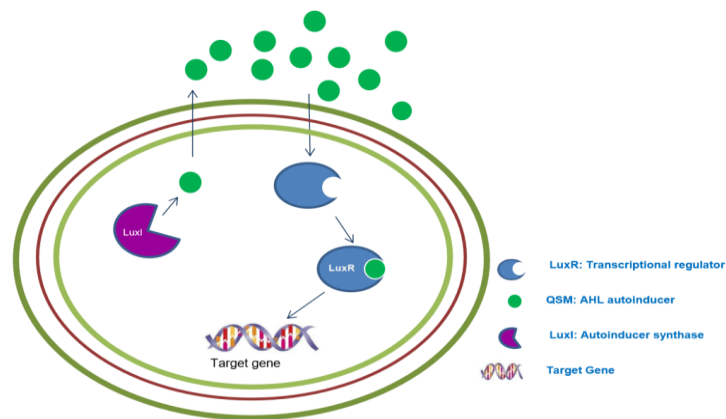


Figure 1.20. QS mechanism in Gram-negative bacteria (Amache, 2014)

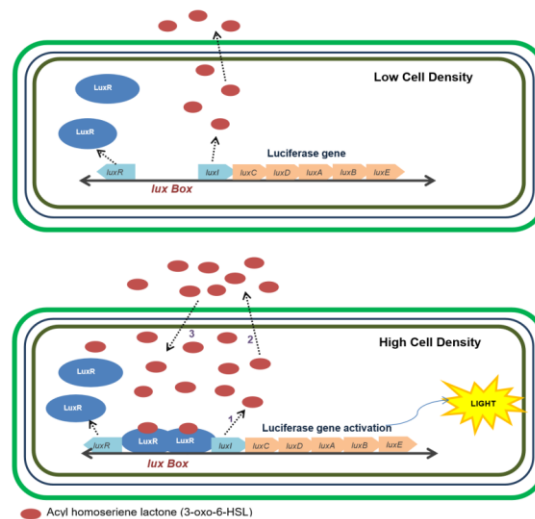


Figure 1.21. QS process effect on the surface of the squid by increasing the cell concentration of *V. fischeri* (Amache, 2014)

1.12.1. QSM types

There are three different types of QS systems with their associated QSM. The first group of QSMs exists in Gram-negative bacteria. Another group of QSMs works in Gram-positive bacteria. The third group is active in both Gram-negative and Gram-positive bacteria, and belongs to universal QS system (Miller and Bassler, 2001).

Previous studies show that all Gram-negative bacteria follow similar QS mechanisms. QS in Gram-negative bacteria occurs by acyl homoserine lactones (AHLs) (Fig 1.22). Acyl homoserine lactones are produced by more than 50 different bacterial species. They difference depends on the length and substituent of their acyl side chain (Fuqua and Eberhard, 1999).

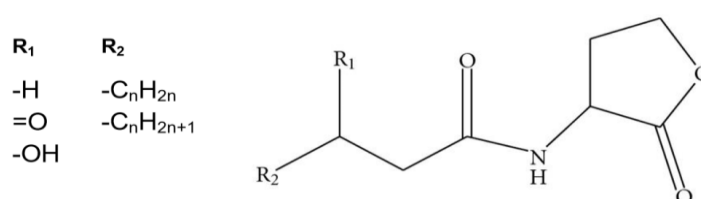


Figure 1.22. Molecular structure of AHLs (Amache, 2014)

AHLs are catalysed by the LuxI family enzymes. LuxI synthesis AHL molecules and release them to the extracellular environment. Increasing in the density of the bacterial cells leads to AHLs autoinducers bind to cytoplasmic regulatory proteins called LuxR which play the transcriptional regulator role. They can activate or repress the target genes by binding to them.

AHLs are one family of QS signals in Gram-negative bacteria that can regulate the biological functions such as biofilm and virulence formation. For example, ALH quorum sensing in *Burkholderia glumae* (*B. glumae*) AU6208 regulates secretion of lipase. Some groups of AHL enzymes are used for degradation of QSMs, for quenching of signals, or to block the QS signals and prevent the infection (Fuqua et al., 2001).

Besides AHLs, some signalling molecules including γ -butyrolactone containing compounds in *Streptomyces spp.* are also acting as a signalling molecule in Gram-negative bacteria. These molecules can be divided into three groups based on their fatty acid side chain (Fig 1.23, A-C). Group I includes the virginiae butanolide type; 6-

α -hydroxy group from *Streptomyces virginiae* (Fig 1.23, A). Group II includes IM-2 type from *Streptomyces lavendulae* FRI-5; 6- β -hydroxy group (Fig 1.23, B), and Group III includes the A-factor type: 6-Keto-group from *Streptomyces griseus* (Fig 1.23, C) (Takano et al., 2000).

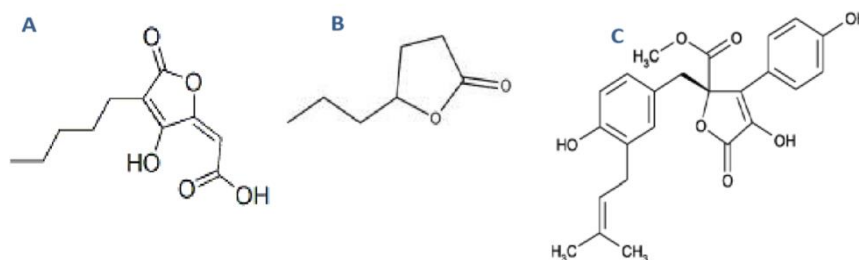


Figure 1.23. Molecular structure of butyrolactone- containing compounds (Amache, 2014).

1.12.2. Application and potential of QSM

QS process may effect a variety of physiological and morphological responses including biofilm formation, bioluminescence, pathogenicity, biosynthesis of antimicrobials, virulence factor secretion, enzyme and pigment production as well as changes in the enzyme activity. For example, by enhancing the activity of enzymes in *Aspergillus terreus* (*A. terreus*), lovastatin, a lipid-lowering drug is produced. In medicine, prevention of some conditions such as athletes foot in diabetics maybe controlled by using quorum quenching molecules to avoid forming biofilm (Manzoni and Rollini, 2002). QSMs are often involved in the formation of biofilms, which are structured communities of microorganisms encased in a protective extracellular matrix. Biofilms can adhere to surfaces and are associated with increased resistance to antibiotics and the host immune system. QSMs coordinate the attachment and maturation of biofilms, making them a crucial factor in biofilm formation (Kalgudi, 2018). In pathogenic bacteria, QSMs can control the production of virulence factors, such as toxins, adhesins, and secretion systems. When the population reaches a quorum, the expression of these virulence factors is upregulated, increasing the pathogenic potential of the microorganisms (Deep et al., 2011; Subramoni et al., 2021). This is particularly relevant in the context of infectious diseases. QSMs also play a role in establishing and maintaining beneficial relationships between microorganisms and their hosts. In mutualistic or symbiotic interactions, QSMs can coordinate activities that benefit both the microorganism and its host, such as nutrient exchange or protection from pathogens (Rutherford et al., 2012; Su et al., 2023). Microbes can

use quorum sensing to optimize the utilization of available resources. For example, when a bacterial population reaches a quorum, it may trigger the expression of genes involved in nutrient acquisition or the utilization of specific carbon sources (Amache, 2014; Kalgudi, 2018).

In this project the effect of quorum sensing will be investigated on enzymatic pretreatment and biofilm production by *I. sakaiensis*. Biofilm formation depends on the environmental factors such as nutrient composition and concentration, oxic and anoxic conditions, shear stress, temperature, and pH (Amache, 2014; Kalgudi, 2018). Researchers have shown that QS enhances biofilm formation in some strains of *Pseudomonas aeruginosa* (*P. aeruginosa*). QS-related enzyme production has been investigated in cultures of the fungus *Ophiostoma piceae* CECT 20416 where secretion of esterase and lipase enzymes are affected. This project focuses part of the investigation on PETase and MHETase which are categorized as esterases (De Salas et al., 2015).

1.12.3. N-(3-oxododecanoyl) L-Homoserine lactone (3-oxo-C₁₂-HSL)

The prominent auto-inducers in Gram-negative bacteria are N-acyl-L-homoserine lactones (AHLs). Previous studies show the Acyl homoserine lactone effect on biofilm formation, and it can regulate the expression of virulence factors in several organisms such as *P. aeruginosa*. These auto-inducers (AHLs) are binding to regulatory proteins belonging to *LuxR* family. AHL auto-inducers have the same homoserine lactone (HSL) ring linked by an amide bond to the fatty acyl side chain with structural differences in the acyl chain length ranging from 4 to 20 carbon atoms and substitutions (3-oxo or 3-hydroxyl function) depending on the bacterial strain. The homoserine ring is N-acylated at the C-1 position with a fatty acyl group ranging from 4 to 18 carbons. The acyl group can be the straight chain or be a double, an oxo group or hydroxyl group (Parsek and Greenberg, 2000; Ampomah-Wireko et al., 2021).

The molecular formula for this molecule is C₁₆H₂₇NO₄ (Fig 1.24). These molecules have essential roles in controlling bacterial functions such as biofilm formation. The autoinducer such as 3-oxo-C₁₂-HSL binds to and activates the receptors to regulate the virulence genes and enzymes (Parsek and Greenberg, 2000; Ampomah-Wireko et al., 2021).

The signal synthase LasI and the transcriptional regulator LasR are involved in the *las* QS system with 3-oxo-C₁₂-HSL as a signalling molecule. The efflux pumps help the

QSM (3-oxo-C₁₂-HSL) to transport to the outside of the cell (Parsek and Greenberg, 2000; Ampomah-Wireko et al., 2021).

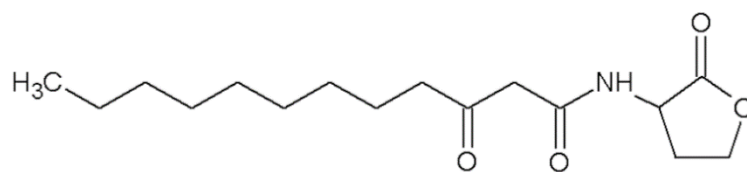


Figure 1.24. Molecular structure of 3-oxo-C₁₂-HSL

1.13. Aim and objectives

The overall aim of this project is to investigate biodegradation of PET and potential enhancement of the biodegradation process using different pre-treatment methods followed by microbial degradation. To address the aim, the following objectives will be considered:

1. To investigate the effect of different pre-treatments on PET biodegradation:
 - a) NaOH treatment
 - b) UV treatment
 - c) Surfactant treatment (Brij-35 and DTAB)
 - d) *F. culmorum* supernatant (containing cutinase) treatment
2. To investigate bacterial biofilm formation on non-treated and treated PET.
3. To investigate the effect of QSM (3-oxo-C₁₂-HSL) on biofilm formation of non-treated and treated PET.
4. To investigate degradation of PET using *I. sakaiensis* and *P. mendocina* as model bacteria capable to degrade PET.
5. To investigate the effect of scale-up on PET biodegradation.

Chapter 2. Materials and Methods

2. Materials and Methods

2.1. Materials

2.1.1. Microorganisms

2.1.1.1. Bacteria

Two microorganisms; *I. sakaiensis* strain 201-F6^T (NBRC 110686) and *P. mendocina* NCIMBCH 50 were used during the experiments. *P. mendocina* strain was available in the School of Life Sciences culture collection. *I. sakaiensis* strain 201-F6^T (NBRC 110686) was ordered from the National Institute of Technology and Evaluation (NITE) Biological Resource Centre (NBRC), Japan.

2.1.1.2. Fungi

Three fungi; *F. graminearum*, *F. culmorum* and *F. asiaticum* were used in experiments. These species were a kind gift from the University of Cranfield.

2.1.2. Media

Nutrient broth (NB) and nutrient agar (NA) were used for growth of *P. mendocina*. NA was used for maintenance of *P. mendocina*. Hipolyeptone broth (HPP broth) and Hipolyeptone agar (HPP agar) were used for growth and maintenance of *I. sakaiensis* respectively. Yeast extract sodium carbonate and vitamins (YSV) and M9 minimal media were used as a defined medium for growth of *P. mendocina* and *I. sakaiensis*. Potato dextrose agar (PDA) and potato dextrose broth (PDB) used for growth and maintenance of *Fusarium* species. List of media, reagents and their applications are outlined in table 2.1. The list of chemicals and reagents can be seen in table 2.2.

Table 2.1. List of media and their applications

Name of media	Application
HPP broth	Growth of <i>I. sakaiensis</i> 201
HPP agar	Growth and maintenance of <i>I. sakaiensis</i> 201
NB	Growth of <i>P. mendocina</i>
NA	Growth and maintenance of <i>P. mendocina</i>
YSV	Defined medium for growth of <i>I. sakaiensis</i> and <i>P. mendocina</i>
M9 minimal medium	Defined medium for growth of <i>I. sakaiensis</i> and <i>P. mendocina</i>
PDB	Growth of <i>F. graminearum</i> , <i>F. culmorum</i> and <i>F. asiaticum</i>
PDA	Growth and maintenance of <i>F. graminearum</i> , <i>F. culmorum</i> and <i>F. asiaticum</i>

Table 2.2. Comprehensive inventory of chemicals employed as media constituents or reagents.

Compounds	Supplier	Product number
Acetic acid	Thermo Fisher	A/0360/PB17
Agar	Sigma	05040
Ammonium chloride	Sigma	A9434
Ammonium sulfate	Amresco	M105
BBL polypeptone	BD	211910
Biotin	sigma	B4639
Boric acid	Sigma	B6768
Calcium carbonate	sigma	239216
Calcium chloride dihydrate	Sigma	C3306
Cobalt chloride hexahydrate	Sigma	C8661
Copper chloride dihydrate	Sigma	307483
Copper sulfate pentahydrate	Sigma	209198
Crystal violet	Sigma	61135
D (+) Glucose	Sigma	G8270
Disodium hydrogen phosphate	Sigma	1.06586
DMSO	Sigma	D8418
Ethanol absolute	VWR	153386FDP
Ethanol 99% denatured with methanol	VWR	23684.444
Ethylenediaminetetraacetic acid	Sigma	ED2SS
Glycerol	Thermo Fisher	G/0600/17
Iron (III) chloride hexahydrate	Sigma	236489
Iron (II) sulfate heptahydrate	Sigma	215422
Magnesium sulfate heptahydrate	Sigma	230391
Manganese (II) chloride tetrahydrate	sigma	M5005
Manganese (II) sulfate monohydrate	Sigma	M7634
Methanol	Thermo Fisher	M/4056/PB17
NB	Sigma	N7519
PBS	Sigma	P4417
PDA	Sigma	P2182
PDB	Sigma	P6685
Peptone from casein	Sigma	70169
Phosphoric acid	Fluka	79607
Potassium chloride	Sigma	P9541
Potassium dihydrogen phosphate	Sigma	P9791
Sodium bicarbonate	sigma	S5761
Sodium chloride	Sigma	S9888
Sodium hydroxide	VWR	28244.295
Sodium phosphate dihydrate	sigma	71643
Sodium phosphate monobasic	Sigma	S3139
Terephthalic acid	Thermo Fisher	180725000
Thiamine-HCl	Sigma	T1270
Vitamin B12	Sigma	V6629
Yeast extract	Sigma	Y1625
Zinc chloride	sigma	208086
Zinc sulfate heptahydrate	Sigma	Z4750

2.1.3. Surfactants

Two surfactants were acquired from Thermo Fisher for the purposes of this project: a cationic surfactant, Dodecyltrimethylammonium bromide (DTAB), and an anionic surfactant, Dodecyl polyethylene oxide ether (Brij-35) (Table 2.3).

Table 2.3. Surfactants suppliers and product numbers

Compound	Supplier	Product number
Brij-35	Thermo Fisher	YBP345500
DTAB	Thermo Fisher	409310250

2.1.4. Quorum sensing molecule

N-(3-oxododecanoyl) L-Homoserine lactone (3-oxo-C₁₂-HSL) was used as a quorum-sensing molecule. Dimethyl sulfoxide (DMSO) was used for solving this molecule (Table 2.4).

Table 2.4. QSM supplier and product number

Compound	Supplier	Product number
3-oxo-C ₁₂ -HSL	Sigma	09139

2.1.5. Plastic

PET sheets (amorphous, 0.25 mm thickness), were ordered from Goodfellow Cambridge Ltd (Table 2.5).

Table 2.5. PET supplier and product number

Compound	Supplier	Product number
PET sheets	Goodfellow	ES30-SH-000250

2.1.6. Equipment

2.1.6.1. FTIR

The FTIR system used in this study was a Spectrum Two FTIR spectrometer (PerkinElmer).

2.1.6.2. Microplate reader

Spectrostar Nano equipped with BMG Labtech's ultrafast UV spectrometer was used as the microplate reader to measure the optical density (OD) of inocula at 600 nm and the OD for biofilm crystal violet assay at 570 nm.

2.1.6.3. High-Performance Liquid Chromatography (HPLC)

UltiMate 3000 HPLC from ThermoFisher Scientific was used for the detection of TPA monomers in the samples.

2.1.6.4. High Resolution Microscopy

The high resolution microscopy was carried out by Zeiss Axio Zoom V16 optical microscope, 20 and 100 magnification.

2.1.6.5. Scanning electron microscopy (SEM)

Scanning electron microscopy (SEM) was performed using Lyra 3 Tescan SEM operating at 4.00 kV, 5700 magnification, courtesy of Imperial College London.

2.1.6.6. Other equipment

In this study, we used specialized equipment for various laboratory procedures. The Rodwell MP24 autoclave from Priorclave Company, which operates at a temperature of 121 °C, was used for sterilizing the media, ancillaries, and decontaminating the biological wastes. The Incu-shake MIDI bench-top shaking incubator from Sciquip Company, which allows for precise temperature control ranging from 5 to 70 °C and adjustable speed of up to 600 rpm, was used for providing the optimal environment for bacterial growth. The GE12R PuriCore Scientific hood from Labcaire Company, which features HEPA filtration and laminar airflow, was used to provide aseptic conditions for experiments. The Ohaus Company scale, which has a maximum capacity of 5000 g and a resolution of 0.01 g, was used for accurate measurements of materials. The VWR Company stirrer, which has a maximum speed of 2000 rpm and can accommodate magnetic flea of different sizes, was used for mixing materials in solution. The Analytik Jena UV equipment from Endress and Hauser Company, which emits UV light at a wavelength of 365 nm, was used for UV treatment. The Electrothermal Engineering Ltd continuous condensation apparatus was used for alkaline treatment. The selection of these equipment and instruments was based on their technical specifications and their suitability for the specific laboratory procedures required for this study.

2.2. Methods

2.2.1. Media preparation

Different volumes of media were prepared as required for the experiments. The preparations were sterilised (autoclaved), where necessary, at 121 °C for 20 minutes.

2.2.1.1. Hipolypeptone broth

Table 2.6. HPP broth ingredients in 1-litre distilled water

Ingredients	Weight (g)
Peptone from casein	5.00
BBL polypeptone	5.00
Yeast extract	2.00
MgSO ₄ .7H ₂ O	1.00

2.2.1.2. Hipolypeptone agar

Table 2.7. HPP agar ingredients in 1-litre distilled water

Ingredients	Weight (g)
Peptone from casein	5.00
BBL polypeptone	5.00
Yeast extract	2.00
MgSO ₄ .7H ₂ O	1.00
Agar	15.00

2.2.1.3. Nutrient broth

Table 2.8. Nutrient Broth ingredients in 1-litre distilled water

Ingredients	Weight (g)
D (+) Glucose	1.00
Yeast extract	3.00
Peptone	15.00
NaCl	6.00

2.2.1.4. Nutrient agar

Table 2.9. Nutrient agar ingredients in 1-litre distilled water

Ingredients	Weight (g)
D (+) Glucose	1.00
Yeast extract	3.00
Peptone	15.00
Agar	15.00
NaCl	6.00

2.2.1.5. Stock solutions for M9 minimal medium preparation

For preparing the M9 minimal medium the following solutions need to be prepared and autoclaved separately, in advance.

2.2.1.5.1. M9 minimal salt (10 X)

Table 2.10. M9 minimal salt (10 X) ingredients in 1-liter distilled water

Ingredients	Weight (g)
$\text{Na}_2\text{HPO}_4 - 2\text{H}_2\text{O}$	75.20
KH_2PO_4	30.00
NaCl	5.00
NH_4Cl	5.00

2.2.1.5.2. Glucose (20% w/v)

2.2.1.5.3. MgSO₄ (1 M)

Table 2.12. Magnesium sulfate (1 M) ingredients in 100 ml distilled water

Ingredients	Weight (g/100 ml)
MgSO ₄ ·7H ₂ O	24.65

2.2.1.5.4. CaCl₂ (1 M)

Table 2.13. Calcium chloride (1 M) ingredients in 100 ml distilled water

Ingredients	Weight (g/100 ml)
CaCl ₂ – 2H ₂ O	14.70

2.2.1.5.5. Biotin

The small aliquots of NaOH (1N) were added until the biotin was dissolved. Then, the solution was sterilised over a 0.22 µm filter and the 1 ml aliquots were prepared and stored at -20°C.

Table 2.14. Biotin ingredients in 100 ml distilled water

Ingredients	Weight (g/ 100 ml)
Biotin	0.10

2.2.1.5.6. Thiamine-HCl

The solution was sterilised over a 0.22 µm filter and the 1 ml aliquots were prepared and stored at -20 °C.

Table 2.15. Thiamine-HCl ingredients in 100 ml distilled water

Ingredients	Weight (g/100 ml)
Thiamine-HCl	0.10

2.2.1.5.7. Trace elements solution (100 X)

The solution was sterilised over a 0.22 µm filter.

Table 2.16. Trace element solution (100X) ingredients in 1-liter distilled water

Ingredients	Weight (mg/L)
EDTA	5000.00
FeCl ₃ – 6H ₂ O	830.00
ZnCl ₂	84.00
CuCl ₂ – 2H ₂ O	13.00
CoCl ₂ – 2H ₂ O	10.00
H ₃ BO ₃	10.00
MnCl ₂ – 4H ₂ O	1.60

2.2.1.5.8. M9 minimal media

M9 minimal medium was prepared by adding following ingredients to 867 ml autoclaved distilled water under aseptic condition.

Table 2.17. M9 minimal medium ingredients in 1-liter distilled water

Ingredients	Volume (ml)
M9 minimal salt (10X)	100.00
Glucose (20 %)	20.00
MgSO ₄ (1 M)	1.00
CaCl ₂ (1 M)	0.30
Biotin	1.00
Thiamine	1.00
Trace elements solution (100X)	10.00

2.2.1.6. YSV medium

Table 2.18. YSV ingredients in 100 ml distilled water

Ingredients	Weight (g/100 ml)
Yeast extract	0.01
Ammonium sulfate	0.10
Calcium carbonate	0.01
Sodium hydrogen carbonate	0.02
Trace elements and vitamins	0.60

2.2.1.6.1. Vitamins for YSV

Table 2.19. YSV vitamins ingredients in 100 ml distilled water

Ingredients	Weight (g/100 ml)
Thiamine-HCl	0.25
biotin	0.005
Vitamin B12	0.05

2.2.1.6.2. Trace element for YSV

Table 2.20. Trace element solution ingredients in 100 ml distilled water

Ingredients	Weight (g/100 ml)
$\text{FeSO}_4 - 7\text{H}_2\text{O}$	0.10
$\text{MgSO}_4 - 7\text{H}_2\text{O}$	0.10
$\text{CuSO}_4 - 5\text{H}_2\text{O}$	0.01
$\text{MnSO}_4 - 5\text{H}_2\text{O}$	0.01
$\text{ZnSO}_4 - 7\text{H}_2\text{O}$	0.01

2.2.1.7. Potato dextrose broth

Table 2.21. Potato dextrose broth ingredients in 1-litre distilled water

Ingredients	Weight (g)
Potato dextrose broth	24.00

2.2.1.8. Potato dextrose agar

Table 2.22. Potato dextrose agar ingredients in 1-litre distilled water

Ingredients	Weight (g)
Potato dextrose agar	39.00

2.2.2. Reagents preparation

2.2.2.1. Phosphate buffer saline

The Phosphate buffer saline (PBS) was used for the serial dilution of cultures. PBS was prepared from a combination of following ingredients.

Table 2.23. PBS ingredients in 1-litre distilled water

Ingredients	Weight (g)
NaCl	8.00
KCl	0.20
Na ₂ HPO ₄	1.44
KH ₂ PO ₄	0.24

2.2.2.2. Phosphate Buffer (20 mM, pH 2.5)

Table 2.24. 20 mM Phosphate Buffer ingredients in 1-litre distilled water

Ingredients	Weight (g)
NaH ₂ PO ₄	2.40
H ₃ PO ₄	2.31

2.2.3. Preparing the pre-treatment solutions

2.2.3.1. NaOH solution

Table 2.25. NaOH (10%) solution ingredients in 100 ml distilled water

Ingredients	Weight (g)
NaOH	10.00

2.2.3.2. Dodecyltrimethylammonium bromide (DTAB)

Table 2.26. DTAB solution ingredients in 100 ml distilled water

Ingredients	Weight (g)
DTAB	0.005

2.2.3.3. Dodecyl polyethylene oxide ether (Brij-35)

Table 2.27. Brij-35 solution ingredients in 100 ml distilled water

Ingredients	Weight (g)
Brij-35	0.005

2.2.4. preparation of QSM

2.2.4.1. N-(3-oxododecanoyl) L-Homoserine lactone (3-oxo-C₁₂-HSL)

Table 2.28. 3-oxo-C₁₂-HSL stock solution in 10 ml DMSO

Ingredients	Weight (g)
3-oxo-C ₁₂ -HSL	0.01

2.2.5. Inocula preparation

2.2.5.1. Long-term storage of bacterial strains

Microorganisms require a specific nutrient environment for their growth and maintenance. In this study, Nutrient Broth was used to prepare the culture of *P. mendocina*, while HPP broth was used for *I. sakaiensis*. The liquid broth was prepared from a single colony of each strain, which helps to ensure the purity of the culture. To preserve the strains for long-term storage, the fresh inoculum was mixed with 20 % glycerol and kept in cryogenic vials at -20 °C and -80 °C in freezer. This method of preservation helps to maintain the viability of the strains over an extended period. The strains were also maintained on agar slants for up to six months, providing a convenient and accessible source of inoculum. For routine use, the strains were kept on agar plates.

2.2.5.2. Preparation of working culture

To initiate the experiments the culture stocks were made using the loop of frozen bacteria to be streaked on the nutrient agar (*P. mendocina*) and HPP agar (*I. sakaiensis*). Then, the plates were put in the incubator at 30 °C for 18-20 hrs and were stored at 4 °C.

Next, the obtained single colony was cultured in 5 ml liquid broth (in 15 ml falcon tubes) to use for experiments. In addition, 6 to 7 slants of inocula were prepared and incubated at 30 °C for 18-20 hrs and were kept at 4 °C. All these processes were performed under aseptic conditions using biological safety cabinet.

2.2.5.2.1. Inoculation for growth curve experiment

To initiate the growth curve experiment, 3 ml of *I. sakaiensis* 201-F6^T was aseptically transferred from the HPP liquid culture into two pre-sterilized 50 ml falcon tube each containing 15 ml of the HPP medium. The falcon tubes were then placed in an incubator at 30 °C and 300 rpm to provide optimal growth conditions for the microorganism.

After 18-20 hrs of incubation, the OD₆₀₀ of liquid culture was adjusted to 0.125 based on McFarland standard ($\sim 1.5 \times 10^8$ cells/ml). Then, 15 ml of the culture was aseptically transferred to a 500 ml shake flask containing 150 ml of pre-sterilized medium. The flask was placed in the incubator under the same conditions as the falcon tube to provide optimal growth conditions. Samples were taken at intervals to construct

a growth curve by measuring the turbidity of the culture at 600 nm using a spectrophotometer. The same process applied for *P. mendocina*.

2.2.5.2.1.1. Equation for the bacteria doubling time

Equation (7) shows the calculation for the maximum specific growth rate (μ_{\max}). Also, doubling time (t_d) can be obtained from equation (8).

$$\mu_{\max} = \frac{\Delta \ln(\text{OD}_{600})}{\Delta t(\text{hrs})} \quad (7)$$

$$t_d = \frac{\ln 2}{\mu_{\max}} \quad (8)$$

2.2.5.2.2. Inoculation for biofilm formation

To prepare the bacterial culture for the biofilm assay, an overnight culture of *I. sakaiensis* was obtained by growing a loop full of inoculum in 5 ml HPP medium at 30 °C, 300 rpm. The culture was then transferred into two 50 ml falcon tube each including 15 ml medium. To ensure a consistent starting culture density, the OD_{600} of the liquid culture was adjusted to 0.125 based on McFarland standard ($\sim 1.5 \times 10^8$ cells/ml) using 17 ml of HPP medium. This step ensures that the bacterial cells are in the exponential phase and have reached a similar growth stage, which is important for accurate and reproducible results.

The adjusted culture was then further diluted 1:100 into fresh HPP medium in a falcon tube to obtain the appropriate cell density for the biofilm assay. This dilution step ensures that the bacterial cells are not overcrowded and have enough nutrients and space to form a biofilm. Additionally, using a fresh medium ensures that the nutrient composition is consistent and that any potential contamination from the overnight culture is minimized.

The McFarland standard is a widely used method to standardize the bacterial cell density. It is based on the turbidity of the culture and provides a standardized method to adjust the cell density to a specific value. This method is essential for comparing the bacterial growth or biofilm formation between different cultures or experiments.

Overall, these steps ensure that the bacterial culture used for the biofilm assay is in the appropriate growth stage and cell density, which is crucial for accurate and reproducible results. The same process applied for *P. mendocina*.

2.2.5.2.3. Inoculation of *I. sakaiensis* for larger scale experiments including DTAB, FSC and QSM

To prepare the bacterial culture for DTAB, FSC and QSM scaleup experiments, a 1 ml overnight culture of *I. sakaiensis* was obtained by growing a loop full of inoculum in 5 ml HPP medium at 30 °C. The culture was then transferred to a 500 ml shaken flask containing 50 ml of YSV medium. The use of a larger volume of medium and a shaken flask ensures that the bacterial culture has sufficient nutrients and oxygen to grow optimally.

2.2.5.2.4. Preparation of fungi species

To initiate the growth of fungi species, PDA was used. PDA is a nutrient-rich agar medium that supports the growth of a wide range of fungal species. The plates were streaked with a fungal spore suspension or mycelial fragments and incubated at 25-30 °C for 7 days. This allows the fungi to grow and form visible colonies on the agar surface.

To maintain the fungal strains for long-term storage, the growth species were cut from the agar plate and transferred to a new plate to grow. After 7 days, the colonies were cut from the plate and transferred to cryogenic vials containing 25 % glycerol. The use of glycerol as a cryoprotectant helps to prevent damage to the fungal cells during freezing and thawing. The cryogenic vials were then stored in a -20 °C freezer for long-term storage.

In addition, the fungal strains were also maintained on agar slants for use as inocula for up to six months. Agar slants are a convenient way to store fungal cultures, as they provide a stable surface for the fungi to grow on and can be easily transported. The use of slants also allows for easy recovery of the fungal culture when needed for further experiments.

2.2.6. PET preparation

To prepare the samples for further experiments, PET sheets were cut into 2×2 mm pieces using a sterile cutter. To ensure the samples were free of any potential microbial contamination, they were sterilized using 70 % ethanol, which is a commonly used disinfectant in microbiology. The PET pieces were then dried under aseptic conditions overnight to remove any residual ethanol and ensure the samples were completely dry before further use.

2.2.7. Pre-treatments of PET pieces

2.2.7.1. Alkaline treatment

Sodium hydroxide (NaOH) was used for alkaline treatment of the PET pieces. PET pieces were treated with 10 % NaOH (w/v) at 80 °C for 30 minutes based on Pita and Castilho's method, 2020 in which they determined the optimized conditions of NaOH treatment for PET.

The PET pieces were treated using continuous condensation set-up (as described in Materials section). The PET (200) pieces were placed in the boiling flask containing 25 ml of 10 % NaOH for 30 minutes at 80 °C. After 30 minutes the solution was discarded, and the PET pieces were washed with sterile distilled water to remove any residual NaOH and other reaction by-products.

2.2.7.2. UV treatment

The PET pieces (200) were placed at a distance of 15 cm under a 6-Watt UV (365 nm wavelength) lamp for 14 days.

2.2.7.3. Surfactant treatment

PET pieces were placed in a falcon tube containing 15 ml of 0.005 % (w/v) the surfactant solution and were treated overnight.

2.2.7.4. FSC treatment

To initiate the FSC treatment experiment, *F. culmorum* was cultured by first transferring it from a storage plate in the fridge onto a fresh PDA plate. After 7 days, spores were extracted and suspended in PBS before being transferred to a 500 ml shaken flask containing 150 ml of PDB medium. The flask was then placed in an incubator set to 30 °C and 180 rpm for overnight growth for 24 hrs. Following this, a 40 ml sample was taken and centrifuged at 4000 rpm for 10 minutes to obtain the supernatant. The supernatant was then added to a petri dish containing sterile PET pieces, to initiate the FSC treatment. then, the petri dish containing the sterile PET pieces and the supernatant was placed in an incubator set to a temperature of 40 °C and a speed of 40 rpm for 2 hrs.

2.2.7.5. FSC-DTAB treatment

To prepare the PET pieces for FSC-DTAB treatment, a series of steps were followed according to the procedures outlined in the figure 2.1. The DTAB treatment was applied to the PET pieces, which involved coating the surface with a thin layer of

DTAB to facilitate FSC adsorption. Following this, the PET pieces were rinsed thoroughly with sterile distilled water to remove any excess DTAB and to ensure that the surface was free of contaminants that could interfere with the FSC-DTAB treatment. Once the rinsing process was complete, the procedure outlined in section 2.2.8.3 was applied to the PET pieces. This involved the addition of the FSC solution to the surface of the PET pieces, which then underwent a controlled incubation period to facilitate the FSC-catalysed degradation of the PET material.

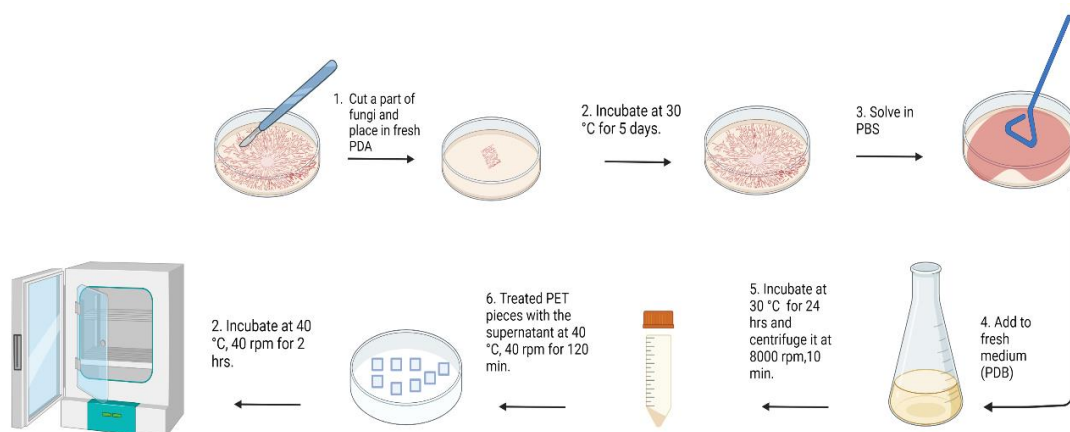


Figure 2.1. The schematic shows the pre-treatment process of PET using FSC.

The fungus was first transferred to a fresh PDA plate and incubated for 7 days. The resulting spores were then washed with PBS and transferred to a shaken flask containing PDB medium, which was then incubated for 24 hrs. The resulting supernatant was obtained by centrifugation at 8000 rpm for 10 minutes. Next, the supernatant was applied to PET pieces in a petri dish, which was then incubated at 40 °C and 40 rpm for 2 hrs.

2.2.8. 3-oxo-C₁₂-HSL concentrations preparation

To prepare for the subsequent experimental treatments, a range of QSM concentrations were prepared by diluting a stock solution of 1 mg/ml to concentrations of 0.5, 1, 5, 10, 15, and 20 µg/ml. The stock solution was prepared by dissolving 10 mg of QSM in 10 ml of DMSO, which was used as a solvent due to its ability to effectively solubilize QSM. The dilution process was carefully performed to ensure that the desired concentration of QSM was accurately obtained.

2.2.8.1. 3-oxo-C₁₂-HSL concentrations biofilm formation

The experiment aimed to determine the optimal concentration of QSM for biofilm formation by conducting a biofilm formation assay. To achieve this, a range of concentrations of QSM was prepared and tested. The experiment was conducted in a sterile 96-well plate, where each well had a total volume of 200 µl. To initiate the

assay, 20 μ l of inoculum was added to each well, followed by the addition of 50 μ l of QSM medium and 130 μ l of growth medium to each well. The plate was then incubated at a temperature of 30 °C for a duration of 24 hrs. The diagram of 96 well-plate outlined follow. Then the biofilm assay applied.

2.2.8.2. DTAB large scale in 3-oxo-C₁₂-HSL supplemented culture

To initiate the scale-up experiment, a 500 ml shake flask was filled with 50 ml of YSV media, 7.5 ml of inoculum (either *I. sakaiensis* or *P. mendocina*), and 17.5 ml of quorum sensing molecules (QSM) at a concentration of 5 μ g/ml. Each flask contained 12 PET pieces, and the different treatments included non-treated PET, non-treated PET in the presence of QSM, DTAB-treated PET, and DTAB-treated PET in the presence of QSM. Sampling was performed in weeks one, four, and eight to monitor the biodegradation process. The schematic diagram (Fig 2.2) clearly illustrates the experimental setup, including the use of shaken flasks and the various treatment groups.

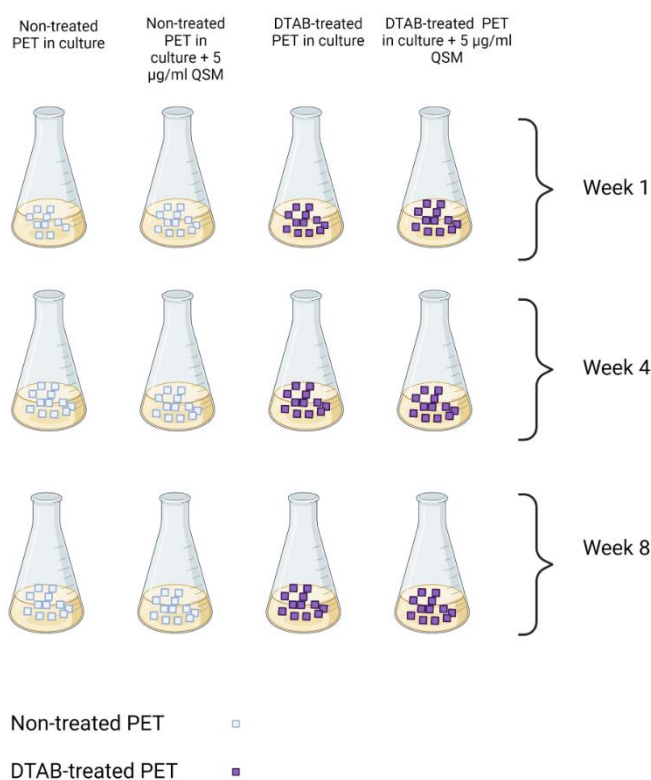


Figure 2.2. The schematic diagram illustrates the experimental setup used to investigate the biodegradation of PET in the presence of QSM and DTAB.

A 500 ml shaken flask was filled with YSV media, inoculum, and QSM, and 12 PET pieces were added to each flask. Different treatment groups were tested, including non-treated PET, non-treated PET with QSM, DTAB-treated PET, and DTAB-treated PET with QSM. Sampling was performed at weeks one, four, and eight to monitor the biodegradation process.

2.2.8.3. FSC larger scale in 3-oxo-C₁₂-HSL supplemented culture

To initiate the experiment, a 500 ml shake flask was filled with 50 ml of YSV media, 7.5 ml of inoculum (either *I. sakaiensis* or *P. mendocina*), and 17.5 ml of QSM at a concentration of 5 µg/ml. The total working volume of the flask was 75 ml (15 % the of total volume). Each flask contained 12 PET pieces, and the different treatments included non-treated PET, non-treated PET in QSM supplemented culture, FSC-treated PET, FSC-treated PET in QSM supplemented culture, FSC-DTAB-treated PET and FSC-DTAB-treated PET in QSM supplemented culture. Sampling was performed in weeks one, four, and eight to monitor the biodegradation process. The schematic diagram clearly illustrates the experimental setup, including the use of shaken flasks and the various treatment groups (Fig 2.3).

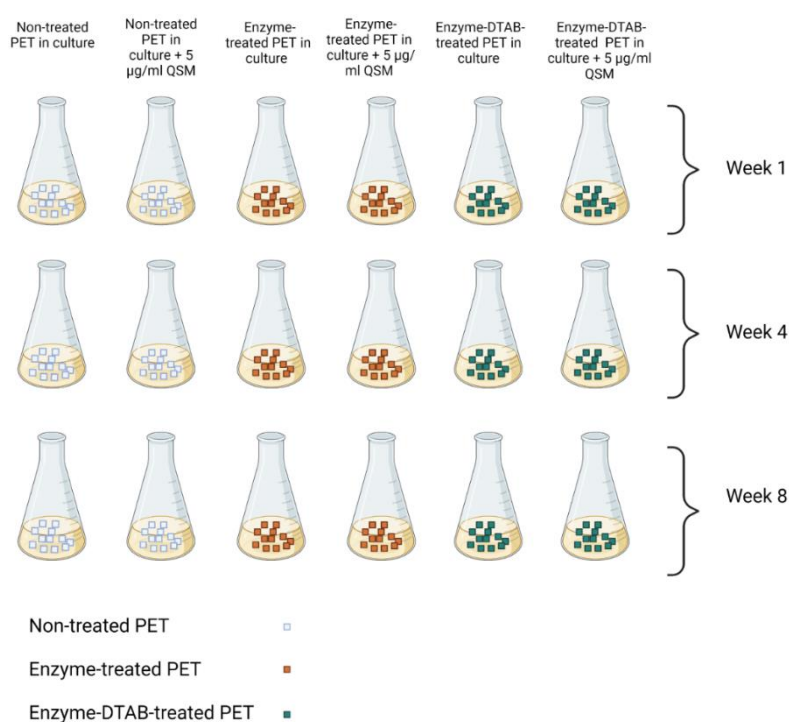


Figure 2.3. The schematic diagram illustrates the experimental setup used to investigate the biodegradation of FSC and FSC-DTAB treated PET in QSM supplemented culture.

A 500 ml shaken flask was filled with YSV media, inoculum, QSM, and 12 treated PET pieces were added to each flask. Different treatment groups were tested, including non-treated PET, non-treated PET with QSM, FSC-treated, FSC-treated with QSM, FSC-DTAB-treated PET, and FSC-DTAB-treated PET with QSM. Sampling was performed at weeks one, four, and eight to monitor the biodegradation process.

2.2.9. Biofilm formation

The 6-well plates were used for investigation of biofilm formation on PET pieces. At first, each one of the media HPP, YSV and M9 was transferred to six 6-well plates aseptically. Then, 10 pieces of pre-treated PET were added to each well of the 6-well plate related to a specific medium. Finally, the adjusted inoculum was added to all wells of all plates and the plates were placed in the incubator at 30 °C and the results of biofilm assay and FTIR was recorded each week. The experiment continued for *I. sakaiensis* for three weeks, and for *P. mendocina* for one week. The following diagram (Fig 2.4) demonstrates the set-up of the experiment and the steps involved for *I. sakaiensis*. The same set-up was provided for *P. mendocina*.

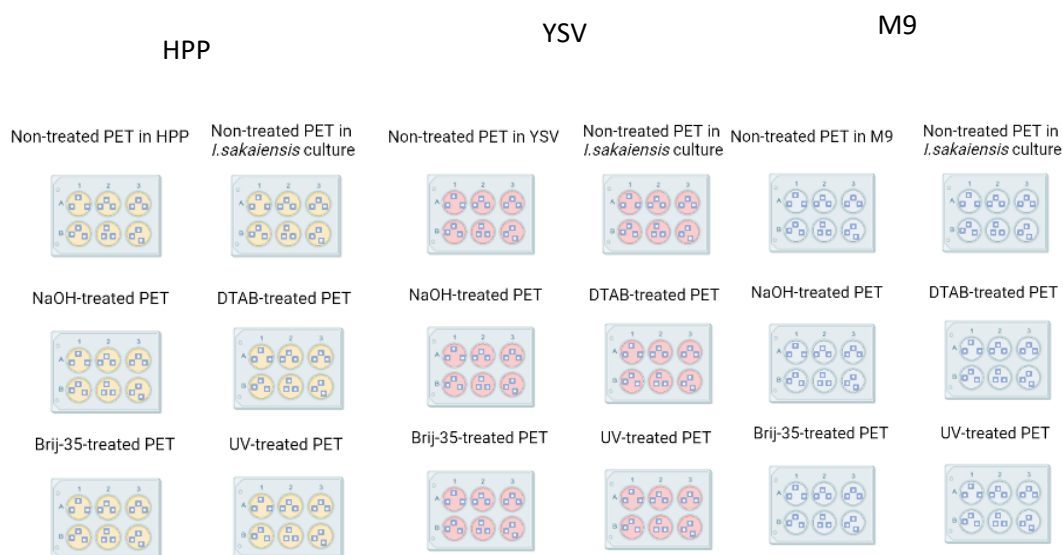


Figure 2.4. Biofilm formation on non-treated and treated PET pieces experiment set-up (created with BioRender.com).

2.2.9.1. Biofilm Assay

2.2.9.1.1. Staining biofilm

After incubation the PET samples were taken and transferred to the 96-well plates with different columns representing different PET treatments. Subsequently, the planktonic cells were removed by gently adding 100 μ l distilled water to each well and discharging the whole liquid from the well. This process was repeated twice to ensure no planktonic cells were left on the PET pieces in the wells. Next, 200 μ l Crystal violetate (0.1 % w/v) was added to each well and incubated at room temperature for 10 minutes. Then, the liquid was removed from the wells and the PET pieces were

washed twice with 200 µl distilled water. Finally, the plate was taken place in the room temperature overnight to become dry.

2.2.9.1.2. Quantifying the biofilm

In final step of biofilm assay 200 µl of 30 % acetic acid was added to dissolve the crystal violate. The solution was mixed gently with pipette tip to reach a homogenous colour. The OD was read at 570 nm, a 30 % acetic acid solution was used as blank.

2.2.10. FTIR

PET samples were used for the investigation and analysis of the changes on the surface of them and were placed directly onto the diamond crystal. The force gauge was chosen at 113 units and the infrared absorption spectrum was measured between the wavelength region of 4000 – 450 cm^{-1} . The spectral resolution was 4 cm^{-1} and spectra were collated based on 5 scans.

2.2.11. HPLC

UltiMate 3000 (ThermoFisher Scientific) equipped with reversed-phase column (Phenomenex, Gemini 5 µm C18 110 Å, 150 x 4.6 mm). The 1 ml of each prepared samples poured in the HPLC 2ml vials and put in the HPLC rack. The Methanol (100 % (v/v)) and 20 mM phosphate buffer (pH 2.5) used as the mobile phase. The flow rate set to 1 ml/min. and the samples was monitored at a wavelength of 240 nm. The typical elution condition was as follows: 0 to 15 min, 25 % (v/v) methanol (isocratic); 15 to 25 min, 25– 100 % (v/v) methanol (linear gradient).

2.2.11.1. TPA standard sample preparation

The TPA stock solution with concentration of 0.01 mg/ml were prepared. The following concentrations were made from 0.01 mg/ml stock solution containing 20, 15, 12, 10, 8, 5, 2.5, and 1.2 µg/ml.

2.2.11.2. The sample preparation

The supernatant of samples from each flask was obtained after week one, four and eight to centrifuge at 4000 rpm for 10 minutes. Then, 2 ml of each sample poured in the HPLC 2 ml vials and put in the HPLC rack.

Chapter 3. Results

3. Overview

The results of this study are organized into four distinct chapters, each of which covers a significant aspect of the experiments.

The first chapter is focused on exploring different pre-treatments on PET and discovering the pre-treatment effects on the biodegradation of PET using biofilm assay and FTIR. This chapter demonstrates the results obtained from two different microbes (*I. sakaiensis* and *P. mendocina*), three media (HPP, YSV, and M9 minimal medium), and four treatments (NaOH, Brij-35, DTAB, and UV) in 6-well plates over a period of three weeks for *I. sakaiensis* and one week for *P. mendocina*.

The second chapter of the study is centred around scaling up the most effective pre-treatment, which was determined to be DTAB from the results obtained in the first chapter. The experiment was conducted for eight weeks, and samples were taken at weeks one, four, and eight. Biofilm assay, FTIR, and HPLC were utilized to assess the results.

The third chapter focuses on the effects of *F. culmorum* supernatant containing cutinase (FSC), on PET degradation. The experiments were carried out using a 96-well plate (200 μ l), a 6-well plate (10 ml) and 500 ml shaken flask (large scale). The 96-well plate experiment was carried out for a duration of 24 hrs, whereas the 6-well plate experiment was conducted over a longer period of three weeks. The large scale experiment was conducted for a total of eight weeks and samples were collected after one, four, and eight weeks. Biofilm assay was carried out on samples in 96-well plate. For the 6-well plate, biofilm assay and FTIR were done on PET samples. In scale up experiment the biofilm assay, FTIR, HPLC, high resolution microscopy and SEM were carried out to investigate the biodegradation of PET.

Finally, the fourth chapter explores the effects of QSMs on optimal treatments of PET, including DTAB treatment, FSC treatment, and FSC-DTAB treatment. The biodegradation of PET was investigated using biofilm assay, FTIR, HPLC, high resolution microscopy and SEM. The experiment was conducted for eight weeks, and samples were taken at weeks one, four, and eight.

Overall, the study provides an investigation into the biodegradation of PET, examining the effects of different pre-treatments, scaling up the most effective pre-treatment, and exploring the role of FSC and QSMs in the biodegradation process. The results of this

study have important implications for the development of more sustainable and efficient approaches to plastic waste management, which is a critical challenge facing our society today.

The experimental design and results of each chapter are presented in a diagram (Fig 3.1), which outlines the experimental design. The optimal results are shown with the pink background.

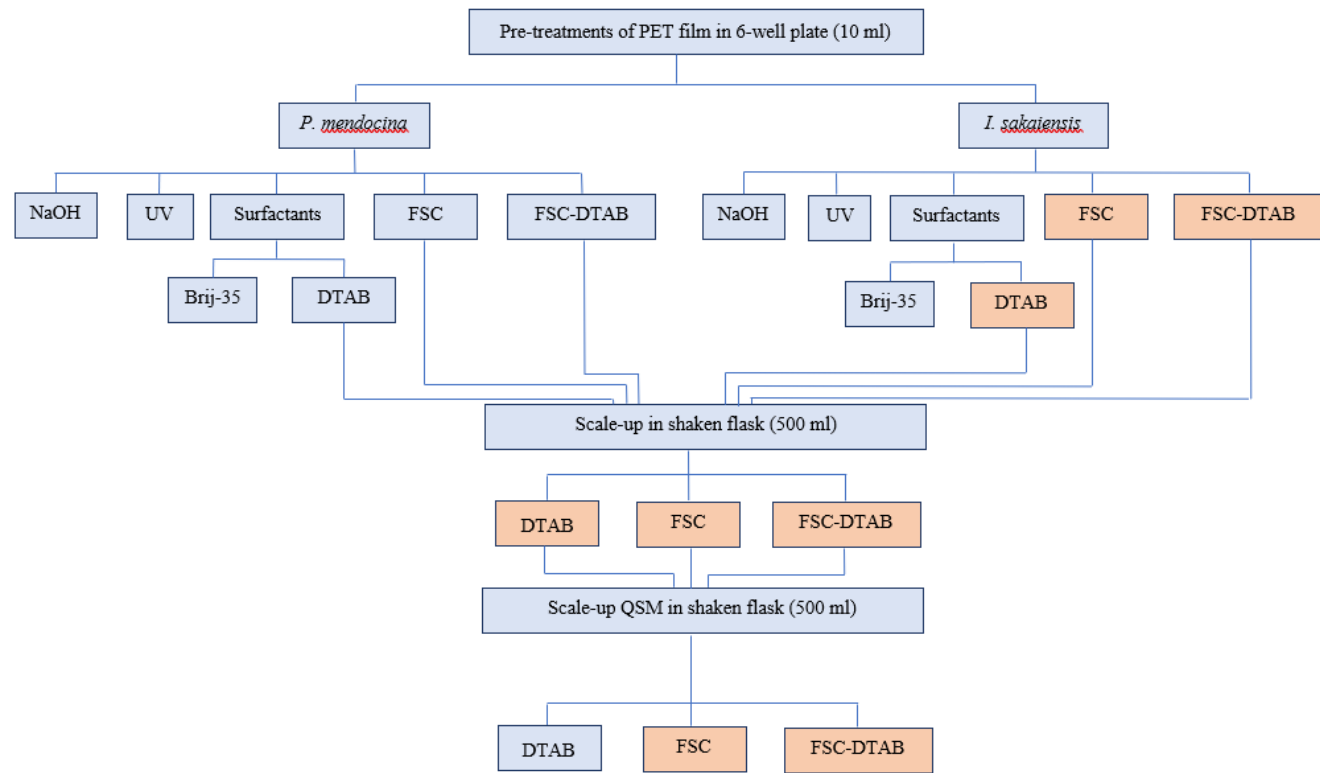


Figure 3.1. Diagram highlighting the experiments and the pathway pursued to attain the optimal approach for the biodegradation of PET film.

Chapter 3.1. Effect of PET pre-treatment on PET biodegradation

3.1. Overview

This chapter begins with the presentation of the growth curve of two selected microbes, namely *I. sakaiensis* and *P. mendocina*. The growth curves of both microbes were analysed by calculating their specific growth rates and doubling times based on culture absorbance (OD₆₀₀). Subsequently, the effectiveness of four different pre-treatment methods for PET degradation, including NaOH, DTAB and Brij-35 surfactants, as well as UV treatment were investigated. These pre-treatment methods were studied to enhance the biodegradability of PET.

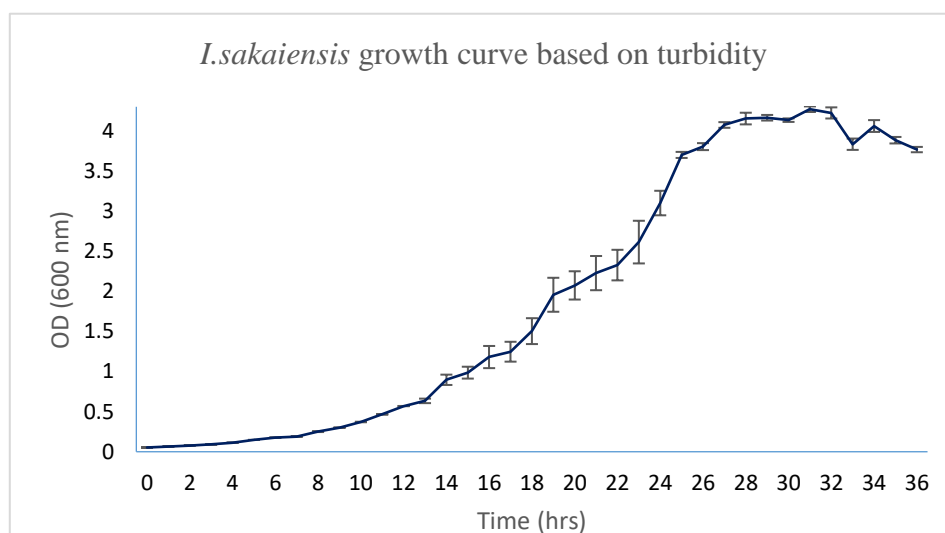
The pre-treated PET pieces were subjected to two different microbes, *I. sakaiensis* and *P. mendocina*, in three different media: HPP, YSV, and M9 minimal medium (as described in Section 2.1.1 and 2.1.2 of the Materials and Methods Chapter). A large matrix of data was obtained based on the two microbes, three media, four pre-treatments and processing time (a period of up to three weeks). The results of the three different pre-treatment methods were compared using biofilm formation assay and FTIR.

Overall, the study highlights the optimal pre-treatment methods for PET biodegradation.

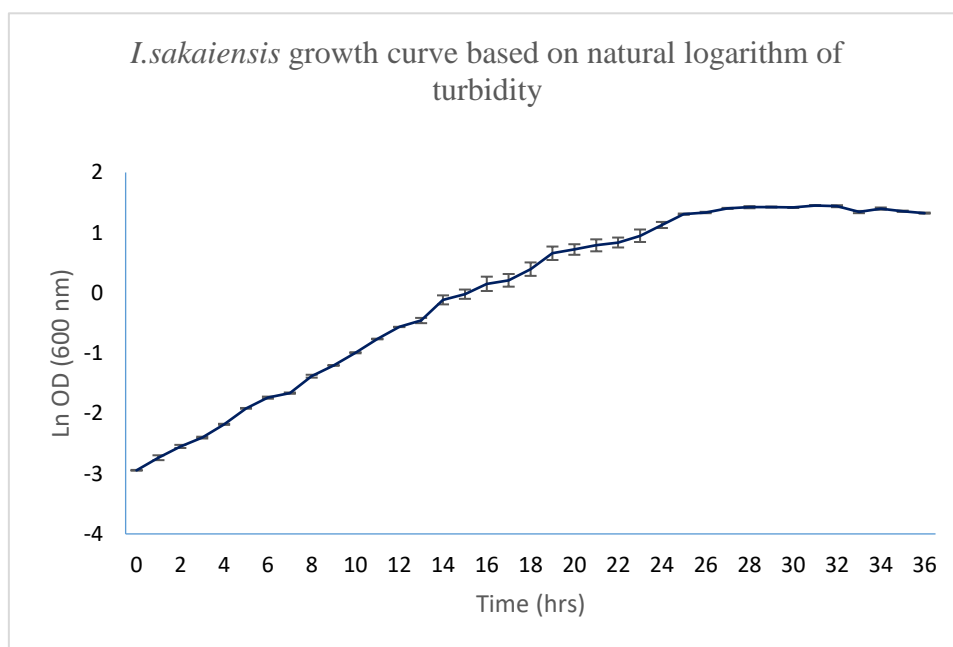
3.1.1. Growth profile

3.1.1.1. *I. sakaiensis* growth profile

The growth profile of *I. sakaiensis* in liquid culture (HPP) based on turbidity measurement is presented in figure 3.2 (a= normal graph, b= logarithmic graph). After a short lag and slow growth, the growth rate increases, and the culture enters the exponential phase of growth followed by stationary phase after 26 hrs.



(a)



(b)

Figure 3.2. The figure shows the results of three independent shaken flask cultures (100 ml culture in 500 ml shaken flask) in HPP medium over 36 hrs of incubation at 30 °C, 180 rpm.

(a) A graph showing growth profile of *I. sakaiensis* based on turbidity OD_{600 nm}. (b) A graph showing growth curve of *I. sakaiensis* based on natural logarithm of turbidity.

Specific growth rate and doubling time are calculated below for *I. sakaiensis* based on OD₆₀₀ (Please note section 2.2.5 of the Materials and Methods Chapter, equation 7 and 8).

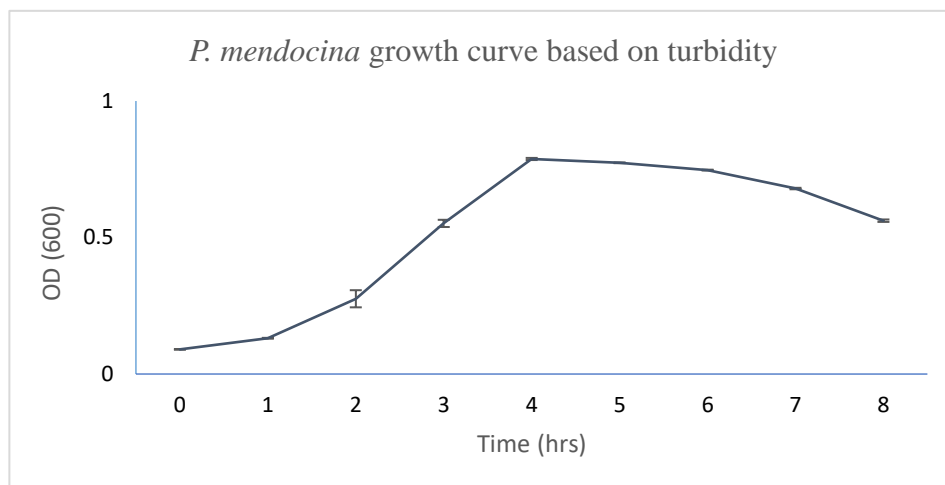
$$\mu_{\max} = \frac{\ln(3.7) - \ln(2.6)}{25 - 23} = 0.18 \quad \text{hrs}^{-1} \text{ (based on turbidity measurement at OD}_{600\text{nm})}$$

$$t_d = \frac{0.693}{0.18} = 3.8 \quad \text{hrs (based on turbidity measurement at OD}_{600\text{nm})}$$

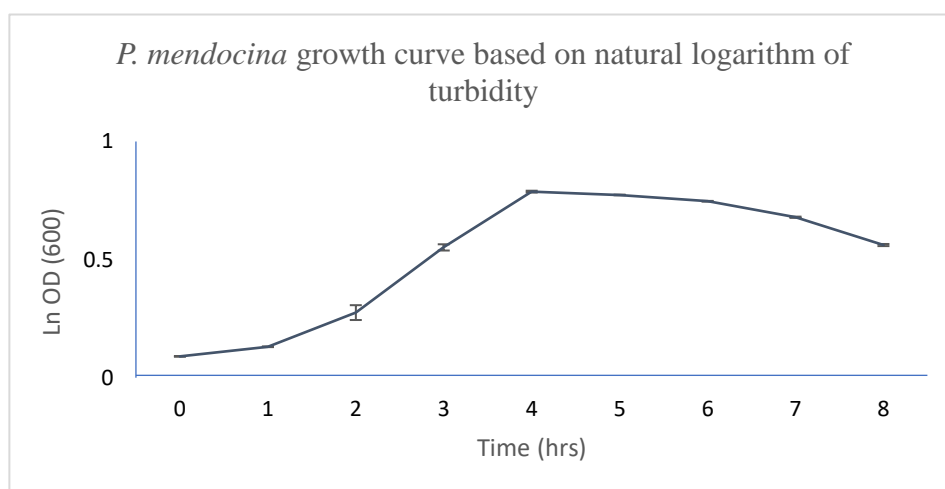
Doubling time calculation for *I. sakaiensis* from three flasks show fastest growth between time 23 and 25 hrs where the doubling time is 3.8 hrs.

3.1.1.2. *P. mendocina* growth profile

The growth profile of *P. mendocina* in liquid culture (YSV) based on turbidity measurement is presented in fig 3.3 (a= normal graph, b= logarithmic graph). After a 1 hr lag, the growth rate increased, and the culture entered the exponential phase of growth followed by stationary phase after 4 hrs.



(a)



(b)

Figure 3.3. The figure shows the results of three independent shaken flask cultures (100 ml culture in 500 ml flask) in YSV medium over 8 hrs of incubation at 30 °C, 180 rpm.

(a) A graph showing growth profile of *P. mendocina* based on turbidity OD₆₀₀. (b) A graph showing growth curve of *P. mendocina* based on natural logarithm of turbidity.

Specific growth rate and doubling time are calculated below for *P. mendocina* based on OD_{600nm} (Please note section 2.2.5 of the Materials and Methods Chapter, equation 13 and 14).

$$\mu_{\max} = \frac{\ln(0.79) - \ln(0.28)}{4 - 2} = 0.52 \text{ hrs}^{-1} \text{ (based on turbidity measurement at OD}_{600\text{nm}})$$

$$t_d = \frac{0.693}{0.52} = 1.33 \text{ hrs (based on turbidity measurement at OD}_{600\text{nm}})$$

Doubling time calculation for *P. mendocina* from three flasks show fastest growth between time 2 and 4 hrs where the doubling time is 1.33 hrs.

3.1.2. Pre-treated PET FTIR profile in the presence of *I. sakaiensis*

In this section, the biofilm and FTIR results of the non-treated (control) and pre-treated (NaOH, DTAB, Brij-35, and UV) PET pieces in cultures of *I. sakaiensis* and *P. mendocina* are compared.

There are three presentations of FTIR results related to non-treated and pre-treated PET samples in the presence of *I. sakaiensis* in the three media grown in 6-well plates, incubated for one to three weeks at 30 °C. The results are presented in bar charts based on:

- The media HPP, YSV and M9 minimal medium (Fig 3.4, 3.5. and 3.6 respectively),
- The treatment including NaOH, DTAB, Brij-35 and UV (Fig 3.7, 3.8, 3.9 and 3.10 respectively).

The results are also presented in tables (Table 3.1, 3.2, 3.3). Next, the biofilm results are presented by bar charts (Fig 3.11, 3.12 and 3.13).

Similar experiment was carried out with *P. mendocina*, but for one week and the results are presented in bar charts based on medium (Fig 3.14), bar charts based on treatment (Fig 3.15, 3.16, 3.17 and 3.18) and table (Table 3.4). Subsequently, the biofilm results are presented by bar chart (Fig 3.19).

As described in section 1.10 of the Introduction Chapter, the peak intensity alterations in the FTIR spectra of the samples are an indication of the energy required to cause vibration in molecules of the sample under study. So, a decrease in the intensity of peaks (higher percentage of transmittance or lower amount of absorbance) suggests that less energy is required to vibrate the related bonds, meaning it is easier to break them down. The raw data showing pre-treated PET FTIR spectra are uploaded into the Appendix (Chapter 6, Fig 6.1- 6.12).

3.1.2.1. PET FTIR profile of samples in different media

In this section the results are presented in bar charts based on the media HPP, YSV and M9 minimal medium.

3.1.2.1.1. PET pre-treatment profile in HPP medium

Considering all four pre-treatment methods in HPP medium, Fig 3.4, the most alteration in transmittance percentage of carbonyl group (C=O) was related to the NaOH treatment. followed by UV pre-treatment. The transmittance of NaOH treated samples changed from 28.95 to 61.71 % after one week of incubation. After two weeks, the transmittance percentage decreased to 51.42. However, after three weeks the transmittance percentage reached 65.95, which was significantly higher than 39.02, the transmittance of non-treated PET in the presence of *I. sakaiensis* culture.

After two and three weeks there was no significant change in the transmittance percentages of PET pieces treated by UV in comparison with week one.

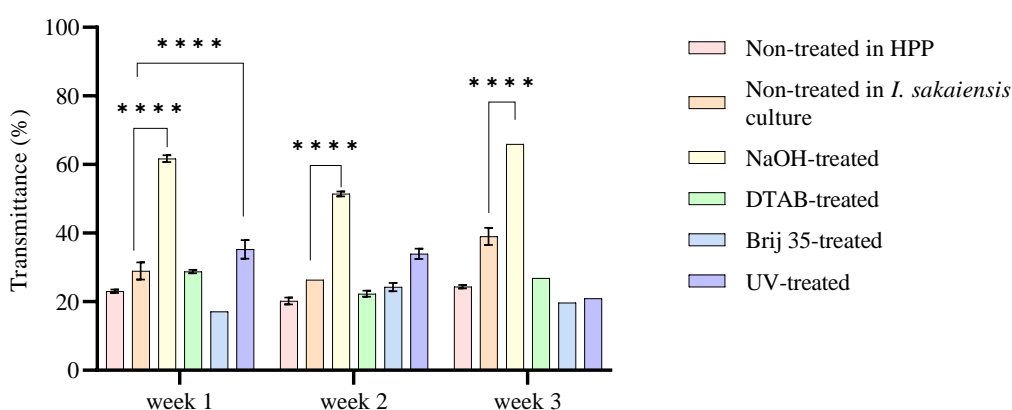


Figure 3.4. FTIR transmittance percentages of carbonyl group after pre-treatment of PET samples and inoculation in HPP in the presence of *I. sakaiensis* culture over three weeks incubation at 30 °C. Data was analysed using a two-way ANOVA with post hoc. Tukey's multiple comparisons test (n=3, P < 0.0001 (****)).

3.1.2.1.2. PET pre-treatment profile in YSV medium

According to the four pre-treatments on PET in YSV medium, Fig 3.5, the prominent changes in the transmittance percentage of carbonyl group (C=O) were related to the DTAB, Brij-35 and NaOH-treated PET, respectively. After subjecting the PET to DTAB treatment, an enhancement in transmittance percentage was observed, increasing from 17.21 to 74.83 within a week. The transmittance percentage of carbonyl group after DTAB treatment increased to 75.72 by the third week.

Following the PET treatment by Brij-35, the transmittance percentage rose to 65.86 after one week. The transmittance percentage of carbonyl group after Brij-35 pre-treatments showed a decrease trend over the three weeks.

The transmittance percentage of carbonyl group after NaOH treatment reached 51.48 in a week. This enhancement continued to progress over the course of two weeks, resulting in an increase to 71.88. The transmittance percentage remained stable throughout the subsequent three-week period.

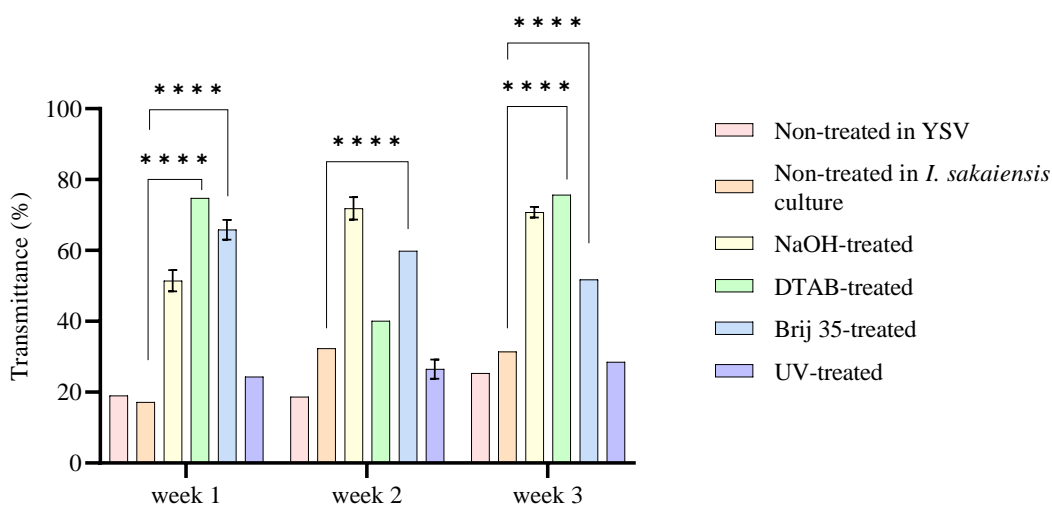


Figure 3.5. FTIR transmittance percentages of carbonyl group after pre-treatment of PET samples and inoculation in YSV in the presence of *I. sakaiensis* culture over three weeks incubation at 30 °C. Data was analysed using a two-way ANOVA with post hoc. Tukey's multiple comparisons test (n=3, P < 0.0001 (****)).

3.1.2.1.3. PET pre-treatment profile in M9 minimal medium

Based on four pre-treatments of PET in M9 minimal medium, Fig 3.6, the significant alteration was in the transmittance percentage of carbonyl group after NaOH and DTAB treatment, respectively. There were notable changes from 33.32 to 53.04 in

carbonyl functional group transmittance after NaOH treatment in a week of incubation. After two weeks, the transmittance percentage of carbonyl group gradually increased until it reached 60.14. This level of transmittance remained constant throughout the following three weeks.

Following one week of incubation, the transmittance percentage of carbonyl group after the DTAB treatment reached 39.03. Subsequently, there was an increase in transmittance percentages after two weeks, with a rise to 44.94. Encouragingly, this level of transmittance remained stable over the subsequent three-week period.

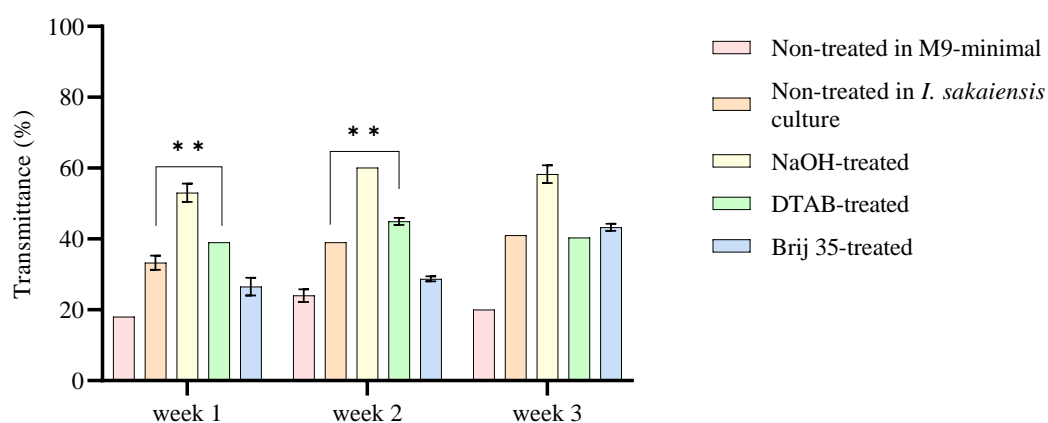


Figure 3.6. FTIR transmittance percentages of carbonyl group after pre-treatment of PET samples and inoculation in M9-minimal in the presence of *I. sakaiensis* culture over three weeks incubation at 30 °C.

Data was analysed using a two-way ANOVA with post hoc. Tukey's multiple comparisons test (n=3, P < 0.01 (**)).

3.1.2.2. PET FTIR profile of samples based on pre-treatment

3.1.2.2.1. NaOH-treatment

Considering the NaOH treatment in all three media, Fig 3.7, the most alteration in the transmittance percentage of carbonyl group was related to YSV medium. Significant changes were observed in the carbonyl group of PET samples after two weeks of treatment. The transmittance percentages after NaOH treatment in YSV changed from 51.48 to 71.88 after two weeks of incubation. After three weeks there was no significant change in the transmittance percentages of PET pieces treated by NaOH in YSV in comparison with week two.

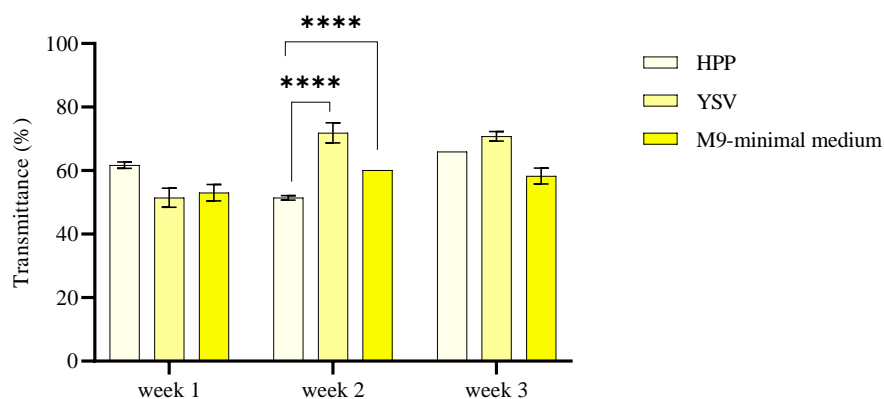


Figure 3.7. FTIR transmittance percentages of carbonyl functional group after NaOH treatment of PET samples and inoculation by HPP, YSV and M9 minimal medium in the presence of *I. sakaiensis* culture over three weeks incubation at 30 °C.

Data was analysed using a two-way ANOVA with post hoc. Tukey's multiple comparisons test (n=3, $P < 0.0001$ (****)).

3.1.2.2.2. DTAB treatment

According to DTAB treatment of PET in all three media, Fig 3.8, the significant change can be seen in the transmittance percentage of carbonyl group of PET in YSV medium. The transmittance percentages after DTAB treatment in YSV changed to 74.83 after one week of incubation. After three weeks there was no significant change in the transmittance percentages of PET pieces treated by DTAB in YSV in comparison with week one.

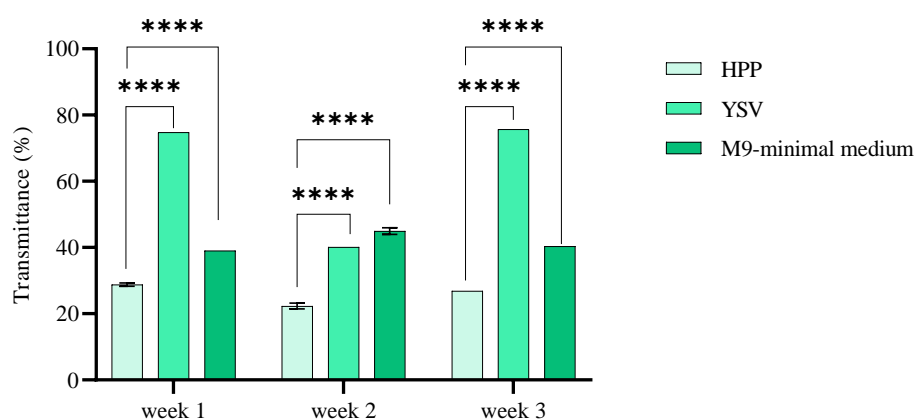


Figure 3.8. FTIR transmittance percentages of carbonyl group after DTAB treatment of PET samples and inoculation by HPP, YSV and M9 minimal medium and *I. sakaiensis* culture after three weeks incubation at 30 °C.

Data was analysed using a two-way ANOVA with post hoc. Tukey's multiple comparisons test (n=3, $P < 0.0001$ (****)).

3.1.2.2.3. Brij-35 treatment

Based on Brij-35 treatment of PET in all three media, Fig 3.9, the most alteration in the intensity of spectra on Brij-35-treated PET was related to YSV. The treatment of PET samples with Brij-35 resulted significant changes in the transmittance percentage of carbonyl group within a week. Notably, the transmittance percentages after undergoing Brij-35 treatment in YSV medium, exhibited a remarkable increase to 65.86 following one week of incubation. However, as the three-week approached, a downward trend in the transmittance percentages of the Brij-35-treated PET pieces in YSV became apparent.

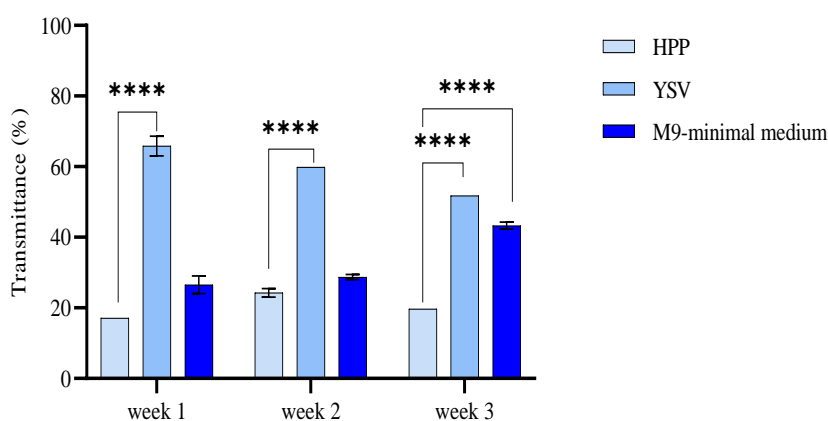


Figure 3.9. FTIR transmittance percentages of carbonyl group after Brij-35 treatment of PET samples and inoculation by HPP, YSV and M9 minimal medium and *I. sakaiensis* culture over three weeks incubation at 30 °C.

Data was analysed using a two-way ANOVA with post hoc. Tukey's multiple comparisons test (n=3, $P < 0.0001$ (****)).

3.1.2.2.4. UV treatment

Considering the UV treatment in all three media, fig 3.10, the most alteration in the intensity of spectra on UV-treated PET was related to HPP. Significant changes were observed in the carbonyl group of PET samples after the treatments within one week. The transmittance percentages after UV treatment in HPP changed to 35.26 after one week of incubation. By week three, there was a decrease trend in the transmittance percentages of PET pieces treated by UV in HPP.

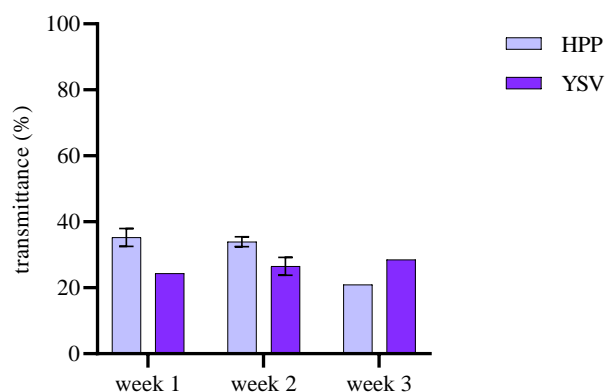


Figure 3.10. FTIR transmittance percentages of each functional group after Brij-35- treatment of PET samples and inoculation by HPP and YSV and *I. sakaiensis* culture after three weeks incubation at 30 °C.

Data was analysed using a two-way ANOVA with post hoc. Tukey's multiple comparisons test (n=3).

3.1.2.3. Comprehensive tables of data

Tables 3.1, 3.2 and 3.3 are provided a consolidated presentation of the transmittance percentage of all functional groups of PET before pre-treatment (non-treated PET in medium and non-treated PET in the presence of *I. sakaiensis* culture) and after pre-treatment of PET (NaOH, DTAB, Brij-35 and UV) in three media (HPP, YSV and M9 minimal medium) over three weeks, respectively.

The transmittance percentages are presented for the following wavenumbers (functional groups); 3391 cm^{-1} (O-H), 2920 cm^{-1} (C-H), 1713 cm^{-1} (C=O), 1240 cm^{-1} (C-O aromatic), 1093 cm^{-1} (C-O aliphatic), 873 cm^{-1} (C-H aliphatic) and 724 cm^{-1} (C-H aromatic). The significant alterations in intensity are identified by red.

Table 3.1 illustrates that the prominent alteration in the transmittance percentage of the functional group in the first week was related to DTAB-treated PET in YSV medium. Regarding table 3.2 in the second week the most remarkable result was related to NaOH-treated PET in YSV medium. However, the significant result was obtained from DTAB-treated PET after three weeks of incubation in YSV medium (Table 3.3).

Table 3.1. Transmittance percentages of non-treated and treated (NaOH, DTAB, Brij-35 and UV) PET samples after one week inoculation in HPP, YSV and M9 minimal medium and *I. sakaiensis* culture at 30 °C.

The transmittance percentages presented in the following wavenumbers (functional groups); 3391 cm⁻¹ (O-H), 2920 cm⁻¹ (C-H), 1713 cm⁻¹ (C=O), 1240 cm⁻¹ (C-O aromatic), 1093 cm⁻¹ (C-O aliphatic), 873 cm⁻¹ (C-H aliphatic) and 724 cm⁻¹ (C-H aromatic). The significant alterations in intensity are identified by red.

Transmittance (%)																						
Medium		HPP						YSV						M9								
Treatments		3391 (O-H)	2920 (C-H)	1713 (C=O)	1240 (C-O aromatic)	1093 (C-O aliphatic)	873(C-H aliphatic)	724(C-H aromatic)	3391 (O-H)	2920 (C-H)	1713 (C=O)	1240 (C-O aromatic)	1093 (C-O aliphatic)	873 (C-H aliphatic)	724 (C-H aromatic)	3391 (O-H)	2920 (C-H)	1713 (C=O)	1240 (C-O aromatic)	1093 (C-O aliphatic)	873 (C-H aliphatic)	724 (C-H aromatic)
Non-treated PET in medium	-	90.65	23.02	17.11	22.41	66.92	18.15	-	94.15	19.05	13.03	18.94	67.76	14.14	-	91.17	18.05	12.69	17.97	65.65	13.50	
Non-treated PET in <i>I. sakaiensis</i> culture	-	89.87	28.95	23.41	28.35	69.82	23.70	-	90.82	17.21	11.79	17.16	63.99	13.25	-	94.15	33.32	26.08	30.67	72.17	25.75	
NaOH-treated PET in <i>I. sakaiensis</i> culture	-	95.83	61.71	59.04	61.93	86.19	57.55	-	95.45	51.48	46.82	50.31	80.50	43.93	-	94.96	53.04	50.43	53.74	82.09	48.31	
DTAB-treated PET in <i>I. sakaiensis</i> culture	-	92.65	28.79	23.27	28.15	69.84	23.61	96.20	99.93	74.83	57.13	58.75	87.22	46.41	97.92	92.76	39.03	28.36	33.34	78.66	24.24	
Brij 35-treated PET in <i>I. sakaiensis</i> culture	-	90.44	17.14	11.85	17.47	65.54	13.25	92.97	93.35	65.86	51.8	53.65	79.30	43.60	-	93.39	26.54	21.65	27.00	70.26	22.13	
UV-treated PET in <i>I. sakaiensis</i> culture	-	93.14	35.26	30.30	34.75	73.57	30.07	-	93.34	24.34	17.51	21.35	66.19	15.96	N/A	N/A	N/A	N/A	N/A	N/A	N/A	

Table 3.2. Transmittance percentages of non-treated and treated (NaOH, DTAB, Brij-35 and UV) PET samples after two week inoculation in HPP, YSV and M9 minimal medium and *I. sakaiensis* culture at 30 °C.

The transmittance percentages are presented in the following wavenumbers (functional groups); 3391 cm⁻¹ (O-H), 2920 cm⁻¹ (C-H), 1713 cm⁻¹ (C=O), 1240 cm⁻¹ (C-O aromatic), 1093 cm⁻¹ (C-O aliphatic), 873 cm⁻¹ (C-H aliphatic) and 724 cm⁻¹ (C-H aromatic). The significant alterations in intensity are identified by red.

Transmittance (%)																						
Medium		HPP						YSV						M9								
Treatments		3391 (O-H)	2920 (C-H)	1713 (C=O)	1240 (C-O aromatic)	1093 (C-O aliphatic)	873 (C-H aliphatic)	724 (C-H aromatic)	3391 (O-H)	2920 (C-H)	1713 (C=O)	1240 (C-O aromatic)	1093 (C-O aliphatic)	873 (C-H aliphatic)	724 (C-H aromatic)	3391 (O-H)	2920 (C-H)	1713 (C=O)	1240 (C-O aromatic)	1093 (C-O aliphatic)	873 (C-H aliphatic)	724 (C-H aromatic)
Wavenumber (cm ⁻¹)	(Functional groups)																					
Non-treated PET in medium		-	92.89	20.18	14.47	19.78	66.20	14.87	-	92.17	18.71	12.69	17.93	65.01	14.85	-	93.26	24.00	17.63	22.74	67.78	17.42
Non-treated PET in <i>I. sakaiensis</i> culture		-	93.89	26.34	21.80	27.14	70.84	22.83	-	94.40	32.39	24.29	28.99	70.93	21.43	-	91.71	39.00	12.69	18.20	64.61	13.93
NaOH-treated PET in <i>I. sakaiensis</i> culture		-	94.27	51.42	48.51	51.79	80.45	46.86	-	97.72	71.88	65.98	68.10	88.51	63.10	-	97.22	60.14	56.97	59.94	84.68	55.92
DTAB-treated PET in <i>I. sakaiensis</i> culture		-	93.02	22.33	15.98	21.29	68.25	15.97	-	93.60	40.09	34.65	39.82	77.45	35.05	99.32	95.16	44.94	37.64	41.32	76.81	34.01
Brij 35-treated PET in <i>I. sakaiensis</i> culture		-	93.03	24.28	17.75	22.79	67.65	16.78	95.00	92.39	59.84	45.47	48.10	78.85	36.63	-	87.74	28.74	19.38	24.24	67.85	17.90
UV-treated PET in <i>I. sakaiensis</i> culture		-	94.38	33.97	25.03	29.26	70.34	21.86	-	93.34	26.51	19.51	24.33	68.73	17.91	N/A	N/A	N/A	N/A	N/A	N/A	N/A

Table 3.3. Transmittance percentages of non-treated and treated (NaOH, DTAB, Brij-35 and UV) PET samples after three weeks inoculation in HPP, YSV and M9 minimal medium and *I. sakaiensis* culture at 30 °C.

The transmittance percentages are presented in the following wavenumbers (functional groups); 3391 cm⁻¹ (O-H), 2920 cm⁻¹ (C-H), 1713 cm⁻¹ (C=O), 1240 cm⁻¹ (C-O aromatic), 1093 cm⁻¹ (C-O aliphatic), 873 cm⁻¹ (C-H aliphatic) and 724 cm⁻¹ (C-H aromatic). The significant alterations in intensity are identified by red.

Transmittance (%)																						
Medium		HPP							YSV							M9						
Treatments		3391 (O-H)	2920 (C-H)	1713 (C=O)	1240 (C-O aromatic)	1093 (C-O aliphatic)	873 (C-H aliphatic)	724 (C-H aromatic)	3391 (O-H)	2920 (C-H)	1713 (C=O)	1240 (C-O aromatic)	1093 (C-O aliphatic)	873 (C-H aliphatic)	724 (C-H aromatic)	3391 (O-H)	2920 (C-H)	1713 (C=O)	1240 (C-O aromatic)	1093 (C-O aliphatic)	873 (C-H aliphatic)	724 (C-H aromatic)
Wavenumber (cm ⁻¹) (Functional groups)		3391 (O-H)	2920 (C-H)	1713 (C=O)	1240 (C-O aromatic)	1093 (C-O aliphatic)	873 (C-H aliphatic)	724 (C-H aromatic)	3391 (O-H)	2920 (C-H)	1713 (C=O)	1240 (C-O aromatic)	1093 (C-O aliphatic)	873 (C-H aliphatic)	724 (C-H aromatic)	3391 (O-H)	2920 (C-H)	1713 (C=O)	1240 (C-O aromatic)	1093 (C-O aliphatic)	873 (C-H aliphatic)	724 (C-H aromatic)
Non-treated PET in medium		-	91.62	24.38	18.21	24.03	69.10	19.71	-	96.65	2.40	48.04	51.51	82.51	45.58	-	95.31	20.00	37.81	43.46	82.19	38.87
Non-treated PET in <i>I. sakaiensis</i> culture		-	93.90	39.02	31.02	35.12	74.26	29.00	-	95.19	31.43	21.83	25.35	77.32	21.55	-	92.90	41.00	12.70	18.38	66.75	13.84
NaOH-treated PET in <i>I. sakaiensis</i> culture		-	94.52	65.95	63.45	66.15	87.14	62.66	96.65	96.03	70.78	63.08	65.09	85.96	58.08	96.98	94.89	58.27	53.92	56.49	81.42	50.81
DTAB-treated PET in <i>I. sakaiensis</i> culture		-	90.39	26.86	18.72	23.39	67.28	17.61	95.00	95.32	75.72	67.04	69.90	93.12	57.74	-	93.70	40.34	31.38	36.19	78.69	26.45
Brij 35-treated PET in <i>I. sakaiensis</i> culture		-	88.08	19.73	13.49	18.95	64.92	14.38	-	93.21	51.75	45.01	49.51	85.09	41.34	-	93.63	43.26	37.47	41.24	20.81	36.17
UV-treated PET in <i>I. sakaiensis</i> culture		-	89.65	20.93	14.49	19.94	66.68	14.88	-	101.00	28.57	21.62	27.52	74.98	20.16	N/A	N/A	N/A	N/A	N/A	N/A	N/A

3.1.3. Pre-treated PET biofilm profile in the presence of *I. sakaiensis*

In the first week, the sequence of biofilm formation from the highest to the lowest concentration on the PET in the presence of *I. sakaiensis* in HPP was on samples treated with Brij-35, DTAB, UV and NaOH. The OD₅₇₀ for Brij-35, DTAB, UV and NaOH treatment in HPP were 0.23, 0.20, 0.16 and 0.15, respectively. The biofilm formation on Brij-35, DTAB and UV decreased by passing weeks. NaOH-treated PET increased for the first two weeks. No change was detected in week three (Fig 3.11, 3.12 and 3.13).

In the first week, the order of biofilm formation on the samples in presence of *I. sakaiensis* in YSV was: UV, Brij-35, DTAB, and NaOH-treated PET. The biofilm formation on Brij-35, DTAB and UV treated samples decreased by passing weeks. NaOH-treated PET increased for two week and no change was observed in week three (Fig 3.11, 3.12 and 3.13).

In the first week, the highest biofilm formation in presence of *I. sakaiensis* in M9 was on DTAB and NaOH-treated PET respectively. The biofilm formation on NaOH treated samples decreased by passing weeks. DTAB and Brij-35-treated PET biofilm increased for the first two weeks and decreased in week three (Fig 3.11, 3.12 and 3.13).

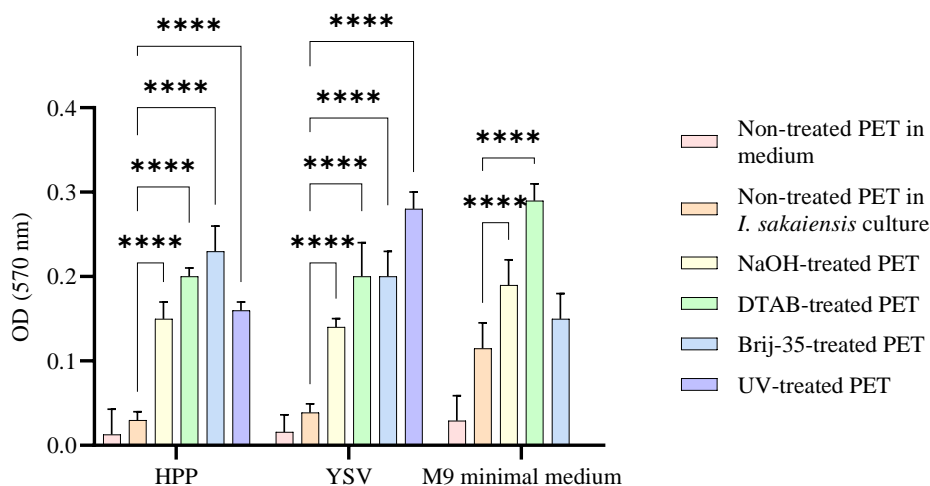


Figure 3.11. The biofilm formation on non-treated and treated (NaOH, DTAB, Brij-35 and UV) PET samples were inoculated in HPP, YSV and M9 minimal medium with *I. sakaiensis*, and were incubated at 30 °C for one week. (n=8, P < 0.0001 (****)).

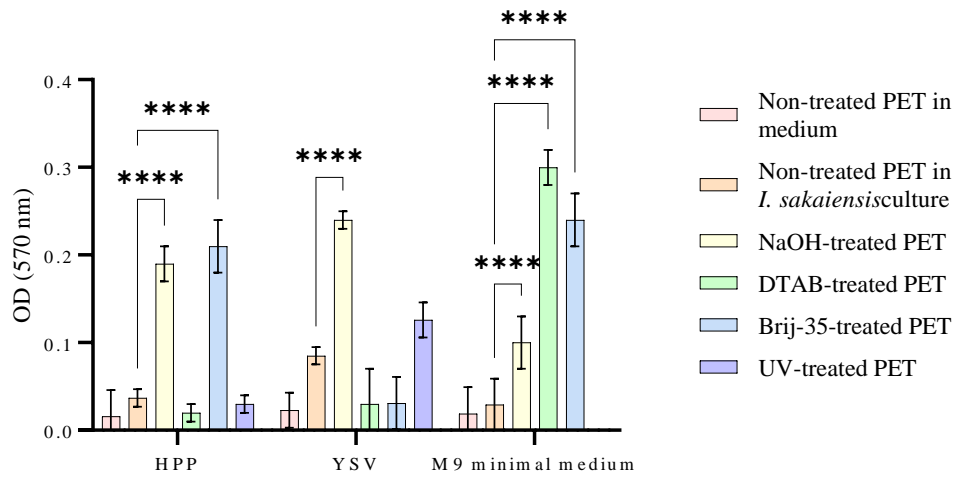


Figure 3.12. The biofilm formation on non-treated and treated (NaOH, DTAB, Brij-35 and UV) PET samples were inoculated in HPP, YSV and M9 minimal medium with *I. sakaiensis*, and were incubated at 30 °C for two week. (n=8, P < 0.0001 (****)).

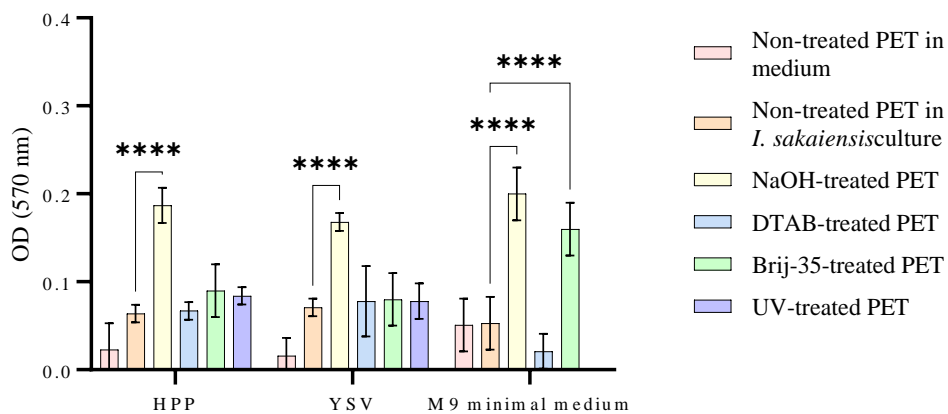


Figure 3.13. The biofilm formation on non-treated and treated (NaOH, DTAB, Brij-35 and UV) PET samples were inoculated in HPP, YSV and M9 minimal medium with *I. sakaiensis*, and were incubated at 30 °C for three weeks. (n=8, P < 0.0001 (***)).

3.1.4. Pre-treated PET FTIR profile in the presence of *P. mendocina*

3.1.4.1. PET FTIR profile for different media

3.1.4.1.1. PET pre-treatment profile in HPP medium

Considering all four pre-treatment methods in HPP medium (Fig 3.14), the most alteration in the transmittance percentage of carbonyl group was related to the NaOH-treated PET in *P. mendocina* culture. The transmittance percentages related to NaOH treatment changed from 32.59 to 46.75 within a week.

3.1.4.1.2. PET pre-treatment profile in YSV medium

According to all four pre-treatment methods in YSV medium (Fig 3.14), the prominent changes in the transmittance percentage of carbonyl group were related to the Brij-35 and NaOH treatments. The transmittance percentages altered from 24.01 to 40.71 after Brij-35 treatment on PET after one week of incubation. Also, the transmittance percentages after NaOH treatment reached 39.84.

3.1.4.1.3. PET pre-treatment profile in M9 minimal medium

Based on all four pre-treatment methods in M9 minimal medium (Fig 3.14), the notable changes in the transmittance percentage of carbonyl group were related to the NaOH, DTAB and UV treatment. The transmittance percentages altered from 31.76 to 58.33 after NaOH treatment of PET within a week. The transmittance percentages related to DTAB reached 55.88. Besides, the UV treatment percentage reached 45.71. Figure 3.14 provides the profile of different treatments of PET in HPP, YSV and M9 minimal medium in the presence of *P. mendocina* after one week of incubation.

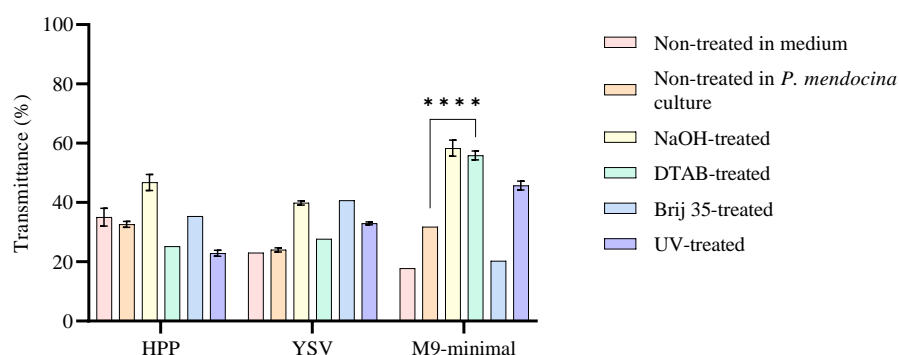


Figure 3.14. FTIR transmittance percentages of carbonyl group after pre-treatment of PET samples and inoculation in HPP, YSV and M9-minimal in the present of *P. mendocina* culture after one week incubation at 30 °C.

Data was analysed using a two-way ANOVA with post hoc. Tukey's multiple comparisons test (n=3, $P < 0.0001$ (****)).

3.1.4.2. PET FTIR profile based on pre-treatment

In this section the results are presented in bar charts based on the treatments including NaOH, DTAB, Brij-35 and UV.

3.1.4.2.1. NaOH treatment

Considering the NaOH treatment in all three media, Fig 3.15, the most alteration in the transmittance percentage of carbonyl group was related to M9 minimal medium. The transmittance percentages after NaOH treatment in M9 minimal medium changed from 31.76 to 58.33 after one week of incubation.

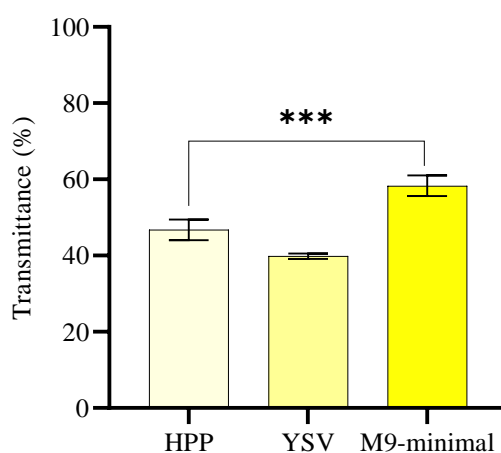


Figure 3.15. FTIR transmittance percentages of carbonyl group after NaOH-treatment of PET samples and inoculation in HPP, YSV and M9-minimal in the presence of *P. mendocina* culture after one week incubation at 30 °C. (n=3, P < 0.001 (***)).

3.1.4.2.2. DTAB treatment

Based on the DTAB treatment in all three media, Fig 3.16, the notable changes in the transmittance percentage of carbonyl group was related to M9 minimal medium. The transmittance percentages after DTAB treatment in M9 minimal medium reached 55.88 after one week of incubation.

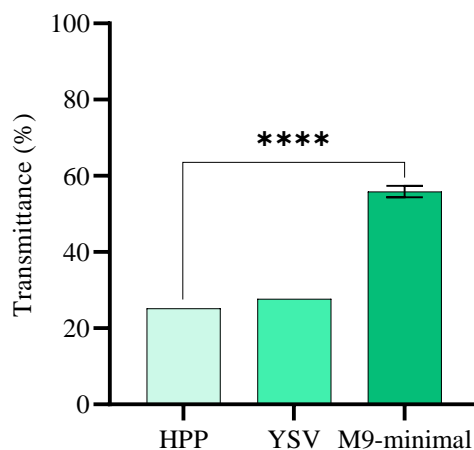


Figure 3.16. FTIR transmittance percentages of carbonyl group after DTAB-treatment of PET samples and inoculation in HPP, YSV and M9-minimal in the presence of *P. mendocina* culture after one week incubation at 30 °C. (n=3, P < 0.0001 (****)).

3.1.4.2.3. Brij-35 treatment

Based on the Brij-35 treatment in all three media, Fig 3.17, the remarkable changes in the transmittance percentage of carbonyl group was related to YSV. The transmittance percentages after Brij-35 treatment in YSV medium reached 38 after one week of incubation.

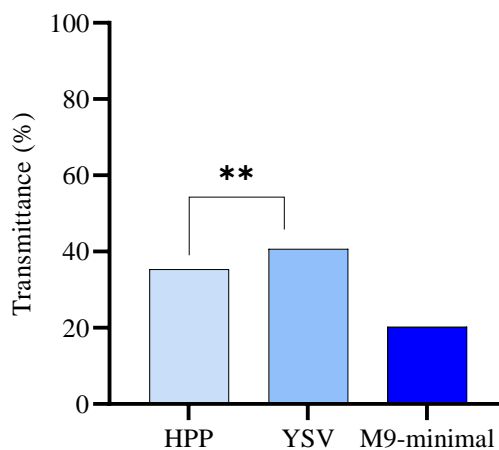


Figure 3.17. FTIR transmittance percentages of carbonyl group after Brij-35-treatment of PET samples and inoculation in HPP, YSV and M9-minimal in the presence of *P. mendocina* culture after one week incubation at 30 °C. (n=3, P < 0.01 (**)).

3.1.4.2.4. UV treatment

Based on the UV treatment in all three media, Fig 3.18, the prominent changes in the transmittance percentage of carbonyl group was related to M9 minimal medium. The transmittance percentages after UV treatment in M9 minimal medium reached 43 after one week of incubation.

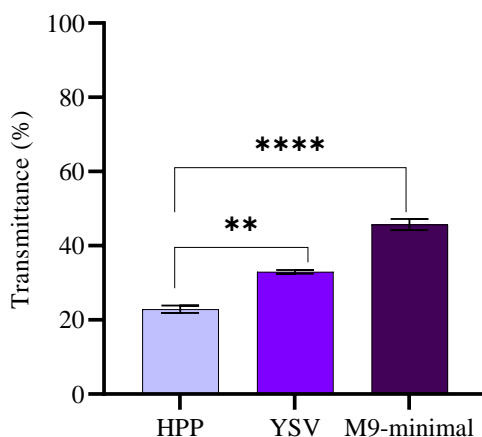


Figure 3.18. FTIR transmittance percentages of carbonyl group after UV-treatment of PET samples and inoculation in HPP, YSV and M9-minimal in the presence of *P. mendocina* culture after one week incubation at 30 °C. (n=3, P < 0.01 (**), P < 0.0001 (****)).

3.1.4.3. Comprehensive table of data

Table 3.4 is provided to show the transmittance percentage of all functional groups of PET before pre-treatment (non-treated PET in medium and non-treated PET in the presence of *P. mendocina* culture) and after pre-treatment of PET samples (NaOH, DTAB, Brij-35 and UV) in three media (HPP, YSV and M9 minimal medium) within one week.

The transmittance percentages are presented in the following wavenumbers (functional groups); 3391 cm^{-1} (O-H), 2920 cm^{-1} (C-H), 1713 cm^{-1} (C=O), 1240 cm^{-1} (C-O aromatic), 1093 cm^{-1} (C-O aliphatic), 873 cm^{-1} (C-H aliphatic) and 724 cm^{-1} (C-H aromatic). The significant alterations in intensity are identified in red.

Table 3.4 illustrates that the prominent alteration in the transmittance percentage of the functional group in the first week was related to NaOH-treated PET in M9 minimal medium.

Table 3.4. Transmittance percentages of non-treated and treated (NaOH, DTAB, Brij-35 and UV) PET samples after one week inoculation in HPP, YSV and M9 minimal medium and *P. mendocina* culture at 30 °C.

The transmittance percentages presented in the following wavenumbers (functional groups); 3391 cm⁻¹ (O-H), 2920 cm⁻¹ (C-H), 1713 cm⁻¹ (C=O), 1240 cm⁻¹ (C-O aromatic), 1093 cm⁻¹ (C-O aliphatic), 873 cm⁻¹ (C-H aliphatic) and 724 cm⁻¹ (C-H aromatic). The most alteration in intensity is identified by red.

Transmittance (%)																						
Medium		HPP						YSV						M9								
Treatments																						
Wavenumber (cm ⁻¹) (Functional groups)		3391 (O-H)	2920 (C-H)	1713 (C=O)	1240 (C-O aromatic)	1093 (C-O aliphatic)	873 (C-H aliphatic)	724 (C-H aromatic)	3391 (O-H)	2920 (C-H)	1713 (C=O)	1240 (C-O aromatic)	1093 (C-O aliphatic)	873 (C-H aliphatic)	724 (C-H aromatic)	3391 (O-H)	2920 (C-H)	1713 (C=O)	1240 (C-O aromatic)	1093 (C-O aliphatic)	873 (C-H aliphatic)	724 (C-H aromatic)
Non-treated PET in medium	-	94.38	35.05	29.71	33.68	73.70	27.84	-	94.24	23.08	18.40	21.45	68.56	19.31	-	92.49	17.75	13.59	19.04	65.10	13.77	
Non-treated PET in <i>P. mendocina</i> culture	-	94.11	32.59	24.22	28.47	70.63	21.07	-	92.56	24.01	18.79	23.75	68.16	19.50	-	94.47	31.76	24.16	28.43	70.95	21.09	
NaOH-treated PET in <i>P. mendocina</i> culture	99.78	94.00	46.75	42.86	46.92	79.04	40.85	-	93.81	39.84	36.57	40.84	75.19	35.61	-	96.49	58.33	55.49	58.43	84.67	54.02	
DTAB-treated PET in <i>P. mendocina</i> culture	-	93.52	25.20	18.89	24.04	69.57	18.40	-	92.56	27.74	21.50	27.53	74.55	21.28	99.34	95.75	55.88	49.53	52.87	82.08	48.95	
Brij 35-treated PET in <i>P. mendocina</i> culture	-	94.66	35.37	30.50	35.07	73.94	29.89	-	94.24	40.71	36.05	40.03	67.48	35.80	-	93.36	20.25	14.01	19.53	66.61	14.77	
UV-treated PET in <i>P. mendocina</i> culture	-	93.10	22.91	16.12	21.38	67.27	15.90	-	94.56	32.97	27.36	32.08	70.51	26.77	-	95.25	45.71	40.62	39.69	70.65	32.27	

3.1.5. Pre-treated PET biofilm profile in the presence of *P. mendocina*

The highest biofilm concentration in HPP medium was on NaOH-treated and Brij-35-treated PET in the presence of *P. mendocina* after one week of incubation. The OD₅₇₀ reached 0.26 and 0.25 after NaOH and Brij-35 treatment, respectively.

The highest biofilm concentration in YSV medium was on NaOH and DTAB in which the OD₅₇₀ reached 0.26 and 0.24, respectively.

The notable biofilm formation in M9 minimal medium was on DTAB-treated PET in which the OD₅₇₀ reached 0.52 after the treatment (Fig 3.19).

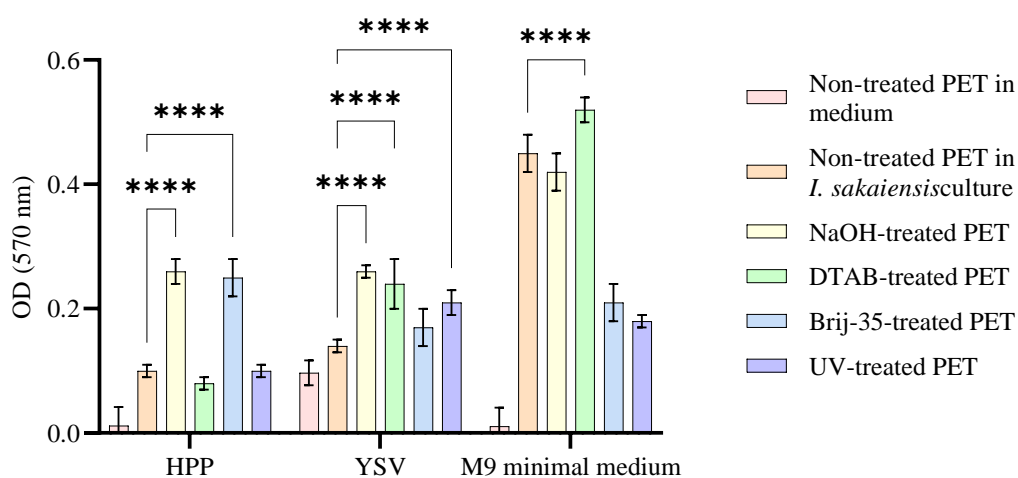


Figure 3.19. The biofilm formation on non-treated and treated (NaOH, DTAB, Brij-35 and UV) PET samples were inoculated in HPP, YSV and M9 minimal medium with *P. mendocina*, and were incubated at 30 °C for one week.

Data was analysed using a two-way ANOVA with post hoc. Tukey's multiple comparisons test ((n=8, $P < 0.0001$ (****))).

Chapter 3.2. Effect of DTAB treatment (in large scale) on PET biodegradation

3.2. Overview

In chapter one, the optimal conditions for PET biodegradation were found to be the DTAB-treated PET films in the presence of *I. sakaiensis* in YSV medium. However, experiments were done at small scale (6-well plate). In this chapter, further investigation is carried out by designing the experiments in a scale-up setup (500 ml shaken flask).

This chapter concerns the scale-up experiment of DTAB-treated PET films. The treatments that were investigated included non-treated PET and DTAB-treated PET in the presence of *I. sakaiensis* or *P. mendocina*. The experiment was run for eight weeks and the samples were taken in weeks one, four and eight. However, the DTAB-treated PET samples completely dissolved by four weeks. So, the FTIR and biofilm assay were done on samples after one week of incubation. The HPLC was run for all samples.

3.2.1. Effect of DTAB treatment on PET degradation: FTIR results

The FTIR spectra showed significant changes in the carbonyl group peak intensities related to PET samples in the presence of *I. sakaiensis* compared to *P. mendocina*. Also, the spectra indicated that DTAB treatment have a significant effect on the functional groups of PET after one week of incubation in the presence of *I. sakaiensis*. However, as PET film was dissolved by week four, FTIR was not a sufficient method for investigating the effect of DTAB treatment on PET degradation. Nonetheless, the transmittance percentage of the carbonyl group was measured for both DTAB-treated and non-treated PET samples after week one. In the presence of *I. sakaiensis*, the transmittance percentage of the carbonyl group in DTAB-treated and non-treated PET samples was 62.2 and 43 respectively, after one week. On the other hand, in the presence of *P. mendocina*, the transmittance percentage of the carbonyl group in DTAB-treated and non-treated PET samples was 18.82 and 19.14, respectively, after one week. These results suggest that DTAB treatment may not affect significantly the functional groups of PET in the presence of *P. mendocina*, but it enhances the degradation of PET in the presence of *I. sakaiensis* during the early of incubation (Fig 3.20). However, further investigations using complementary analytical techniques such as HPLC is necessary to obtain a more comprehensive understanding of the underlying mechanisms of DTAB treatment-mediated PET degradation after four and eight weeks.

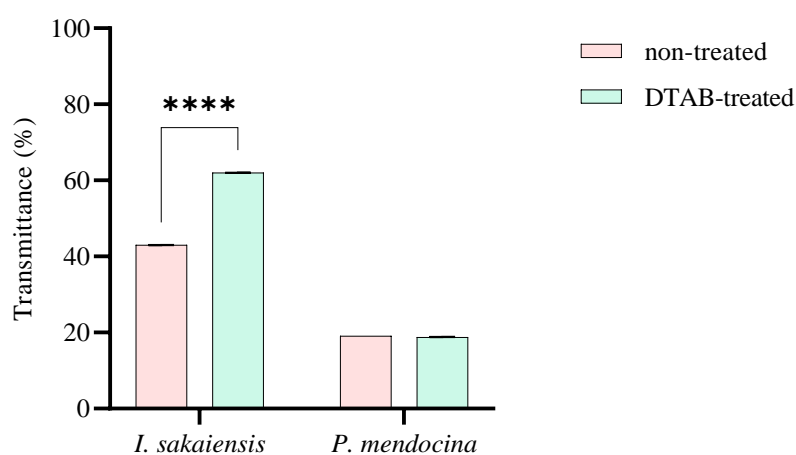


Figure 3.20. The carbonyl percentage of non-treated and DTAB-treated PET samples inoculated in YSV medium in the presence of *P. mendocina*, or *I. sakaiensis*. Cultures were incubated at 30 °C for one week. Data was analysed using a two-way ANOVA with post hoc. Tukey's multiple comparisons test (n=3, $P < 0.0001$ (****)).

3.2.2. Effect of DTAB treatment on PET degradation: biofilm results

The biofilm assay results revealed that DTAB treatment had a significant impact on PET degradation in the presence of *I. sakaiensis* during the scale-up experiment. The OD₅₇₀ of the biofilm was measured after incubating the samples for one week. The OD₅₇₀ of the DTAB-treated PET pieces was observed to be 0.15 after one week of incubation, which was significantly higher than the OD₅₇₀ of non-treated PET pieces (0.07) (Fig 3.21). These results indicate that DTAB treatment was effective in promoting biofilm formation on the PET surface during the early stages of incubation.

The results of the biofilm assay demonstrated that DTAB treatment did not have a significant impact on PET degradation in the presence of *P. mendocina* during the scale-up experiment. The OD₅₇₀ of the biofilm was measured after incubating the samples for one week. The OD₅₇₀ of the DTAB-treated PET pieces was observed to be 0.02 which was not significantly different from the OD₅₇₀ of non-treated PET pieces (0.04) (Fig 3.21). These results suggest that DTAB treatment may not be an effective approach for promoting PET degradation in the presence of *P. mendocina*. However, further investigations using complementary techniques such as FTIR spectroscopy and HPLC provide a more comprehensive understanding of the underlying mechanisms and potential limitations of DTAB treatment in promoting PET degradation.

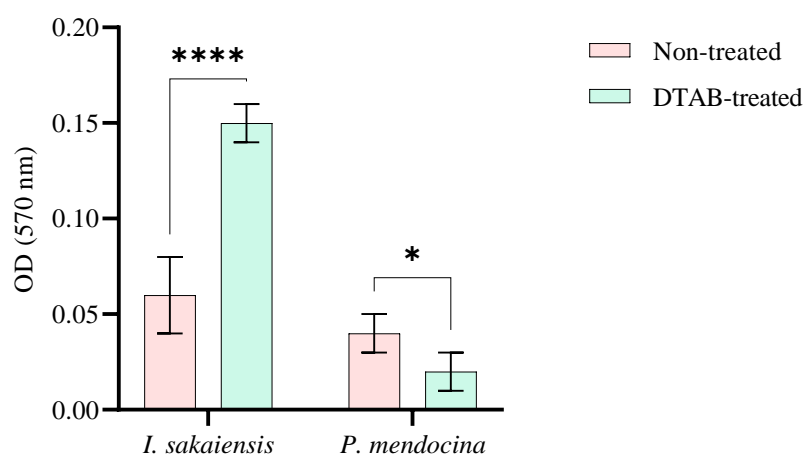


Figure 3.21. The biofilm formation on non-treated and DTAB-treated PET samples. Cultures were inoculated in YSV medium in the presence of *P. mendocina*, and *I. sakaiensis*, and were incubated at 30 °C for one week.

Data was analysed using a two-way ANOVA with post hoc. Tukey's multiple comparisons test (n=8, $P < 0.05$ (*), $P < 0.0001$ (****)).

3.2.3. Effect of DTAB treatment on PET degradation: HPLC results

HPLC analysis was conducted to investigate the presence of TPA in all samples, which is an indicator of PET depolymerization to its monomers. TPA calibration curve was provided using TPA standards, with concentrations ranging 1.2, 2.5, 5, 8, 10, 12, 15, 20 $\mu\text{g/ml}$. HPLC was done on all the cited concentrations. The area of the peaks for the above concentrations was calculated and the obtained values were used to derive the following equation: $Y = 19.137x + 1.6917$ with an R-squared value of 1 (Fig 3.22). The retention time of TPA was found to be approximately 6.46 minutes. Figures 3.23 shows the HPLC results related to YSV medium.

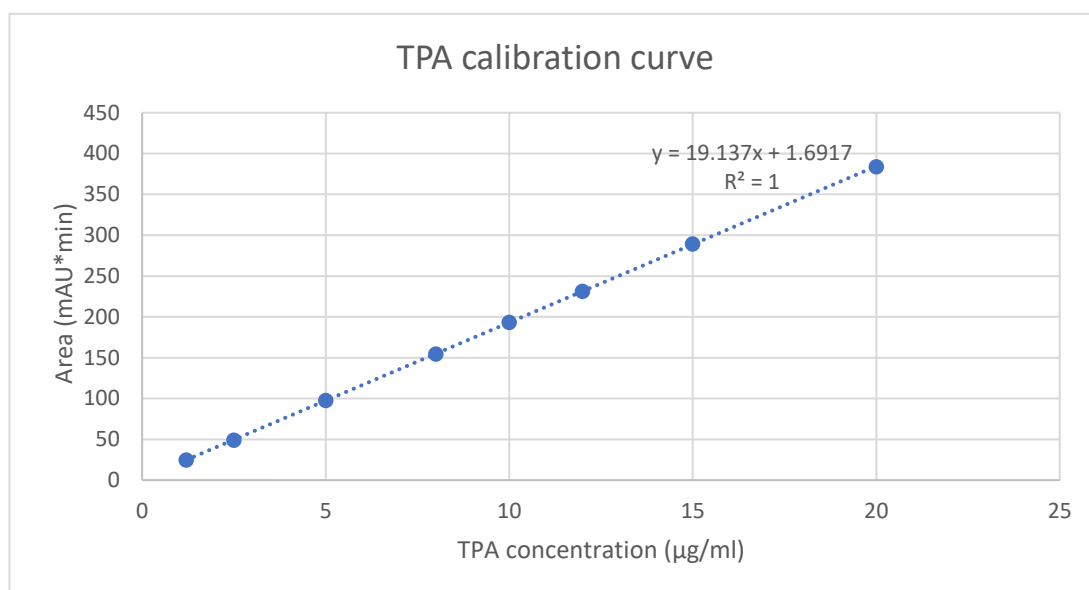


Figure 3.22. TPA calibration curve. The area related to different TPA concentrations containing 1.2, 2.5, 5, 8, 10, 12, 15, 20 $\mu\text{g/ml}$ were collected by HPLC.



Figure 3.23. Chromatograms of YSV medium.

Figures 3.24 and 3.25 show the HPLC results related to non-treated and DTAB-treated PET samples in the presence of *I. sakaiensis* and *P. mendocina* over eight weeks of incubation, respectively. As can be seen in figure 3.24, the spectra related to *I. sakaiensis* show the TPA peaks (red arrow) after treating PET samples with DTAB over week four and eight. However, the spectra related to *P. mendocina* did not show any peaks related to the TPA (Fig 3.25).

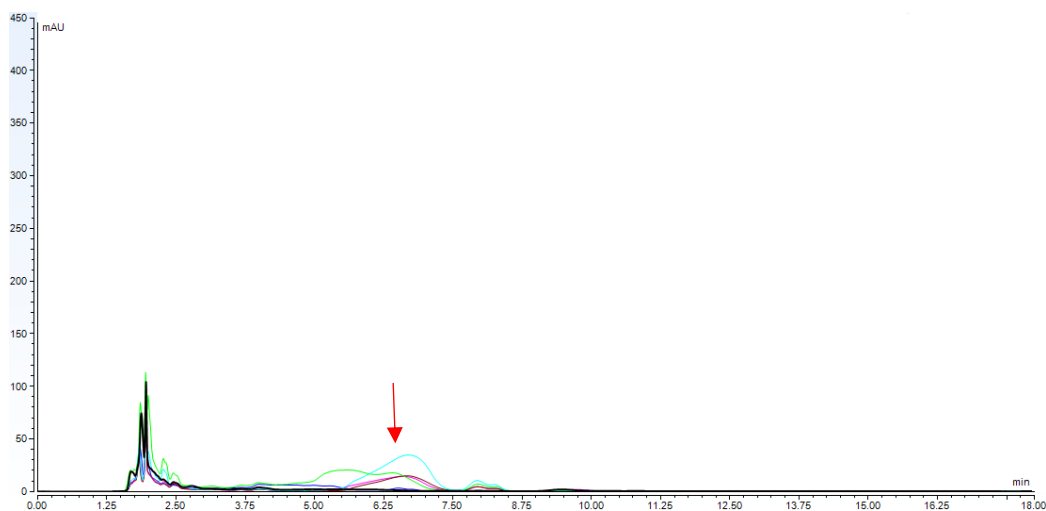


Figure 3.24. Chromatograms of non-treated and DTAB-treated PET samples after incubation in the presence of *I. sakaiensis* over eight weeks.

The samples were taken in week one, four and eight. TPA concentrations investigated by comparing with TPA calibration chromatograms and curves. Non-treated week one (black), DTAB-treated week one (dark blue), non-treated week four (pink), DTAB-treated week four (brown), non-treated week eight (green), DTAB-treated week eight (blue).



Figure 3.25. Chromatograms of non-treated and DTAB-treated PET samples after incubation in the presence of *P. mendocina* over eight weeks.

The samples were taken in week one, four and eight. TPA concentrations investigated by comparing with TPA calibration chromatograms and curves. Non-treated week one (black), DTAB-treated week one (dark blue), non-treated week four (pink), DTAB-treated week four (brown), non-treated week eight (green), DTAB-treated week eight (blue).

The amount of TPA in each sample was calculated using the following equation $Y = 19.137X + 1.6917$, and the results are presented in Fig 3.26. These results indicate the effectiveness of the DTAB treatment in the presence of *I. sakaiensis* in PET depolymerization, as evidenced by the higher levels of TPA detected in the samples treated with DTAB in comparison to the non-treated samples.

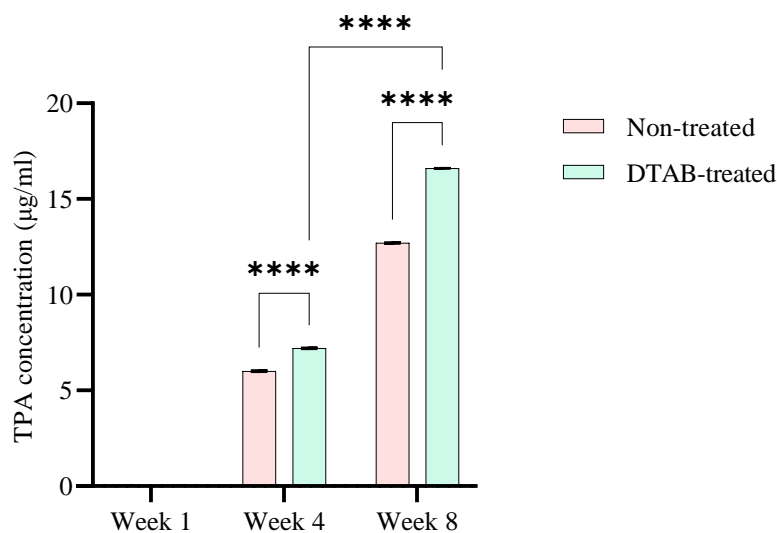


Figure 3.26. The TPA concentration ($\mu\text{g/ml}$) of non-treated and DTAB-treated PET samples were inoculated in YSV medium in the presence *I. sakaiensis* was incubated at 30 °C over eight weeks. Data was analysed using a two-way ANOVA with post hoc. Tukey's multiple comparisons test ($n=2$, $P < 0.0001$ (****)).

Chapter 3.3. Effect of *F. culmorum* supernatant treatment on PET biodegradation

3.3. Overview

This chapter aims to investigate the effects of FSC treatment on both non-treated and DTAB-treated PET films in the presence of *I. sakaiensis*. In this chapter, the term "FSC" specifically refers to the *F. culmorum* supernatant containing cutinase.

To investigate the effects of FSC treatment, the study design different scales, including a 96-well plate (200 μ l), a 6-well plate (10 ml), and a shaken flask (500 ml). The treatments subjected to investigation comprised non-treated PET, FSC-treated PET for 6-well plate experiment. In scale-up experiment and 96-well plate the treatments including non-treated PET, FSC-treated PET and FSC-DTAB treated PET all in the presence of *I. sakaiensis*. The large scale process, conducted using the 500 ml shaken flask.

The degradation of PET was studied and assessed through a variety of analytical techniques. These techniques included biofilm assay, Fourier-transform infrared spectroscopy (FTIR), high-performance liquid chromatography (HPLC), high-resolution microscopy, and scanning electron microscopy (SEM).

By exploring these aspects across different scales, the study aimed to establish a foundation for future applications of FSC-based treatments in enhancing biofilm formation, promoting PET degradation, and potentially contributing to more sustainable waste management practices.

3.3.1. Effect of *F. culmorum* supernatant and DTAB in 96-well plate: biofilm results

The effect of FSC on PET films in a 96-well plate was investigated through a series of treatments. These films were categorized into three distinct groups: non-treated, FSC-treated, and FSC-DTAB-treated. Additionally, the presence of *I. sakaiensis*, a specific microorganism, was taken into consideration during the entire incubation period. The results obtained from this study demonstrated that both the FSC treatment and FSC-DTAB treatment can enhance the biofilm formation significantly.

Specifically, when the PET films were subjected to the FSC treatment, a remarkably significant enhancement in biofilm formation was observed compared to the non-treated PET films. This enhancement was evident from the measurements of the OD₅₇₀, which increased substantially from 1.34 to 2.60 for the FSC-treated PET films.

Similarly, the FSC-DTAB treated PET films, in the presence of *I. sakaiensis* during the 24-hrs incubation period at a temperature of 30 °C, also resulted in an increase in biofilm formation. The OD₅₇₀ for FSC-DTAB-treated PET films increased from 1.34 to 2.34 (Fig 3.27). These findings indicate that both the FSC treatment and the FSC-DTAB treatment can effectively enhance biofilm formation on PET films in the presence of *I. sakaiensis* over a 24-hr period.

In conclusion, this study provides evidence for the positive effects of FSC and FSC-DTAB treatments on biofilm formation on PET films.

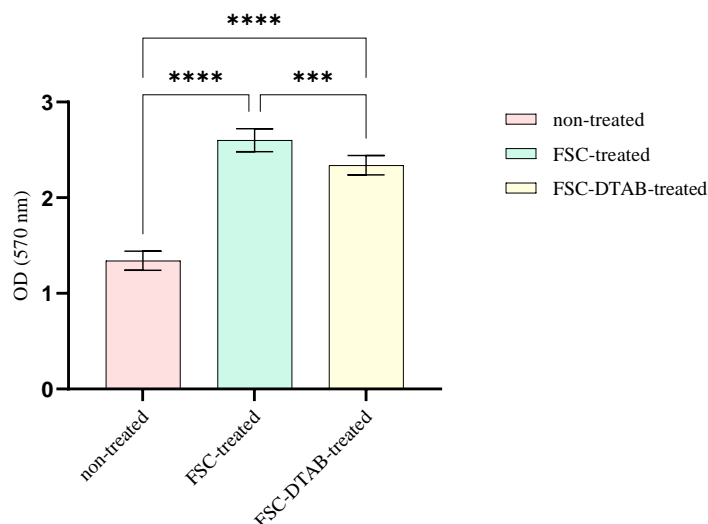


Figure 3.27. Biofilm formation on different treated PET (non, FSC, FSC-DTAB) in the presence of *I. sakaiensis* in 96-well plate after 24 hrs at 30 °C. Data was analysed using a one-way ANOVA. Dunnett's multiple comparisons test (n=8, P < 0.001 (***), P < 0.0001 (****)).

3.3.2. Effect of *F. culmorum* supernatant in 6-well plate

3.3.2.1. Effect of *F. culmorum* supernatant in 6-well plate: biofilm results

The effect of FSC on a 6-well plate was investigated over an extended period of three weeks, aiming to understand the impact of FSC treatment on biofilm formation. The experimental setup involved the incubation of PET films treated with FSC in the presence of *I. sakaiensis*.

The results obtained from this experiment shed light on the effects of FSC treatment on biofilm formation. An analysis of the data, presented in the form of a bar chart (Fig 3.28), clearly illustrated that the FSC treatment could enhance the biofilm formation compared to the non-treated PET films.

However, it is important to note that the efficacy of the FSC treatment exhibited a diminishing trend over time. In the initial week of incubation at a temperature of 30 °C, the OD₅₇₀ increased from 0.6 to 0.8 (Fig 3.28). This indicates a slight improvement in biofilm formation compared to the non-treated PET films. However, as the experiment progressed into weeks two and three, no significant changes in biofilm formation were observed. However, in comparison with week one, the less biofilm formed. These findings suggest that while the FSC treatment initially enhances biofilm formation on

PET films, its effectiveness gradually diminishes over the course of a three-week incubation period in the presence of *I. sakaiensis* in a 6-well plate.

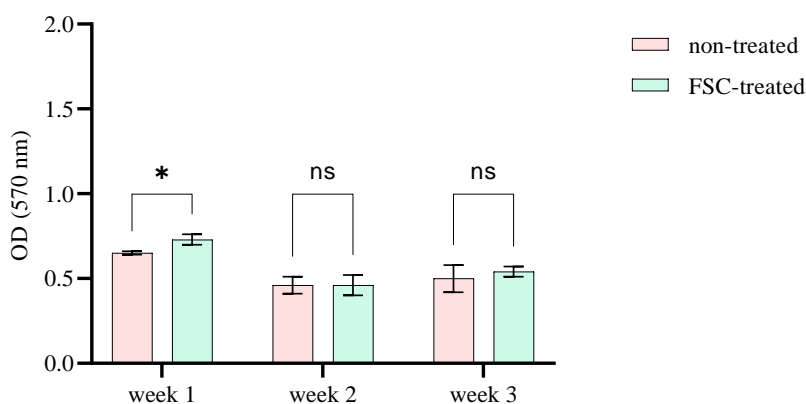


Figure 3.28. Biofilm formation of non-treated and FSC-treated PET in 6-well plate in the presence of *I. sakaiensis* over three weeks at 30 °C.

Data was analysed using a two-way ANOVA with post hoc. Tukey's multiple comparisons test (n=8, $P < 0.05$ (*)).

3.3.2.2. Effect of *F. culmorum* supernatant in 6-well plate: FTIR results

FTIR was conducted to analyse PET samples to gain insights into the alteration of surface functional groups. Our findings revealed an enhancement in the degradation process over the course of three weeks.

Interestingly, the FSC treatment had a notable impact on the transmittance percentage of carbonyl groups, indicating a potential role for cutinases in promoting the degradation of PET. The FTIR results clearly showed that the transmittance percentage of carbonyl groups increased when FSC treatment was applied compared to non-treated PET.

To illustrate this, the bar chart was prepared to demonstrate the alteration in carbonyl transmittance percentage over time (Fig 3.29). After one week of incubation, the transmittance percentage of carbonyl groups increased from 34.48 to 42.44 following FSC treatment (Fig 3.29). This indicates that the enzymatic action facilitated the breakdown of the polymer chains.

As the incubation period progressed to the second week, further enhancement was observed in the transmittance percentage of carbonyl groups. The values rose from 46 to 53 after FSC treatment, indicating an ongoing degradation process (Fig 3.29).

Upon reaching the third week of incubation, the transmittance percentage of carbonyl groups significantly increased to 62 (Fig 3.29). This finding suggests that the degradation process continued to progress, leading to a higher presence of carbonyl functional groups on the surface of the PET samples.

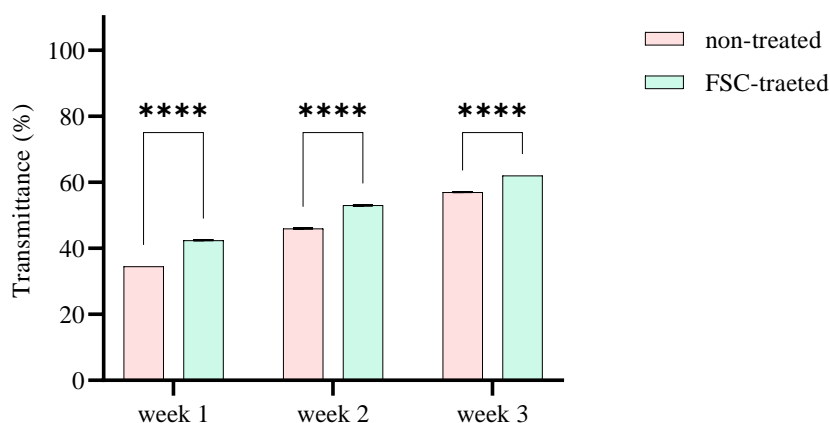


Figure 3.29. FTIR of non-treated and FSC-treated PET in YSV medium in the presence of *I. sakaiensis* over three weeks in 6-well plate.

Data was analysed using a two-way ANOVA with post hoc. Tukey's multiple comparisons test (n=3, $P < 0.0001$ (****)).

3.3.3. Effect of *F. culmorum* supernatant and DTAB in large scale

3.3.3.1. Effect of *F. culmorum* supernatant and DTAB in large scale: biofilm results

The investigation into the FSC effect in larger scale involved a study conducted over a span of eight weeks, during which treated PET films were subjected to incubation in the presence of *I. sakaiensis*. Three different treatments were compared including non-treated PET, FSC-treated PET and FSC-DTAB-treated PET. In order to gain an understanding of the biofilm formation process, samples were collected at different intervals, specifically at weeks one, four, and eight.

To present the biofilm formation over eight weeks, a bar chart was generated, displaying the OD₅₇₀ (Fig 3.30). This chart effectively illustrated the notable enhancements resulting from FSC treatment of the PET films after one week of incubation. The initial OD₅₇₀ measurement of 0.46 remarkably increased to 0.91 after FSC treatment. Also, the FSC-DTAB treatment enhance the biofilm formation on PET films from 0.46 to 0.78 after passing one week (Fig 3.30).

In week four the less biofilm formation was observed on FSC-treated PET and FSC-DTAB-treated PET in comparison with week one. However, in comparison with non-treated PET still FSC-treated PET enhanced the biofilm formation in week four. During the fourth week, however, the OD₅₇₀ measurements exhibit significant downward changes across the PET films, irrespective of the treatment. This trend suggested a possible detachment of the biofilm formation during this period.

As the incubation period reached its highest amount at week eight, the OD₅₇₀ measurements revealed remarkable progress in the biofilm formation on FSC-DTAB treated PET. Comparing the non-treated PET, the OD₅₇₀ reached to the 1.80 after FSC-DTAB-treated PET. The findings showcased the FSC remarkable impact during the initial week, and the enhancement in biofilm formation achieved by FSC-DTAB treatment after eight weeks.

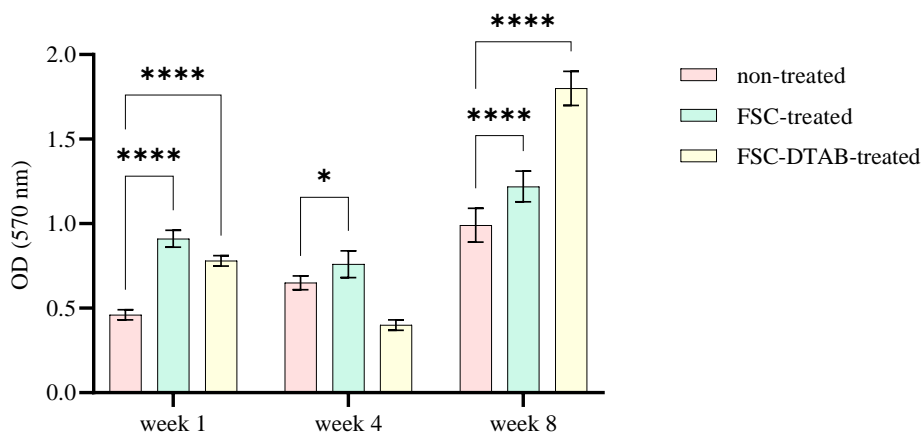


Figure 3.30. Biofilm formation of different treatments of PET (non, FSC and FSC-DTAB) in 500 ml shaken flask in the presence of *I. sakaiensis* over eight weeks.

Data was analysed using a two-way ANOVA with post hoc. Tukey's multiple comparisons test (n=8, P < 0.05 (*), P < 0.0001 (****)).

3.3.3.2. Effect of *F. culmorum* supernatant and DTAB in large scale: FTIR results

In addition to the biofilm assay, the Fourier Transform Infrared Spectroscopy (FTIR) was carried out on PET samples to investigate the alterations in surface functional groups. The FTIR results not only complemented the findings of the biofilm formation assay, but also provided valuable insights into the specific changes in the surface chemistry of the samples.

The FTIR analysis confirmed that the FSC-treated PET samples, following one week of incubation, yielded the most significant outcomes in terms of the transmittance percentage of the carbonyl group. Specifically, the transmittance percentage of the

carbonyl group in the PET samples showed a remarkable increase from 35.22 to 79.67 after one week of FSC treatment in the presence of *I. sakaiensis* (Fig 3.31). This significant enhancement suggests that the FSC treatment effectively modified the PET surface, resulting in a higher degree of transparency.

Moreover, the effects of FSC-DTAB treatment on the transmittance percentage of the carbonyl group in the PET samples was investigated. After one week of incubation with FSC-DTAB, the alteration in the transmittance percentage was observed. The results revealed that the FSC-DTAB treatment led to a transmittance percentage of 53.58, indicating a notable change in the molecular structure and functional groups present on the PET surface (Fig 3.31).

However, as the incubation period extended to four weeks, there was no longer a significant difference between the non-treated and FSC-treated PET samples. Interestingly, the transmittance percentage of the FSC-DTAB-treated PET samples exhibited a notable decrease after four weeks of incubation, indicating that the FSC-DTAB treatment may have caused some structural degradation or alterations to the PET surface.

Nevertheless, after an extended incubation period of eight weeks, both the FSC-treated and FSC-DTAB-treated PET samples demonstrated a remarkable recovery in terms of the transmittance percentage of the carbonyl group. The FSC-treated PET samples reached a transmittance percentage of 91.69, while the FSC-DTAB-treated PET samples showed an even higher transmittance percentage of 94.44 (Fig 3.31).

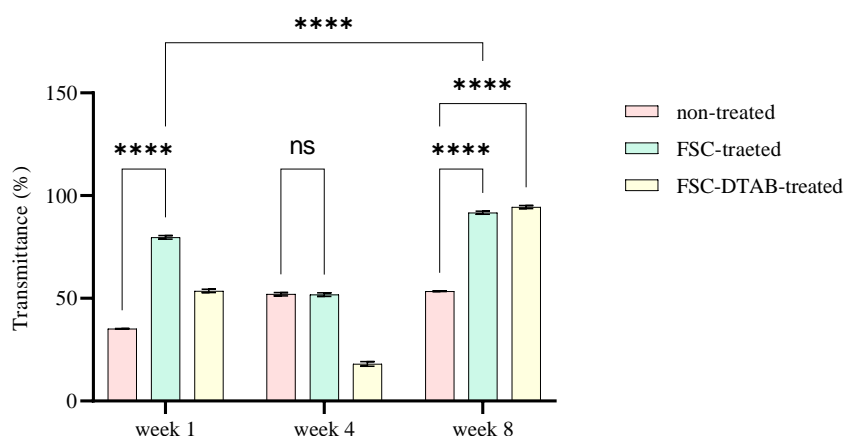


Figure 3.31. FTIR on different treatments of PET (non, FSC, FSC-DTAB) in 500 ml shaken flask in the presence of *I. sakaiensis* over eight weeks.

Data was analysed using a two-way ANOVA with post hoc. Tukey's multiple comparisons test (n=3, $P < 0.0001$ (****)).

3.3.3.3. Effect of *F. culmorum* supernatant and DTAB in large scale: HPLC results

To gain further insights into the degradation of FSC-treated and FSC-DTAB treated PET samples, High-Performance Liquid Chromatography (HPLC) analysis was conducted after incubation periods of one, four, and eight weeks in the presence of *I. sakaiensis*. This analytical technique is widely used for separating, identifying, and quantifying individual components in a liquid mixture (Appendix, Chapter 6, Fig 6.19).

The HPLC results demonstrated a notable increase in TPA concentration over an eight-week period following the application of FSC and FSC-DTAB on PET, in the presence of *I. sakaiensis*. In comparison to non-treated PET, all the treated samples exhibited the enhancement. After one week of incubation, there was no detectable TPA (one of the degradation products of PET) in any of the samples (non-treated, FSC-treated, or FSC-DTAB-treated).

However, as time progressed, TPA was detected. After four weeks, the TPA concentration reached 0.33 $\mu\text{g/ml}$ in the FSC-DTAB-treated PET samples, while the FSC-treated PET showed no measurable TPA concentration. Nonetheless, by the end of eight weeks, the TPA concentration in the FSC-DTAB treated PET samples surged to 0.87 $\mu\text{g/ml}$, and even the FSC-treated PET samples exhibited a notable TPA concentration of 0.83 $\mu\text{g/ml}$.

3.3.3.4. Effect of *F. culmorum* supernatant and DTAB in large scale: high resolution microscopy results

The investigation of surface alterations on PET was conducted using advanced high-resolution microscopy technique. The primary objective of this study was to assess the effects of FSC and FSC-DTAB treatments on the surface properties of PET over a period of one, four, and eight weeks of incubation in the presence of *I. sakaiensis*. By employing high-resolution microscopy, specifically at magnifications of $\times 20$ and $\times 100$. The obtained findings were documented in figures 3.32 and 3.33, which provide visual representation of the observed results.

Comparing the non-treated PET samples after one week of incubation with those after eight weeks, a striking change is evident. The latter exhibit a visibly thicker dark edge (Fig 3.32, red arrow), suggesting alterations to the surface morphology. In contrast, when PET samples subjected to FSC treatment after one week of incubation were compared to non-treated samples from the same time frame, no significant changes were observed.

However, after an extended period of eight weeks, notable transformations became apparent in the FSC-treated PET samples, particularly when contrasted with the non-treated PET samples over the same duration. The edges of the PET became remarkably thin, displaying signs of degradation, and the presence of multiple holes along these edges became clearly visible (Fig 3.32, red arrow). Additionally, the surface of the PET exhibited conspicuous pores resulting from the enzymatic treatment (Fig 3.33).

Furthermore, when examining the surface characteristics of non-treated PET and FSC-DTAB treated PET after one week of incubation, a notable change was detected. Although not as pronounced as the changes seen in the FSC-treated PET samples, an apparent difference in surface properties was observed. Similarly, after an extended incubation period of eight weeks, highly notable alterations were noticed in the structure of the FSC-DTAB treated PET. The edges of the PET displayed extensive breakdown, featuring a fragmented appearance, while deeper pores were readily observable on the PET surface (Fig 3.32, red arrow).

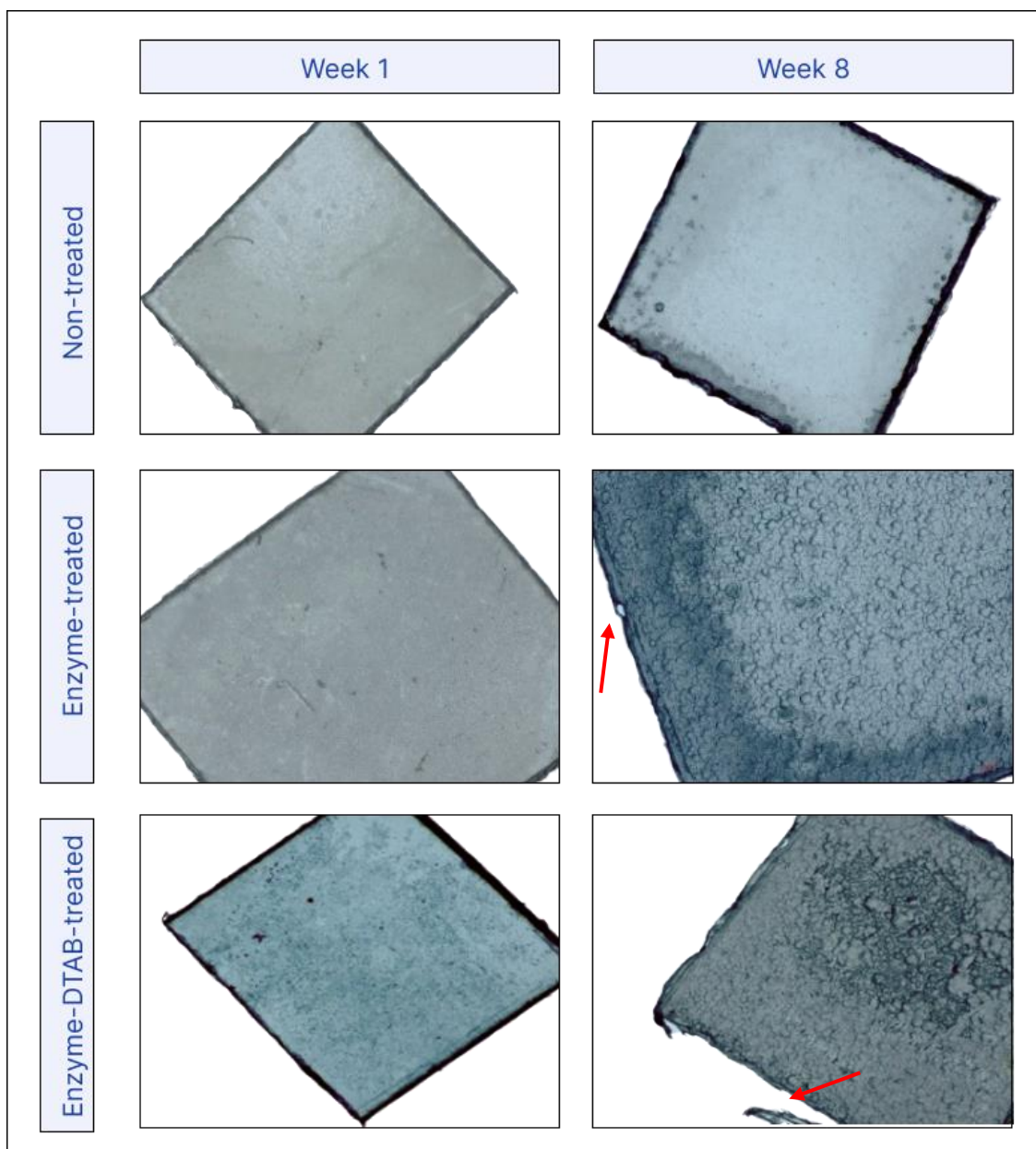


Figure 3.32. Using high resolution microscopy to visual presentation of the non-treated, FSC-treated and FSC-DTAB-treated PET after one and eight weeks of incubation in the presence of *I. sakaiensis* at 30 °C (magnification $\times 20$).

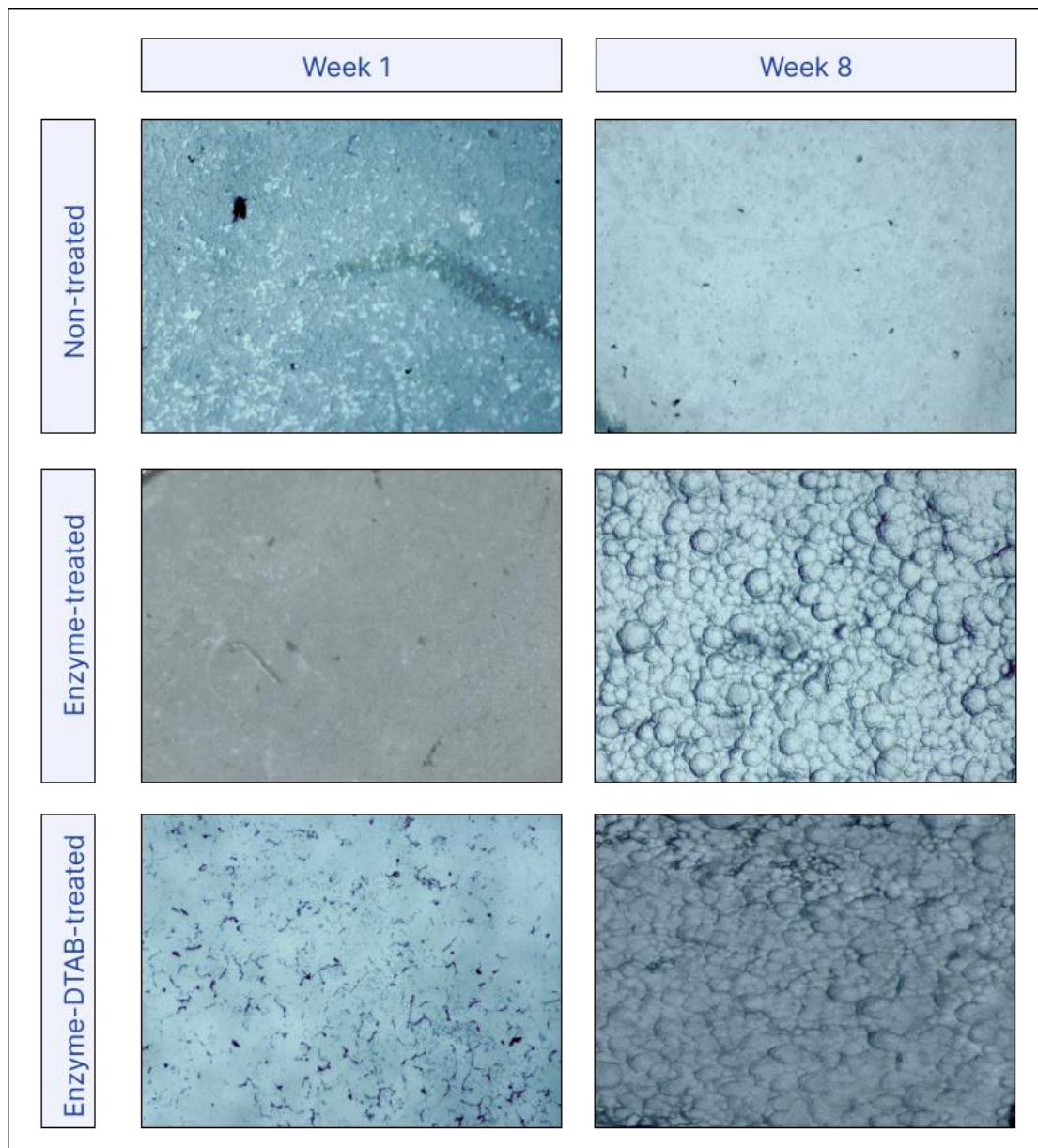


Figure 3.33. Using high resolution microscopy to visual presentation of the non-treated, FSC-treated and FSC-DTAB-treated PET after one and eight weeks of incubation in the presence of *I. sakaiensis* at 30 °C (magnification $\times 100$).

3.3.3.5. Effect of *F. culmorum* supernatant and DTAB in large scale: SEM results

Scanning Electron Microscopy (SEM) was employed to analyse the structural changes of non-treated, FSC-treated, and FSC-DTAB-treated PET samples after one and eight weeks of incubation in the presence of *I. sakaiensis* (Fig 3.34).

After one week of incubation, the SEM analysis revealed distinct differences in the surface characteristics such as roughness of the PET films. The non-treated PET films displayed a relatively smooth surface, with minimal irregularities. In contrast, the FSC-treated PET samples exhibited a slightly rougher surface, characterized by small-scale irregularities. This indicates that the enzymatic treatment effected alterations in the surface topography, due to the enzymatic action on the PET polymer chains. Similarly, the FSC-DTAB-treated PET samples displayed surface roughness, although to a lesser extent compared to the FSC-treated PET samples (Fig 3.34).

Upon extending the incubation period to eight weeks, the SEM analysis revealed further changes in the surface morphology of the PET samples. Notably, both the FSC-treated and FSC-DTAB-treated PET samples displayed more alterations in the surface topography compared to the non-treated PET films. The surfaces of these treated samples exhibited an increased number of pores and irregularities, indicating a higher degree of degradation (Fig 3.34). These observations suggest that the enzymatic treatment, as well as the combination of FSC and DTAB treatment, facilitated the breakdown of the PET polymer chains over time, resulting in the formation of pores on the surface. The presence of these pores implies that the enzymatic degradation process initiated by *I. sakaiensis* was progressing and causing physical changes in the PET samples.

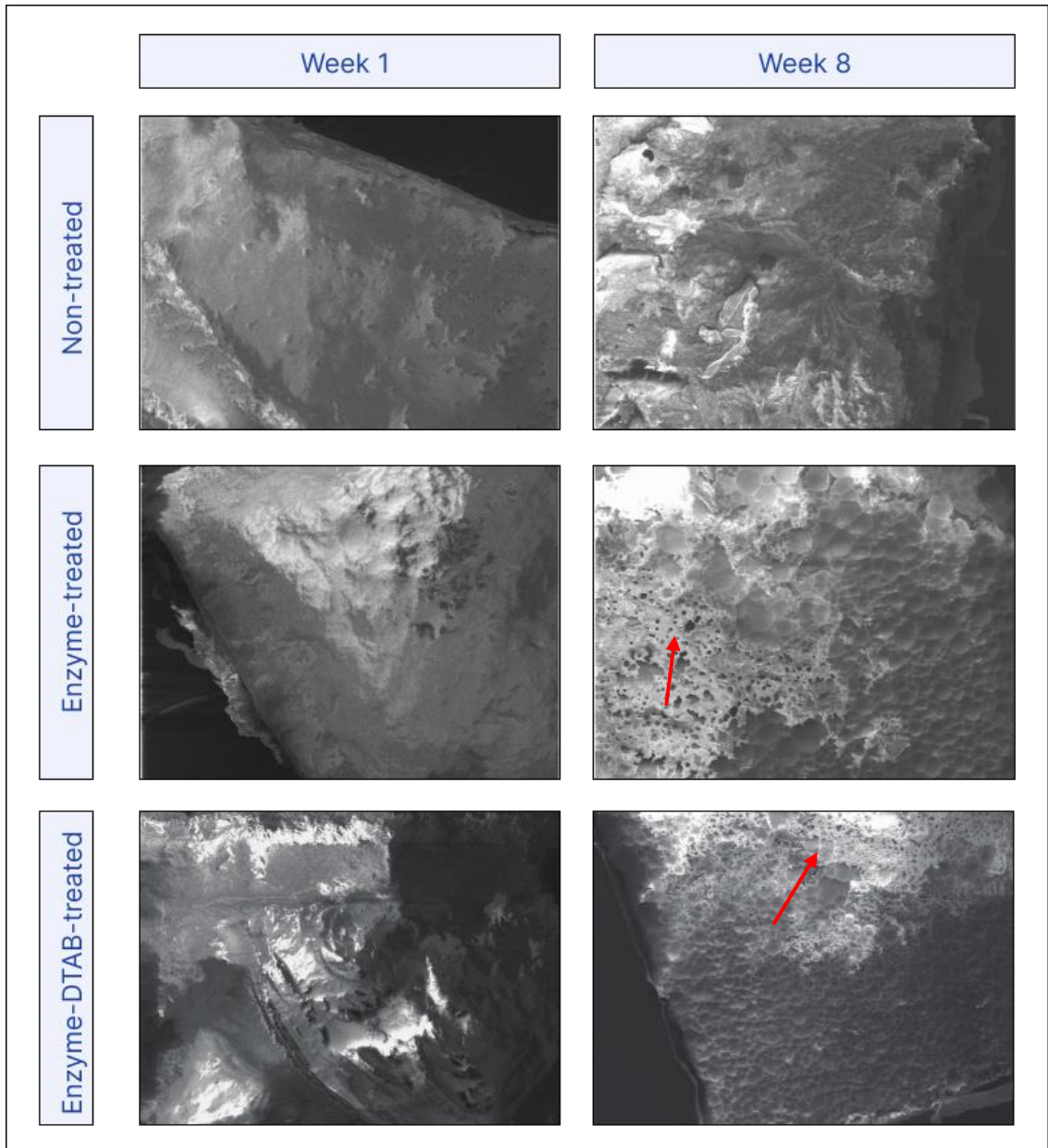


Figure 3.34. SEM presentation of the non-treated, FSC-treated and FSC-DTAB-treated PET samples after one and eight weeks of incubation in the presence of *I. sakaiensis* at 30 °C.

Chapter 3.4. The effect of 3-oxo-C₁₂-HSL on Pre-treated PET by DTAB, FSC, and FSC-DTAB

3.4. Overview

This chapter presents an investigation into the influence of 3-oxo-C₁₂-HSL on PET samples treated with DTAB, FSC, and a combination of FSC and DTAB. The study explores the changes observed over an extended period of eight weeks in the presence of *I. sakaiensis*. The sampling intervals were carefully chosen at weeks one, four, and eight to capture and analyse the characteristics of the samples throughout the duration of the experiment.

This chapter is divided into four distinct sections. The first part focuses on investigating the effect of 3-oxo-C₁₂-HSL concentrations varying from 0.5 µg/ml to 20 µg/ml on *I. sakaiensis* biofilm formation. The primary objective of this part is to identify the optimal concentration of 3-oxo-C₁₂-HSL that yields the most significant results in terms of biofilm formation. The second part of the chapter is devoted to exploring the impact of 3-oxo-C₁₂-HSL on DTAB-treated PET biodegradation within the context of a larger-scale experiment.

Similarly, the third part of the chapter focuses on the effects of 3-oxo-C₁₂-HSL on FSC-treated PET and FSC-DTAB-treated PET in a larger-scale experiment.

To evaluate the outcome of the experiments, a range of assays were employed, including biofilm assays, Fourier-transform infrared spectroscopy (FTIR), and high-performance liquid chromatography (HPLC). These analyses were specifically conducted on PET films treated with DTAB. Furthermore, further assessments such as high-resolution microscopy and scanning electron microscopy (SEM) were employed to evaluate the effects of 3-oxo-C₁₂-HSL on PET films treated with FSC as well as the combined FSC-DTAB treatment.

3.4.1. Effect of different concentrations of 3-oxo-C₁₂-HSL on PET samples

3.4.1.1. Effect of different concentrations of 3-oxo-C₁₂-HSL on PET samples: biofilm results

In this study, the 3-oxo-C₁₂-HSL was selected as a QSM to evaluate its capability in facilitating the formation of biofilms. The investigation aimed to understand the influence of the 3-oxo-C₁₂-HSL on biofilm development both in the presence of PET film and in its absence. To achieve this, different concentrations of the 3-oxo-C₁₂-HSL were examined, including 0.5, 1, 5, 10, 15, and 20 µg/ml in the presence of *I. sakaiensis* for 24 hrs in 96-well plates.

The bar chart presented in Figure 3.35 provides insights into the relationship between concentration of 3-oxo-C₁₂-HSL and biofilm formation in the presence and absence of PET. Notably, the chart indicates that the optimal concentration for promoting biofilm development was 5 µg/ml in which OD₅₇₀ reached to 1.11. Based on this observation, the concentration of 5 µg/ml was selected as the most effective for subsequent experiments.

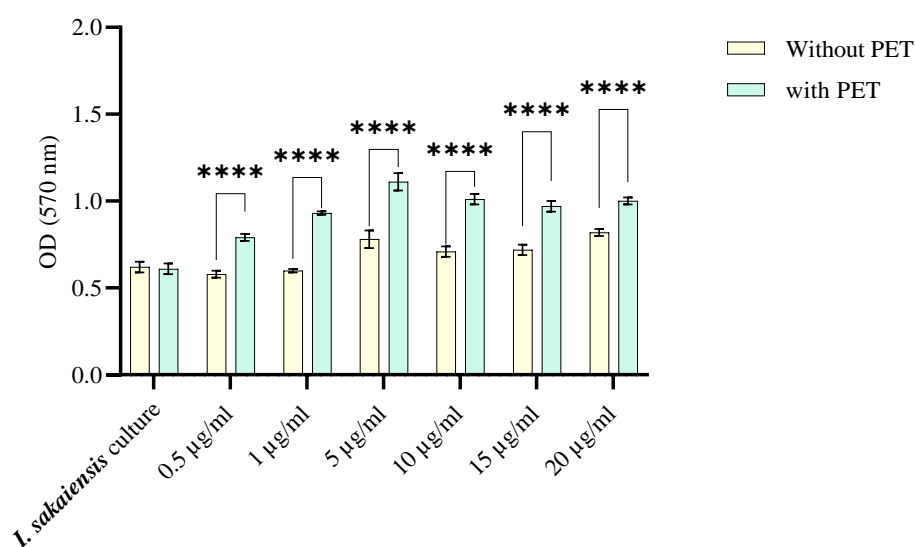


Figure 3.35. *I. sakaiensis* biofilm formation in YSV medium in the presence of different concentrations (0.5, 1, 5, 10, 15 and 20 µg/ml) of QSM (3-oxo-C₁₂-HSL) was investigated.

There are two series of data in the presence of PET and the absence of it in 96-well plate for 24 hrs (n=8, P < 0.0001 (****)).

3.4.1.2. Effect of different concentrations of 3-oxo-C₁₂-HSL on PET samples: FTIR results

The PET pieces were subjected to Fourier Transform Infrared (FTIR) analysis to evaluate any alteration on the surface of the PET resulting from exposure to various concentrations of 3-oxo-C₁₂-HSL after 24 hrs of incubation. The resulting FTIR spectra are represented in figure 3.36.

Among the range of concentrations tested, it was observed that the highest increase in transmittance percentage for the carbonyl group was associated with the concentration of 5 µg/ml of 3-oxo-C₁₂-HSL. The carbonyl transmittance percentage reaches to 90.

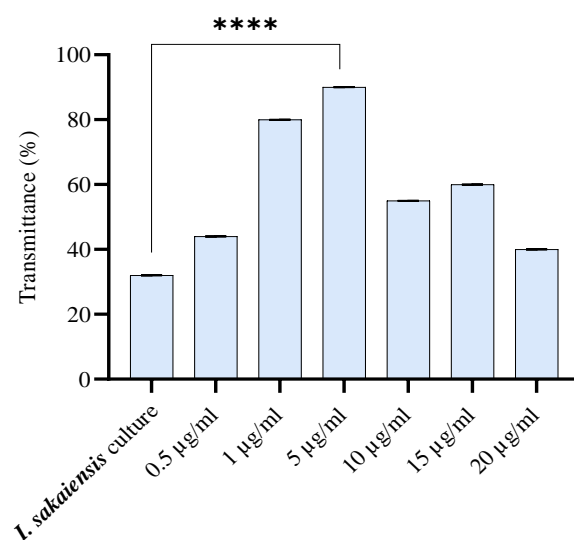


Figure 3.36. Carbonyl group transmittance percentage in the presence of different concentrations (0.5, 1, 5, 10, 15 and 20 µg/ml) of QSM (3-oxo-C₁₂-HSL) was investigated.

There are two series of data in the presence of PET and the absence of it (n=3, P < 0.0001 (****)).

3.4.2. Effect of 3-oxo-C₁₂-HSL on DTAB-treated PET samples in large scale

This study aimed to explore the influence of 3-oxo-C₁₂-HSL at a larger scale, particularly in relation to the incubation of both non-treated and DTAB-treated PET films in the presence of *I. sakaiensis* over an extended period of eight weeks. To assess the progression, samples were collected at regular intervals during weeks one, four, and eight. The investigation primarily focused on the formation of biofilms and the alteration of surface functional groups, along with the quantification of terephthalic acid (TPA) using High-Performance Liquid Chromatography (HPLC). Also, the morphological changes on the surface of the PET were assayed by high resolution microscopy and SEM.

3.4.2.1. Effect of 3-oxo-C₁₂-HSL on DTAB-treated PET samples in large scale:

biofilm results

The results of the biofilm formation analysis are presented in figure 3.37. It was found that the DTAB treatment, in culture supplemented with QSM, yielded the most impact on the PET pieces during the fourth week of incubation.

After a week of incubation, the results of the study indicated a notable effect of QSM on non-treated PET biofilm ($OD_{570} = 0.45$). This was lower compared to QSM-supplemented culture ($OD_{570} = 0.59$), suggesting that the presence of QSM had a positive impact on biofilm formation on the PET surface.

In contrast, the biofilm formation on DTAB-treated PET showed a slightly higher initial OD_{570} of 0.55 after a week, and the introduction of QSM led to a decrease in biofilm formation, as evidenced by the subsequent OD_{570} of 0.46. This reduction suggested that QSM had a moderating effect on biofilm formation on the DTAB-treated PET (Fig 3.37).

Moving forward to the fourth week of incubation, an interesting observation emerged regarding non-treated PET, DTAB-treated PET, and QSM-added culture. It was found that the presence of QSM resulted in higher biofilm formation on DTAB-treated PET compared to non-treated PET. The OD_{570} increased significantly ($P < 0.0001$) from 0.47 to 0.81, indicating a potential synergistic effect between DTAB treatment and QSM supplementation in promoting biofilm growth on the surface of the PET pieces. Meanwhile, in the presence of QSM, the non-treated PET also exhibited a relatively higher OD_{570} of 0.61, further highlighting the influence of QSM on biofilm formation (Fig 3.37).

As the study progressed to the eighth week, the most significant finding was related to the biofilm formation on DTAB-treated PET in the presence of QSM. The biofilm OD_{570} reached a much higher value of 1.01, suggesting a significant ($P < 0.0001$) increase in biofilm growth on the surface of the DTAB-treated PET compared to the levels of previous weeks.

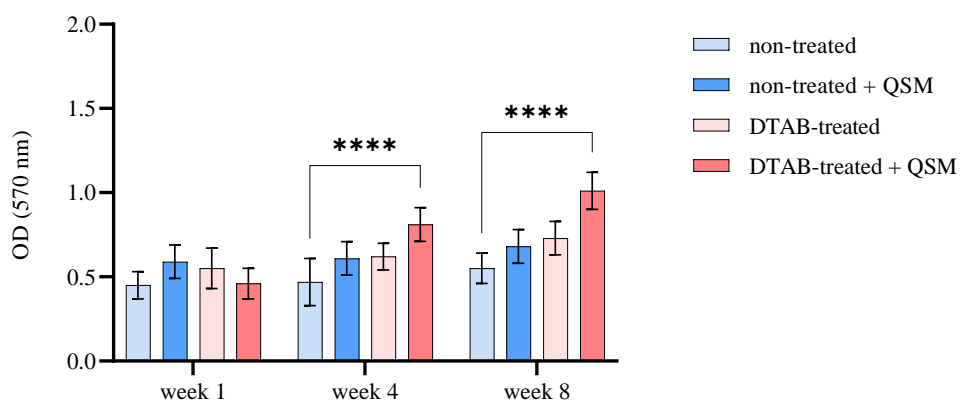


Figure 3.37. Biofilm formation on non-treated and DTAB-treated PET in 500 ml shaken flask in the presence of *I. sakaiensis* and QSM over eight weeks. Data was analysed using a two-way ANOVA with post hoc. Tukey's multiple comparisons test (n=8, $P < .0001$ (****)). The Concentration of QSM is 5 $\mu\text{g/ml}$.

3.4.2.2. Effect of 3-oxo-C₁₂-HSL on DTAB-treated PET samples in large scale: FTIR results

In order to look deeper into the changes occurring on the PET surface, Fourier Transform Infrared (FTIR) spectroscopy was performed on the PET samples. The FTIR analysis served as a complementary tool to confirm the effect of biofilm formation on PET biodegradation. The data obtained from FTIR supported the notion that DTAB-treated PET, in the presence of QSM, delivered the most satisfactory biodegradation outcome. This treatment resulted a highest transmittance percentage of the carbonyl group among the non-treated, non-treated, QSM supplemented culture, and DTAB-treated PET, suggesting a positive alteration in the surface functional groups of the PET.

After one week of incubation, the presence of QSM had a significant ($P < 0.0001$) impact on both DTAB-treated and non-treated PET. The carbonyl transmittance percentage for DTAB-treated PET was recorded at 53.75, while for non-treated PET, it was 41.92. These findings indicated that the presence of QSM influenced the transmission of the carbonyl group, with a higher transmittance observed in the DTAB-treated PET compared to the non-treated PET (Fig 3.38).

As the study progressed to the fourth week, the most notable result was observed in the case of DTAB-treated PET in the presence of QSM. The transmittance percentage of the carbonyl group significantly ($P < 0.0001$) increased to 69.41, indicating a higher degree of light transmission through the material. This result suggested that the combination of

DTAB treatment and QSM presence had a potential synergistic effect in enhancing the transmittance of the carbonyl group (Fig 3.38).

Upon reaching the eighth week, significant ($P < 0.0001$) results were observed in different scenarios. Firstly, the non-treated PET in the presence of QSM demonstrated a transmittance percentage of 68.58 for the carbonyl group. Secondly, the DTAB-treated PET exhibited a transmittance percentage of 64.78. Lastly, the DTAB-treated PET in the presence of QSM showcased the highest transmittance percentage of 74.09 % for the carbonyl group. These findings indicated that the presence of QSM had a positive impact on the transmittance of the carbonyl group in both non-treated and DTAB-treated PET, with the highest enhancement observed in the latter scenario (Fig 3.38).

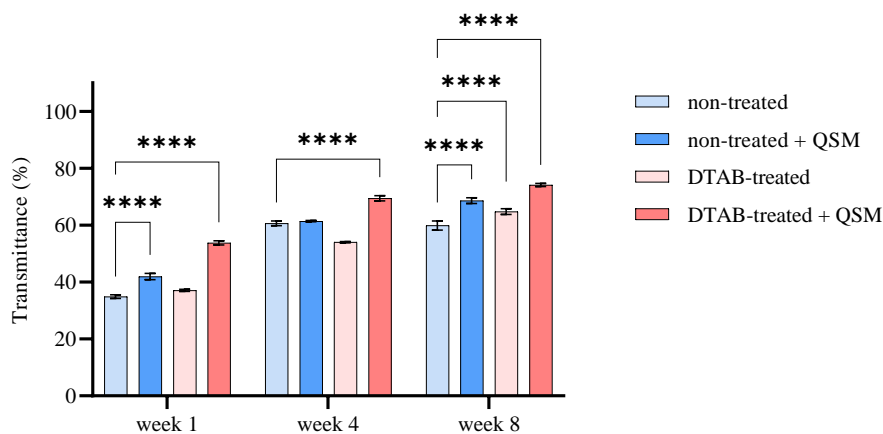


Figure 3.38. FTIR on non-treated and DTAB-treated PET in 500 ml shaken flask in the presence of *I. sakaiensis* and QSM over eight weeks.

Data was analysed using a two-way ANOVA with post hoc. Tukey's multiple comparisons test ($n=3$, $P < .0001$ (****)). The Concentration of QSM is 5 $\mu\text{g/ml}$.

3.4.2.3. Effect of 3-oxo-C₁₂-HSL on DTAB-treated PET samples in large scale:

HPLC results

HPLC analysis was conducted to quantitatively evaluate the levels of terephthalic acid (TPA) formed over time. The results indicated that the TPA concentration increases from 0 to 0.03 $\mu\text{g/ml}$ over eight weeks.

3.4.3. Effect of 3-oxo-C₁₂-HSL on FSC-treated and FSC-DTAB-treated PET samples in 96-well plate

3.4.3.1. Effect of 3-oxo-C₁₂-HSL on FSC-treated and FSC-DTAB-treated PET samples in 96-well plate: biofilm results

The biofilm formation was thoroughly examined over a 24-hr period on non-treated, FSC-treated, and FSC-DTAB-treated PET in the presence of 5 µg/ml of 3-oxo-C₁₂-HCL. The introduction of QSM demonstrated a notable reduction in biofilm formation on both FSC-treated and FSC-DTAB-treated PET surfaces. The OD₅₇₀ decreased from 2.26 to 1.66 and 1.58 following FSC and FSC-DTAB treatments, respectively (Fig 3.39). However, the presence of QSM resulted in an enhanced biofilm formation on non-treated PET films in 96-well plate.

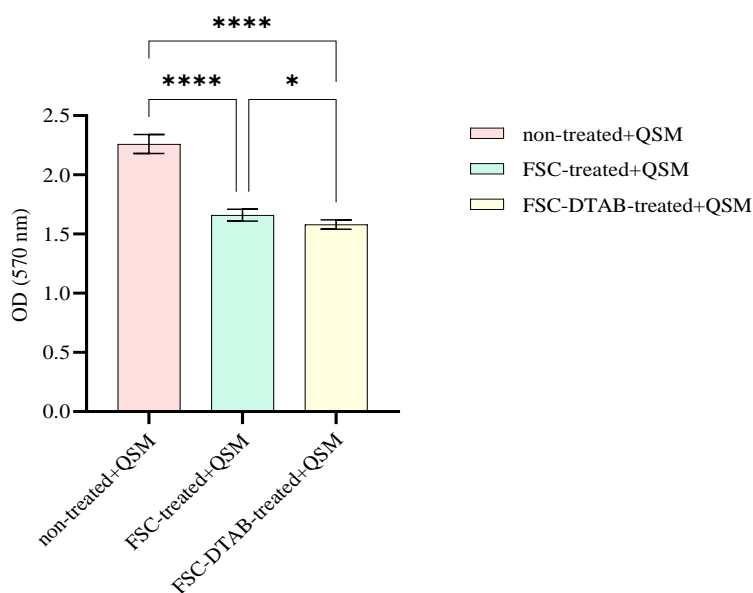


Figure 3.39. Biofilm formation on non-treated, FSC-treated and FSC-DTAB-treated PET in 96-well plate in the presence of *I. sakaiensis* and QSM after 24 hrs.

Data was analysed using a two-way ANOVA with post hoc. Tukey's multiple comparisons test (n=8, P < .0001(****)). The Concentration of QSM is 5 µg/ml.

3.4.4. Effect of 3-oxo-C₁₂-HSL on FSC-treated and FSC-DTAB-treated PET samples in large scale

3.4.4.1. Effect of 3-oxo-C₁₂-HSL on FSC-treated and FSC-DTAB-treated PET samples in large scale: biofilm results

This study aimed to examine the effect of biofilm formation on non-treated (control), FSC-treated and FSC-DTAB-treated PET pieces in the presence of 5 µg/ml of 3-oxo-C₁₂-HCL in *I. sakaiensis* culture in large scale (500 ml).

In Figure 3.40, the bar chart demonstrates the enhanced biofilm formation on FSC-treated PET after a week of incubation with 3-oxo-C₁₂-HCL in the presence of *I. sakaiensis*. It is worth noting that the OD₅₇₀ of the FSC-treated PET reached a value of 1.11 after one week, indicating an increase in biofilm formation compared to non-treated PET surfaces.

However, as the investigation progressed to the fourth week, interesting findings emerged. At this stage, there were no significant differences observed between the biofilm formation on non-treated PET surfaces and those treated with either FSC or FSC-DTAB. Additionally, it was observed that the biofilm on FSC-treated PET surfaces exhibited a decrease in the OD values over the four-week period. The OD measurements for non-treated, FSC-treated, and FSC-DTAB-treated PET were recorded as 0.77, 0.79, and 0.83, respectively (Fig 3.40).

Notably, a significant alteration in biofilm formation became apparent after eight weeks. Both the FSC-treated PET and FSC-DTAB-treated PET surfaces displayed a remarkable increase in biofilm density, as evidenced by their respective OD values of 1.5 and 1.89. These findings suggest that the presence of 3-oxo-C₁₂-HCL, along with the enzymatic treatment, exerted an influence on biofilm formation on PET surfaces over an extended incubation period.

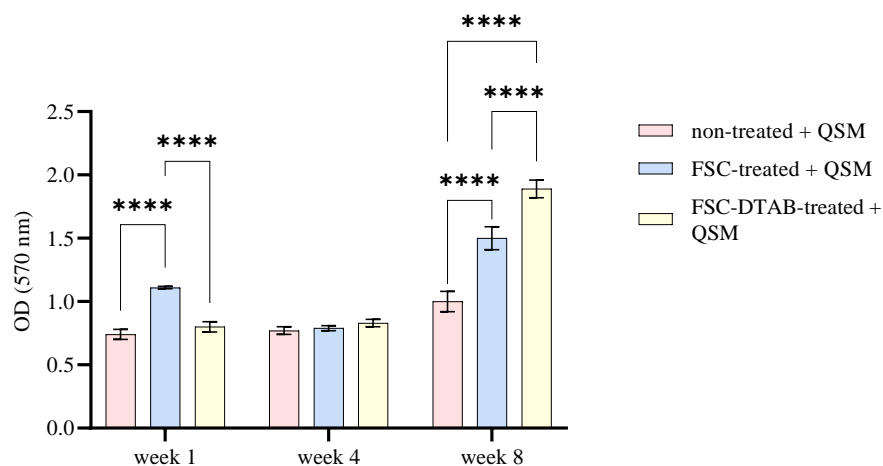


Figure 3.40. Biofilm formation on non-treated, FSC-treated and FSC-DTAB-treated PET in 500 ml shaken flask in the presence of *I. sakaiensis* and QSM after over eight weeks. Data was analysed using a two-way ANOVA with post hoc. Tukey's multiple comparisons test (n=8, $P < .0001$ (****)). The Concentration of QSM is 5 $\mu\text{g/ml}$.

3.4.4.2. Effect of 3-oxo-C₁₂-HSL on FSC-treated and FSC-DTAB-treated PET samples in large scale: FTIR results

Fourier-transform infrared spectroscopy (FTIR) was employed to analyze the alteration on the surface of various PET samples, including non-treated PET, FSC-treated PET, and PET treated with a combination of FSC and DTAB, in the presence of 5 $\mu\text{g/ml}$ of 3-oxo-C₁₂-HCL.

The FTIR analysis revealed that the carbonyl transmittance percentage of FSC-treated PET reached 88.89 after one week. This observation indicated an enhancement in the breakdown of ester bonds and, notably, a reduction in the energy required for their cleavage. These results demonstrated the effectiveness of FSC treatment in facilitating the degradation of ester bonds within the PET material.

As the study progressed to the four-week mark, changes in transmittance percentage became evident across all treatments. The FTIR analysis indicated a decrease in transmittance percentage for non-treated PET, FSC-treated PET, and FSC-DTAB-treated PET. The transmittance values recorded after four weeks were 68.65, 51.68, and 74.21, respectively (Fig 3.41).

Interestingly, after eight weeks, a noteworthy difference was observed in the transmittance percentages. Although the transmittance percentage of non-treated PET decreased to 58, the most notable changes were observed in FSC-treated PET and FSC-DTAB-treated PET. These treatments resulted in transmittance percentages of 100

compared to non-treated PET after eight weeks. These findings suggest that the combined treatment of FSC and DTAB had a profound effect on the PET degradation, leading to increased transmittance percentages (Fig 3.41).

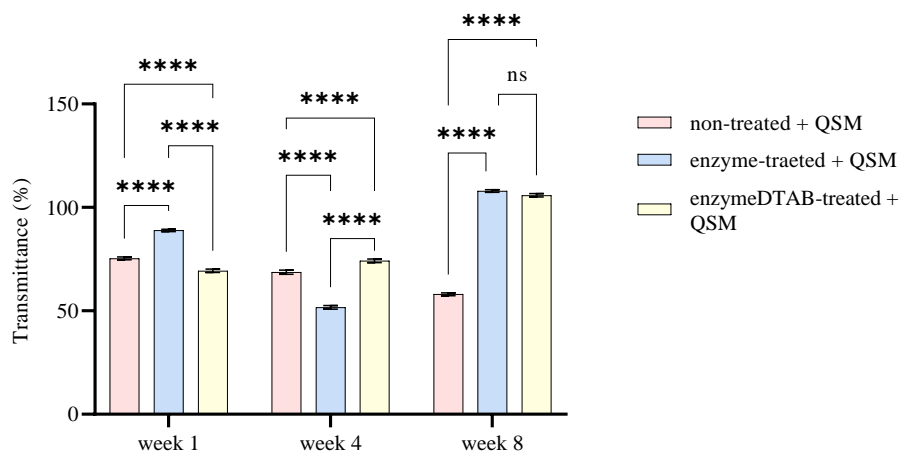


Figure 3.41. FTIR on non-treated and DTAB-treated PET in 500 ml shaken flask in the presence of *I. sakaiensis* and QSM over eight weeks.

Data was analysed using a two-way ANOVA with post hoc. Tukey's multiple comparisons test (n=8, $P < .0001$ (****)). The Concentration of QSM is 5 $\mu\text{g/ml}$.

3.4.4.3. Effect of 3-oxo-C₁₂-HSL on FSC-treated and FSC-DTAB-treated PET samples in large scale: HPLC results

To gain further insights into the changes of the FSC-treated and FSC-DTAB treated PET samples in QSM supplemented culture, HPLC was conducted and samples were analysed after incubation periods of one, four, and eight weeks in the presence of *I. sakaiensis*. The area of TPA peak and TPA concentration were calculated based on the following equation which obtained from TPA calibration curve $Y = 19.137x + 1.6917$ (Result, Chapter 3.2, Section 3.2.3, Fig 3.22).

The TPA concentration reached 2.20 $\mu\text{g/ml}$ after FSC treatment in the presence of *I. sakaiensis* and QSM, after one week of incubation. The TPA concentration decreases after eight weeks to 0.92 $\mu\text{g/ml}$. The TPA concentrations related to the FSC-DTAB treatment were 0.98, 0.13 and 0 for week one, four and eight, respectively (Appendix, Chapter 6, Fig 6.20).

3.4.4.4. Effect of 3-oxo-C₁₂-HSL on FSC-treated and FSC-DTAB-treated PET samples in large scale: high resolution microscopy results

The investigation of surface alterations on PET was conducted using advanced high-resolution microscopy technique. The primary objective of this study was to assess the effects of FSC and FSC-DTAB treatments on the surface properties of PET over the period of one, four, and eight weeks of incubation in the presence of *I. sakaiensis*.

The high-resolution microscopy was carried out at magnifications of $\times 20$. The obtained findings are documented in figure 3.42, which provide visual representation of the observed results.

The PET samples subjected to FSC treatment after one week of incubation were compared to eight weeks. After an extended period of eight weeks, notable transformations was apparent in the FSC-treated PET samples. The edges of the PET became remarkably thin, displaying signs of degradation, and the presence of multiple holes along these edges became clearly visible. Additionally, the surface of the PET exhibited noticeable pores resulting from the enzymatic treatment. Similar changes were observed for FSC-DTAB-treated PET (Fig 3.42).

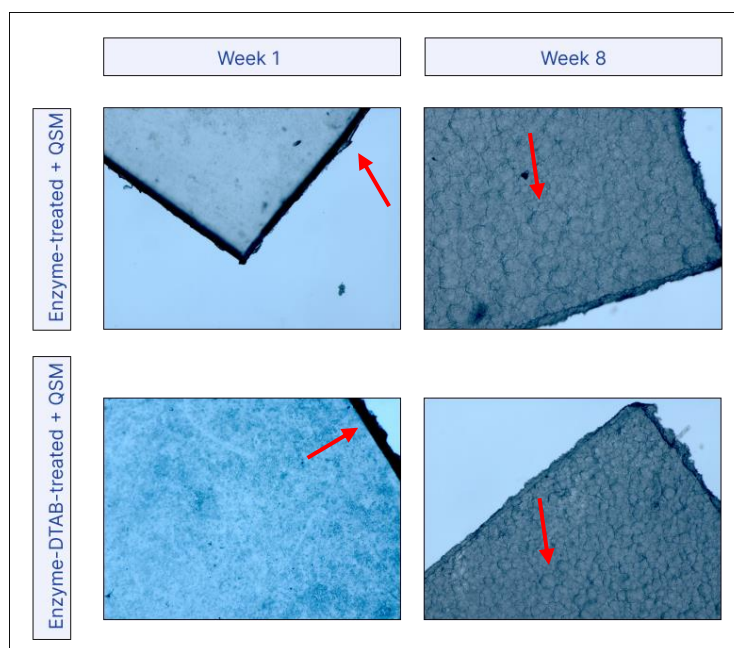


Figure 3.42. High resolution microscopy on FSC-treated and FSC-DTAB-treated PET in the presence of *I. sakaiensis* and QSM over eight weeks (magnification $\times 20$).

3.4.4.5. Effect of 3-oxo-C₁₂-HSL on FSC-treated and FSC-DTAB-treated PET samples in large scale: SEM results

Scanning Electron Microscopy (SEM) was employed to analyse the structural changes in non-treated, FSC-treated, and FSC-DTAB-treated PET samples after one and eight weeks of incubation in the presence of *I. sakaiensis*. After one week of incubation, the SEM analysis revealed distinct differences in the surface characteristics of the PET films. The FSC-treated PET films displayed a relatively smooth surface, with minimal irregularities on surface after one week of incubation in the presence of QSM. In contrast, the FSC-treated PET samples in the presence of QSM exhibited a significant rougher surface after eight weeks. This indicates that the enzymatic treatment induced alterations in the surface topography, potentially due to the enzymatic action on the PET polymer chains in the presence of QSM after eight weeks. Similarly, the FSC-DTAB-treated PET samples displayed surface roughness after eight weeks (Fig 3.43).

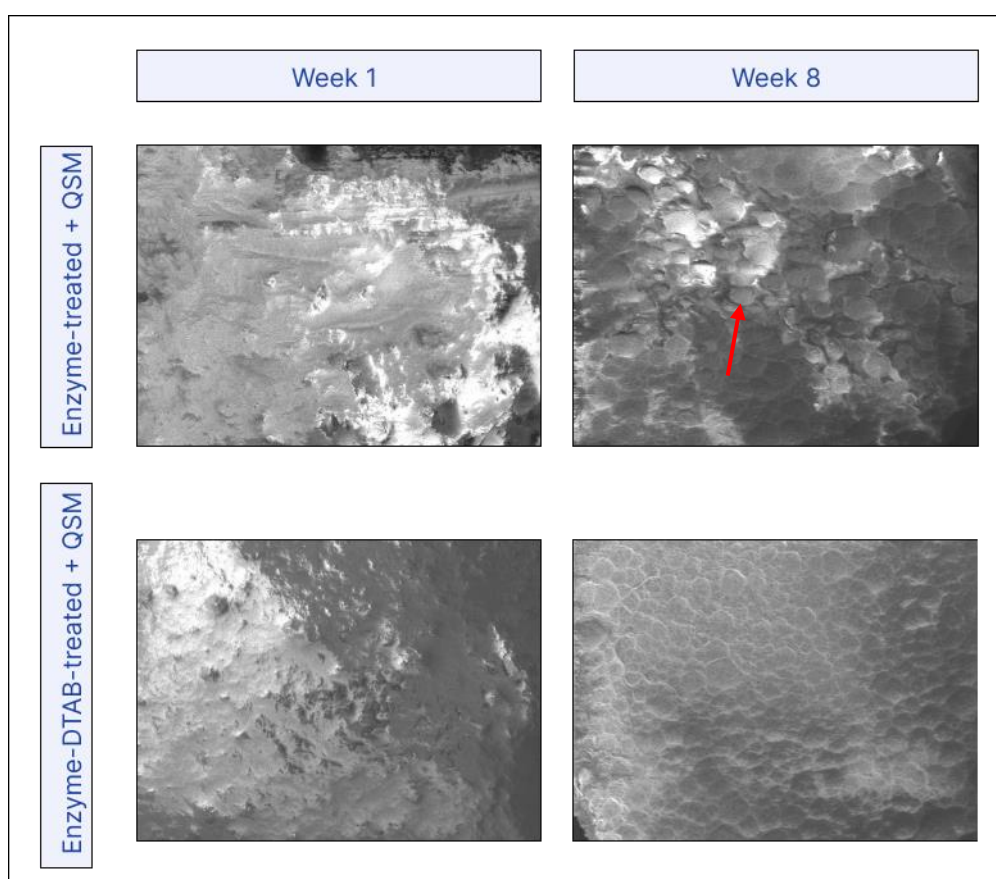


Figure 3.43. SEM on FSC-treated and FSC-DTAB-treated PET in the presence of *I. sakaiensis* and QSM over eight weeks. Red arrow shows the pores.

Chapter 4. Discussion

4.1. Overview

This chapter is divided into four parts including discussions about the effect of different pre-treatments on PET biodegradation at a small scale (10 ml), the effect of DTAB at a larger scale (500 ml), the effect of FSC from a 96-well plate to larger scale and effect of QSM on DTAB treatment, FSC treatment, and combination with the two.

4.2. Different pre-treatment effects on PET biodegradation

The section is divided into two parts. In the first part, the results from FTIR spectroscopy and biofilm formation assay of different treatments (NaOH, DTAB, Brij-35 and UV) on PET pieces in the three media (HPP, YSV and M9) in the presence of *I. sakaiensis* are discussed. In the second part, the same is discussed for *P. mendocina*.

4.2.1. PET pre-treatment in the presence of *I. sakaiensis*: FTIR and biofilm

Plastic polymers may require decades to break down unless their surface hydrophilicity is enhanced through preparatory steps. The degradation of plastics is accelerated by treatments like thermal oxidation, UV photooxidation, oxidative chemicals, or surfactants (Gilan et al. 2004; Arkatkar et al. 2010; Devi et al. 2016). Photodegradation initiates chain fragmentation of plastic molecules via mechanisms mediated by free radicals, resulting in smaller molecules that microorganisms can absorb (Devi et al. 2016). Additionally, scrutiny of PP using infrared spectroscopy revealed that brief UV exposure introduced keto carbonyl peaks, while thermal treatment introduced ester carbonyl peaks (Arkatkar et al. 2010). This led to the suggestion that *P. stutzeri* might preferentially target ester bonds, as thermally treated PP displayed greater weight loss than PP exposed to short UV treatment (Arkatkar et al. 2010). However, neither UV nor thermal pretreatment augmented *P. azotoformans*' ability to degrade PP (Arkatkar et al. 2010).

Oxidative chemicals, such as sulphuric acid, nitric acid, hydrochloric acid, and hydrogen peroxide, also effectively generate hydroxyl group radicals that oxidize polymer surfaces (Arkatkar et al. 2010; Sen and Raut 2015). Nitric acid, in particular, is a common method that oxidizes polymers, introducing carbonyl groups and double bonds into the chain structure (Rajandas et al. 2012; Sen and Raut 2015). Similarly, incorporating pro-oxidant additives was found to heighten the hydrophilicity of high-molecular-weight PE by introducing carbonyl functional groups and generating lower molecular weight components (Chiellini et al. 2006; Singh and Sharma 2008).

In tandem with chemical oxidants, surfactants are employed to encourage microbial degradation by enhancing the polymer's surface hydrophilicity. Nonionic surfactants like

Tween 80 have been employed to increase *P. aeruginosa* adhesion to LDPE (Albertsson et al. 1993). However, for naturally hydrophobic *Pseudomonas* sp. AKS2, Tween 80 reduced adhesion and degradation of LDPE, while mineral oil, which boosts hydrophobic interactions, increased adhesion and degradation capabilities (Tribedi and Sil, 2013). As such, pre-treatments manifest species-specific effects and must be tailored to each degradation scenario.

The challenge associated with the degradation of PET stems from its elevated glass transition temperatures (T_g), typically falling within the range of 75–80 °C when exposed to ambient conditions, and an even higher degradation temperature exceeding 300 °C, attributable to its aromatic polyester structure. Contrastingly, microorganisms typically flourish within a temperature range of 25-40 °C, and the melting temperatures (T_m) of enzymes involved in PET degradation often lie below the T_g of PET, generally ranging between 40 to 80 °C. Notably, specific enzymes, such as *H. insolens* cutinase, exhibit a T_m as high as 80 °C, while enzymes like PETase and *F. oxysporum* cutinase possess a T_m of approximately 45 °C. Consequently, the stark disparity between the required high temperatures for PET degradation and the enzyme T_m necessitates a preliminary pretreatment step to facilitate biodegradation, as reported by Kawai et al. (2019), and Mohanan et al. (2020).

The capacity of bacterial cells to adhere to and break down plastic polymers relies on the configuration of the polymer's surface characteristics (Donlan 2002). Often, introducing hydrophilic functional groups to plastic polymers becomes necessary to encourage the bonding of cell surfaces, given that cell surfaces typically possess a hydrophilic nature that doesn't naturally attract hydrophobic polymers. Consequently, increased surface unevenness and hydrophilicity of the polymer have been demonstrated to facilitate both the improved attachment of bacterial colonies and the accessibility of externally secreted enzymes to the polymer's surface (Sanin et al. 2003; Tribedi and Sil 2013; Nauendorf et al. 2016).

Pre-treatment is a necessary step for PET degradation due to its durability (Taniguchi et al., 2019; Kawai et al., 2019; Li et al., 2020). The pre-treatment approaches can change the physicochemical properties of the surface of the PET, such as hydrophobicity, enhancing the bacterial adhesion to the surface. This improves the exposure of PET pieces to degradative enzymes (Section 1.8 of the Introduction Chapter). The most prominent result obtained from the investigation on PET samples, using FTIR and biofilm assay, is DTAB treatment on PET pieces in YSV medium and in the presence of *I. sakaiensis*.

Based on FTIR results of DTAB-treated PET in YSV medium in the presence of *I. sakaiensis* all functional groups reach the higher transmittance percentages (decreased intensity). The aim of FTIR analysis is to interpret the alterations in functional groups' intensity, specifically an increase of O-H and a decrease of other functional groups' (C-H, C=O, C-O) intensities as an indicator of degradation to investigate the most efficient treatment to degrade the PET. However, the main focus is on the C=O bond due to the importance of ester cleavage in PET degradation. Ester bond hydrolysis occurs as a result of the serine oxygen's nucleophilic attack on the carbonyl carbon within the ester bond (Han et al., 2017; Roberts et al., 2020; Urbanek et al., 2021) which leads to the intermediate products of degradation, BHET and MHET. DTAB surfactant leads to an increase of transmittance percentage of the carbonyl group which suggests lower energy to break down the PET. Besides, in the spectrum of both surfactants-treated PET pieces, the O-H group can be observed at 3391 cm^{-1} . As can be seen, the figure 4.1 shows the molecular structure of PET.

The PET molecular structure involves; 1) ester bond ($\text{RCO}_2\text{R}'$) which has carbonyl group (C=O), aromatic ether (C-O) and aliphatic ether (C-O) functional groups, 2) benzene ring which has aromatic C-H functional group, 3) hydrocarbon chain which contains aliphatic C-H functional groups is shown in figure 4.1 (Robert et al., 2020).

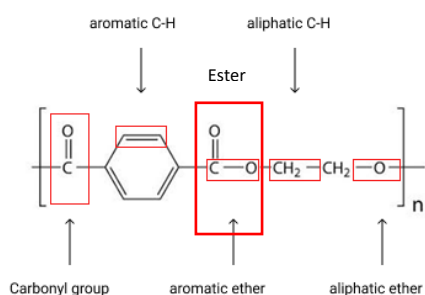


Figure 4.1. Presence of functional groups in molecular structure of PET (Roberts et al., 2020).

During the hydrolysis reaction, the ester bonds become weaker and finally break down which leads to the presence of hydroxyl group (O-H) and carboxylic acid groups (COOH) in the spectrum. Carboxylic acid contains the carbonyl group and hydroxyl group (Roberts et al., 2020). Figure 4.2 illustrates the degradation products of PET and presence

of the hydroxyl group during this process. Table 4.1 shows the PET functional groups and their specific wavenumber based on the literature (Pereira et al., 2017).

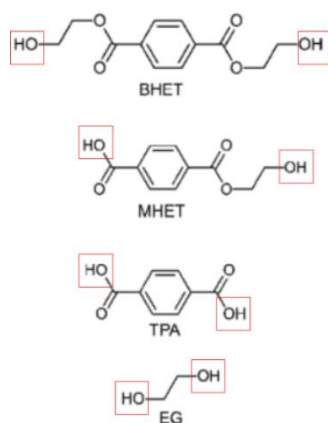


Figure 4.2. The PET sample after hydrolysis reaction breaks down to Bis (2-hydroxyethyl) terephthalate (BHET), Mono (2-hydroxyethyl) terephthalate MHET, Terephthalic acid (TPA) and ethylene glycol (EG). The figure shows the presence of hydroxyl groups in cited molecules (Roberts et al., 2020).

Table 4.1. Functional groups of PET and the related wavenumber

Functional groups	Wavenumber (cm ⁻¹)
O-H	3391
C=O	1715
C-O (aromatic)	1245
C-O (aliphatic)	1100
C-H (aliphatic)	870
C-H (aromatic)	730

The biofilm assay results show higher biofilm formation on DTAB-treated PET. However, it cannot be concluded that higher transparency causes increased biofilm formation directly, as other results cannot confirm that. The biofilm formation results related to DTAB treatment in the presence of *I. sakaiensis* in YSV medium indicate high OD₅₇₀ after one week of incubation. However, after two weeks the graph (Result, Chapter 3.1, Section 3.1.3, Fig 3.11 and 3.12) indicates a decreasing trend. This can be attributed to the dislodgment of the biofilm adhered to the PET surface. The dislodgment event is a

well-known stage within the biofilm formation process. The biofilm formation process encompasses several sequential steps, including the reversible and irreversible attachment of cells to the substrate, followed by the establishment of micro-colonies, subsequent development of macro-colonies, and eventual maturation of the biofilm through the accelerated generation and accumulation of extracellular polymeric substances (EPS). Ultimately, this culminates in the dispersal of cells from within the mature biofilm structure, as outlined by Douterelo et al. (2014). Consequently, the biofilm arrives at the dispersal stage after a span of two weeks, initiating a renewed cycle whereby planktic cells embark on the biofilm formation process once again, reinstating the biofilm's presence and attributes. Biofilms provide a protective environment for the bacteria and their associated enzymes, creating localized concentrations which facilitate the degradation of PET. This approach has shown promise in enhancing PET degradation efficiency (Muhammad et al., 2020).

Biofilm formation is highly critical for the degradation of PET due to its effecting changes in the physicochemical properties of PET such as alteration in functional groups and enhancement of the hydrophilicity of the PET surface (Han et al., 2020). Biofilm formation can enhance the hydrophilicity of PET through several mechanisms. When microorganisms colonize the PET surface and form a biofilm, they secrete extracellular polymeric substances (EPS). EPS is a complex mixture of polysaccharides, proteins, lipids, and nucleic acids that make up the matrix of the biofilm (Muhammad et al., 2020).

One way in which biofilm formation enhances hydrophilicity is through the production of exopolysaccharides. These polysaccharides are hydrophilic in nature, meaning they have an affinity for water. As the biofilm grows and accumulates on the PET surface, the exopolysaccharides become more abundant, creating a hydrated matrix. This hydrated matrix increases wettability of PET, making it more hydrophilic (Muhammad et al., 2020; Han et al., 2020; Ramírez-Larrota et al., 2022).

Based on the results acquired from different treatments on PET pieces in *I. sakaiensis* culture in YSV (Result, Chapter 3.1, Section 3.1.2.1.2, Fig 3.5), it can be interpreted that DTAB treatment has a higher impact on PET pieces in the defined medium rather than the complex medium. Even the non-treated PET pieces show a higher percentage transmittance in defined medium rather than a complex medium (HPP). This is expected due to the good growth of *I. sakaiensis* in a rich medium such as HPP. In such medium, there is little need to use any other difficult source of carbon for assimilation (such as PET). In a defined medium, the lack (or low concentration of carbon source) drives the

cells towards any consumable source of carbon, in this case, PET. The cells form biofilm on the PET film, and through the enzymatic process, assimilate the carbon source in the PET backbone.

The effectiveness of DTAB as a cationic surfactant is expected due to the surfactant; it facilitates the hydrolysis of PET. Surfactant treatment can increase the wettability and adhesion properties of PET (Urbanek et al., 2021; Sagong et al., 2020; Samak et al., 2020; Furukawa et al., 2019). Surfactants can accelerate the hydrolysis of PET films, which leads to a decrease in the molecular weight of the polymer and a decrease in the mechanical properties by the penetration of water into the PET film structure (Soong et al., 2022). DTAB interacts with the PET surface, causing it to form micelles or aggregates. This increases the surface area of the PET, providing more sites for enzymatic attack. Also, it is found that DTAB stabilizes the enzymes involved in PET degradation, such as cutinases and lipases. These enzymes can efficiently break down PET into its constituent monomers, terephthalic acid and ethylene glycol. The DTAB micelles help to solubilize the PET polymer, making it more accessible to the enzymes. This enhances the enzymatic hydrolysis process. The combination of DTAB and enzymes accelerates the hydrolysis of PET, leading to a faster breakdown of the polymer into its monomers. The PET surface is activated by treating it with anionic surfactants. The surfactants adsorb onto the surface, reducing its contact angle and increasing its surface energy. This modification allows water or other coatings to spread more uniformly on the surface (Furukawa et al., 2018).

Sodium dodecyl sulfate (SDS) is used as an anionic surfactant for pre-treatment of PET pieces in the presence of *I. sakaiensis* (Furukawa et al., 2018). This anionic surfactant can accelerate the hydrolysis reaction on PET due to the positive electrical charge of PETase and the negative charge of SDS. A 120-fold-increase in the hydrolytic activity of PETase has been reported (Furukawa et al., 2018; Sagong et al., 2020; Soong et al., 2022). The thickness of the PET film decreased by 22% following a 36 hrs degradation process at a temperature of 30°C in the presence of *I. sakaiensis*. Under this particular condition, the surfactants played a crucial role in enhancing the binding between the hydrophilic PETase and the hydrophobic surface of PET. It's worth noting that the surfactant concentration utilized in this degradation method was remarkably low, standing at only 0.005% (Samak et al., 2020).

Furukawa et al., 2018, investigated the effect of a cationic surfactant (dodecyltrimethylammonium chloride). They found a decrease in the enzyme activity of

PETase after the surfactant treatment. However, in their later study, they reported an enhancement in the activity of the wild type *T. fusca* cutinase in the presence of this surfactant (Furukawa et al., 2019). This study showed that the degradation rate increased 12.7 times compared to the degradation in the absence of the cationic surfactant. Also, Mukherjee et al., 2017, studied the effect of the anionic surfactant, SDS, on polyethylene at 60 °C for one month in the presence of *Lysinibacillus fusiformis* (*L. fusiformis*). Besides the effect of other surfactants including sodium dodecyl benzene sulphonate (anionic), CTAB (cationic) and Tween 80 (non-ionic) was investigated on PE. polyethylene is oxidised by sodium dodecyl sulphate and solubilized by sodium dodecyl benzene sulphonate (Mukherjee et al., 2017; Kawai et al., 2022).

The two strains *I. sakaiensis* and *P. mendocina* (Yoshida et al., 2016; Ronkvist et al., 2009) have been reported to degrade PET, but the degradation efficiency is very low. *I. sakaiensis* can completely degrade the PET after six weeks. PET had 5% weight loss at 50 °C in the presence of *P. mendocina*. However, there has been a lack of investigation of cationic and nonionic surfactants on PET in the presence of these two strains. The pre-treatment of PET with the surfactants DTAB and Brij-35 was investigated in this project as a novel approach for potential improved biodegradation.

So, based on Result Chapter (3.1) figure 3.5 to 3.11, the most effective pre-treatment of PET pieces is related to DTAB treatment in the YSV medium. As can be seen in figure 3.5 the C=O functional group transmittance percentages present that DTAB treatment in YSV has the most effect on PET pieces. It appears that the choice of media may have a role in the carbonyl group percentage and subsequently on the degradation of PET. Also, after passing one week the biofilm formation on DTAB-treated PET shows a significant ($P < 0.0001$) enhancement rather than non-treated PET.

Based on previous studies such as Furukawa et al., 2018, the initial anticipation was that DTAB would exhibit limited efficacy in the presence of *I. sakaiensis* due to positive charge of PETase and DTAB. However, this study shows that DTAB has the potential to enhance the surface property of PET in the presence of the *I. sakaiensis* due to which leads to the enhancement of the biodegradation process. DTAB can improve the adsorption of PET-degrading enzymes onto the PET surface. Enzyme adsorption is a crucial step in the degradation process, as it brings the enzymes into close proximity with the PET substrate. DTAB surfactant properties can help enzymes overcome the hydrophobic barrier presented by PET, allowing for better enzyme-PET interactions.

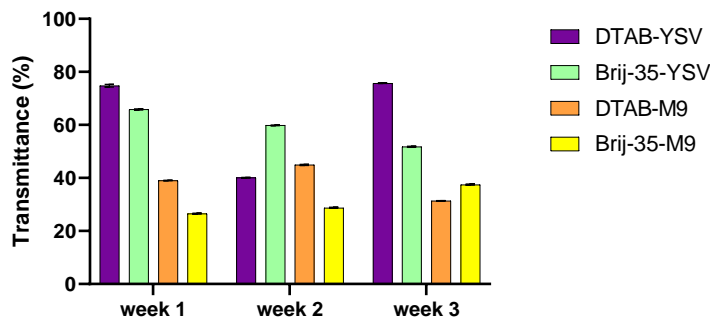


Figure 4.3. Transmittance percentages of carbonyl group related to DTAB and Brij-35 pre-treated PET pieces in YSV and M9 minimal medium over three weeks of incubation with *I. sakaiensis* at 30 °C.

Below are further treatments that have demonstrated effectiveness in diverse media. The obtained results from the different treatments on PET pieces in the presence of *I. sakaiensis* culture in HPP medium (Result, Chapter 3.1, Tables 3.1, 3.2 and 3.3), indicate that the most effective method for degradation of PET pieces in this culture (HPP) is NaOH pre-treatment after one week. Several papers studied the effect of NaOH on pre-treatment of PET (Karayannidis et al., 2007; Caparanga et al., 2009; Biswas et al., 2022; Giraldo-Narcizo et al., 2021). The recent paper Giraldo-Narcizo et al., 2021 demonstrated that the NaOH treatment can modify the surface of the PET and improving the accessibility of PETase to hydrolysable chemical bonds and enhance the production of TPA and MHET. Based on the results obtained (Result, Chapter 3.1, Section 3.1.2.2.1, Fig 3.7) regarding carbonyl transmittance percentage, it is apparent that there were no significant variations observed in transmittance percentages across different mediums or over time. This indicates that the influence of the NaOH treatment on PET was primarily confined to the treatment process itself and did not manifest after the culture was introduced (Result, Chapter 3.1, Section 3.1.2.2.1, Fig 3.7). Also, using sodium hydroxide (NaOH) can have negative environmental effects such as water pollution, soil contamination, high energy consumption during production, and waste generation. (National Research Council (US) Committee on Toxicology, 1984).

The second considerable pre-treatment is the application of UV. There has been a lack of investigation of UV treatment in the presence of *I. sakaiensis* and *P. mendocina*. However, Taghavi et al., 2021 investigated the effect of UV light on the degradation of PET. They used UV light (245 nm) for 72 and 120 hrs in two different distances of 24

and 12 cm. They found that the best result was related to the shorter distance (12 cm) and higher period of exposure (120 hrs). In the current project, the UV light under a higher wavelength (365 nm) was investigated. The higher wavelength was used to mimic the UVA which contains 95% of sunlight and can mimic the exposure conditions more realistically. The findings from this project (Result, Chapter 3.1, Section 3.1.2.2.4, Fig 3.10) show that UV treatment show significant potential for priming PET for subsequent degradation processes in HPP medium in the presence of *I. sakaiensis*. Notably, a higher transmittance percentage can be observed in the HPP medium, indicating improved PET transparency. This enhancement can be attributed to the effects of UV light, which facilitates PET degradation by increasing the transmittance percentage of carbonyl groups through a photooxidation process. This photooxidation process is a result of the interaction between UV light and ester bond in PET structure, promoting structural changes that render PET more amenable to degradation. Such alterations in PET's chemical composition and structure are essential for its successful breakdown in various environmental contexts.

Based on the first week results, this can be seen that NaOH and UV treatments can encourage the biodegradation process of PET in *I. sakaiensis* culture in HPP (Result, Chapter 3.1, Section 3.1.2.1.1, Fig 3.4). By three weeks, no significant changes were observed in the transmittance percentages of PET pieces treated with NaOH and UV. The complex medium (HPP) provides more nutritious environment for bacterial growth, so, there is no need for bacteria to consume the PET pieces in the medium as a carbon source. The defined medium provides the suitable environment for bacteria to use the PET as a carbon source. In comparison between YSV and M9 minimal medium, the YSV includes vitamins and trace elements needed for the metabolic activities of the microbe.

The results of the different treatments using *I. sakaiensis* culture in M9 minimal medium, confirm that DTAB treatments have the most impact on PET pieces over the three weeks. Besides, Brij-35 treatment has a notable effect on PET pieces after three weeks. The results of UV-treated PET pieces in *I. sakaiensis* culture in M9 minimal medium are unavailable due to contamination.

In the M9 minimal medium, the evaluation of biofilm formation demonstrates notable variations among the treatments over the three-week period. Specifically, the DTAB treatment exhibits superior performance, with a slight increase observed after the first week, followed by a gradual declining trend in biofilm formation after the third week. A comparable pattern is observed in the case of Brij-35 treatment, where biofilm formation

follows a trajectory akin to that of DTAB. Conversely, the NaOH treatment showcases distinct dynamics, with biofilm formation reaching a comparable level in both the first and third weeks but experiencing a decrease in the second week. These nuanced temporal trends in biofilm formation highlight the varying impacts of these treatments on the adherence and growth of microorganisms over the specified three-week experimental duration within the M9 minimal medium. This could be due to detachment of part of the formed biofilm. Comparing the biofilm formation results and transmittance percentages, in DTAB treatment, the trend of biofilm and transmittance is similar. However, in Brij-35 and NaOH treatment the biofilm formation and transmittance percentages present the opposite trend. So, the opposite trends can be explained by the fact that Brij-35 enhances biofilm formation by improving microorganism attachment, but its surfactant properties may slightly affect transmittance. On the other hand, NaOH treatment hinders biofilm formation by degrading the PET surface, but it may improve transmittance by making the PET surface smoother and more transparent.

4.2.2. PET pre-treatment in the presence of *P. mendocina*: FTIR and biofilm

The most prominent finding is that the treatment of PET pieces with DTAB in M9 minimal medium demonstrated efficacy in the presence of *P. mendocina*. This outcome suggests that *P. mendocina* exhibited superior growth and PET degradation capabilities in M9 minimal medium after DTAB treatment, implying a preference for this medium over the YSV medium that was found to be conducive to the growth of *I. sakaiensis*. Different requirements for metabolic activities of *P. mendocina* and *I. sakaiensis* are the probable reason for the observed variation. *Pseudomonas* species have shown limited effectiveness in breaking down PET. For instance, a lipase obtained from an unspecified *Pseudomonas* species couldn't facilitate the degradation of PET, as observed in the study by Muller et al. in 2005. Similarly, in a study by Jun et al. in 1994, an extracellular lipase from an unspecified *Pseudomonas* species was ineffective in breaking down a mixture containing poly(ϵ -caprolactone) and more than 50 % PET. However, a different enzyme, cutinase, derived from *P. mendocina*, demonstrated a strong attraction to PET with low crystallinity. This cutinase managed to reduce the film's weight by 5 %, although the original weight of the film wasn't specified, as indicated in the research by Ronkvist et al. in 2009.

In this study, the FTIR analysis on PET samples after one week revealed significant insights in the presence of *P. mendocina*. Notably, the highest transmittance was observed in PET pieces subjected to DTAB treatment.

The results from the different treatments in *P. mendocina* culture in HPP indicate that the NaOH treatment has a higher impact compared to other treatments on PET pieces. The next main alteration in the intensity of transmittance is related to the Brij-35 treatment. For the YSV medium, Brij-35 treatment showed a significant effect on PET pieces based on results obtained from transmittance percentage. Brij-35 is a non-ionic surfactant known for its ability to improve the wetting properties of hydrophobic surfaces like PET. In YSV medium, the surfactant properties of Brij-35 may reduce the contact angle between the medium and the PET surface, making it more hydrophilic. This enhanced wettability encourages better contact between the medium, microbial culture, and the PET surface.

Considering the growth media, both DTAB and NaOH treatments emerged as factors influencing PET pieces in M9 minimal medium. This emphasises the importance of surface modification in suitability for microbial colonization and degradation.

The biofilm assay results in agreement with FTIR spectra further underscored the positive impact of DTAB and NaOH treatments on biofilm formation on PET surfaces, highlighting their role in facilitating microbial adhesion and growth.

The biofilm formation results related to each treatment in the presence of *P. mendocina* in HPP medium indicate higher OD₅₇₀ records from NaOH and Brij-35-treated PET pieces. Also, biofilm formation and transmittance percentages follow similar trends which means by increasing the biofilm formation, higher transmittance percentages were obtained. In terms of biofilm formation, the best result was obtained from NaOH treatment. However, the difference of biofilm formation between the different PET pre-treatments by NaOH or Brij-35 is not significant (Result, Chapter 3.1, Section 3.1.5, Fig 3.19).

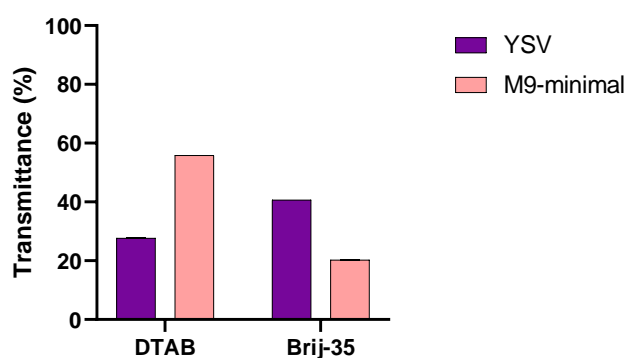


Figure 4.4. Transmittance percentages of carbonyl group related to DTAB and Brij-35 pre-treated PET pieces in YSV and M9 minimal medium after one week of incubation with *P. mendocina* at 30 °C.

It can be concluded based on obtained results of FTIR and biofilm formation that DTAB treatment in the presence of *I. sakaiensis* in YSV medium presents significant potential to enhance the degradation of PET. Also, Brij-35 in YSV medium can pre-treat the PET and make it ready for bacterial adhesion compared to DTAB. More biofilm was formed on DTAB-treated PET in M9 minimal medium in the presence of *I. sakaiensis*. Also, in the presence *P. mendocina*, DTAB treatment in M9 medium and Brij-35 in YSV medium seem to be the most effective treatments based on biofilm formation and transmittance percentage of carbonyl group.

M9 minimal media typically contain only essential nutrients for bacterial growth, which could be limiting for some bacteria. The presence of DTAB on PET surfaces might have provided additional nutrients or co-factors that were not available in the M9 minimal medium alone, promoting the growth and biofilm formation of *P. mendocina*. In addition, DTAB treatment could have altered the PET surface in a way that stabilized the biofilm structure. This may result in stronger interactions between the bacterial cells and the modified PET surface, leading to a thicker and more stable biofilm.

4.2.3. Comparison between *I. sakaiensis* and *P. mendocina*

The comparison of the results between *I. sakaiensis* and *P. mendocina* biodegradation of PET is based on one week. The main reason for this was that the best results obtained in the first week by *I. sakaiensis*, and also it was a more efficient and effective microbe compared to *P. mendocina* for degradation. However, it is important to arrive at higher biodegradation in a shorter time due to operational and economic reasons. In this context, the results based on one week are scrutinized (Fig 4.4, 4.5 and 4.6).

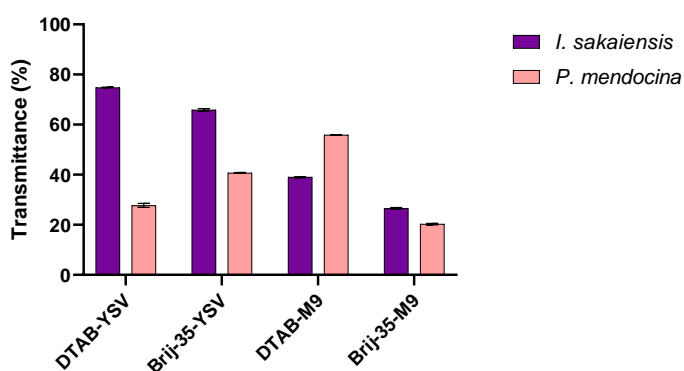


Figure 4.5. Comparing the carbonyl functional groups related to DTAB and Brij-35- treated PET pieces in the presence of *I. sakaiensis* and *P. mendocina* in defined media (YSV and M9) after one week.

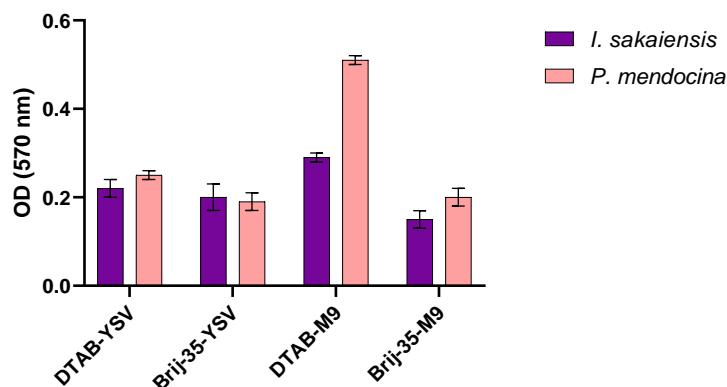


Figure 4.6. Comparing the biofilm formation related to DTAB and Brij-35- treated PET pieces in the presence of *I. sakaiensis* and *P. mendocina* in defined media (YSV and M9) after one week.

The DTAB treatment on PET could alter its optical properties, affecting light transmittance independently of the biofilm (Fig 4.5 and 4.6). Changes in surface roughness and refractive index due to DTAB treatment may play a role in transmittance. If the refractive index of the biofilm and the surrounding medium (e.g., M9 minimal medium) is aligned light scattering at the biofilm-medium interface may be minimized, leading to lower transmittance despite significant biofilm formation.

Based on the results, the highest carbonyl group transmittance percentage was obtained after DTAB-treated PET in the presence of *I. sakaiensis* within a 6-well plate after one week (Result, Chapter 3.1, Section 3.1.2.1.2, Fig 3.5). This finding signifies the potential of DTAB-treatment for further exploration on a larger scale. Also, the same outcome was observed for *P. mendocina*.

In conclusion, the findings of this study offer valuable insights into the different responses of *P. mendocina* and *I. sakaiensis* to varying growth media and treatments on PET pieces. The observed preference of *P. mendocina* for M9 minimal medium and its enhanced PET degradation capabilities when subjected to DTAB treatment highlight the importance of metabolic adaptations in microbial responses. The FTIR analysis and biofilm formation results provide an understanding of the surface modifications induced by treatments, shedding light on their contributions to biofilm formation and the transparency of PET substrates. This study contributes to our knowledge of microbial interactions with PET materials and offers potential avenues for optimizing PET degradation strategies and biofilm-related applications.

4.3. DTAB-treatment at larger scale: effect on PET biodegradation

Further investigation was carried out to discover the effect of (DTAB) on PET pieces in a larger scale experiment ($\times 15$ higher volume and for a longer period of time) a) in the presence of *I. sakaiensis* and b) *P. mendocina* in YSV medium.

FTIR spectra studies revealed that the DTAB-treated PET pieces have higher transmittance percentages compared to non-treated PET after one week of incubation in the presence of *I. sakaiensis*. This indicates that DTAB, is capable of altering the functional groups of PET after one week. After four weeks, all the PET pieces in the two flasks out of the three were dissolved in the presence of *I. sakaiensis*. However, there were no changes in FTIR spectra of DTAB-treated PET and non-treated PET in the presence of *P. mendocina* throughout the eight weeks of incubation.

The biofilm formation on the DTAB-treated PET pieces in the presence of *I. sakaiensis* and *P. mendocina*, separately, in the larger scale experiment were investigated for eight weeks. The biofilm formation on DTAB-treated PET pieces in the presence of *P. mendocina* did not show any significant effect between DTAB-treated PET in comparison with non-treated PET pieces over the eight weeks. However, the biofilm formation in the presence of *I. sakaiensis* significantly increased after DTAB treatment within one week of incubation. It was not possible to investigate biofilm formation of *I. sakaiensis* in two out of the three flasks as PET pieces were completely dissolved. The results obtained from the FTIR analysis, coupled with the assessment of biofilm formation, in relation to the third flask, indicate that the PET surface treated with DTAB exhibited a greater potential for enhanced biofilm formation and increased transmittance percentages when compared to non-treated PET (Result, Chapter 3.2, Section 3.2.1 and 3.2.2, Fig 3.20 and 3.21). This observation was made after one week of incubation in the presence of the bacterium *I. sakaiensis*, highlighting the effectiveness of DTAB treatment in promoting biofilm development and optical properties of PET materials under these experimental conditions.

To further explore the biodegradation process, HPLC analyses were conducted on both DTAB-treated and non-treated PET samples in the presence of *I. sakaiensis* and *P. mendocina* at three different time points of one, four and eight weeks.

The HPLC results for samples containing *I. sakaiensis* demonstrated presence of TPA as a product of PET degradation. Notably, the quantity of TPA progressively increased from an initial level of 0 $\mu\text{g/ml}$ to a significant concentration of 16.6 $\mu\text{g/ml}$ after the eight-week

incubation period (Result, Chapter 3.2, Section 3.2.3, Fig 3.24). This substantial rise in TPA production indicates the efficacy of *I. sakaiensis* in catalysing the degradation of PET, successfully breaking down the polymer into TPA.

Conversely, the HPLC results concerning *P. mendocina* exhibited an entirely different outcome. Surprisingly, no TPA production was detected even after an extended incubation period of eight weeks. This finding suggests that *P. mendocina* may not be as effective in breaking down PET or generating TPA under the experimental conditions employed.

These HPLC results provide valuable insights into the divergent abilities of *I. sakaiensis* and *P. mendocina* to degrade PET. While *I. sakaiensis* exhibited TPA production over time, indicating its potential application in PET biodegradation, *P. mendocina* did not. These findings underscore the significance of understanding the different abilities of microorganisms in the biodegradation process and may guide the selection of more efficient biodegradation strategies in the future.

However, the peaks reported (Result, Chapter 3.2, Section 3.2.3, Fig 3.24 and 3.25) did not exhibit sharpness. Consequently, the relevant TPA chromatograph area was considered. An investigation into the underlying causes of wide peak revealed several factors such as contaminants in the column can affect peak shape, sample solubility and purity, sample overloading, column age and mobile phase issues.

Addressing these factors through proper column maintenance and optimization of chromatographic conditions can help achieve sharper HPLC peaks. Also, further improvement of the obtained results is possible through further purification of the samples before the HPLC is done.

In conclusion based on the obtained results from FTIR and HPLC indicate that there is negligible disparity between the performance of DTAB-treated and non-treated PET in the presence of *P. mendocina*. As such, it became apparent that the focus of subsequent experiments should shift towards FSC-treatment and the investigation of QSM in the presence of *I. sakaiensis*. This decision was motivated by the striking contrast in the effectiveness of *I. sakaiensis*, as compared to *P. mendocina*, in the biodegradation process. So, the further experiments were carried out solely on *I. sakaiensis*.

4.4. FSC-treatment effect on PET biodegradation

The most prominent result for PET degradation was obtained from FSC-treatment of PET in the presence of *I. sakaiensis* during the eight weeks in both 6-well plate and larger scale (500 ml shaken flasks) (Result, Chapter 3.3, Section 3.3.2.2, Fig 3.29; section 3.3.3.2, Fig 3.31).

To gain a deeper understanding of the chemical changes occurring in the PET samples, FTIR analysis was performed. The results demonstrated that the transmittance percentage of the carbonyl group in FSC-treated PET was consistently higher than that of non-treated PET in the 6-well plate. Over the course of three weeks, the transmittance percentage increased to 62 (Result, Chapter 3.3, Section 3.3.2.2, Fig 3.29). This shows that FSC is able to break down the ester bonds in the PET structure. However, for further confirmation, HPLC was carried out to record presence of monomers such as TPA and EG.

Additionally, the FTIR results from the larger scale experiment showed even more pronounced effects compared to 6-well plate. In the FSC-treated PET samples, the transmittance percentage of the carbonyl group increased up to 79.67 and 91.69 by the weeks one and eight, respectively. Furthermore, HPLC results (Appendix, Chapter 6, Fig 6.19) suggest that the FSC treatment not only increases the abundance of carbonyl groups but also leads to their complete conversion in the later stages of the experiment.

This study revealed significant differences in biofilm formation between non-treated PET and FSC-treated PET. In a 96-well plate after 24 hrs, the biofilm formation on FSC-treated PET was considerably higher compared to non-treated PET. This suggests that the FSC treatment enhances the substrate's ability to support biofilm growth. The enzymes can support biofilm growth through several mechanisms. These mechanisms include surface modification of PET by breaking down or altering the chemical composition of the polymer. For example, enzymes like lipases can hydrolyse PET, creating surface irregularities or functional groups that make it more suitable for microbial attachment. Another mechanism includes enzyme-facilitated production of extracellular polymeric substances (EPS) by microorganisms. EPS is a critical component of biofilms. Enzymes like exopolysaccharidases can promote the synthesis of polysaccharides and other EPS components, providing structural stability and adhesion sites for microbial cells. Also, some enzymes can influence quorum sensing, a cell-to-cell communication system used by bacteria in biofilms to coordinate their behaviour (Amache, 2014). By modulating quorum sensing signals, enzymes can promote microbial aggregation and biofilm

development. In addition, enzymes can break down complex organic molecules in the surrounding environment, releasing nutrients that can promote microbial growth and biofilm formation. This can be especially important in environments where nutrient availability is limited. Cell Attachment is another mechanism that certain enzymes, such as proteases, can cleave proteins and promote the exposure of adhesion molecules on the PET surface. This enhances the initial attachment of microbial cells to the polymer.

Moreover, in a 6-well plate, the FSC-treated PET exhibited a higher amount of biofilm after one week of incubation. After passing four weeks the biofilm formation reduced and the biofilm formation recovered after eight weeks. Similarly, in scale-up experiment the biofilm formation on FSC-treated PET show higher optical density. However, after four weeks the biofilm formation reduces and after eight weeks the biofilm formation increased. This phenomenon may be related to the different stages of biofilm formation in which the biofilm dislodges and the released cells convert to the planktonic state again. There is little evidence about the effect of FSC on biofilm formation of bacteria. However, Li et al., 2022 studied the effect of alcalase, neutrase and α -amylase on biofilm formation of *Shewanella marisfavi* ECSMB14101 (*S. marisfavi*). The study shows the reduction in biofilm formation. The reason for this phenomenon may be the enzyme disruption of bacteria leading to its death. Based on previous studies, cutinases have emerged as key players in the realm of environmentally friendly PET degradation. These complex biological catalysts, such as PETase and cutinase, have shown potential in facilitating the breakdown of PET by selectively hydrolysing its ester bonds. By leveraging the power of these cutinases, the degradation process of PET can be significantly enhanced (Ronkvist et al., 2009; Acero et al., 2011).

Scientific investigations have demonstrated the capability of cutinases derived from *H. insolens*, *T. fusca*, and *F. solani* to enhance the degradation of PET (Ronkvist et al., 2009; Acero et al., 2011; Sulaiman et al., 2012; Furukawa et al., 2019). Also, in 2021 Spina et al. investigated *F. oxysporum*, *F. falciforme* and *Purpureocillum lilacinum* degradation ability of PE. A study conducted by Aguilar Alvarado et al. in 2015 investigated the growth of *F. culmorum* on media that included di (2-ethyl hexyl) phthalate (DEHP). Their findings showcased the organism's capability to break down esterified compounds. However, the scientific literature lacks comprehensive studies on the potential of cutinases from *F. culmorum* in PET degradation. To address this research gap, and contribute to improvement of biodegradation process, the present project employed *F. culmorum* to produce cutinase and employed its supernatant containing

cutinase (FSC) in the pre-treatment of PET pieces. The primary objective was to assess the potential of this particular fungal species to effectively degrade PET in the presence of *I. sakaiensis*.

On the other hand, the HPLC analysis illustrates an increase in TPA production after FSC and FSC-DTAB treatment over the eight weeks. The introduction of FSC-DTAB combination treatment signifies a potential synergistic effect, enhancing their ability to cleave PET bonds and accelerate degradation and lead to improved efficiency and productivity in TPA production. As regards surface modification, DTAB can adsorb onto the surface of PET due to its hydrophobic tail and positively charged headgroup. This adsorption alters the surface properties of PET, increasing its wettability and rendering it more accessible to enzymes. This modification improves the contact between enzymes and the PET surface. DTAB-coated PET surfaces can attract enzymes more effectively due to the electrostatic interactions between the positively charged surfactant headgroup and the negatively charged regions on enzyme molecules. This increased enzyme adsorption helps in concentrating enzymes at the PET surface. The presence of DTAB on the PET surface can also disrupt the crystalline structure and reduce the hydrophobicity of PET. This, in turn, makes the PET surface more susceptible to enzymatic attack. Enzymes that can break down PET, such as PETases, can work more efficiently on a surface modified by DTAB. This can be crucial for prolonged enzymatic degradation processes.

It is important to note that the effectiveness of DTAB in preparing PET for enzymatic degradation may vary depending on factors like specific enzymes used, the concentration of DTAB, and the characteristics of the PET substrate (e.g., molecular weight, crystallinity, surface area). Additionally, the environmental and regulatory considerations of using surfactants like DTAB in PET degradation processes should be carefully evaluated, as surfactants may have environmental impacts and require appropriate disposal or treatment. To overcome this problem the biosurfactants such as rhamnolipid can be used for PET degradation (Taghavi et al., 2022). However, they are expensive to use.

Also, surfactants can enhance the enzymatic PET hydrolysis (Maurya et al., 2020). Surfactants can have an impact on the functioning of enzymes. By binding with enzymes, surfactants can modify the secondary and tertiary structure and influencing its kinetic properties (Rubingh, 1996; Maurya et al., 2020). Furthermore, the use of surfactants can enhance the dispersal of PET particles, potentially increasing the accessibility of the

substrate to enzyme. In a study conducted by Chen et al. (2010), the presence of the surfactant sodium taurodeoxycholate in the reaction mixture led to a notable increase in the degradation of PET film (73.65 %) by cutinase from *F. solani pisi*. Similarly, the addition of the surfactant alkyl trimethyl ammonium chloride in the reaction medium resulted in complete degradation of PET after 30 hrs at various temperatures using the *T. fusca* double-mutant cutinase (TfCut2) (Furukawa et al., 2019; Maurya et al., 2020). The FSC treatment was done on DTAB-treated PET in this study.

High resolution microscopy and SEM were done to investigate the structure of the PET after FSC treatment and FSC-DTAB treatment. It shows that there are more pores on the surface of the FSC-treated PET and FSC-DTAB-treated PET than non-treated PET after eight weeks.

In conclusion, the results obtained from the study indicate that the FSC-treated PET exhibits enhanced biofilm formation compared to non-treated PET, both in a 96-well plate and at larger scale experiments. FTIR analysis revealed an increase in the transmittance percentage of the carbonyl group, suggesting chemical changes induced by the FSC treatment in 6-well plate and at large scale (Result, Chapter 3.3, Section 3.3.2.2, Fig 3.29; section 3.3.3.2, Fig 3.31).

Relating the results of biofilm formation to the HPLC analysis involves understanding the potential impact of biofilm formation on the production process and the overall TPA yield. Biofilms can act as a protective barrier, encapsulating enzymes and other microorganisms within their matrix. Depending on the type of biofilm and its composition, it may either enhance or hinder enzyme activity. If the biofilm promotes better enzyme stability or protects the enzyme from harsh reaction conditions, it could lead to increased TPA production, which would be reflected in the HPLC analysis as higher TPA concentrations. The microenvironment within the biofilm can vary significantly from the bulk solution, with different pH, oxygen levels, and nutrient availability. Enzymes may exhibit altered activity and specificity within the biofilm, affecting the reaction kinetics and TPA production rate. By comparing biofilm-grown reactions to planktonic cultures using HPLC, differences in TPA yield can be assessed. Biofilm communities often exhibit distinct metabolic pathways and interactions between different microorganisms. Some microorganisms within the biofilm may produce metabolites or by-products that influence TPA production or act as co-factors for enzymes involved in the synthesis pathway. HPLC analysis can be used to detect these metabolites and assess their impact on the overall TPA production process.

4.5. QSM effect on PET biodegradation

The presence of quorum sensing molecules in this project showed an enhancement of biofilm formation on PET surfaces that had undergone specific treatments. In this study, PET samples were treated with DTAB FSC, and a combination of both treatments. Surprisingly, the presence of QSMs demonstrated a significant enhancement of biofilm formation on all the treated PET samples.

This study evaluated the impact of QSMs on the chemical structure of PET by assessing the transmittance of the carbonyl group, a key indicator of PET degradation. Remarkably, the presence of QSMs significantly increased the carbonyl transmittance percentage after FSC treatment on PET after one week of incubation with *I. sakaiensis* (Result, Chapter 3.4, Section 3.4.4.2, Fig 3.41) suggesting that QSMs might contribute to the chemical breakdown of PET.

Considering the objective of accelerating PET degradation and the findings of this study, the most effective and environmentally friendly treatment approach appears to be the use of enzymes, particularly FSCs, in conjunction with QSMs. Further research is warranted to explore the underlying mechanisms and optimize this approach for potential applications in PET waste management and environmental sustainability.

Specifically, the FSC-treated PET showed a remarkable increase in biofilm formation after just one week of incubation in the presence of *I. sakaiensis*, in QSM supplemented culture. The OD₅₇₀ measurement, a proxy for biofilm growth, reached an impressive value of 1.1 after one week. On the other hand, the DTAB-treated PET exhibited a slower rate of biofilm formation, with an OD₅₇₀ of 0.4 achieved after one week of incubation under similar conditions. After eight weeks, the OD₅₇₀ of FSC-treated and DTAB-treated PET reached to 1.5 and 1.0, respectively.

The study also explored the combined treatment of the FSC and DTAB, along with the presence of QSMs. This combination demonstrated even greater potential for enhancing biofilm formation. After eight weeks of incubation, the biofilm on the FSC-DTAB-treated PET reached an OD₅₇₀ value of 1.89, indicating a substantial increase compared to the other treatments. The results verified the result of 6-well and in fact produce more effective outcomes (Result, Chapter 3.3, Section 3.3.2.2, Fig 3.28; Chapter 3.4, Section 3.4.4.2, Fig 3.41).

In the early stages of biofilm formation, bacteria communicate with one another using QSMs to coordinate the expression of genes involved in the production of the

extracellular matrix. In the early stages of biofilm formation, QSMs can also play a role in regulating the expression of genes involved in nutrient acquisition, motility, and virulence.

To date, there are no publications on the potential effect of QSMs on DTAB-treated PET surfaces. However, it is possible that QSMs could influence the behaviour of bacteria on these surfaces, potentially affecting biofilm formation and adhesion.

However, the extent to which QSMs can enhance the degradation of PET through biofilm formation is not yet fully understood and may depend on various factors, including the type of bacteria involved, the properties of the plastic, and the environmental conditions. Further research is needed to determine the mechanisms underlying this process and to develop strategies.

For example, some QSMs, such as acyl-homoserine lactones (AHLs), have been shown to promote biofilm formation on various surfaces (Huang et al., 2022). After DTAB treatment on PET surface, AHLs could potentially enhance bacterial attachment and biofilm formation, leading to increased surface fouling and reduced material performance.

Overall, the specific effect of QSMs on DTAB-treated PET surfaces will depend on the specific QSMs, the bacterial species involved, and the conditions of the system. More research is needed to fully understand the potential interplay between QSMs, DTAB, and bacterial behavior on PET surfaces.

There is currently a lack of comprehensive research studying the effects of QSMs on the degradation of PET. However, a noteworthy study conducted by Ayush et al. in 2022 aimed to shed light on the impact of QSMs on biofilm formation, focusing on *P. aeruginosa* and its interaction with different microplastics, including PE, PS, PP, and PTFE. Interestingly, their findings indicated a decrease in biofilm formation when a mixture of QSMs, specifically C4-HSL and 3-oxo-C₁₂-HSL, was present. However, the QS mechanisms, driven by QSMs, allow microorganisms to communicate and coordinate their activities. This enhances microbial adaptation to dynamic environments by regulating phenotypic characteristics and metabolic processes.

Biofilm Production is another way that QSM can enhance the degradation. QS activities demand energy and are initiated when a concentration of QSMs reach a critical threshold. One of the key mandates controlled by QS is biofilm production, which involves microorganisms working together in a coordinated manner to form protective structures. Also, some bioactive molecules produced by microorganisms can interact with receptors

in host organisms. It allows microorganisms to coordinate gene activation or inhibition, impacting their collective behaviour and bioactivity.

The HPLC results also confirm that FSC treatment had a significant impact on PET degradation and subsequently the TPA production. The TPA concentration reached to 0.98 $\mu\text{g/ml}$ after one week of incubation.

In addition, advanced techniques such as high-resolution microscopy and scanning electron microscopy (SEM) were employed to examine the morphological alterations induced by the presence of QSM on the treated PET samples.

The microscopic analysis of the treated PET samples revealed distinguishable changes on the surface of the PET. The FSC-treated PET exhibited notable modifications on its surface. More rigidity and the formation of pores can be seen on the surface. These alterations indicated that the enzymatic treatment, in combination with QSMs, had an impact on the surface morphology of the PET material.

The emergence of a more rigid structure suggests a potential breakdown of the PET polymer chains, potentially caused by the enzymatic activity facilitated by the QSMs. Furthermore, the presence of distinct pores on the surface of FSC-treated PET may indicate the initiation of localized degradation or the creation of additional sites for bacterial colonization and biofilm formation.

Chapter 5. Conclusion and Future work

5.1. Conclusion

In conclusion, this study represents a comprehensive exploration of various PET pre-treatment methods, shedding light on the remarkable potential of DTAB as a key catalyst for PET degradation. The investigations, conducted using the YSV medium and employing the bacterial strains *I. sakaiensis* and *P. mendocina*, showcased DTAB's efficacy in accelerating PET breakdown over a three-week period. The expedited transformation of PET, especially in the presence of *I. sakaiensis*, underscores the significance of DTAB as a promising agent in the quest to address the persistent problem of plastic waste.

Moreover, the research took a deeper dive into the realm of enzymatic PET degradation by examining the impact of FSC (*Fusarium* supernatant containing cutinase). This approach yielded impressive outcomes, with significant PET degradation achieved within just one week, emphasizing the potential of cutinase enzymes from *Fusarium* sp. in expediting PET breakdown.

Furthermore, when subjecting PET to a synergistic treatment involving DTAB and FSC in the presence of *I. sakaiensis*, a notable enhancement in the degradation of PET becomes evident. This augmentation in PET degradation can be distinctly observed through advanced analytical techniques such as FTIR spectroscopy, high-resolution microscopy, and scanning electron microscopy (SEM).

Additionally, the introduction of Quorum Sensing Molecules (QSM) into the experimental framework provided valuable insights into their role in enhancing the effectiveness of PET degradation. Notably, the synergy between FSC-treated PET and *I. sakaiensis* culture supplemented with QSM showcased a prominent enhancement in the degradation process in one week, reinforcing the importance of QSM in augmenting the efficiency of this environmentally crucial process.

The combination of DTAB, FSC, and QSM presents a compelling approach to addressing the global challenge of plastic pollution, offering hope for more sustainable and effective solutions in the future. Further research and development in this direction hold great promise for mitigating the adverse environmental impacts associated with PET plastic waste.

5.2. Future work

Using the synergistic effects of co-culture of *I. sakaiensis* and *P. mendocina* may enhance the degradation of PET by using the potentials of each microorganism. Microbes in a co-culture can engage in cross-feeding, where one microbe consumes the metabolic byproducts or waste products of another. This process may be able to minimize the accumulation of inhibitory intermediates and enhance the overall efficiency of PET degradation. Besides, each microorganism possesses distinct enzymes or enzyme systems optimized for different stages of PET degradation. For example, *I. sakaiensis* is known for its PETase enzyme, which can break down PET into intermediate products, such as MHET. *P. mendocina* produce carboxylic ester hydrolases capable of further metabolizing these intermediates. In co-culture, they work together to efficiently degrade PET.

Using extremophiles and high-temperature enzymes for PET degradation represent a promising avenue in the field of biotechnology and environmental science. Extremophiles, microorganisms adapted to thrive in extreme conditions such as high temperatures, for example *H. insolens*, have shown remarkable capabilities in breaking down PET plastics. This approach holds great potential for addressing the global plastic pollution problem as it offers a sustainable and eco-friendly method for PET waste management.

Gas Chromatography-Mass Spectrometry (GC-MS) can be carried out as a powerful analytical tool to probe the presence of EG as a monomeric byproduct of PET degradation. This analysis is useful for confirming the success of the degradation process and understanding the specific breakdown pathways involved.

Furthermore, the research can be extended to the use of other QSMs (e.g., C₄-HSL and C₆-HSL) that might have the potential to enhance the efficiency and effectiveness of subsequent degradation processes through influencing microbial metabolism.

Another perspective for future work is the use of biosurfactants. Microorganisms such as *P. aeruginosa*, *Bacillus subtilis*, and *Candida* spp. have been investigated and research in this area is expanding. Biosurfactants help in adhering microbes to the surface of the PET material, enhancing their colonisation and growth. The produced enzymes from these microbes can then break down the PET polymer over time.

Hydrophobins can be used for enhancing PET degradation. The hydrophobic nature of hydrophobins makes them potential candidates for PET degradation as PET is also a

hydrophobic polymer. The idea is that hydrophobins could be used to facilitate microbial attachment to the PET surface, enabling the growth of microorganisms that possess the ability to degrade PET. For example, the fungal hydrophobin RolA affects the enhancement of PETase hydrolysis (Puspitasari et al., 2020).

Chapter 6. Appendix

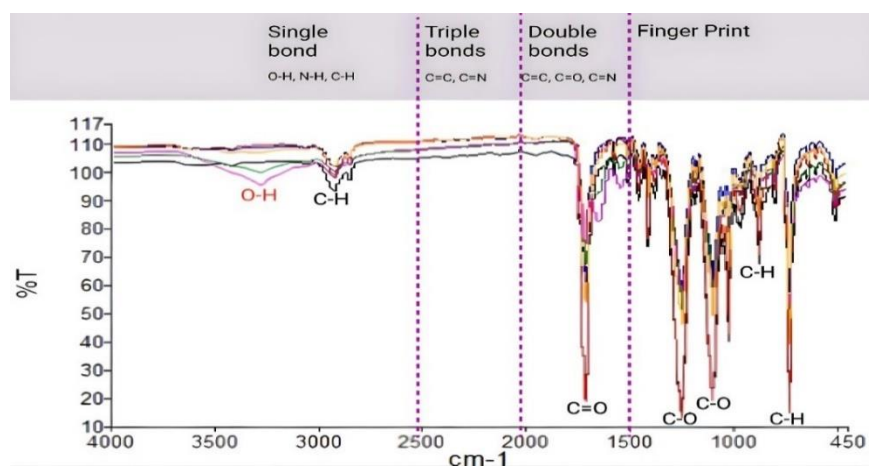


Figure 6.1. FTIR of PET samples (non-treated and treated) using HPP and *I. sakaiensis* culture after one week incubation at 30 °C

(**—** Non-treated PET in HPP, **—** Non-treated PET in HPP and *I. sakaiensis* culture, **—** NaOH-treated PET, **—** DTAB-treated PET, **—** Brij-35-treated PET and **—** UV-treated PET). The peaks on the FTIR spectrum related to the following wavenumbers and functional groups; 3391 cm^{-1} (O-H), 2920 cm^{-1} (C-H), 1713 cm^{-1} (C=O), 1240 cm^{-1} (C-O aromatic), 1093 cm^{-1} (C-O aliphatic), 873 cm^{-1} (C-H aliphatic) and 724 cm^{-1} (C-H aromatic).

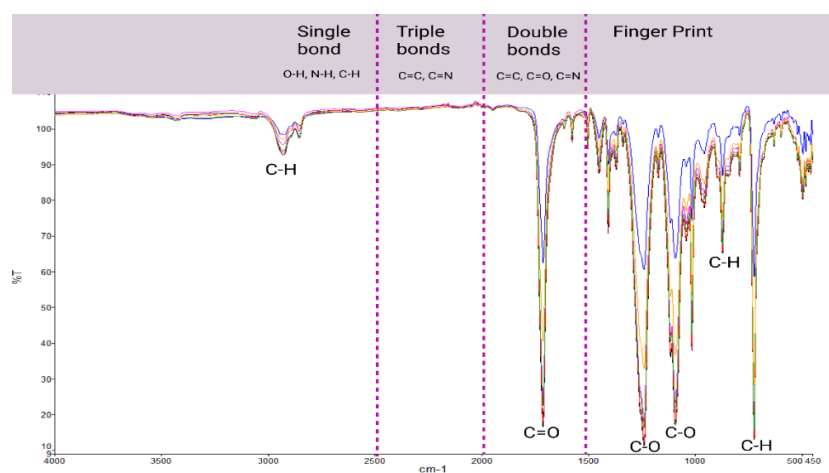


Figure 6.2. FTIR on PET samples (non-treated and treated) using HPP and *I. sakaiensis* culture after two week incubation at 30 °C.

(**—** Non-treated PET in HPP, **—** Non-treated PET in HPP and *I. sakaiensis* culture, **—** NaOH-treated PET, **—** DTAB-treated PET, **—** Brij-35-treated PET and **—** UV-treated PET). The peaks on the FTIR spectrum related to the following wavenumbers and functional groups; 3391 cm^{-1} (O-H), 2920 cm^{-1} (C-H), 1713 cm^{-1} (C=O), 1240 cm^{-1} (C-O aromatic), 1093 cm^{-1} (C-O aliphatic), 873 cm^{-1} (C-H aliphatic) and 724 cm^{-1} (C-H aromatic).

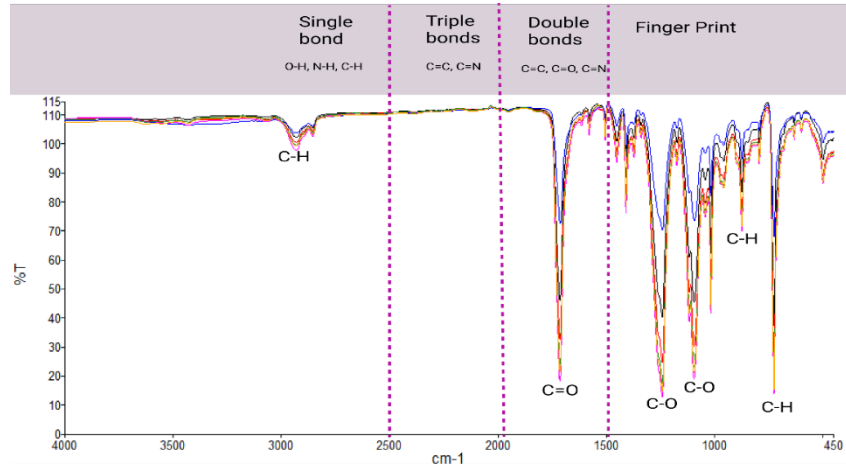


Figure 6.3. FTIR on PET samples (non-treated and treated) using HPP and *I. sakaiensis* culture after three weeks incubation at 30 °C.

(**—** Non-treated PET in HPP, **—** Non-treated PET in HPP and *I. sakaiensis* culture, **—** NaOH-treated PET, **—** DTAB-treated PET, **—** Brij-35-treated PET and **—** UV-treated PET). The peaks on the FTIR spectrum related to the following wavenumbers and functional groups; 3391 cm^{-1} (O-H), 2920 cm^{-1} (C-H), 1713 cm^{-1} (C=O), 1240 cm^{-1} (C-O aromatic), 1093 cm^{-1} (C-O aliphatic), 873 cm^{-1} (C-H aliphatic) and 724 cm^{-1} (C-H aromatic).

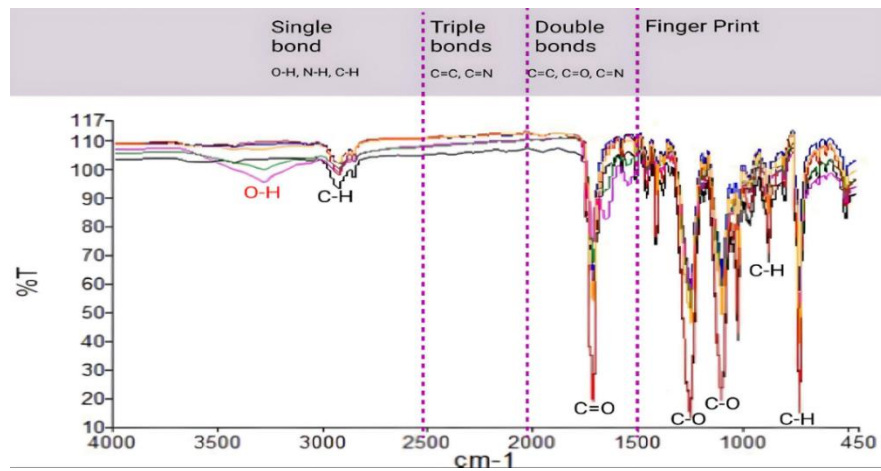


Figure 6.4. FTIR on PET samples (non-treated and treated) using YSV and *I. sakaiensis* culture after one week of incubation at 30 °C.

(**—** Non-treated PET in YSV, **—** Non-treated PET in YSV and *I. sakaiensis* culture, **—** NaOH-treated PET, **—** DTAB-treated PET, **—** Brij-35-treated PET and **—** UV-treated PET). The peaks on the FTIR spectrum related to the following wavenumbers and functional groups; 3391 (O-H), 2920 cm^{-1} (C-H), 1713 cm^{-1} (C=O), 1240 cm^{-1} (C-O aromatic), 1093 cm^{-1} (C-O aliphatic), 873 cm^{-1} (C-H aliphatic) and 724 cm^{-1} (C-H aromatic).

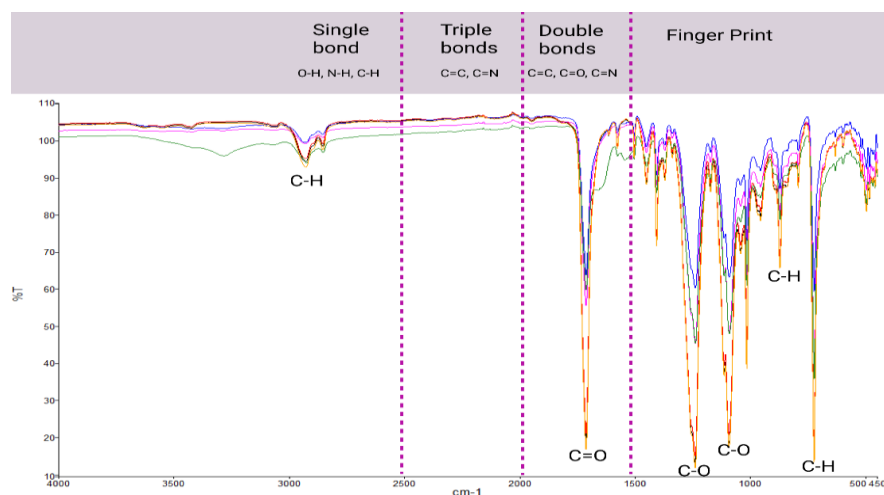


Figure 6.5. FTIR on PET samples (non-treated and treated) using YSV and *I. sakaiensis* culture after two week of incubation at 30 °C.

(█ Non-treated PET in YSV, █ Non-treated PET in YSV and *I.sakaiensis* culture, █ NaOH-treated PET, █ DTAB-treated PET, █ Brij-35-treated PET and █ UV-treated PET), The peaks on the FTIR spectrum related to the following wavenumbers and functional groups; 3391 cm^{-1} (O-H), 2920 cm^{-1} (C-H), 1713 cm^{-1} (C=O), 1240 cm^{-1} (C-O aromatic), 1093 cm^{-1} (C-O aliphatic), 873 cm^{-1} (C-H aliphatic) and 724 cm^{-1} (C-H aromatic).

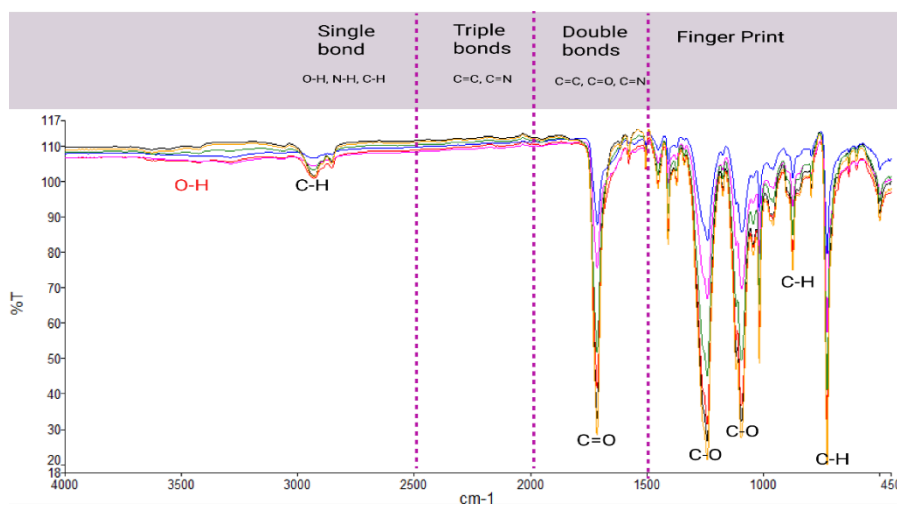


Figure 6.6. FTIR on PET samples (non-treated and treated) using YSV and *I. sakaiensis* culture after three weeks of incubation at 30 °C.

(█ Non-treated PET in YSV, █ Non-treated PET in YSV and *I.sakaiensis* culture, █ NaOH-treated PET, █ DTAB-treated PET, █ Brij-35-treated PET and █ UV-treated PET), The peaks on the FTIR spectrum related to the following wavenumbers and functional groups; 3391 cm^{-1} (O-H), 2920 cm^{-1} (C-H), 1713 cm^{-1} (C=O), 1240 cm^{-1} (C-O aromatic), 1093 cm^{-1} (C-O aliphatic), 873 cm^{-1} (C-H aliphatic) and 724 cm^{-1} (C-H aromatic).

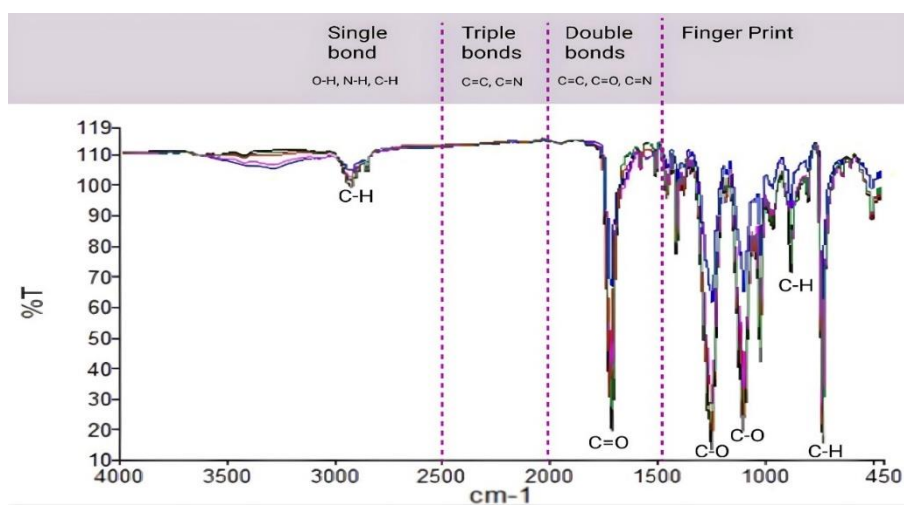


Figure 6.7. FTIR on PET samples (non-treated and treated) using M9 minimal and *I. sakaiensis* culture after one week of incubation at 30 °C.

(■ Non-treated PET in M9 minimal, ■ Non-treated PET in M9 minimal and *I. sakaiensis* culture ■, NaOH-treated PET, ■ DTAB-treated PET, ■ Brij-35-treated PET and ■ UV-treated PET), The peaks on the FTIR spectrum related to the following wavenumbers and functional groups; 3391 cm^{-1} (O-H), 2920 cm^{-1} (C-H), 1713 cm^{-1} (C=O), 1240 cm^{-1} (C-O aromatic), 1093 cm^{-1} (C-O aliphatic), 873 cm^{-1} (C-H aliphatic) and 724 cm^{-1} (C-H aromatic).

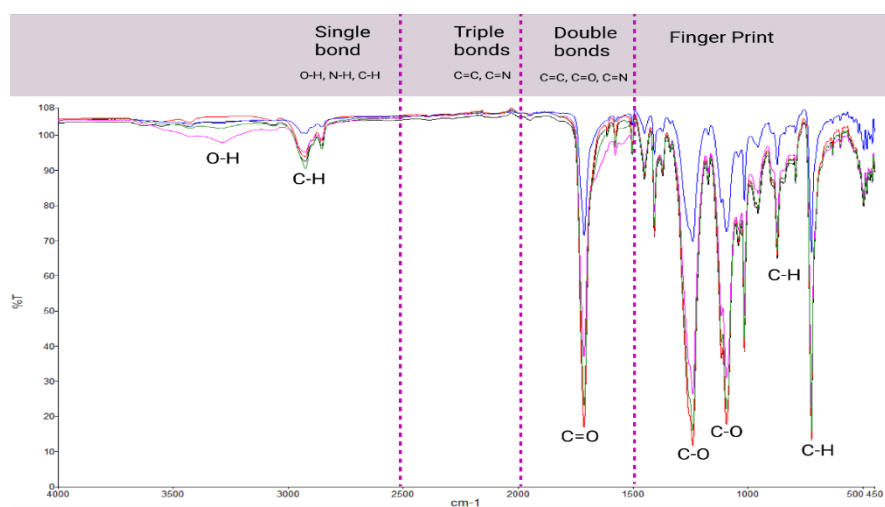


Figure 6.8. FTIR on PET samples (non-treated and treated) using M9 minimal and *I. sakaiensis* culture after two week of incubation at 30 °C.

(■ Non-treated PET in M9 minimal, ■ Non-treated PET in M9 minimal and *I. sakaiensis* culture ■, NaOH-treated PET, ■ DTAB-treated PET, ■ Brij-35-treated PET and ■ UV-treated PET), The peaks on the FTIR spectrum related to the following wavenumbers and functional groups; 3391 cm^{-1} (O-H), 2920 cm^{-1} (C-H), 1713 cm^{-1} (C=O), 1240 cm^{-1} (C-O aromatic), 1093 cm^{-1} (C-O aliphatic), 873 cm^{-1} (C-H aliphatic) and 724 cm^{-1} (C-H aromatic).

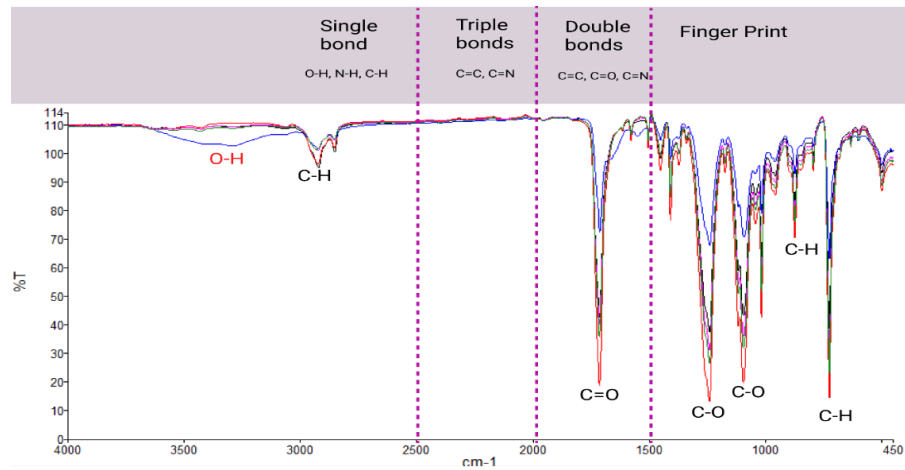


Figure 6.9. FTIR on PET samples (non-treated and treated) using M9 minimal and *I. sakaiensis* culture after three weeks of incubation at 30 °C. (**■** Non-treated PET in M9 minimal, **■** Non-treated PET in M9 minimal and *I. sakaiensis* culture **■**, NaOH-treated PET, **■** DTAB-treated PET, **■** Brij-35-treated PET and **■** UV-treated PET), The peaks on the FTIR spectrum related to the following wavenumbers and functional groups; 3391 cm^{-1} (O-H), 2920 cm^{-1} (C-H), 1713 cm^{-1} (C=O), 1240 cm^{-1} (C-O aromatic), 1093 cm^{-1} (C-O aliphatic), 873 cm^{-1} (C-H aliphatic) and 724 cm^{-1} (C-H aromatic).

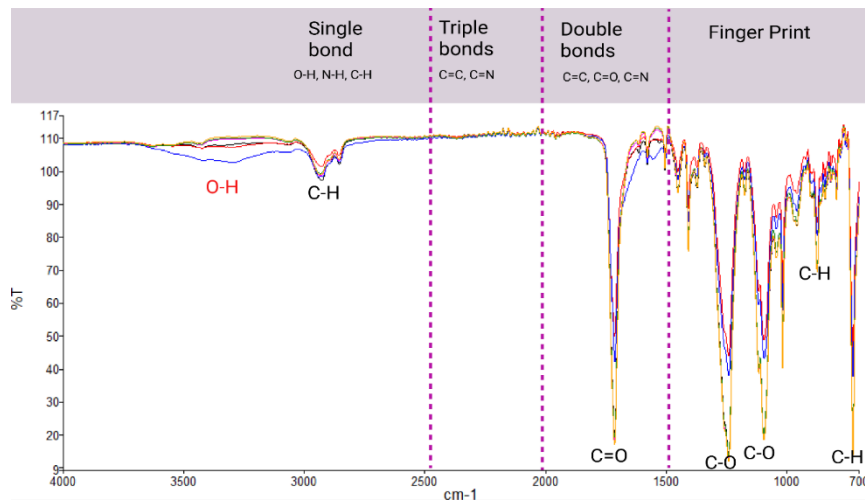


Figure 6.10. FTIR on PET samples (non-treated and treated) using HPP and *P. mendocina* culture after one week of incubation at 30 °C. (**■** Non-treated PET in HPP, **■** Non-treated PET in HPP and *P. mendocina* culture, **■** NaOH-treated PET, **■** DTAB-treated PET, **■** Brij-35-treated PET and **■** UV-treated PET), The peaks on the FTIR spectrum related to the following wavenumbers and functional groups; 3391 cm^{-1} (O-H), 2920 cm^{-1} (C-H), 1713 cm^{-1} (C=O), 1240 cm^{-1} (C-O aromatic), 1093 cm^{-1} (C-O aliphatic), 873 cm^{-1} (C-H aliphatic) and 724 cm^{-1} (C-H aromatic).

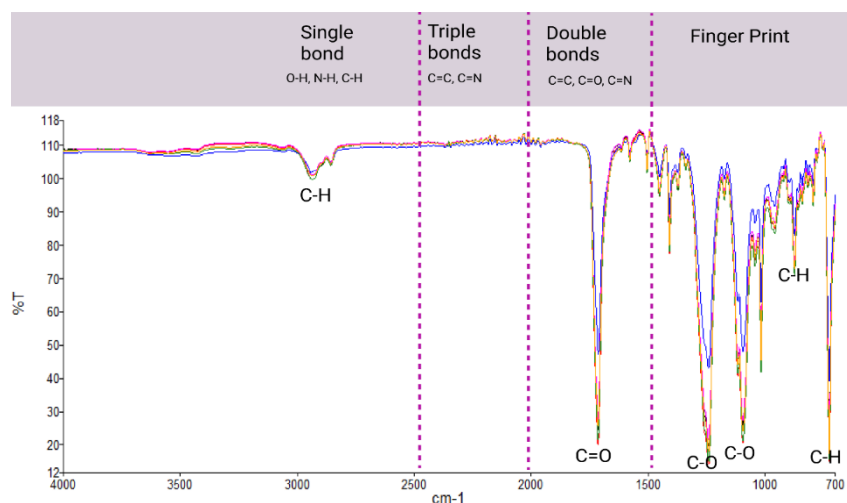


Figure 6.11. FTIR on PET samples (non-treated and treated) using YSV and *P.mendocina* culture after one week of incubation at 30 °C.

(**■** Non-treated PET in YSV, **■** Non-treated PET in YSV and *P. mendocina* culture, **■** NaOH-treated PET, **■** DTAB-treated PET, **■** Brij-35-treated PET and **■** UV-treated PET), The peaks on the FTIR spectrum related to the following wavenumbers and functional groups; 3391 cm^{-1} (O-H), 2920 cm^{-1} (C-H), 1713 cm^{-1} (C=O), 1240 cm^{-1} (C-O aromatic), 1093 cm^{-1} (C-O aliphatic), 873 cm^{-1} (C-H aliphatic) and 724 cm^{-1} (C-H aromatic).

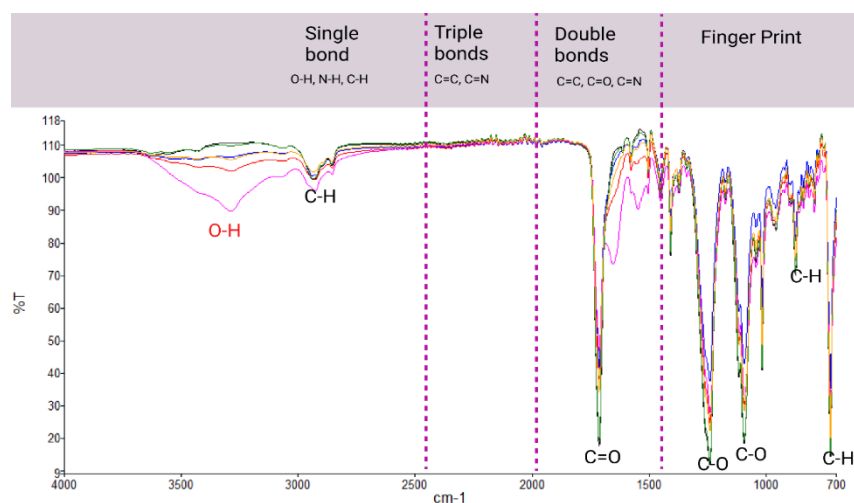


Figure 6.12. FTIR on PET samples (non-treated and treated) using M9 minimal and *P.mendocina* culture after one week of incubation at 30 °C.

(**■** Non-treated PET in M9, **■** Non-treated PET in M9 and *P. mendocina* culture, **■** NaOH-treated PET, **■** DTAB-treated PET, **■** Brij-35-treated PET and **■** UV-treated PET), The peaks on the FTIR spectrum related to the following wavenumbers and functional groups; 3391 cm^{-1} (O-H), 2920 cm^{-1} (C-H), 1713 cm^{-1} (C=O), 1240 cm^{-1} (C-O aromatic), 1093 cm^{-1} (C-O aliphatic), 873 cm^{-1} (C-H aliphatic) and 724 cm^{-1} (C-H aromatic).

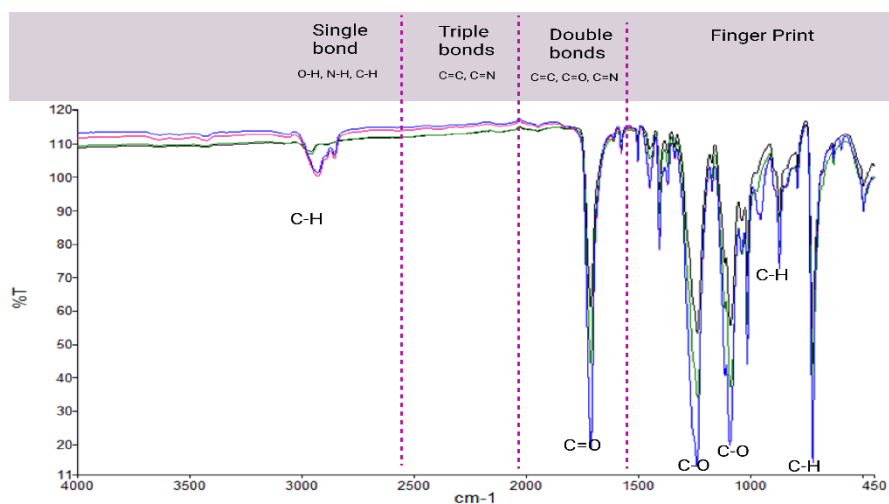


Figure 6.13. FTIR on non-treated and DTAB-treated PET samples using YSV medium in the presence of *I. sakaiensis* and *P.mendocina* culture after one week of incubation at 30 °C (large-scale). (— Non-treated PET in *I. sakaiensis* culture, — DTAB-treated PET in *I. sakaiensis* culture, — Non-treated PET in *P. mendocina* culture, — DTAB-treated PET in *P. mendocina* culture. The peaks on the FTIR spectrum related to the following wavenumbers and functional groups; 3391 cm^{-1} (O-H), 2920 cm^{-1} (C-H), 1713 cm^{-1} (C=O), 1240 cm^{-1} (C-O aromatic), 1093 cm^{-1} (C-O aliphatic), 873 cm^{-1} (C-H aliphatic) and 724 cm^{-1} (C-H aromatic).

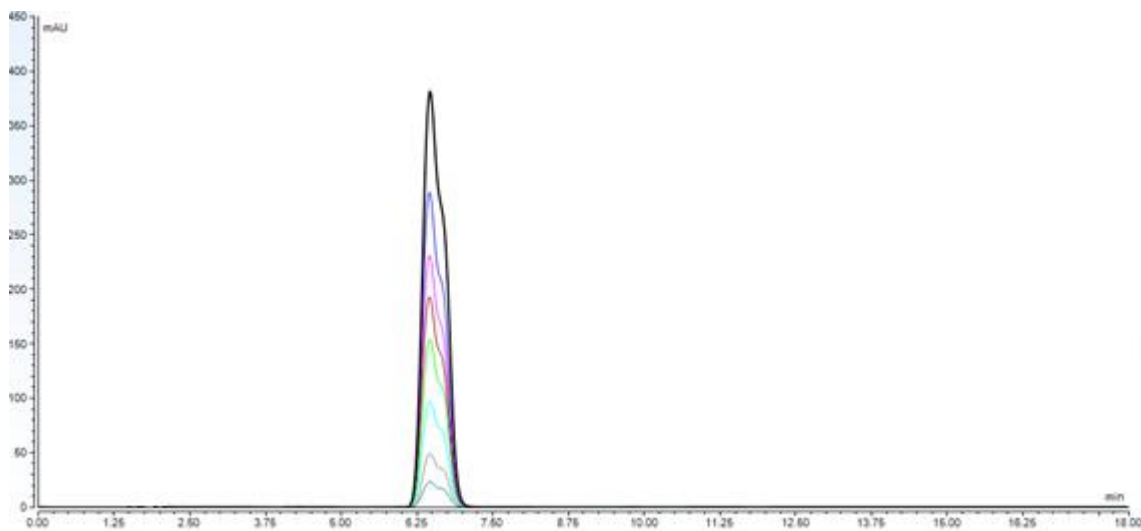


Figure 6.14. HPLC chromatogram of TPA standard samples with concentrations ranging 1.2, 2.5, 5, 8, 10, 12, 15, 20 $\mu g/ml$.

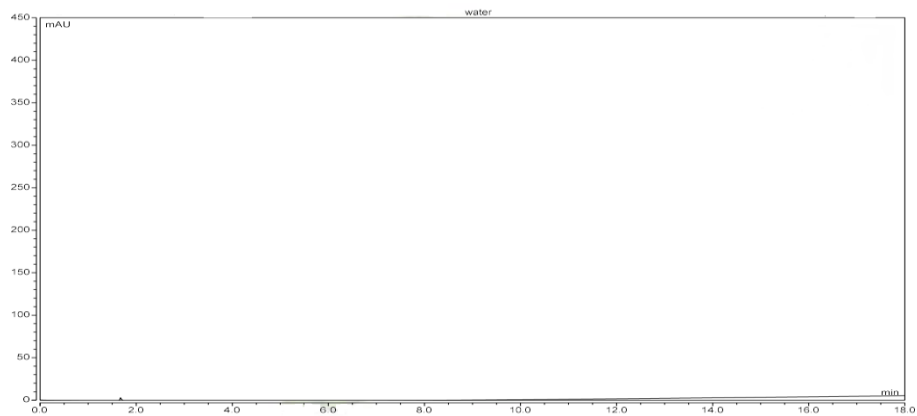


Figure 6.15. HPLC chromatograms of water.

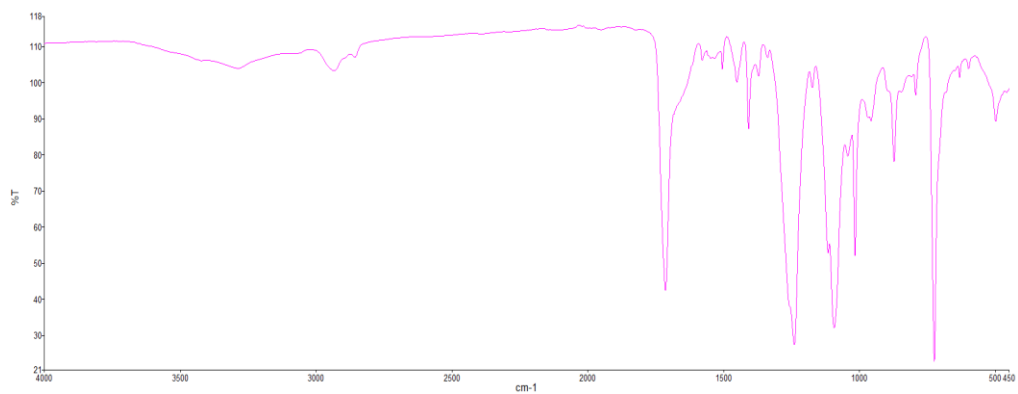


Figure 6.16. FTIR on FSC-treated PET in the presence of *I. sakaiensis* in 6-well plate after one week.

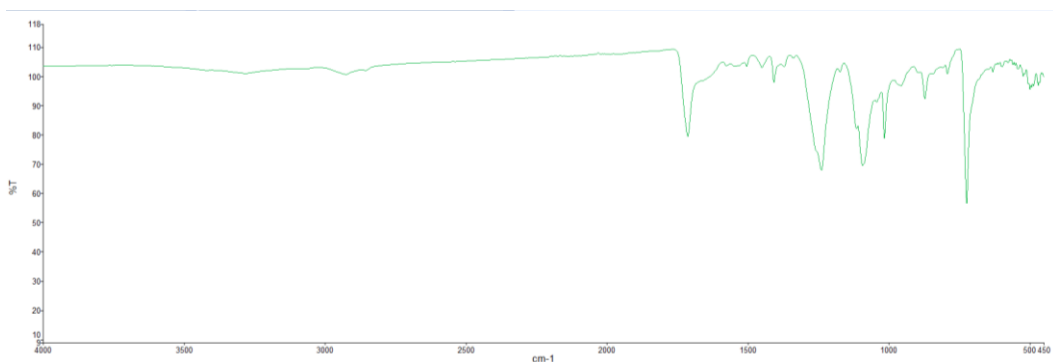


Figure 6.17. FTIR on FSC-treated PET with QSM in the presence of *I. sakaiensis* in large scale after one week.

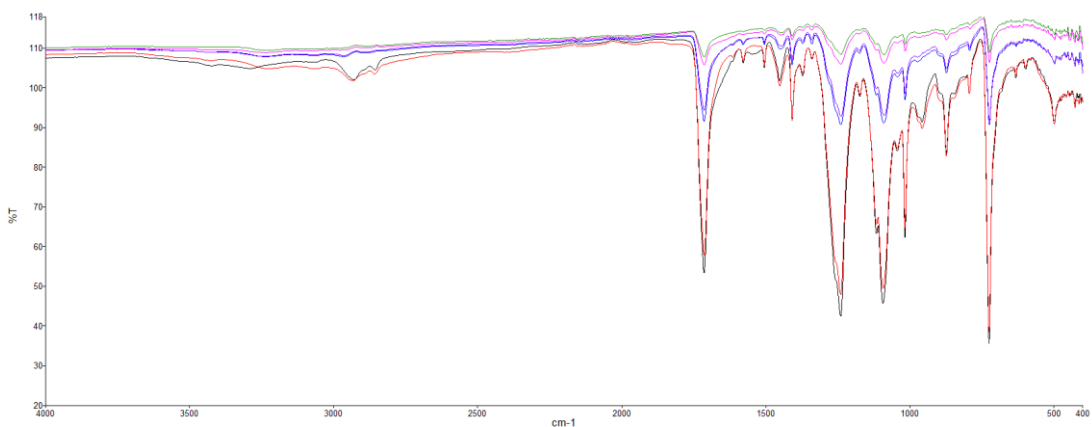


Figure 6.18. FTIR on different treatments of PET (non, non with QSM, FSC, FSC with QSM FSC-DTAB and FSC-DTAB with QSM) in the presence of *I. sakaiensis* in large scale after eight weeks.



Figure 6.19. HPLC chromatogram on non-treated, FSC-treated and FSC-DTAB-treated PET in the presence of *I. sakaiensis* in large scale after one week. — Non-treated, — FSC-treated and — FSC-DTAB-treated.

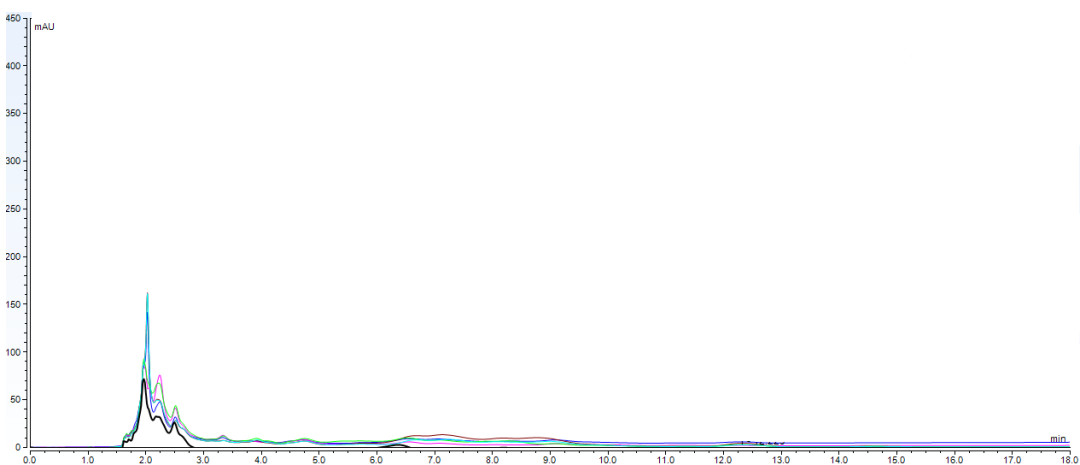


Figure 6.20. HPLC chromatogram on non-treated, non-treated with QSM, FSC-treated, FSC-treated with QSM, FSC-DTAB-treated and FSC-DTAB-treated PET in the presence of *I. sakaiensis* in large scale after one week. — Non-treated, — non-treated with QSM, — FSC-treated, — FSC-treated with QSM, — FSC-DTAB-treated and — FSC-DTAB-treated.

References

- Adıgüzel, A. O. Tunçer, M. (2017). Purification and characterization of cutinase from *Bacillus* sp. KY0701 isolated from plastic wastes. *Prep. Biochem. Biotechnol.* 47, 925–933.
- Aguado, J. Serrano, D. (1999). Feedstock recycling of plastic wastes. *The Royal Society of Chemistry.* 30-50.
- Aguilar-Alvarado, Y. Báez-Sánchez, M. R. Martínez-Carrera, D. Ahuactzin-Pérez, M. Cuamatzi-Muñoz, M. Sánchez, C. (2015). Mycelial growth and enzymatic activities of fungi isolated from recycled paper wastes grown on di (2-ethylhexyl) phthalate. *Pol J Environ Stud.* 24, 1897–1902.
- Ahmaditabatabaei, S. Kyazze, G. Iqbal, H.M.N. Keshavarz, T. (2021). Fungal Enzymes as Catalytic Tools for Polyethylene Terephthalate (PET) Degradation. *J. Fungi,* 7, 931.
- Albertsson, A. C. Karlsson, S. (1993). Aspects of biodeterioration of inert and degradable polymers, *International Biodeterioration & Biodegradation.* 31 (3), 161-170.
- Alisch-Mark, M. Herrmann, A. Zimmermann, W. (2006). Increase of the hydrophilicity of polyethylene terephthalate fibres by hydrolases from *Thermomonospora fusca* and *Fusarium solani* f. sp. pisi. *Biotechnol. Lett.* 28, 681–685.
- Al-Salem, S. M. Lettieri, P. Baeyens, J. (2009). Recycling and recovery routes of plastic solid waste (PSW): a review. *Waste Manag.* 29 (10), 2625-2643.
- Amache, R. (2014). Quorum sensing for improved production of industrially useful products from filamentous fungirashid. 1-30.
- Ampomah-Wireko, M. Luo, C. Cao, Y. Wang, H. Nininahazwe, L. Wu, C. (2021). Chemical probe of AHL modulators on quorum sensing in Gram-Negative Bacteria and as antiproliferative agents: A review, *European Journal of Medicinal Chemistry.* 226, 113864.
- Anbalagan, S. Venkatakrishnan, H. R. R. Ravindran, J. Sathyamoorthy, J. Rangabashyam, K. A. Ragini, Y. P. Sureshbabu, K. (2022). Hydrolytic Degradation of Polyethylene Terephthalate by Cutinase Enzyme Derived from Fungal Biomass–Molecular Characterization. *BioInterface Res. Appl. Chem.* 12, 653–667.
- Ammala, A. Bateman, S. Dean, K. Petinakis, E. Sangwan, P. Wong, S. Yuan, Q. Yu, L. Patrick, C. Leong, K. H. (2011). An overview of degradable and biodegradable polyolefins, *Progress in Polymer Science.* 36 (8), 1015-1049.
- Arkatkar, A. Juwarkar, Asha A. Bhaduri, S. Uppara, P. Doble, M. (2010). Growth of *Pseudomonas* and *Bacillus* biofilms on pretreated polypropylene surface. *International Biodeterioration & Biodegradation.* 64, 530-536.

- Austin, H. P. Allen, M. D. Donohoe, B. S. Beckham, G. T. (2018). Characterisation and engineering of a plastic-degrading aromatic polyesterase. *Proc. Natl. Acad. Sci.* 115 (19), e4350–e4357.
- Ayush, P.T. Ko, J. H. Oh, H. S. (2022). Characteristics of Initial Attachment and Biofilm Formation of *Pseudomonas aeruginosa* on Microplastic Surfaces. *Appl. Sci.* 12, 5245.
- Aziz, Z. (2021). Investigating microbial quorum sensing potential for enhanced production of biodegradable polymers, University of Westminster.
- Badmus, S.O. Amusa, H.K. Oyehan, T.A. Saleh, T.A. (2021), Environmental risks and toxicity of surfactants: overview of analysis, assessment, and remediation techniques, *Environmental science and pollution research international*. 28 (44), 62085-62104.
- Barth, M. Oeser, T. Wei, R. Then, J. Schmidt, J. Zimmermann, W. (2015). Effect of hydrolysis products on the enzymatic degradation of polyethylene terephthalate nanoparticles by a polyester hydrolase from *Thermobifida fusca*. *Biochem. Eng. J.* 93, 222–228.
- Benavides Fernández, C. D. Guzmán Castillo, M. P. Quijano Pérez, S. A. Carvajal Rodríguez, L. V. (2022). Microbial degradation of polyethylene terephthalate: a systematic review, *SN applied sciences*. 4 (10), 1-13.
- Bermúdez-García, E. Peña-Montes, C. Castro-Rodríguez, J. A. González-Canto, A. Navarro-Ocaña, A. Farrés, A. (2017). AN CUT2, a thermo-alkaline cutinase from *Aspergillus nidulans* and its potential applications. *Appl. Biochem. Biotechnol.* 182, 1014–1036.
- Bhagwat, G. O'Connor, W. Grainge, I. Palanisami, T. (2021). Understanding the fundamental basis for biofilm formation on plastic surfaces: Role of conditioning films, *Frontiers in microbiology*. 12, 687118.
- Bhogle, C. S. Pandit, A. B. (2018). Ultrasound-Assisted Alkaline Hydrolysis of Waste Poly (Ethylene Terephthalate) in Aqueous and Non- aqueous Media at Low Temperature Ultrasound-Assisted Alkaline Hydrolysis of Waste Poly (Ethylene Terephthalate) in Aqueous and Non-aqueous Media at Low. *Indian Chemical Engineer*. 60 (2), 122-140.
- Biswas, N. K. Srivastav, A. Saxena, S. Verma, A. Dutta, R. Srivastava, M. Satsangi, V. R. Shrivastav, R. Dass, S. (2022). Role of varying ionic strength on the photoelectrochemical water splitting efficiency, *Solar Energy*. 247, 543-552.
- Boucher, J. Friot D. (2017). *Primary Microplastics in the Oceans: A Global Evaluation of Sources*. Gland, Switzerland.
- Branda, S. S. Vik, S. Friedman, L. Kolter, R. (2005). Biofilms: the matrix revisited. *Trends in Microbiology*. 13 (1), 20-26.

- Canavati-Alatorre, M.S. Águila, I. Barraza-Soltero, I. K. Castellón, E. Correa-Barrón, A. L. Sánchez-López, E. Conde-Avila, V. González-Marquez, Á. Méndez-Iturbide, D. Ruvalcaba, D. Sánchez, C. (2016). Growth and cutinase activity of *Fusarium culmorum* grown in solid state fermentation. *Mexican Journal of Biotechnology*. 2, 8-19.
- Cao, Q. Yuan, G. Yin, L. Chen, D. He, P. Wang, H. (2016). Morphological characteristics of polyvinyl chloride (PVC) dechlorination during pyrolysis process: Influence of PVC content and heating rate. *Waste Management*. 58, 241-249.
- Caparanga, A. R. Basilia, B. A. Dagbay, K. B. Salvacion, J. W. L. (2009). Factors Affecting Degradation of Polyethylene Terephthalate (PET) during Pre-flotation Conditioning. *Waste Management*. 29, 2425–2428.
- Carniel, A. Valoni, É. Junior, J. N. Gomes, A. Castro, A. M. (2017). Lipase from *Candida antarctica* (CALB) and cutinase from *Humicola insolens* act synergistically for PET hydrolysis to terephthalic acid. *Process Biochem*. 59, 84–90.
- Carr, C. M. Clarke, D. J. Dobson, A. D. W. (2020), Microbial Polyethylene Terephthalate Hydrolases: Current and Future Perspectives, *Frontiers in microbiology*. 11, 571265.
- Castro, A. M. Carniel, A. Junior, J. N. Gomes, A. C. Valoni, É. (2017). Screening of commercial enzymes for poly (ethylene terephthalate) (PET) hydrolysis and synergy studies on different substrate sources. *J. Ind. Microbiol. Biotechnol*. 44, 835–844.
- Chambliss, W. G. (1983). The forgotten dosage form: enteric-coated tablets. *J Pharm Technol*. 7, 124-40.
- Chen, S. Su, L. Billig, S. Zimmermann, W. Chen, J. Wu, J. (2010). Biochemical characterization of the cutinases from *Thermobifida fusca*. *J. Mol. Catal. B Enzym*. 63, 121–127.
- Chen, C. C. Han, X. Ko, T. P. Liu, W. Guo, R. T. (2018). Structural studies reveal the molecular mechanism of PETase. *FEBS J*. 285, 3717–3723.
- Chen, K. Hu, Y. Dong, X. Sun, Y. (2021). Molecular Insights into the Enhanced Performance of EKylated PETase toward PET Degradation. *ACS Catal*. 11, 7358–7370.
- Chiellini, E. Corti, A. D'Antone, S. and Baciú, R. (2006) Oxo-Biodegradable Carbon Backbone Polymers—Oxidative Degradation of Polyethylene under Accelerated Test Conditions. *Polymer Degradation and Stability*. 91, 2739-2747.
- Chow, J. Perez-Garcia, P. Dierkes, R. Streit, W.R. (2023). Microbial enzymes will offer limited solutions to the global plastic pollution crisis, *Microbial biotechnology*, 16 (2), 195-217.
- Costerton, J. (2007). *The biofilm primer*. Berlin: Springer, 36-43.
- Dave, N and Joshi, T. (2017). A Concise Review on Surfactants and Its Significance. *International Journal of Applied Chemistry*. 13. 663-672.

- De Salas, F. Martínez, M. J. Barriuso, J. (2015). Quorum-sensing mechanisms mediated by farnesol in *Ophiostoma piceae*: effect on secretion of sterol esterase. *Appl Environ Microbiol.* 8, 4351–4357.
- Deep, A. Chaudhary, U. Gupta, V. (2011). Quorum sensing and Bacterial Pathogenicity: From Molecules to Disease. *J Lab Physicians.* 3 (1), 4-11.
- Devi, R.S. Kannan, V.R. Natarajan, K. Nivas, D. Kannan, K. Chandru, S. Arokiaswamy, R.A. (2016). The role of microbes in plastic degradation. Environmental waste management. Boca Raton, CRC, 341–70.
- Dimarogona, M. Nikolaivits, E. Kanelli, M. Christakopoulos, P. Sandgren, M. Topakas, E. (2015). Structural and functional studies of a *Fusarium oxysporum* cutinase with polyethylene terephthalate modification potential. *Biochim. Biophys. Acta Gen. Subj.* 1850, 2308–2317.
- Din, S. U. Kalsoom, Satti, S. M. Uddin, S. Mankar, S. V. Ceylan, E. Hasan, F. Khan, S. Badshah, M. Beldüz, A. O. Çanakçı, S. Zhang, B. Linares-Pastén, J. A. Shah, A. A. (2023), The Purification and Characterization of a Cutinase-like Enzyme with Activity on Polyethylene Terephthalate (PET) from a Newly Isolated Bacterium *Stenotrophomonas maltophilia* PRS8 at a Mesophilic Temperature, *Applied sciences*, 13 (6), 3686.
- Dong, Y. H. Wang, L. H. Xu, J. L. Zhang, H. B. Zhang, X. F. Zhang, L. H. (2001). Quenching quorum-sensing-dependent bacterial infection by an N-acyl homoserine lactonase. *Nature.* 411, 813-817.
- Donlan RM. (2002). Biofilms: microbial life on surfaces. *Emerg Infect Dis.* 8 (9), 881-90.
- Douterelo, I. Boxall, J. Deines, P. Sekar, R. Fish, K. and Biggs, C. (2014). Methodological approaches for studying the microbial ecology of drinking water distribution systems. *Water Research*, 65, 134-156.
- Dussud, C. Ghiglione, J. F. (2014). bacterial degradation of synthetic plastics.
- Eberl, A. Heumann, S. Brückner, T. Araujo, R. Cavaco-Paulo, A. Kaufmann, F. Guebitz, G.M. (2009). Enzymatic surface hydrolysis of poly (ethylene terephthalate) and bis (benzoyloxyethyl) terephthalate by lipase and cutinase in the presence of surface active molecules. *J. Biotechnol.* 143, 207–212.
- Elasri, M. Delorme, S. Lemanceau, P. Stewart, G. Laue, B. Glickmann, E. Oger, P. M. Dessaux, Y. (2001). Acyl-homoserine lactone production is more common among plant-associated *Pseudomonas spp.* than among soilborne *Pseudomonas spp.* *Applied and environmental microbiology.* 67, 1198-1209.
- Espino-Rammer, L. Ribitsch, D. Przylucka, A. Marold, A. Greimel, K. J. Herrero Acero, E. Druzhinina, I. S. (2013). Two novel class II hydrophobins from *Trichoderma spp.*

stimulate enzymatic hydrolysis of poly (ethylene terephthalate) when expressed as fusion proteins. *Appl. Environ. Microbiol.* 79, 4230–4238.

Eyerer, P. (2010). *Plastics: Classification, Characterization, and Economic Data In Polymers - Opportunities and Risks I*. The Handbook of Environmental Chemistry. Springer, Berlin, Heidelberg. 11.

Falkenstein, P. Gräsing, D. Bielytskyi, P. Zimmermann, W. Matysik, J. Wei, R. Song, C. (2020). UV Pretreatment Impairs the Enzymatic Degradation of Polyethylene Terephthalate. *Frontiers in Microbiology*, 11.

Fechinec, G. Rabellob, M. Souto Maiora , R. Catalani, L. (2004). Surface characterization of photodegraded poly (ethylene terephthalate). The effect of ultraviolet absorbers. *Polymer*. 45, 2303-2308.

Fecker, T. Galaz-Davison, P. Engelberger, F. Narui, Y. Sotomayor, M. Parra, L. P. Ramírez-Sarmiento, C. A. (2018). Active site flexibility as a hallmark for efficient PET degradation by *I. sakaiensis* PETase. *Biophys. J.* 114, 1302–1312.

Franden, M. A. Jayakody, L. N. Li, W. J. Wagner, N. J. Cleveland, N. S. Michener, W. E. Hauer, B. Blank, L. M. Wierckx, N. Klebensberger, J. Beckham, G. T. (2018). Engineering *Pseudomonas putida* KT2440 for efficient ethylene glycol utilization. *Metab Eng.* 48, 197-207

Fukuoka, T. Shinozaki, Y. Tsuchiya, W. Suzuki, K. Watanabe, T. Yamazaki, T. Kitamoto, H. (2016). Control of enzymatic degradation of biodegradable polymers by treatment with biosurfactants, mannosylerythritol lipids, derived from *Pseudozyma* spp. Yeast strains. *Appl. Microbiol. Biotechnol.* 100, 1733–1741.

Fuqua, C. Eberhard, A. (1999). Signal generation in autoinduction systems: synthesis of acylated homoserine lactones by LuxI-type proteins. *Cell-cell signaling in bacteria*. ASM Press, Washington, DC. 211-230.

Fuqua, C. Parsek, M. R. Greenberg, E. P. (2001). Regulation of gene expression by cell-to-cell communication: acyl-homoserine lactone quorum sensing. *Annual review of genetics*. 35, 439-468.

Furukawa, M. Kawakami, N. Tomizawa, A. Miyamoto, K. (2019). Efficient degradation of poly (ethylene terephthalate) with *Thermobifida fusca* cutinase exhibiting improved catalytic activity generated using mutagenesis and additive-based approaches. *Sci. Rep.* 9, 16038.

Furukawa, M. Kawakami, N. Oda, K. Miyamoto, K. (2018). Acceleration of Enzymatic Degradation of Poly (ethylene terephthalate) by Surface Coating with Anionic Surfactants. *ChemSusChem*. 11, 4018.

Geyer, R. Jambeck, Jenna R. Lavender Law, K. (2017). Production, use, and fate of all plastics ever made. *Science Advances*. 3 (7), 170-782.

- Ghosh, S. K. Pal, S. Ray, S. (2013). Study of microbes having potentiality for biodegradation of plastics. *Environmental Science and Pollution Research*. 20, 4339-4355.
- Gilan, I. Hadar, Y. Sivan, A. (2004). Colonization, biofilm formation and biodegradation of polyethylene by a strain of *Rhodococcus ruber*. *Appl. Microbiol. Biotechnol.* 65 (1), 97-104.
- Giraldo-Narcizo, S. Guenani, N. Sánchez-Pérez, A. M. Guerrero, A. (2022). Accelerated Polyethylene Terephthalate (PET) Enzymatic Degradation by Room Temperature Alkali Pre-treatment for Reduced Polymer Crystallinity, *ChemBioChem*. 24, e202200503.
- Goel, N. Fatima, S.W. Kumar, S. Sinha, R. Khare, S.K. (2021). Antimicrobial resistance in biofilms: Exploring marine actinobacteria as a potential source of antibiotics and biofilm inhibitors, *Biotechnology Reports*. 30, e00613.
- Gong, J. Li, Y. Wang, H. Li, H. Zhang, J. (2018). Depolymerization and Assimilation of Poly (Ethylene Terephthalate) By Whole-Cell Bioprocess, *Conf. Ser.: Mater. Sci. Eng.* 394, 022047.
- Grassie, N. Scott, G. (1985). *Polymer Degradation and Stabilization*, Cambridge: Cambridge University Press. 222.
- Han, X. Liu, W. Huang, J. W. Ma, J. Zheng, Y. Ko, T. P. Xu, L. Cheng, Y. S. Chen, C. C. Guo, R. T. (2017). Structural insight into catalytic mechanism of PET hydrolase. *Nat Commun.* 8 (1), 2106.
- Han, Y. Wei, M. Han, F. Fang, C. Wang, D. Zhong, Y. Guo, C. Shi, X. Xie, Z. Li, F. (2020), Greater Biofilm Formation and Increased Biodegradation of Polyethylene Film by a Microbial Consortium of *Arthrobacter* sp. and *Streptomyces* sp. *Microorganisms*. 8 (12), 1979.
- Hardman, A. M. Stewart, G. S. Williams, P. (1998). Quorum sensing and the cell-cell communication dependent regulation of gene expression in pathogenic and non-pathogenic bacteria. *Antonie Van Leeuwenhoek*. 74, 199-210.
- Hassan, T. Srivastwa, A.K. Sarkar, S. Majumdar, G. (2022). Characterization of Plastics and Polymers: A Comprehensive Study. *Materials Science and Engineering*. 1225 (1), 12033.
- Herrero Acero, E. Ribitsch, D. Steinkellner, G. Gruber, K. Greimel, K. Eiteljoerg, I. Trotscha, E. Wei, R. Zimmermann, W. Zinn, M. Cavaco-Paulo, A. Freddi, G. Schwab, H. Guebitz, G. (2011). Enzymatic Surface Hydrolysis of PET: Effect of Structural Diversity on Kinetic Properties of Cutinases from *Thermobifida*, *Macromolecules*. 44 (12), 4632-4640.
- Ho, B. T. Roberts, T. K. Lucas, S. (2018). An overview on biodegradation of polystyrene and modified polystyrene: the microbial approach. *Crit. Rev. Biotechnol.* 38, 308–320.

- Hu, X. Gao, Z. Wang, Z. Su, T. Yang, L. Li, P. (2016). Enzymatic degradation of poly (butylene succinate) by cutinase cloned from *Fusarium solani*. *Polym. Degrad. Stab.* 134, 211–219.
- Huang, S. Liu, X. Yang, W. Ma, L. Li, H. Liu, R. Qiu, J. Li Y. (2022). Insights into Adaptive Mechanisms of Extreme Acidophiles Based on Quorum Sensing/Quenching-Related Proteins. *mSystems.* 7 (2), e0149121.
- Hunsen M. Azim A. Mang H. Wallner S. R. Ronkvist A. Xie W. Gross, R. A. (2007). A cutinase with polyester synthesis activity. *Macromolecules.* 40, 148–150.
- Hurd, D. J. (2014). Best Practices and Industry Standards in PET plastic recycling, *Washington State Department of Community, Trade and Economic Development's Clean Washington Center.*
- Ishigaki, T. Kawagoshi, Y. Fujita, M. I. M. (1999). Biodegradation of a polyvinyl-alcohol starch blend plastic film. *World J Microbiol Biotechnol.* 15 (3), 321-327.
- Iwahashi, Y. (2018). Analysis of the regulatory mechanism of deoxynivalenol production using omics. *AMB Express.* 8 (1), 161.
- Jia, R. Hu, Y. Liu, L. Jiang, L. Huang, H. (2013). Chemical modification for improving activity and stability of lipase B from *Candida antarctica* with imidazolium-functional ionic liquids. *Org. Biomol. Chem.* 11, 7192–7198.
- Joo, S. Cho, I. J. Seo, H. Son, H. F. Sagong, H. Y. Shin, T. J. Kim, K. J. (2018). Structural insight into molecular mechanism of poly (ethylene terephthalate) degradation. *Nat. Commun.* 9, 382.
- Jun, H. S. Kim, B. O. Kim, Y. C. Chang, H. N. Woo, S. I. (1994). Synthesis of copolyesters containing poly (ethylene terephthalate) and poly (ε-caprolactone) units and their susceptibility to *Pseudomonas* sp. lipase. *J Env Polym Degrad.* 2, 9–18.
- Kaczorek, E. Pacholak, A. Zdarta, A. Smulek, W. (2018). The Impact of Biosurfactants on Microbial Cell Properties Leading to Hydrocarbon Bioavailability Increase. *Colloids Interfaces.* 2, 35.
- Kalgudi, R. (2018). Quorum Quenching: A study of the inhibition of *Pseudomonas aeruginosa* Quorum-sensing controlled biofilm formation and virulence.
- Kanelli, M. Vasilakos, S. Nikolaivits, E. Ladas, S. Christakopoulos, P. Topakas, E. (2015). Surface modification of poly (ethylene terephthalate) (PET) fibers by a cutinase from *Fusarium oxysporum*. *Proc. Biochem.* 50, 1885–1892.
- Kao, C. M. Liu, J. K. Chen, Y. L. Chai, C. T., and Chen S. C. (2005). Factors affecting the biodegradation of PCP by *Pseudomonas mendocina* NSYSU. *Journal of hazardous materials.* 124, 68-73.
- Karayannidis, G. P. Achilias, D.S. (2007), Chemical Recycling of Poly (ethylene terephthalate). *Macromol. Mater. Eng.* 292, 128-146.

Kawai, F. Kawabata, T. Oda, M. (2019). Current knowledge on enzymatic PET degradation and its possible application to waste stream management and other fields. *Appl. Microbiol. Biotechnol.* 103, 4253–4268.

Kawai, F. Furushima, Y. Mochizuki, N. Muraki, N. Yamashita, M. Iida, A. Mamoto, R. Tosha, T. Iizuka, R. Kitajima, S. (2022), Efficient depolymerization of polyethylene terephthalate (PET) and polyethylene furanoate by engineered PET hydrolase Cut190, *AMB Express*, 12 (1), 134.

Khairul Anuar, N. F. S. Huyop, F. Ur-Rehman, G. Abdullah, F. Normi, Y. M. Sabullah, M. K. Abdul Wahab, R. (2022), An Overview into Polyethylene Terephthalate (PET) Hydrolases and Efforts in Tailoring Enzymes for Improved Plastic Degradation, *International journal of molecular sciences*, 23 (20), 12644.

Khaneghah, A. M. Limbo, S. Shoeibi, S. Mazinani, S. (2014). HPLC study of migration of terephthalic acid and isophthalic acid from PET bottles into edible oils. *J Sci Food Agric.* 94 (11), 2205-9.

Kitadokoro, K. Kakara, M. Matsui, S. Osokoshi, R. Thumarat, U. Kawai, F. Kamitani, S. (2019). Structural insights into the unique polylactate-degrading mechanism of *Thermobifida alba* cutinase. *FEBS J.* 286, 2087–2098.

Knott, B. C. Erickson, E. Allen, M. D. Gado, J. E. Graham, R. Kearns, F. L. Pardo, I. Topuzlu, E. Anderson, J. J. Austin, H. P. Dominick, G. Johnson, C. W. Rorrer, N. A. Szostkiewicz, C. J. Copié, V. Payne, C. M. Woodcock, H. L. Donohoe, B. S. Beckham, G. T. McGeehan, J. E. (2020), Characterization and engineering of a two-enzyme system for plastics depolymerization, *Proceedings of the National Academy of Sciences – PNAS.* 117 (41), 25476-25485.

Kobayashi, J. Akiyama, Y. Yamato, M. Okano, T. (2019). *Biomaterials: Temperature-Responsive Polymer, Comprehensive Biotechnology*, 3rd ed, Pergamon, 457-470.

Komorniczak, M. (2009). Bacterial growth, https://en.wikipedia.org/wiki/Bacterial_growth.

Koshti, R. Mehta, L. Samarth, N. (2018). Biological recycling of polyethylene terephthalate: a mini-review. *J. Polym. Environ.* 26, 3520–3529.

Kruse, A. Krüger, G. Baalman, A. Hennemann O. D. (1995) Surface pretreatment of plastics for adhesive bonding, *Journal of Adhesion Science and Technology*, 9 (12), 1611-1621.

Li, Y. Xiao, P. Wang, Y. Hao, Y. (2020). Mechanisms and Control Measures of Mature Biofilm Resistance to Antimicrobial Agents in the Clinical Context. *ACS Omega.* 5 (36), 22684-22690.

Liebming, S. Eberl, A. Sousa, F. Heumann, S. Fischer-Colbrie, G. Cavaco-Paulo, A. Guebitz, G. M. (2007). Hydrolysis of PET and bis-(benzoyloxyethyl) terephthalate with a new polyesterase from *Penicillium citrinum*. *Biocatal. Biotransform.* 25, 171–177.

- Lin, Y. H. Yang, M. H. 2009. Tertiary recycling of commingled polymer waste over commercial FCC equilibrium catalysts for producing hydrocarbons. *Polym. Degrad. Stabil.* 94 (1), 25-33.
- Longhi, S. Cambillau, C. (1999). Structure-activity of cutinase, a small lipolytic enzyme. *Biochem Biophys Acta.* 1441, 185–196.
- Lu, H. Diaz, D. J. Czarnecki, N. J. Zhu, C. Kim, W. Shroff, R. Acosta, D. J. Alexander, B. R. Cole, H. O. Zhang, Y. Lynd, N. A. Ellington, A. D. Alper, H. S. (2022). Machine learning-aided engineering of hydrolases for PET depolymerization, *Nature.* 604 (7907), 662-667.
- Ma, Y. Yao, M. Li, B. Ding, M. He, B. Chen, S. Zhou, X. Yuan, Y. (2018). Enhanced Poly (ethylene terephthalate) Hydrolase Activity by Protein Engineering, *Engineering*, 4 (6), 888-893.
- Magalhães, R. P. Cunha, J. M. Sousa, S. F. (2021). Perspectives on the Role of Enzymatic Biocatalysis for the Degradation of Plastic PET, *Int. J. Mol. Sci.* 22, 11257.
- Manzoni, M. Rollini, M. (2002). Biosynthesis and biotechnological production of statins by filamentous fungi and application of these cholesterol-lowering drugs. *Applied Microbiology and Biotechnology.* 58, 555-564.
- Mariotti, N. Ascione, G. S. Dario, C. Cuomo, F. (2019). Critical barriers for plastic recycling. A case study in Turin. *Procedia Environmental Science, Engineering and Management.* 6 (2), 169-180.
- Martinez, C. De Geus, P. Lauwereys, M. Matthyssens, G. Cambillau, C. (1992). *Fusarium solani* cutinase is a lipolytic enzyme with a catalytic serine accessible to solvent. *Nature.* 356, 615–618.
- Masaki, K. Kamini, N. R. Ikeda, H. Iefuji, H. (2005). Cutinase-like enzyme from the yeast *Cryptococcus* sp. strain S-2 hydrolyzes polylactic acid and other biodegradable plastics. *Appl. Environ. Microbiol.* 71, 7548–7550.
- Maurya, A. Bhattacharya, A. Khare, S.K. (2020). Enzymatic Remediation of Polyethylene Terephthalate (PET)–Based Polymers for Effective Management of Plastic Wastes: An Overview. *Front. Bioeng. Biotechnol.* 8, 602325.
- McIntyre, J. E. (2004). *The historical development of polyesters. In Modern Polyesters: Chemistry and Technology of Polyesters and Copolyesters.* UK, John Wiley & Sons, Ltd., 1–28.
- Meereboer, K. W. Misra, M. Mohanty, A. K. (2020). Review of recent advances in the biodegradability of polyhydroxyalkanoate (PHA) bioplastics and their composites, *Green Chem.* 22, 5519-5558.
- Mihucz, V. G. Zaray, G. (2016). Occurrence of antimony and phthalate esters in polyethylene terephthalate bottled drinking water. *Appl. Spectrosc. Rev.* 51 (3), 183-209.

- Miller, M. B. Bassler, B. L. (2001). Quorum sensing in bacteria. *Annual Reviews in Microbiology*. 55, 165-199.
- Miyakawa, T. Mizushima, H. Ohtsuka, J. Oda, M. Kawai, F. Tanokura, M. (2015) Structural basis for the Ca²⁺-enhanced thermostability and activity of PET-degrading cutinase-like enzyme from *Saccharomonospora viridis* AHK190. *Appl. Microbiol. Biotechnol.* 99, 4297–4307.
- Moges, B. (2022), Chemical De-polymerization for reuse of Polyethylene Terephthalate (PET) towards a circular economy.
- Mohanan, N. Montazer, Z. Sharma, P.K. Levin, D.B. (2020), Microbial and Enzymatic Degradation of Synthetic Plastics, *Frontiers in microbiology*. 11, 580709.
- Muhammad, M. H. Idris, A. L. Fan, X. Guo, Y. Yu, Y. Jin, X. Qiu, J. Guan, X. Huang, T. (2020). Beyond Risk: Bacterial Biofilms and Their Regulating Approaches, *Front. Microbiol.* 11, 928.
- Mukherjee, S. RoyChaudhuri, U. Kundu, P. P. (2017). Anionic surfactant induced oxidation of low density polyethylene followed by its microbial bio-degradation, *International biodeterioration & biodegradation*, 117, 255-268.
- Müller, R. J. Schrader, H. Profe, J. Dresler, K. Deckwer, W. D. (2005). Enzymatic degradation of poly (ethylene terephthalate): rapid hydrolyse using a hydrolase from *Thermobifida fusca*. *Macromol. Rapid Commun.* 26, 1400–1405.
- Murphy, K. S. Enders, N. A. Mahjour, M. Fawzi, M. B. (1986). A comparative evaluation of aqueous enteric polymers in capsule coatings. *Pharm Technol.* 36-45.
- National Center for Biotechnology Information. (2021). PubChem Compound Summary.
- National Research Council. (2000). *Waste Incineration and Public Health*. Washington, DC, The National Academies Press.
- National Research Council (US) Committee on Toxicology. (1984). *Emergency and Continuous Exposure Limits for Selected Airborne Contaminants*, Washington, National Academies Press.
- Nauendorf, A. Krause, S. Bigalke, N. K. Gorb, E. V. Gorb, S. N. Haeckel, M. Wahl, M. Treude, T. (2016). Microbial colonization and degradation of polyethylene and biodegradable plastic bags in temperate fine-grained organic-rich marine sediments. *Mar Pollut Bull.* 103 (1-2), 168-178.
- Nealson, K. Hastings, J. W. (1979). Bacterial bioluminescence: its control and ecological significance. *Microbiological reviews*, 43, 496.
- Obuekwe, C. Al-Jadi, Z. K. Al-Saleh, E. (2009). Hydrocarbon degradation in relation to cell-surface hydrophobicity among bacterial hydrocarbon degraders from petroleum-contaminated Kuwait desert environment. *Int. Biodeter. Biodeg.* 63, 273–279.
- Oda, M. Yamagami, Y. Inaba, S. Oida, T. Yamamoto, M. Kitajima, S. Kawai, F. (2018). Enzymatic hydrolysis of PET: Functional roles of three Ca²⁺ ions bound to a cutinase-

like enzyme, Cut190*, and its engineering for improved activity. *Appl. Microbiol. Biotechnol.*, 102, 10067–10077.

O'Toole, G. and Wong, G. (2016). Sensational biofilms: surface sensing in bacteria. *Current Opinion in Microbiology*, 30, 139-146.

Parsek, M. R. E. P. Greenberg. (2000). Acyl-homoserine lactone quorum sensing in Gram-negative bacteria: a signaling mechanism involved in associations with higher organisms. *PNAS*. 97, 8789–8793.

Palleroni, N. J. M. Doudoroff, R. Y. Stanier, R. E. Solanes, M. Mandel. (1970). Taxonomy of the aerobic pseudomonads: the properties of the *Pseudomonas stutzeri* group. *Journal of general microbiology*. 60, 215-231.

Pathak, V.M. Navneet. (2017). Review on the current status of polymer degradation: a microbial approach. *Bioresour. Bioprocess*. 4, 15.

Peirce, J. Vesilind, P. Weiner, Ruth F. (1997). *Environmental Pollution and Control*, 4th ed. Elsevier Science & Technology Books. pages 167-177.

Pellis, A. Ferrario, V. Zartl, B. Brandauer, M. Gamerith, C. Acero, E. H. Ebert, C. Gardossi, L. Guebitz, G. M. (2016). Enlarging the tools for efficient enzymatic polycondensation: structural and catalytic features of cutinase 1 from *Thermobifida cellulosilytica*. *Catal. Sci. Technol.* 6, 3430–3442.

Pereira, A. Silvaa, M. Júniora, E. Paulaa, A. Tommasinia, F. (2017). Processing and Characterization of PET Composites Reinforced with Geopolymer Concrete Waste. *Materials Research*. 20, 411-420.

Petrova, O. and Sauer, K. (2012). Dispersion by *Pseudomonas aeruginosa* requires an unusual posttranslational modification of BdlA. *Proceedings of the National Academy of Sciences*. 109 (41), 16690-16695.

PlasticsEurope. *Plastics—The Facts*. (2018). An Analysis of European Plastics Production, Demand and Waste Data.

Ploux, L. Ponche, A. Anselme, K. (2010). Bacteria/Material Interfaces: Role of the Material and Cell Wall Properties. *Journal of Adhesion Science and Technology*. 24 (13-14), 2165-2201.

Pop Ristova, P. Pichler, T. Friedrich, M. Bühring, S. (2017). Bacterial Diversity and Biogeochemistry of Two Marine Shallow-Water Hydrothermal Systems off Dominica (Lesser Antilles). *Frontiers in Microbiology*. 8, 2400.

Pospisil, J. Nespurek, S. (1997). Highlights in chemistry and physics of polymer stabilization. *Macromol Symp*. 115, 143–63.

Proshad, R. Kormoker, T. Saiful Islam, Md. Asadul Haque, M. Mahfuzur Rahman, M. d. Mahabubur Rahman Mithu, Md. (2018). Toxic effects of plastic on human health and

environment: A consequences of health risk assessment in Bangladesh, *International Journal of Health*. 6 (1) 1-5.

Qi, X. Yan, W. Cao, Z. Ding, M. Yuan, Y. (2022). Current Advances in the Biodegradation and Bioconversion of Polyethylene Terephthalate, *Microorganisms*. 10 (1), 39.

Rahman, M. East, G. C. (2009). Titanium Dioxide Particle-induced Alkaline Degradation of Poly(ethylene Terephthalate): Application to Medical Textiles, *Textile Research Journal*. 79 (8), 728-736.

Rajandas, H. Parimannan, S. Sathasivam, K. Ravichandran, M. Yin, L. S. (2012). A novel FTIR-ATR spectroscopy based technique for the estimation of low-density polyethylene biodegradation, *Polymer Testing*. 31 (8), 1094–1099.

Ramakrishnan, R. Singh, A.K. Singh, S. Chakravorty, D. Das, D. (2022). Enzymatic dispersion of biofilms: An emerging biocatalytic avenue to combat biofilm-mediated microbial infections, *The Journal of biological chemistry*, 298 (9), 102352.

Ramírez-Larrota, J. S. Eckhard, U. (2022). An Introduction to Bacterial Biofilms and Their Proteases, and Their Roles in Host Infection and Immune Evasion. *Biomolecules*. 12 (2), 306.

Reimschuessel, H. K. (1980). Poly (ethylene terephthalate) Formation. Mechanistic and Kinetic Aspects of the Direct Esterification Process, *Ind. Eng. Chem. Prod. Res. Dev.* 19, 117-125.

Ribitsch, D. Heumann, S. Trotscha, E. Herrero-Acero, E. Greimel, K. Leber, R. Birner-Gruenberger, R. Deller, S. Eiteljoerg, I. Remler, P. Weber, T. Siegert, P. Maurer, K. H. Donelli, I. Freddi, G. Schwab, H. Guebitz, G. M. (2011). Hydrolysis of polyethyleneterephthalate by p-nitrobenzylesterase from *Bacillus subtilis*. *Biotechnol. Prog.* 27 951–960.

Ribitsch, D. Acero, E. H. Greimel, K. Eiteljoerg, I. Trotscha, E. Freddi, G. Schwab, H. Guebitz, G. M. (2012). Characterization of a new cutinase from *Thermobifida alba* for PET-surface hydrolysis. *Biocatal. Biotransformation*. 30 2–9.

Robards, K. Haddad, P.R. Jackson, P.E. (2004). High-performance Liquid Chromatography—Instrumentation and Techniques, Principles and Practice of Modern Chromatographic Methods, *Academic Press*. 227-303.

Robards, K. and Ryan, D. (2022). *High performance liquid chromatography: Separations, Principles and Practice of Modern Chromatographic Methods*, 2nd ed. Academic Press, 283-336.

Roberts C, Edwards S, Vague M, León- Zayas R, Scheffer H, Chan G, Swartz NA, Mellies JL. (2020). Environmental consortium containing *Pseudomonas* and *Bacillus* species synergistically degrades polyethylene terephthalate plastic. *mSphere* 5-20.

Rohman, A. Ghazali, M. Windarsih, A. Irnawati, Riyanto, S. Yusof, F. M. Mustafa, S. (2020). Comprehensive Review on Application of FTIR Spectroscopy Coupled with

Chemometrics for Authentication Analysis of Fats and Oils in the Food Products. *Molecules (Basel, Switzerland)*, 25(22), 5485.

Ronkvist, Å.M. Xie, W. Lu, W. Gross, R.A. (2009). Cutinase-catalyzed hydrolysis of poly (ethylene terephthalate). *Macromolecules*. 42, 5128–5138.

Roth, C. Wei, R. Oeser, T. Then, J. Föllner, C. Zimmermann, W. Norbert, S. (2014). Structural and functional studies on a thermostable polyethylene terephthalate degrading hydrolase from *Thermobifida fusca*. *Appl. Microbiol. Biotechnol.* 98 7815–7823.

Ru, J. Huo, Y. Yang, Y. (2020). Microbial degradation and valorization of plastic wastes. *Front. Microbiol.* 11, 442.

Rubingh, D.N. (1996). The influence of surfactants on enzyme activity. *Curr. Opin. Colloid Interface Sci.* 1, 598–603.

Ruby, E. G. (1996). Lessons from a cooperative, bacterial-animal association: the *Vibrio fischeri-Euprymna scolopes* light organ symbiosis. *Annual Reviews in Microbiology*. 50, 591-624.

Rutherford, S. T. Bassler, B. L. (2012). Bacterial quorum sensing: its role in virulence and possibilities for its control. *Cold Spring Harb Perspect Med.* 2 (11), a012427.

Sagong, H.-Y. Seo, H. Kim, T. Son, H.F. Joo, S. Lee, S.H. Kim, S. Woo, J.-S. Hwang, S. Y. Kim, K.-J. (2020). Decomposition of the PET Film by MHETase Using Exo-PETase Function. *ACS Catal.* 10, 4805–4812.

Samak, N.A. Jia, Y. Sharshar, M.M. Mu, T. Yang, M. Peh, S. Xing, J. (2020), Recent advances in biocatalysts engineering for polyethylene terephthalate plastic waste green recycling, *Environment international*, 145, 106144.

Sánchez, C. (2020). Fungal potential for the degradation of petroleum-based polymers: An overview of macro-and microplastics biodegradation. *Biotechnol. Adv.* 40, 107501.

Sanin, S.L. Sanin, F.D. Bryers, J.D. (2003). Effect of starvation on the adhesive properties of xenobiotic degrading bacteria. *Process Biochem.* 38, 909–914.

Scherf-Clavel, O. (2016). Impurity Profiling of Challenging Active Pharmaceutical Ingredients without Chromophore.

Schmidt-Heydt, M., Parra, R., Geisen, R. Magan, N. (2010). Modelling the relationship between environmental factors, transcriptional genes and deoxynivalenol mycotoxin production by strains of two *Fusarium* species. *J R Soc Interface.* 8, 117-26.

Scott, G. Wiles, DM. 2001. Programmed-life plastics from polyolefins: a new look at sustainability. *Biomacromolecules.* 2 (3), 15-22.

Sen, S. K. and Raut, S. (2015). Microbial degradation of low density polyethylene (LDPE): A review, *Journal of Environmental Chemical Engineering*, 3, 462-473.

Shah, A. Hasan, F. (2008). Biological degradation of plastics: A comprehensive review. *Biotechnology Advances.* 26, 246–265.

- Shi, L. Liu, P. Tan, Z. Zhao, W. Gao, J. Gu, Q. Ma, H. Liu, H. and Zhu, L. (2023). Complete Depolymerization of PET Wastes by an Evolved PET Hydrolase from Directed Evolution Wiley. 62 (14), e202218390.
- Shirke, A.N. White, C. Englaender, J.A. Zwarycz, A. Butterfoss, G.L. Linhardt, R.J. Gross, R.A. (2018). Stabilizing leaf and branch compost cutinase (LCC) with glycosylation: Mechanism and effect on PET hydrolysis. *Biochemistry*. 57, 1190–1200.
- Shen, L. Worrell, E. Patel, M.K. (2010). Open-loop recycling: a LCA case study of PET bottle-to-fibre recycling. *Resources, Conservation and Recycling*. 55, 34-52.
- Shen, L. Nieuwlaar, E. Worrell, E. Patel, M.K. (2011). Life cycle energy and GHG emissions of PET recycling: change-oriented effects. *International Journal of Life Cycle Analysis*. 16, 522-536.
- Shimao, M. (2001). Biodegradation of plastics, *Current Opinion in Biotechnology*, 12 (3), 242-247.
- Singh, B. and Sharma, N. (2008). Mechanistic implications of plastic degradation. *Polymer Degradation and Stability*. 93 (3) 561-584.
- Singh, R.K. Tiwari, M.K. Singh, R. Lee, J.K. (2013). From protein engineering to immobilization: Promising strategies for the upgrade of industrial enzymes. *Int. J. Mol. Sci*. 14, 1232–1277.
- Song, S. Wood, T.K. (2021), The Primary Physiological Roles of Autoinducer 2 in *Escherichia coli* Are Chemotaxis and Biofilm Formation. *Microorganisms*. 9 (2), 386.
- Soong, Y.V. Sobkowicz, M.J. Xie, D. (2022), Recent Advances in Biological Recycling of Polyethylene Terephthalate (PET) Plastic Wastes, *Bioengineering (Basel)*, 9 (3), 98.
- Spina, F. Tummino, M. L. Poli, A. Prigione, V. Ilieva, V. Cocconcelli, P. Puglisi, E. Bracco, P. Zanetti, M. Varese, G. C. (2021). Low density polyethylene degradation by filamentous fungi, *Environmental Pollution*. 274, 116548.
- Stanbury, P. F. Whitaker, A. Hall, S. J. (1995). *Principles of fermentation technology. second edition*. Pergamon press.
- Stewart, P. S. Franklin, M. J. (2008). Physiological heterogeneity in biofilms. *Nat Rev Microbiol*. 6 (3), 199-210.
- Su, Y. Ding, T. (2023). Targeting microbial quorum sensing: the next frontier to hinder bacterial driven gastrointestinal infections. *Gut Microbes*. 15 (2), 2252780.
- Subramoni, S. Muzaki, M.Z.B.M. Booth, S.C.M. Kjelleberg, S. Rice, S.A. (2021). N-Acyl Homoserine Lactone-Mediated Quorum Sensing Regulates Species Interactions in Multispecies Biofilm Communities. *Frontiers in Cellular and Infection Microbiology*. 11.
- Sulaiman, S. Yamato, S. Kanaya, E. Kim, J. J. Koga, Y. Takano, K. Kanaya, S. (2012). Isolation of a novel cutinase homolog with polyethylene terephthalate-degrading activity

- from leaf-branch compost by using a metagenomic approach. *Appl Environ Microbiol.* 78 (5), 1556-62.
- Taghavi, N. Zhuang, W. Baroutian, S. (2021). Enhanced biodegradation of non-biodegradable plastics by UV radiation: Part 1, *Journal of Environmental Chemical Engineering.* 9 (6), 106464.
- Taghavi, N. Zhuang, W. Q. Baroutian, S. (2022). Effect of rhamnolipid biosurfactant on biodegradation of untreated and UV-pretreated non-degradable thermoplastics: Part 2, *Journal of Environmental Chemical Engineering.* 10, 107033.
- Takano, E. Nihira, T. Hara, Y. Jones, J. J. Gershter, C. J. Yamada, Y. Bibb, M. (2000). Purification and structural determination of SCB1, γ -Butyrolactone That Elicits Antibiotic Production in *Streptomyces coelicolor* A3 (2). *Journal of Biological Chemistry.* 275, 11010-11016.
- Taniguchi, I. Yoshida, S. Hiraga, K. Miyamoto, K. Kimura, Y. Oda, K. (2019). Biodegradation of PET: Current Status and Application Aspects, *ACS Catal.* 9, 4089–4105.
- Then J. Wei R. Oeser T. Barth M. Belisário-Ferrari M. R. Schmidt J. Zimmermann W. (2015). Ca²⁺ and Mg²⁺ binding site engineering increases the degradation of polyethylene terephthalate films by polyester hydrolases from *Thermobifida fusca*. *Biotechnol. J.* 10, 592–598.
- Thevenon, F. Carroll, C. Sousa, J. (editors). 2014. *Plastic Debris in the Ocean: The Characterization of Marine Plastics and their Environmental Impacts, Situation Analysis Report.* Gland, Switzerland.
- Tiwari, S. Mall, H. Solanki, P. P. (2018). Surfactants and its applications: A review, *International Journal of Engineering Research and Application*, 9, 61-66.
- Tokiwa, Y. Calabia, B. P. Ugwu, C. U. Aiba, S. (2009). Biodegradability of plastics. *Int. J. Mol. Sci.* 10, 3722–3742.
- Tomšič, M. Bešter-Rogač, M. Kunz, A. Touraud, D. Bergmann, A. Glatter, O. (2004). Nonionic Surfactant Brij 35 in Water and in Various Simple Alcohols: Structural Investigations by Small-Angle X-ray Scattering and Dynamic Light Scattering. *The Journal of Physical Chemistry B.* 108 (22), 7021-7032
- Tournier, V. Topham, C.M. Gilles, A. David, B. Folgoas, C. Moya-Leclair, E. Marty, A. (2020). An engineered PET depolymerase to break down and recycle plastic bottles. *Nature*, 580, 216–219.
- Tribedi, P. and Sil, A.K. (2013). Low-Density Polyethylene Degradation by *Pseudomonas* sp. AKS2 Biofilm. *Environmental Science and Pollution Research.* 20, 4146-4153.
- Vegt, A. K. Govaert, L. E. (2005). *Polymeren: van keten tot kunststof*, 5th ed. VSSD.

- Vertommen, M.A.M.E. Nierstrasz, V.A. Van Der Veer, M. Warmoeskerken, M.M.C.G. (2005). Enzymatic surface modification of poly(ethylene terephthalate). *J. Biotechnol.* 120, 376–386.
- Ügdüler, S. Van Geem, K. Denolf, R. Roosen, M. Mys, N. Ragaert, K. and De Meester, S. (2020). Towards closed-loop recycling of multilayer and coloured PET plastic waste by alkaline hydrolysis, *Green Chem.* 22, 5376-5394.
- Urbanek, A.K. Kosiorowska, K.E. and Mirończuk, A.M. (2021). Current Knowledge on Polyethylene Terephthalate Degradation by Genetically Modified Microorganisms, *Frontiers in bioengineering and biotechnology.* 9, 771133.
- Wagner-Egea, P. Aristizábal-Lanza, L. Tullberg, C. Wang, P. Bernfur, K. Grey, C. Zhang, B. Linares-Pastén, J.A. (2023). Marine PET Hydrolase (PET2): Assessment of Terephthalate- and Indole-Based Polyesters Depolymerization. *Catalysts.* 13, 1234.
- Wang, Daniel L. C. Cooney, Charles L. Demain, Arnold L. Dunnill, P. Humphrey, Arthur E. Lille, Malcolm D. (1979). *Fermentation and enzyme technology.* Chichester and New York: John Wiley & Sons Ltd. 374.
- Wang, X. Lu, D. Jönsson, L. J. Hong, F. (2008). Preparation of a PET-Hydrolyzing lipase from *Aspergillus oryzae* by the addition of bis(2-hydroxyethyl) terephthalate to the culture medium and enzymatic modification of PET fabrics. *Eng. Life Sci.* 8, 268–276.
- Webb, H. Arnott, J. Crawford, R. Ivanova, E. (2013). Plastic degradation and its environmental implications with special reference to poly (ethylene terephthalate). *Polymers.* 5, 1–18.
- Wei R. Oeser T. Then J. Kuhn N. Barth M. Schmidt J. Zimmermann, W. (2014). Functional characterization and structural modeling of synthetic polyester-degrading hydrolases from *Thermomonospora curvata*. *AMB Express.* 4, 44.
- Wei, R. Oeser, T. Schmidt, J. Meier, R. Barth, M. Then, J. Zimmermann, W. (2016). Engineered bacterial polyester hydrolases efficiently degrade polyethylene terephthalate due to relieved product inhibition. *Biotechnol. Bioeng.* 113, 1658–1665.
- Wei, R. Zimmermann, W. (2017). Microbial enzymes for the recycling of recalcitrant petroleum-based plastics: how far are we? *Microb. Biotechnol.* 10, 1308–1322.
- Wei, R. Breite, D. Song, C. Gräsing, D. Ploss, T., Hille, P., Zimmermann, W. (2019). Biocatalytic degradation efficiency of postconsumer polyethylene terephthalate packaging determined by their polymer microstructures. *Adv. Sci.* 6, 1900491.
- Weinberger, S. Canadell, J. Quartinello, F. Yeniad, B. Arias, A. Pellis, A. Guebitz, G. M. (2017). Enzymatic degradation of poly (ethylene 2, 5-furanoate) powders and amorphous films. *Catalysts.* 7, 318.
- Wood, T. (2014). Biofilm dispersal: deciding when it is better to travel. *Molecular Microbiology.* 94, 747-750.

Worrell, E. Reuter, M. A. (2014). Handbook of recycling: state-of-the-art for practitioners, analysts, and scientists, United States of America: *Elsevier*, 179-189.

Yoshida, S. Hiraga, K. Takehana, T. Taniguchi, I. Yamaji, H. Maeda, Y. et al. (2016). A bacterium that degrades and assimilates poly (ethylene terephthalate). *Science*. 351, 1196–1199.

Yoshida, S. Hiraga, K. Taniguchi, I. Oda, K. (2021). *Ideonella sakaiensis*, PETase, and MHETase: From identification of microbial PET degradation to enzyme characterization. *Methods Enzymol*. 648,187-205.

Zhang, Y. Pedersen, J.N. Eser, B.E. Guo, Z. (2022). Biodegradation of polyethylene and polystyrene: From microbial deterioration to enzyme discovery. *Biotechnology advances*. 60, 107991.

Zimmermann, W. Billig, S. (2011). Enzymes for the biofunctionalization of poly (ethylene terephthalate). *Adv Biochem Eng Biotechnol*. 125, 97-120.